Population/ Nonlinear mixed-effects modelling of pharmacokinetics and pharmacodynamics of tuberculosis treatment

by

Maxwell Tawanda Chirehwa

Thesis Presented for the Degree of

DOCTOR OF PHILOSOPHY

in the Division of Clinical Pharmacology

Department of Medicine

UNIVERSITY OF CAPE TOWN

Primary supervisor: Doctor Paolo Denti
Co-supervisor: Professor Helen McIlleron

January 2018

Hove dzinokwira dzine muronga

… Progress depends on tried paths

“Shona proverb”

Contributions to the field

This thesis includes some of the following contributions to the field of pharmacometrics and clinical pharmacology:

Full length original articles

1. Chirehwa MT, McIlleron HM, Wiesner L, Affolabi D, Bah Sow O, Merle C, & Denti P Effect of efavirenz-based antiretroviral therapy on pharmacokinetics of isoniazid and acetyl-isoniazid. *In manuscript format*

2. Chirehwa MT, McIlleron H, Rustomjee R, Mthiyane T, Onyebujoh P, Smith P, & Denti P (2017) Pharmacokinetics of pyrazinamide and optimal dosing regimens for drug-sensitive and -resistant tuberculosis. *Antimicrobial Agents Chemotherapy* 61(8): e00490-17. doi: 10.1128/AAC.00490-17

3. Chirehwa MT, Rustomjee R, Mthiyane T, Onyebujoh P, Smith P, McIlleron H, & Denti P (2016) Model-based evaluation of higher doses of rifampicin using a semimechanistic model incorporating autoinduction and saturation of hepatic extraction. *Antimicrobial Agents Chemotherapy* 60(1): 487–94. doi: 10.1128/AAC.01830-15

Scientific conference presentations

1. Chirehwa MT, McIlleron HM, Wiesner L, Affolabi D, Bah Sow O, Denti P, & Merle C (2016) Population pharmacokinetics of 1st-line antituberculosis drugs administered under three treatment strategies in TB/ HIV patients from West Africa. In: *9th International Workshop on Clinical Pharmacology of Tuberculosis Drugs*. Liverpool, United Kingdom Abstr P_23

2. Chirehwa MT, McIlleron HM, Wiesner L, Affolabi D, Bah-Sow O, Bienczak A, Merle C & Denti P (2016) Semimechanistic pharmacokinetic model for isoniazid and acetyl-isoniazid in a cohort of TB/HIV co-infected patients. In: *Population Approach Group Europe (PAGE) 25 meeting*. Lisboa, Portugal Abstr 5993

3. Chirehwa MT, Rustomjee R, Mthiyane T, Onyebujoh PC, Smith P, McIlleron HM, & Denti P (2015) Model-based evaluation of higher doses of rifampicin using a semimechanistic model incorporating autoinduction and saturation of hepatic extraction. In: *8th International Workshop on Clinical Pharmacology of Tuberculosis Drugs*. San Diego, USA Abstr 10

4. Chirehwa MT, Rustomjee R, Mthiyane T, Onyebujoh PC, Smith P, McIlleron HM, & Denti P (2015) Model-based evaluation of higher doses of rifampicin using a semimechanistic model incorporating autoinduction and saturation of first-pass hepatic extraction. In: *Population Approach Group Europe (PAGE) 24 meeting*. Hersonissos, Crete, Greece Abstr 3336

5. Chirehwa M, Rustomjee R, Mthiyane T, Onyebujoh P, Smith P, McIlleron H, & Denti P (2014) Population pharmacokinetics of pyrazinamide in HIV/TB co-infected patients at different levels of immunosuppression in South Africa. In: *World Congress on Pharmacology* Cape Town, South Africa p Abstract. 264

The author also made the following contributions not included in the thesis to the field of clinical pharmacology and pharmacometrics at the time when registered for doctoral studies:

Full length original articles

1. Court R, Chirehwa MT, Wiesner L, Wright B, Smythe WA, Kramer N, et al (2018) Quality assurance of rifampicin-containing fixed drug combinations in South Africa – a pragmatic response. The International Journal of Tuberculosis and Lung Disease. (*In Press*)

2. Naidoo A, Ramsuran V, Chirehwa M, Denti P, McIlleron H, Naidoo K, Yende-Zuma N, Singh R, Ngcapu S, Chaudhry M, Pepper M.S & Padayatchi N (2018) Effect of genetic variation in UGT1A and ABCB1 on moxifloxacin pharmacokinetics in South African patients with tuberculosis. Pharmacogenomics 19(1): 17-29. doi: 10.2217/pgs-2017-0144

3. Naidoo A, Chirehwa M, McIlleron H, Naidoo K, Essack S, Yende-Zuma N, Kimba-Phongi E, Adamson J, Govender K, Padayatchi N & Denti P (2017) Effect of rifampicin and efavirenz on moxifloxacin concentrations when co-administered in patients with drug-susceptible TB. J Antimicrobial Chemotherapy 72(5): 1441-49. doi: 10.1093/jac/dkx004

4. Rockwood N, Meintjes G, Chirehwa M, Wiesner L, McIlleron H, Wilkinson RJ, & Denti P (2016) HIV-1 coinfection does not reduce exposure to rifampicin, isoniazid, and pyrazinamide in South African tuberculosis outpatients. Antimicrobial Agents Chemotherapy 60(10): 6050–9. doi: 10.1128/AAC.00480-16

Declaration of work

I, Maxwell Tawanda Chirehwa, hereby declare that the work on which this dissertation/thesis is based is my original work (except where acknowledgements indicate otherwise) and that neither the whole work nor any part of it has been, is being, or is to be submitted for another degree in this or any other university. Chapter three and four of the thesis have been published in an international journal and contents remain unchanged from the printed versions excepted where formatting was required to maintain consistency in the thesis. All co-authors gave their written consent to include the publications as part of a PhD. I confirm that co-authors of manuscript presented in chapter 5 (not published) are aware that the manuscript is part of a PhD within a primary study.

I empower the university to reproduce for the purpose of research either the whole or any portion of the contents in any manner whatsoever.

SIGNATURE: Signed by candidate

DATE: 22 May 2018

STUDENT NAME:

CHIREHWA MAXWELL TAWANDA

STUDENT NUMBER: CHRMAX003

I confirm that I have been granted permission by the University of Cape Town's Doctoral Degrees Board to include the following publication(s) in my PhD thesis, and where co-authorships are involved, my co-authors have agreed that I may include the publication(s):

1. Chirehwa MT, McIlleron H, Rustomjee R, Mthiyane T, Onyebujoh P, Smith P, & Denti P (2017) Pharmacokinetics of pyrazinamide and optimal dosing regimens for drug-sensitive and -resistant tuberculosis. *Antimicrobial Agents Chemotherapy* 61(8): e00490-17. doi: 10.1128/AAC.00490-17

2. Chirehwa MT, Rustomjee R, Mthiyane T, Onyebujoh P, Smith P, McIlleron H, & Denti P (2016) Model-based evaluation of higher doses of rifampicin using a semimechanistic model incorporating autoinduction and saturation of hepatic extraction. *Antimicrobial Agents Chemotherapy* 60(1): 487–94. doi: 10.1128/AAC.01830-15

SIGNATURE: 

DATE: 22 May 2018

STUDENT NAME:

CHIREHWA MAXWELL TAWANDA

STUDENT NUMBER: CHRMAX003

Acknowledgements

I would like to offer my special thanks to the following whom/which contributed to the successful completion of the research

Supervision

Dr Paolo Denti for introducing pharmacometrics modelling methods, training on reporting standards through feedback on research output and ensuring progress throughout the studies. He also provided funding to attend conferences and supported my applications for funding.

Professor Helen McIlleron for critically reviewing the modelling work from a medical perspective and assistance with interpreting modelling results. She also provided and pointed to useful resources to further my understanding of the tuberculosis disease and its treatment. Funding to attend some conferences were provided from her research projects.

Funding

The European and Developing Countries Clinical Trials Partnership (EDCTP) funded the PhD project under the RAFA randomised clinical trial (PACTR201105000291300). The financial assistance of the National Research Foundation (NRF) towards this research is hereby acknowledged (Grant UID: 95106). Opinions expressed, and conclusions arrived at, are those of the author and are not necessarily to be attributed to the NRF.

Research study

Special thanks to the study participants and study teams of the TB-HAART and RAFA study for dedicating their time towards the success of the project. I would like to express my gratitude to Dr Corinne Merle for leading the RAFA study and all co-authors for their feedback on my research outputs.

Division of Clinical Pharmacology, University of Cape Town

I would like to thank Prof Gary Maartens, Prof Peter Smith and Marilyn Solomons for providing scientific and administrative support for the research. I appreciate the scientific input on pharmacokinetic sample processing and assay analysis received from Dr Lubbe Wiesner and Jennifer Norman of the analytical laboratory. Discussions with and advice from colleagues in the pharmacometrics modelling group has been of great help. The research would not have been smooth without the conducive environment in the division of clinical pharmacology.

Research collaboration and support

I am grateful for the opportunity provided by Dr Colin Pillai, Akiko Keller, and the Next Generation Scientist (NGS) program team to be one of the NGS interns. The mentorship from Dr Ivan Demin and the Novartis Pharma modelling and simulation group will forever be remembered. My participation in the 2017 Uppsala Summer School was made possible through funding provided by Novartis Pharma.

I am thankful for the support from Prof Mats Karlsson, Dr Elin Svensson and the department of pharmaceutical biosciences for the discussions and support during the Uppsala Pharmacometrics Summer School and the research exchange visit at Uppsala University.

Some modelling work were performed using facilities provided by the University of Cape Town's ICTS High-Performance Computing team: http://hpc.uct.ac.za

Personal

You need a strong family because, in the end, they will love you and support you unconditionally. I thank God that I have Mr and Mrs Chirehwa, Maslline, Uno, Ernest, Florence, and Medlyne. The encouragement and support from Chirehwa, Guta, Katiyo and Nyagato families was immense.

Abstract

Population nonlinear mixed-effects modelling of pharmacokinetics and pharmacodynamics of tuberculosis treatment

Maxwell Tawanda Chirehwa - 2018

The pharmacokinetics of rifampicin, isoniazid, pyrazinamide and ethambutol in TB/HIV coinfected patients recruited in two phase III clinical trials (61 patients in TB-HAART and 222 patients in RAFA study) were described using nonlinear mixed-effects modelling. Concentration-time data for rifampicin (TB-HAART study) was used to develop a semimechanistic pharmacokinetic model incorporating autoinduction and saturable pharmacokinetics. A model describing the pharmacokinetics of pyrazinamide (TB-HAART study) was developed and used to evaluate the 24-hour area under the concentration-time curve ($AUC_{0–24}$), and maximum concentrations (C_{max}) achieved with the currently recommended weight-adjusted doses for drug-susceptible and -resistant tuberculosis. Concentration-time data from the RAFA study were used to characterise the pharmacokinetics of the four drugs of the fixed dose combination (FDC) therapy including desacetyl-rifampicin, and acetyl-isoniazid. Binary recursive techniques were applied in the conditional inference framework to determine predictors including drug exposure of time-to-stable culture conversion and poor long-term treatment outcomes.

The model describing the pharmacokinetics of rifampicin predicted that increasing the dose results in a more than proportional increase in exposure. Clearance of rifampicin increased by 90% from baseline to steady-state due to autoinduction and the process takes up to 21 days. Monte Carlo simulations showed that rifampicin doses of at least 25 mg/kg would be required to achieve an $AUC_{0–24}$/MIC ratio of at least 271. Based on the model describing the pharmacokinetics of isoniazid, co-administration of isoniazid and efavirenz-based antiretroviral therapy results in a 54% reduction in isoniazid exposure only in fast acetylators. There were disparities in exposure across weight bands for all the four drugs: patients with lower weight had reduced exposure. To match drug exposure across the weight bands, we recommend the addition of one FDC tablet to patients with weight less than 55 kg. There is need to explore the use of fat-free mass-adjusted dosing since cumulative evidence shows its superiority over total body weight in driving exposure via allometric scaling for all first-line antituberculosis drugs. Individual drug exposures were not predictive of either time-to-stable culture conversion or long-term tuberculosis treatment outcomes. Baseline X-ray grading, HIV stage as TB diagnosis, and treatment arm were predictive of time-to-stable culture conversion while the presence of cavities, patient's level of physical activity and CD4 count were the drivers of long-term treatment outcomes.

CONTENTS

List of tables

List of figures

Abbreviations and acronyms

AcINH	Acetyl-isoniazid
AIC	Akaike Information Criterion
ALT	Alanine Aminotransferase
ART	Antiretroviral Therapy
AST	Aspartate transaminase
ATT	Antituberculosis Treatment
AUC_{0-24}	24-hour area under the concentration-time curve
BLQ	Below the Limit of Quantification
BOV	Between-Occasion Variability
BSV	Between-Subject Variability
CAR	Constitutive Androstane Receptor
CART	Classification and Regression Trees
CFR	Cumulative Fraction of Response
CFU	Colony Forming Units
CI	Confidence Interval
CL	Clearance
CL_H	Hepatic clearance
CL_{int}	Intrinsic clearance
$CL_{int,max}$	Maximum Intrinsic clearance
C_{max}	Maximum plasma concentration
C_{min}	Minimum plasma concentration
DNA	Deoxyribonucleic acid
EBA	Early Bactericidal Activity
EFV	Efavirenz
E_H	Hepatic extraction
F	Oral bioavailability

FDC	Fixed Dose Combination
FFM	Fat-Free Mass
FOCE-I	First-Order Conditional Estimation with eta-epsilon Interaction
F_{prehep}	Prehepatic oral bioavailability
f_u	Unbound fraction
GOF	Goodness of Fit
HAART	Highly Active Antiretroviral Therapy
HIV	Human Immunodeficiency Virus
INA	Isonicotinic acid
INH	Isoniazid
K_a	Absorption rate constant
K_m	Michaelis-menten constant
$K_{transit}$	Absorption intercompartment transfer rate
LLOQ	Lower Limit of Quantification
M. tuberculosis	Mycobacterium tuberculosis
MARS	Multivariate Adaptive Regression Splines
MDR-TB	Multidrug Resistant-tuberculosis
MIC	Minimum Inhibitory Concentration
mRNA	Messenger Ribonucleic acid
MTT	Mean Transit Time
NAT2	N-acetyltransferase 2
NCA	Noncompartmental Analysis
NN	Number of absorption transit compartments
OFV	Objective Function Value
PAS	Para-Aminosalicylate Sodium
PD	Pharmacodynamics
PK	Pharmacokinetics

PK-PD	Pharmacokinetics-pharmacodynamics
P-pg	P-glycoprotein
PsN	Perl-speaks-NONMEM
PTA	Probability of Target Attainment
PXR	Pregnane X receptor
Q	Intercompartmental clearance
Q_H	Hepatic plasma flow
SIR	Sampling Importance Resampling
TB	Tuberculosis
TBW	Total Body Weight
T_{max}	Time to maximum plasma concentration
TTE	Time-to-event
V	Volume of distribution
V_C	Volume of distribution of the central compartment
V_H	Volume of distribution of the liver
V_P	Volume of distribution of the peripheral compartment
VPC	Visual Predictive Check
WHO	World Health Organization

Chapter 1: Introduction and literature review

1.1 Global disease burden of tuberculosis

In 2015, new cases of tuberculosis were estimated to be around 10.4 million worldwide (World Health Organization, 2016). The incidence of tuberculosis continues to grow because of the high prevalence of Human Immunodeficiency Virus (HIV), bacterial resistance to medications, migration from regions of high prevalence, and living conditions (Knechel, 2009). New tuberculosis cases are unevenly distributed by geographical region, sex, and age. Slightly more than half (56%) of the new tuberculosis cases are men, and the remaining proportion is shared between women (34%) and children (10%). A quarter of the new infections in 2015 occurred in the World Health Organization (WHO) African region. In the same year, the incidence rate for three countries in the Southern Africa region (Lesotho, Mozambique and South Africa) was estimated to be above 500 per 100 000 people. Figure 1 shows the incidence rates of tuberculosis in 2016 at country level. Above a tenth of all new tuberculosis cases were people living with HIV (World Health Organization, 2016). Among new and relapse cases of tuberculosis, HIV prevalence was highest in the African region with most countries in Southern Africa recording prevalence above 50%. Tuberculosis remained one of the top 10 causes of mortality, and around 1.4 million and 0.39 million TB deaths were estimated in 2015 among HIV-negative and HIV-positive people, respectively. In the African region, the proportion of deaths due to TB among HIV-positive people is more than double that of HIV-negative people (77% vs 32%).

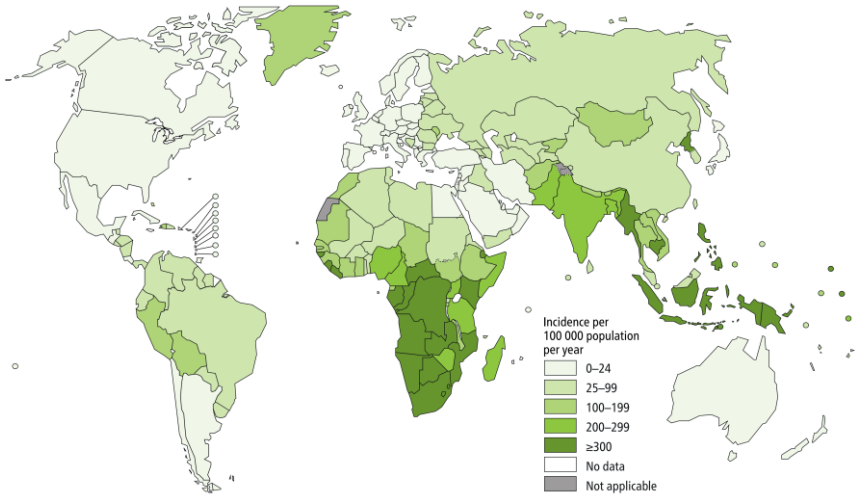

Figure 1.1 Estimated tuberculosis incidence rates, 2016[1]

1.2 Tuberculosis disease

Mycobacterium tuberculosis (*M. tuberculosis)* is the causative agent for tuberculosis. It is a rod-shaped, non-spore forming, and aerobic bacterium that grows slowly compared to other bacteria (Grange, 2009). It has a complex and well-developed cell wall that is responsible for acid-fastness, slow growth rate, host defence mechanism, and resistance (Brennan & Nikaido, 1995; Knechel, 2009). The cell wall is also a barrier to penetration of antituberculosis drugs: the hydrophilic nature of the peptidoglycan and arabinogalactan layer reduces penetration of hydrophobic compounds (Brennan & Nikaido, 1995) and the combination of mycolic acids and long chain fatty acids hinders the penetration of hydrophobic and hydrophilic drugs (Liu, Rosenberg, & Nikaido, 1995). Molecules that escape these barriers are exposed to the multidrug efflux pumps in the cell membrane which pump them out before reaching intracellular targets (Nikaido, 2001). Essential to *M. tuberculosis* survival within macrophages is the lipoarabinomannan, an immunogenic carbohydrate structural antigen component of the cell wall that down-regulates macrophage effector functions (Chan, Fan, Hunter, *et al.*, 1991; Lee, Li, Chatterjee, *et al.*, 2004). *M. tuberculosis* can survive and grow within macrophages thus presenting an additional layer of complexity for drugs to penetrate and this layer also

[1] Reprinted from Global tuberculosis report 2017. Geneva: World Health Organization; 2017. Licence: CC BY-NCSA 3.0 IGO with permission from the World Health Organization.

exposes the drug molecules to host cell efflux transporters (Hartkoorn *et al.*, 2007). Thus antituberculosis drug concentrations inside macrophages become inadequate to eradicate the subpopulation of bacilli in macrophages (Dartois, 2014). Macrophages together with other immune cells form granulomas in an attempt to contain the infection (Ramakrishnan, 2012). The presence of granulomas creates a barrier for antituberculosis drugs reaching the target as it also protects the bacilli within lesions (Dartois & Barry, 2010). The bacilli in the granulomas could then be activated during or after treatment resulting in relapse.

Populations of *M. tuberculosis* can be described as consisting of subpopulations. These can be broadly classified as: (1) actively growing, (2) slow/non-replicating *M. tuberculosis* bacteria that undergo spurts of metabolism, (3) intracellular bacilli present in the acidic compartments of macrophages or lung lesions, and (4) *M. tuberculosis* persisters found in hypoxic microenvironments (Mitchison, 1979). As will be described in the next section, the activity of antituberculosis drugs is preferential to these subpopulations: the drug activity either increases or decreases depending on growth rate of the bacilli , and/or pH at the site of infection (Mitchison, 1979; Vernon, 2011).

1.3 Tuberculosis treatment

The World Health Organisation currently recommends a six-month regimen for the treatment of drug-susceptible tuberculosis. Patients are administered rifampicin, isoniazid, pyrazinamide, and ethambutol daily as Fixed Dose Combination (FDC). Treatment of drug-susceptible tuberculosis consists of an intensive (first two months) and a continuation phase. All four drugs are administered in the intensive phase and only rifampicin and isoniazid in the continuation phase. Adult tuberculosis patients administer weight-adjusted daily doses of the FDC, with each tablet containing 150 mg of rifampicin, 75 mg of isoniazid, 400 mg of pyrazinamide, and 375 mg of ethambutol. Patients with a weight between 30–37 kg receive

two tablets and those with weighing 38–54 kg, 55–70 kg, and above 70 kg receive three, four, and five tablets respectively (World Health Organization, 2010c).

1.4 Pharmacology of antituberculosis drugs

1.4.1 Pharmacology of rifampicin

Rifampicin is the cornerstone of the current drug regimen for the treatment of drug-susceptible tuberculosis. It prevents DNA-directed mRNA synthesis by binding to the β subunit of DNA dependent RNA polymerase (*rpoB*) (Donald & McIlleron, 2009; Gumbo, 2010). Mutations to the *rpoB* gene cause resistance to rifampicin and close to 90% happen at codons 526 and 531. Rifampicin-resistant strains occur in approximately 1 in 10^7 to 1 in 10^8 bacilli (Mitchison, 2000; Somoskovi, Parsons, & Salfinger, 2001). The Minimum Inhibitory Concentrations (MICs) of rifampicin in drug-susceptible *M. tuberculosis* clinical isolates ranged from 0.016 to 0.5 mg/L and the distribution is similar in different geographic regions (Chigutsa *et al.*, 2015; Lee & Heifets, 1987; Schon *et al.*, 2009).

Rifampicin is administered orally, and its absorption is highly variable (Burman, Gallicano, & Peloquin, 2001; Wilkins *et al.*, 2008). Following a 600 mg oral dose, rifampicin concentrations reach a peak (C_{max}) of 6–14 mg/L within 1.5–4 hours post-dose (Donald & McIlleron, 2009; Sirgel *et al.*, 2005). Pharmacokinetic parameters of rifampicin are affected by food intake: C_{max} is reduced by a third and time to C_{max} (T_{max}) is doubled (Acocella, 1978; Lin, Yu, Liu, *et al.*, 2014; Peloquin, Namdar, Singleton, & Nix, 1999; Zent & Smith, 1995). Intake of rifampicin on an empty stomach also reduces the variability in exposure (Peloquin, Namdar, Singleton, & Nix, 1999). In a cross-over study, the absolute bioavailability of rifampicin was found to be 71% in the fed state compared to the 87% observed in the fasted state (Saktiawati *et al.*, 2016). The absorption process of rifampicin has been described with population modelling as a first-order process with or without delay using a lag time or transit compartments (Rockwood *et al.*, 2016; Smythe *et al.*, 2012)

Rifampicin undergoes extensive first-pass metabolism before reaching the systemic circulation, and it is approximately 80% bound to plasma protein especially albumin (Acocella, 1983; Boman & Ringberger, 1974). It is metabolised by liver esterase which deacetylates it within the hepatocytes to form desacetyl-rifampicin (Acocella, 1978). Both rifampicin and desacetyl-rifampicin are largely excreted in bile with a minor proportion excreted renally. At doses of around 450 mg, the capacity of the liver to extract rifampicin is saturated hence increasing the dose results in a more than linear increase in exposure. A 50% increase in the dose (600 mg to 900 mg) resulted in nearly double the concentrations and tripling of exposure was observed after doubling the dose from 10 mg/kg to 20 mg/kg (Acocella, 1978; Decroix *et al.*, 1969). The saturation may be due to the achievement of a transport maximum in bile at doses of around 450 mg.

Rifampicin induces a number of drug metabolising enzymes via the nuclear pregnane X receptor (PXR) and constitutive androstane receptor (CAR) (Chen & Raymond, 2006). This induction also affects rifampicin's own metabolism, such that the exposure on the first day of treatment is greater than at steady state as a result of a change in clearance (Acocella, 1978). It is also a substrate of the P-glycoprotein (P-gp), a drug efflux pump encoded by the ABCB1 gene (Schuetz, Schinkel, Relling, *et al.*, 1996). Reports show widely varying time to full induction: one week to one month (Niemi et al., 2003; Smythe et al., 2012). Recent research results reported after the publication of results in this thesis were in keeping with the previously estimated values (Svensson, Aarnoutse, *et al.*, 2017). A dose-dependent effect of autoinduction, which tends to decrease the elimination half-life of rifampicin over the first two weeks of treatment, has also been observed: the change in half-life was higher for the 900 mg dose compared to the 600 mg dose (Acocella, Pagani, Marchetti, *et al.*, 1971). Population pharmacokinetic modelling was applied to quantify the extent of autoinduction and Svensson et al. reported that the induction process takes around 24 days to complete and Smythe et al.

reported a longer duration of 40 days, assuming 5 half-lives of the induction process. (Smythe *et al.*, 2012; Svensson, Aarnoutse, *et al.*, 2017)

The population pharmacokinetics of rifampicin has been described using a one-compartment disposition model after a single dose or at steady state. At steady state, the apparent clearance (CL/F) reported in African patients ranges between 11 L/h and 25 L/h (Chigutsa *et al.*, 2011; Denti, Martinson, *et al.*, 2015; Rockwood *et al.*, 2016; Smythe *et al.*, 2012; Wilkins *et al.*, 2008). In TB/HIV co-infected patients from South Africa, HIV-infected and ART naïve patients had 21% reduced clearance, and a 46% reduction in clearance was reported among HIV-infected patients on double dose lopinavir/ritonavir (Rockwood *et al.*, 2016). Pregnant women from South Africa were shown to have 14% reduced clearance of rifampicin compared to non-pregnant counterparts (Denti, Martinson, *et al.*, 2015). Comparing single-drug to FDC formulation, Wilkins et al. reported a 23% increase in oral clearance among patients who received single-drug formulation. However, this relationship could be a result of the effect of formulation on bioavailability, rather than clearance itself, as there was a near 100% correlation between CL/F and apparent volume of distribution (V/F) (Wilkins *et al.*, 2008). Genetic polymorphism in SLCO1B1 rs41490932 has been reported to reduced exposure to rifampicin. Patients with the heterozygous mutation have 18% reduced bioavailability while those with the homozygous mutation have 28% lower bioavailability compared to the wild-type (Chigutsa *et al.*, 2011). A 30% reduced volume of distribution in females reported by Chigutsa et al. could reflect the effect of body size and composition on disposition parameters. The model by Chigutsa et al. and that of Wilkins et al. applied allometric scaling using total body weight whereas the models by Denti et al. and Rockwood et al. used fat-free mass. The effect of sex on V/F was not significant in the models by Denti et al. and Rockwood et al., possibly because of the difference in body composition between males and females had been accounted for by allometric scaling. Related to these findings are pharmacokinetic results from Malawi, where males were reported to have 20% increased clearance after adjustment for body size using total body weight (Sloan *et al.*, 2017). Females have higher fat compared to

males, hence receive higher doses per kg of fat-free mass than males when dosed using the currently recommended weight-adjusted dosing. This results in a disparity in exposure, as presented by McIlleron et al. who showed that males with lower weight have significantly reduced exposure than the rest of the patients (McIlleron *et al.*, 2012). Clearance of rifampicin is modified in patients with liver damage, who show increased elimination half-life (Jeanes, Jessamine, & Eidus, 1972). The reduction in rifampicin clearance as a result of renal impairment does not warrant dose modification, but renally impaired patients should be monitored for acute interstitial nephritis or further deterioration of renal function (Acocella, 1978; Malhotra, 2003; Neugarten, Gallo, & Baldwin, 1983).

Besides variability due to patient characteristics, some formulations of rifampicin have been shown to have reduced bioavailability and others are unstable *ex vivo*. In a pooled analysis of drug formulations from tuberculosis programmes and pharmacies in six countries, rifampicin content was reduced to less than 85% in 13% of analysed samples. More FDCs than single-drug tablets had reduced rifampicin content (Laserson, Kenyon, Kenyon, *et al.*, 2001). Under accelerated storage conditions of temperature and humidity, decomposition of rifampicin was observed (Bhutani, Mariappan, & Singh, 2004; Singh & Mohan, 2003). A 98% degradation of rifampicin in the presence of isoniazid compared to rifampicin alone or with pyrazinamide reported by Seifart et al. suggest that the two drugs could have interacted in the formulation environment during storage (Seifart, Parkin, & Donald, 1991).

An integrated pharmacokinetic model for rifampicin and desacetyl-rifampicin has been developed for healthy Asian adults and African children with tuberculosis (Denti *et al.*, 2017; Seng *et al.*, 2015b). In the model by Seng et al., pharmacokinetics of desacetyl-rifampicin was described using a two-compartment model with input from the central plasma compartment of rifampicin. In their model, the clearance of desacetyl-rifampicin was estimated to be 95.8 L/h. Concurrently with the work presented in this, Denti et al. developed a elegant semimechanistic

well-stirred liver model with jointly saturable hepatic extraction for both rifampicin and desacetyl-rifampicin. The authors defined two pathways associated with the clearance of rifampicin: formation of desacetyl-rifampicin and other metabolites or excretion. Disposition of desacetyl-rifampicin was characterised by a one-compartment model (Denti *et al.*, 2017).

The currently recommended rifampicin dose of 10 mg/kg (approximately 600 mg daily) was selected based on (1) concentrations above the Minimum Inhibitory Concentration (MIC), (2) the fact that adverse events were thought to be likely to be dose-related, and (3) cost (van Ingen *et al.*, 2011). The relationship between the dose and toxicity is of less importance as recent evidence shows that daily doses of up to 35 mg/kg of body weight are well tolerated (Boeree *et al.*, 2015). In this study, the adverse events observed were not related to any specific dose of rifampicin. Increased doses of rifampicin had been evaluated in the early studies by comparing doses from 10 mg/kg to 12.5 mg/kg of body weight. The rate of sputum conversion was similar in the two treatment groups, but the 25% increase in dose might have been too conservative (Long, Snider, & Farer, 1979). The recent study by Boeree et al. also showed that doses of 30 mg/kg and 35 mg/kg resulted in greater estimated fall in bacterial load than 10 mg/kg during the first 14 days of treatment (Boeree *et al.*, 2015). Prior to the publication of the results by Boeree et al., several pharmacodynamic indices for rifamycins had been proposed using data from *in vitro* and *in vivo* experiments. Nuermberger and Grosset suggested that rifamycins, have concentration-dependent killing hence the ratio of C_{max}/MIC and area under the concentration-time curve (AUC) over MIC (AUC/MIC) will correlate best with the rate of bacterial killing (Nuermberger & Grosset, 2004). Some researchers argue that of the two indices, $AUC_{0–24}$/MIC is the best index associated with bacterial killing (Gumbo, Louie, Deziel, *et al.*, 2007; Jayaram *et al.*, 2003). Using an aerosol infection model, Jayaram et al. identified that $AUC_{0–24}$/MIC ratio ≥ 271 was important to achieve a 1-$\log_{10}$ CFU decline *in vivo*. For the prevention of resistance to rifampicin, Gumbo et al. reported that a C_{max}/ MIC ratio of ≥ 175 is required (Gumbo, Louie, Deziel, *et al.*, 2007). In order to achieve the required pharmacodynamic targets ($AUC_{0–24}$/MIC and C_{max}/MIC), Goutelle et al. suggested the use of

a 1 200 mg dose which is approximately 20 mg/kg (Goutelle *et al.*, 2009). However, the bacteriological response in the 10 mg/kg, 15 mg/kg, and 20 mg/kg treatment groups was compared during eight weeks of treatment, and no evidence of superiority of the >10 mg/kg doses was observed, supporting the idea that higher doses of rifampicin need to be evaluated over longer treatment durations (Aarnoutse *et al.*, 2017). The need for higher doses of rifampicin is further strengthened by the results reported by Boeree et al.: the decline in bacterial load as measured by time-to-positivity in liquid media was significantly longer for only the 30 mg/kg and 35 mg/kg dose compared to the 10 mg/kg dose (Boeree *et al.*, 2015). In a separate study (the main study of the results presented in this thesis), 12-month mortality was not significantly reduced in the 15 mg/kg dose treatment arm, however, the PK-PD relationship could have been modified by severe immune suppression as the effect of the higher dose of rifampicin was observed only in patients with $CD4^+$ count of <100 cells/µL (Merle *et al.*, 2016). In support of the argument for the need for higher doses, doses of at least 30 mg/kg were reported to eradicate persistent *M. tuberculosis*, allowing relapse free, and shorter treatment duration in a Cornell mouse model (Liu *et al.*, 2017). A possible reason is that the higher doses will also result in a more than linear increase in the concentrations of rifampicin inside the bacteria due to saturation of bacterial efflux pumps (Gumbo, Louie, Deziel, *et al.*, 2007).

Induction of the expression of several proteins that alter the metabolism of other drugs is a major side-effect of rifampicin. Enzyme induction by rifampicin could potentially reduce the efficacy of the co-administered drugs and increase the formation of toxic metabolite(s). (Donald & McIlleron, 2009). Other untoward effects that occur in less than 4% of patients taking rifampicin include rash, fever, nausea, and vomiting. Patients who receive another hepatoxic agent could also be at increased risk of hepatoxicity (Gumbo, 2010).

1.4.2 Pharmacology of isoniazid

Isoniazid was introduced for the treatment of tuberculosis in 1952 and has remained as one of the backbone drugs of tuberculosis chemotherapy. It has excellent bactericidal activity against *M. tuberculosis*, a wide therapeutic margin (around 16 for a 300 mg dose[2]), it is cheap and prevents resistance to companion drugs (Donald & Schaaf, 2011; Mitchison, 2000). Isoniazid is a prodrug that enters the mycobacterial cell by passive diffusion and is then activated by *M. tuberculosis* katG-encoded catalase-peroxidase (Timmins & Deretic, 2006). The activated isoniazid targets the NADH-dependent enoyl-acyl carrier protein reductase coded for by the inhA gene, which is responsible for the synthesis of long fatty acyl chains of mycolic acids (Zhang, Heym, Allen, *et al.*, 1992). The MIC of isoniazid in drug-susceptible *M. tuberculosis* ranges from 0.02 to 0.125 mg/L in broth and from 0.1 to 0.2 mg/L on solid media (Chigutsa *et al.*, 2015; Lee & Heifets, 1987; Suo, Chang, Lin, *et al.*, 1988). Mutation of the katG gene results in resistance due to inactivation of isoniazid. Resistance to isoniazid, and lack of its protective effect results in poor treatment outcomes.

Isoniazid is water-soluble and readily absorbed in the gastrointestinal tract with a short delay (approximately 20 minutes) before reaching the systemic circulation. However, this delay is characterised by large variability (Wilkins *et al.*, 2011). The speed and extent of absorption of isoniazid is not affected by intake of antacids, but it is greatly influenced by concomitant food intake. The maximum concentration is reduced by 51% while the time to reach the maximum concentration is increased by 89% (Peloquin, Namdar, Dodge, *et al.*, 1999), and comparable results have been reported by other researchers (Melander *et al.*, 1976; Saktiawati *et al.*, 2016). Zent and Smith also reported that the pharmacokinetics of isoniazid are affected by concomitant food intake, however with modest effects: C_{max} reduced by 20%, AUC_{0-8} reduced by 19% and T_{max} prolonged by 21% (Zent & Smith, 1995). Isoniazid is primarily metabolised

[2] "The therapeutic margin is the ratio between the usual dose size and the dose that yields detectable EBA" (Mitchison, 2000)

by N-acetyltransferase-2 enzyme (NAT2) isoforms to its principal metabolite acetyl-isoniazid and other metabolites (Ellard & Gammon, 1976; Gumbo, 2010). NAT2 is predominantly found in the liver and intestines and is coded by a polymorphic gene. Mutations of NAT2 result in different rates of acetylation of isoniazid and individuals can be classified as fast, intermediate and slow acetylators (Deguchi, Mashimo, & Suzuki, 1990; Parkin *et al.*, 1997). Because of this genetic variability, NAT2 contributes to around 88% of the variability in isoniazid clearance (Kinzig-Schippers *et al.*, 2005; Sim, Abuhammad, & Ryan, 2014). Seng et al. showed that inclusion of NAT2 in a population pharmacokinetic model reduces the between-subject variability from 86% to 14% (Seng *et al.*, 2015a). The difference in acetylation could potentially influence therapeutic response and toxicity. Pre-systemic elimination including hepatic first-pass extraction is affected by NAT2 phenotype, with significant extraction in fast and to a lesser extent in intermediate and slow acetylators. As a result, peak concentrations of isoniazid, usually observed between 1 to 2 hours post a 300 mg dose depends on the acetylator status. On average, C_{max} for fast acetylators is around 1.8 mg/L while that for intermediate and slow acetylators is 3 mg/L and 6 mg/L, respectively (Parkin *et al.*, 1997; Peloquin *et al.*, 1997; Requena-Méndez *et al.*, 2014). In fast acetylators, the rate of elimination via the acetylation pathway is around four times that of other routes while in slow acetylators the rate of elimination via acetylation is comparable to other routes (Ellard, 1976). Figure 2 shows a schematic representation of isoniazid metabolism.

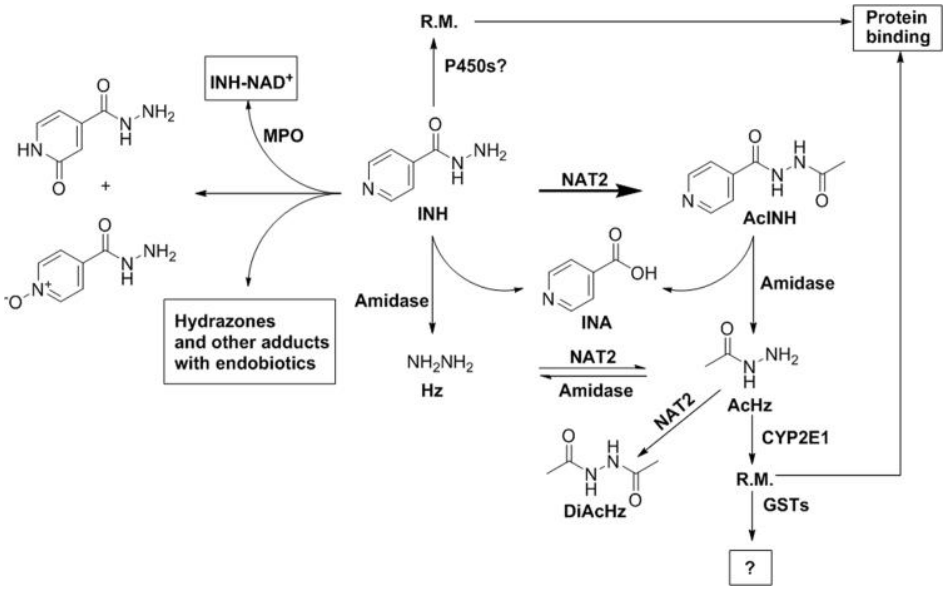

Figure 1.2 A schematic representation of isoniazid (INH) metabolism and the enzymes involved in the metabolic pathways of isoniazid AcHz: acetylhydrazine; AcINH, acetyl-isoniazid; DiAcHz: diacetylhydrazine; GST: glutathione S-transferases; Hz: Hydrazine; INA: isonicotinic acid; MPO: myeloperoxidase; NAT2: N-acetyltransferase 2; P450: cytochrome P450; R.M.: reactive metabolite. (from Wang et al., 2016)[3]

The proportion of fast acetylators varies between 13% and 74% in studies conducted in South Africa, and around 50% in West Africa (Donald *et al.*, 2004; Schaaf *et al.*, 2005; Smythe, 2016; Wilkins *et al.*, 2011). In a cohort of South African patients, CL/F among fast acetylators was estimated to be more than double that of slow acetylators (21.6 vs 9.7 L/h) (Wilkins *et al.*, 2011). In keeping with these results, Smythe also reported a 2-fold increase in CL/F among fast compared to slow acetylators in a cohort of TB/HIV co-infected patients from West Africa (23 vs 10.3 L/h). A smaller difference of 68% higher CL/F in fast acetylators was reported among Tanzanian tuberculosis patients (Denti, Jeremiah, *et al.*, 2015). Mixture modelling was applied to assign patients to the most probable acetylator status in the study by Wilkins et al. and Symthe, while in the study by Denti et al. genotyping results were available. Regardless

[3] Reprinted from Acta Pharm Sin B, 6(5): 384-392, Wang P et al., Isoniazid metabolism and hepatotoxicity, Figure 1, Page 386, Copyright 2016. This is an open access article under the CC BY-NC-ND license (http://creativecommons.org/licenses/by-nc-nd/4.0/)

of acetylator status, allometric scaling was included on CL/F using fat-free mass, which was superior to total body weight as body size descriptor, except for the model presented by Wilkins et al., where fat-free mass was not evaluated. Besides acetylator status, and body size, clearance of isoniazid is influenced by HIV infection, ART intake, and age. Isoniazid clearance in TB/HIV co-infected patients was 23% lower than HIV negative tuberculosis patients (Rockwood *et al.*, 2016). In a similar setting, Wilkins et al. showed that HIV positive patients have 17% reduced clearance compared to HIV negative patients (Wilkins *et al.*, 2011). In a cohort of TB/HIV patients from Mozambique, nevirapine did not affect the pharmacokinetics of isoniazid. However, efavirenz, a widely used antiretroviral therapy drug, reduced isoniazid AUC_{0-24} by 29% (Bhatt *et al.*, 2014). The influence of age on isoniazid clearance reported by Kergueris et al. reflects reduced renal function associated with older age, and the effect would be more pronounced in slow acetylators whose renal clearance accounts for around 25% of the total clearance. (Kergueris, Bourin, & Larousse, 1986; Weber & Hein, 1979).

Isoniazid is responsible for the initial kill of around 95% of the bacteria in the first two days of treatment (Mitchison, 2000). An early bactericidal activity (EBA) of 0.72 $\log_{10}$ CFU/day was achieved with a dose of 300 mg (Jindani, Aber, Edwards, *et al.*, 1980; Jindani, Doré, & Mitchison, 2003). Donald et al. presented corroborating results and also showed that the EBA of isoniazid remains unchanged with or without co-administered drugs (Donald *et al.*, 1997). A decline of at least 0.55 $\log_{10}$ CFU/mL of sputum per day is associated with reduced infectivity and risk of resistance to isoniazid (Donald & McIlleron, 2009). Isoniazid sterilising activity is limited in the presence of rifampicin and pyrazinamide, and its activity is hypothesized as diminishing with a decrease in metabolic activity and depletion of the bacilli (Dickinson & Mitchison, 1981; Donald & McIlleron, 2009). Contrary to this hypothesis, Gumbo et al. showed that the decline in isoniazid activity is related to the development of drug resistance and

postulated that the resistance could be a result of mutation of the katG or the isoniazid-related induction of multidrug resistance pumps (Gumbo, Louie, Liu, Ambrose, *et al.*, 2007).

Acetyl-isoniazid in the product of acetylation of isoniazid by NAT2. Concentrations of acetyl-isoniazid are usually higher in fast acetylators vs slow acetylators, and peak concentrations occur earlier in fast acetylators (Hutchings, Monie, Spragg, *et al.*, 1988). The apparent half-life of acetyl-isoniazid is double that of isoniazid (4.57 hours vs 2 hours). Population pharmacokinetics of acetyl-isoniazid have been reported in healthy Asian volunteers. A two-compartment model adequately described the pharmacokinetics of acetyl-isoniazid formed from acetylation of isoniazid (Seng *et al.*, 2015a). The model estimated fraction of isoniazid converted to acetyl-isoniazid of 97.3% was same regardless of acetylator phenotype. Two pathways for the clearance of acetyl-isoniazid were identified: formation of isonicotinic acid and other metabolites. The same authors also observed a marginal but significant change in clearance of isoniazid for every 10% change in creatinine clearance from a reference value of 113 mL/min.

Based on mouse models, an $AUC_{0–24}$/MIC ratio of approximately 500 was identified as the best explanatory PK-PD index associated with bactericidal activity of isoniazid after 4 to 6 days of exposure followed by C_{max}/MIC ratio (Jayaram *et al.*, 2004). In an *in vitro* experiment, Gumbo et al. also showed that the ratio of the $AUC_{0–24}$/MIC is the PK-PD index associated with microbial kill (Gumbo, Louie, Liu, Brown, *et al.*, 2007). By using classification and regression trees, $AUC_{0–24}$ of isoniazid was reportedly associated with long-term tuberculosis treatment outcomes with a cut-off value of 53 mg·h/L separating poor and favourable outcomes in patients with pyrazinamide $AUC_{0–24}$ > 363 mg·h/L and rifampicin $AUC_{0–24}$ < 13 mg·h/L. At two months, peak concentrations were identified as best predictors of culture conversion, and again isoniazid was included in the decision tree after pyrazinamide and

rifampicin (Pasipanodya *et al.*, 2013). AUC and 2-hour post-dose concentrations were identified as PK-PD indices associated with optimal EBA defined as 90% of the maximum EBA. Achieving $AUC_{0-\infty}$ of at least 10.52 mg·h/L or 2-hour concentrations > 2.19 mg/L was associated with achieving the optimal EBA (Donald *et al.*, 2007).

The two main metabolic pathways (acetylation and hydrolysis) of isoniazid contribute to hepatotoxicity via hydrazine metabolites. In slow acetylators, direct hydrolysis of isoniazid forms hydrazines that could cause liver damage (Scales & Timbrell, 1982). In a meta-analysis of 14 studies, the odds of developing INH-induced hepatotoxicity in slow acetylators was 4.6 times higher compared to fast acetylators (Wang, Xie, Hao, *et al.*, 2012). The risk of hepatotoxicity was 7-fold higher in slow acetylators with CYP2E1 C1/C1 genotype (Huang *et al.*, 2003). Results from a study of 218 Indian patients also showed that slow acetylator status and CYP2E1 C/D or C/C genotype together were associated with a high frequency of drug-induced liver injury (Bose *et al.*, 2011). In fast acetylators, hydrolysis of acetylhydrazine, a product of metabolism of acetyl-isoniazid, results in the formation of the toxic isoniazid hydrazine (Scales & Timbrell, 1982). Overall, hepatotoxicity is fatal in less than 1% of patients receiving isoniazid. Neurotoxicity is another side effect of isoniazid intake and is closely related to the dose. Patients who are slow acetylators and malnourished have higher chances of neurotoxicity (Donald & McIlleron, 2009).

1.4.3 Pharmacology of pyrazinamide

Pyrazinamide is a pro-drug that was first used for the treatment of pulmonary tuberculosis in 1952 (Yeager, Munroe, & Dessau, 1952). Its use was limited, due to hepatic toxicity associated with high doses, until the early 80's, when its ability to shorten treatment duration was discovered (British Thoracic Association, 1982; Fox, 1981). The British Thoracic association reported a higher proportion of two-months culture negative results in patients receiving pyrazinamide-containing regimens compared to control regimen (77% vs 64%, p-value<0.01).

There are relatively few population pharmacokinetics models for pyrazinamide, and the disposition of pyrazinamide is presented as a one-compartment model (Alsultan *et al.*, 2017; Chigutsa, McIlleron, & Holford, 2010; Denti, Jeremiah, *et al.*, 2015; Peloquin *et al.*, 1997, 1998; Rockwood *et al.*, 2016; Smythe, 2016; Wilkins *et al.*, 2006; Zhu *et al.*, 2002). However, some components of the models differ significantly. Pyrazinamide absorption is known to be rapid, reaching a maximum concentration of around 53 mg/L in a fasted state, between 1-2 hours post-dose (Peloquin *et al.*, 1998). To describe the absorption of pyrazinamide, Wilkins et al. applied a sequential zero-order and first-order absorption process with the former characterising the release of the drug from its oral formulation into the absorption compartment. Their model could also identify two sub-populations with different rates of absorption (Wilkins *et al.*, 2006). Denti et al. and Rockwood et al. accounted for a delay in absorption of pyrazinamide using a chain of transit compartments (Denti, Jeremiah, *et al.*, 2015; Rockwood *et al.*, 2016), whereas data from other studies did not support a delay in absorption (Alsultan *et al.*, 2017; Wilkins *et al.*, 2006) or a delay was not reported. Concomitant food intake has little to no impact on both absorption and bioavailability of pyrazinamide (Peloquin *et al.*, 1998; Zent & Smith, 1995).

Pyrazinamide is rapidly distributed and has a longer non-dose dependent elimination half-life (~9.5 hours) compared to the co-administered drugs in the FDC (Ellard, 1969; Lacroix *et al.*, 1989; Peloquin *et al.*, 1997). Pyrazinamide is first hydrolyzed to its active form pyrazinoic acid by microsomal deamidase in the liver and then oxidised to 5-hydroxypyrazinoic acid by xanthine oxidase (Weiner & Tinker, 1972). Only 4% of the dose is excreted unchanged in bile and approximately a third of the dose as pyrazinoic acid (Ellard, 1969). Xanthine oxidase is also involved in the conversion of pyrazinamide to 5-hydroxypyrazinamide. Clearance of pyrazinamide ranges between 2.8–5.06 L/h in African patients (Alsultan *et al.*, 2017; Denti, Jeremiah, *et al.*, 2015; Rockwood *et al.*, 2016; Smythe, 2016; Vinnard *et al.*, 2017; Wilkins *et al.*, 2006). Clearance of pyrazinamide was reported to change with time on treatment with the other first-line anti-TB agents. In patients from Tanzania, pyrazinamide clearance increased by 16% in the first two months of treatment (Denti, Jeremiah, *et al.*, 2015). A higher increase of 30% was reported in a cohort of patients from West Africa (Smythe, 2016). In a study by Chigutsa et al. pyrazinamide clearance was described using a parallel first-order and mixed-order elimination model which was superior to the first-order elimination (Chigutsa, McIlleron, & Holford, 2010). Results of a recent study conducted in Botswana showed a 22% reduced clearance in patients who had activation of $\%CD38^{+}DR^{+}CD8^{+}$ (Vinnard *et al.*, 2017). Allometric scaling has been applied in the population pharmacokinetics models using either total body weight or fat-free mass. In models where allometric scaling was applied based on total body weight, authors identified the effect of sex on bioavailability, volume of distribution, or clearance consistently. Chigutsa et al. reported a 26% increased bioavailability in females (Chigutsa, McIlleron, & Holford, 2010). Wilkins et al. and Alsultan et al. showed that males had 4.55 L and 7.5 L higher volume of distribution respectively (Alsultan *et al.*, 2017; Wilkins *et al.*, 2006). Females had 40% lower clearance in a cohort of tuberculosis patients from Botswana (Vinnard *et al.*, 2017).

Pyrazinamide is more effective against slowly- or non-replicating bacteria that are characterised by reduced metabolism, lower energy reserves and decreased membrane potential (Zhang, Wade, Scorpio, *et al.*, 2003). The activity of pyrazinamide is highly dependent on its conversion to pyrazinoic acid (Konno, Feldmann, & McDermott, 1967). Pyrazinamide enters the tuberculosis bacilli by passive diffusion (Zhang *et al.*, 1999) and possibly active transport (Raynaud *et al.*, 1999), and then is converted by bacterial pyrazinamidase into pyrazinoic acid. In an acidic environment (low pH), a small proportion of uncharged protonated pyrazinoic acid, which permeates through the cell membrane, facilitates the accumulation of pyrazinoic acid anions and protons, and kills the bacteria (Zhang *et al.*, 1999; Zhang & Mitchison, 2003). Pyrazinoic acid kills the bacteria by inhibiting both protein and RNA synthesis, serine uptake, and disruption of membrane potential (Zhang, Wade, Scorpio, Zhang, & Sun, 2003). Pyrazinoic acid leaves the cell via passive diffusion and excreted by weak efflux pump (Zhang *et al.*, 1999). The mechanism associated with pyrazinamide resistance involves mutation of the *pncA* gene that encodes pyrazinamidase and results in reduced or loss of enzyme activity (Hirano, Takahashi, Kazumi, *et al.*, 1997; Juréen, Werngren, Toro, *et al.*, 2008).

The effect of exposure to pyrazinamide on tuberculosis treatment outcome has been explored using a number of metrics: AUC_{0-24}, C_{max}, AUC_{0-24}/MIC, C_{max}/MIC and time above the MIC (Gumbo, Dona, Meek, *et al.*, 2009). In a cohort of predominantly TB/HIV co-infected patients from Botswana, Chideya et al. reported that patients with low pyrazinamide C_{max} (<35 mg/L) had poor treatment outcome compared to those with C_{max} of at least 35 mg/L (50% vs 16%; p-value<0.01). Poor treatment outcome was defined as treatment failure or death during tuberculosis treatment (Chideya *et al.*, 2009). The results of CART analyses on the data from two separate studies also showed that pyrazinamide C_{max} is a significant predictor of treatment outcome. The proportion of patients who were culture positive at two months after treatment initiation was higher among patients with pyrazinamide C_{max} < 58.3 mg/L compared to those

with a C_{max} of at least 58.3 mg/L (14% vs 2%; P value= 0.035) (Pasipanodya *et al.*, 2013). Pyrazinamide AUC_{0-24} was reported to be correlated with long-term treatment outcomes (treatment failure, death, or relapse) and AUC_{0-24} of 363 mg·h/L separated poor from favourable treatment outcomes (Pasipanodya *et al.*, 2013). Using Multivariate Adaptive Regression Splines (MARS), Chigutsa et al. reported that pyrazinamide AUC_{0-24}/MIC > 11.3 is correlated with culture conversion among patients with rifampicin C_{max} ≥ 8.3 mg/L. An *in vitro* study using hollow-fiber systems also identified pyrazinamide AUC_{0-24}/MIC as the PK-PD index linked to microbial killing, and time above MIC as the index associated with suppression of resistance (Gumbo, Dona, Meek, & Leff, 2009). In some studies, MICs are rarely determined hence the use of indices computed using MIC is reduced. In such cases, researchers will have to use either AUC and C_{max} to evaluate the probability of treatment success. Between these two, AUC is expected to be more robust than C_{max} because the latter is dependent on blood sampling time, precision of drug intake time, and drug absorption, which is highly variable (Urso, Blardi, & Giorgi, 2002).

Hepatoxicity is the most serious adverse effect associated with pyrazinamide (Girling, 1977). Signs and symptoms of hepatic disease appear if high daily oral doses of around 40–50 mg/kg are administered for extended periods (Donald & McIlleron, 2009; Gumbo, 2010). Pyrazinamide may also result in elevated plasma uric acid concentrations that could cause acute episodes of gout. Other side effects of pyrazinamide include arthralgias, anorexia, nausea and vomiting, dysuria, malaise, and fever (Alsultan & Peloquin, 2014a; Gumbo, 2010).

1.4.4 Pharmacology of ethambutol

Ethambutol is the “fourth drug” in the FDC for the treatment of drug-susceptible tuberculosis (Bass *et al.*, 1994). In comparison to Para-Aminosalicylic Acid (PAS), ethambutol was found to be more effective and well tolerated as a companion drug to isoniazid (Bobrowitz & Robins, 1967). At doses of 15 mg/kg of body weight, ethambutol exerts a bacteriostatic effect (Hopewell, 2010). Ethambutol MICs ranges from 0.6–2 mg/L in clinical isolates of *M. tuberculosis* from South Africa (Chigutsa *et al.*, 2015). The primary reason for including ethambutol as part of the FDC therapy is to reduce the risk of resistance to rifampicin in patients with known strains that have primary resistance to isoniazid (Bass *et al.*, 1994). Its mechanism of action involves alteration of the mycobacterium cell wall structure by inhibiting biosynthesis of the arabinan component of the mycobacterial cell wall core (Deng *et al.*, 1995; Rastogi, Labrousse, & Goh, 1996; Takayama & Kilburn, 1989).

Approximately 80% of the oral dose of ethambutol reaches the systemic circulation, and plasma protein binding is around 10–40% (Gumbo, 2010; Lee, Brater, Gambertoglio, *et al.*, 1980; Lee, Gambertoglio, Brater, *et al.*, 1977). Peak plasma concentrations of ethambutol are dose proportional and occur between 2–4 hours after a dose. With the currently recommended doses of 15 mg/kg, the peak concentrations are expected to be around 4 mg/L (Bass *et al.*, 1994). Ethambutol is mostly excreted unchanged in urine, in a proportion that was reported to vary widely (40–80%) in early studies of ethambutol pharmacokinetics (Lee, Brater, Gambertoglio, & Benet, 1980). However, recent reports are in agreement that around 80% of the drug is renally eliminated unchanged (Donald & McIlleron, 2009; Gumbo, 2010) and less than 15% of the dose is recovered in urine as metabolites. Metabolism of ethambutol involves oxidation by alcohol dehydrogenase to an aldehyde intermediate. The metabolite is further oxidised to dicarboxylic acid by aldehyde dehydrogenase (Peets, Sweeney, Place, *et al.*, 1965).

Ethambutol is widely distributed in body tissues, and more recently, it has been shown to accumulate in diseased tissues and penetrates lesions with a lesion-to-plasma ratio between 9 and 12 (Zimmerman *et al.*, 2017). The decline in plasma concentration of ethambutol after C_{max} is biphasic, and if a one-compartment model is applied, a disappearance half-life of between 3 and 4 hours is expected. The slower terminal phase may be observed from 10–12 hours post-dose and has a half-life of 10–15 hours (Peloquin *et al.*, 1999). Population pharmacokinetics of ethambutol have been reported among healthy volunteers and patients from the United States and Africa (Peloquin et al. 1999; Zhu et al. 2004; Denti et al. 2015; Smythe 2016; Jönsson et al. 2011; Hall et al. 2012).

Plasma concentrations of ethambutol have been described using a two-compartment disposition model with different absorption models and first-order elimination. In three of the models, a first-order absorption was implemented with a delay characterised by using a chain of transit compartments with a mean absorption time of 2–3 hours (Denti, Jeremiah, *et al.*, 2015; Jönsson *et al.*, 2011; Smythe, 2016). Hall et al. also described the absorption as a first-order process, but without a delay. Peloquin et al. and Zhu et al. described the absorption of ethambutol as a zero-order process, which they found superior to the first-order absorption process. All these models identified first-order elimination of ethambutol. In three studies conducted in African tuberculosis patients, the clearance of ethambutol was comparable and ranging from 39 to 46 L/h (Denti, Jeremiah, *et al.*, 2015; Jönsson *et al.*, 2011; Smythe, 2016). Allometric scaling was applied to account for the effect of body size and composition on disposition parameters. Jönsson et al. and Denti et al. accounted for this effect by using total body weight on all clearance and volume of distribution parameters whereas Smythe applied allometric scaling using fat-free mass on clearance and total body weight on volume of distribution.

Concomitant intake of antacids reduces exposure to ethambutol, and Peloquin et al. reported a 29% and 10% reduction in C_{max} and $AUC_{0-\infty}$ respectively (Peloquin *et al.*, 1999). Another

study also reached a similar conclusion and recommendations were made to avoid taking antacids concomitantly or just before ethambutol (Mattila, Linnoila, Seppälä, *et al.*, 1978). Intake of food before or concomitantly reduces the rate of absorption minimally, but does not affect the extent of absorption (Ameer, Polk, Kline, *et al.*, 1982; Peloquin *et al.*, 1999). HIV has been reported to reduce plasma concentrations of ethambutol: Zhu et al. observed a 20% reduction in $C_{max,}$ and McIlleron et al. reported a 27% reduction in AUC in HIV positive patients (McIlleron *et al.*, 2006; Zhu *et al.*, 2004). In separate studies, Jönsson et al. and Smythe reported a 15% reduction in bioavailability in HIV positive patients (Jönsson *et al.*, 2011; Smythe, 2016). Smythe also reported a 11.4% increase in bioavailability of ethambutol from the first dose to steady-state (Smythe, 2016). The effect of age on clearance of ethambutol in Tanzanian patients reported by Denti et al. is consistent with its elimination via the kidneys, since drug clearance in the older patients is expected to be lower as a result of reduced renal function (Denti, Jeremiah, *et al.*, 2015). The effect of age was also reported in a cohort of tuberculosis patients from South Africa (McIlleron *et al.*, 2006).

Optimal antimicrobial kill of *M. tuberculosis* by ethambutol is associated with the $AUC_{0–24}$/MIC index, and the time above MIC was found to be significant in suppressing efflux pump related drug resistance (Srivastava *et al.*, 2010). Chigutsa et al. applied MARS techniques and discovered that the sterilising effect of ethambutol was evident in patients with ethambutol C_{max}/MIC > 0.46 and rifampicin $AUC_{0–24}$ < 35.4 mg·h/L (Chigutsa *et al.*, 2015). EBA of ethambutol is dose-dependent, and a daily dose of 15 mg/kg has an EBA of 0.05 $\log_{10}$ CFU/mL sputum/day.

The most common adverse effect associated with ethambutol intake is optic neuritis, and routine visual acuity testing is recommended for patients with pre-existing ocular problems (Forget & Menzies, 2006; Girling, 1977). Upon termination of ethambutol intake, gradual improvement in vision is possible (Alsultan & Peloquin, 2014a). Doses of at least 30 mg/kg

are most likely associated with toxicity, but patients with impaired renal function may also be affected at the currently recommended dose (Girling, 1977). Elevated plasma uric acid has also been reported, and other less common side effects include cholestatic jaundice, interstitial nephritis, thrombocytopenia, and neutropenia (Forget & Menzies, 2006).

1.5 Multidrug nature of tuberculosis treatment

The four drugs described above do not work in isolation but function together with potential synergism and antagonism while targeting different *M. tuberculosis* subpopulations. With the current combination therapy of both antituberculosis drugs and antiretroviral therapy, there is paucity of information on synergism and antagonism of drugs driving treatment response. In an *in vitro* experiment, the combination of rifampicin, isoniazid and ethambutol was reported to show synergism in isoniazid-resistant isolates (Rey-Jurado, Tudó, Martínez, *et al.*, 2012). Monotherapy with pyrazinamide only showed minimum sterilising activity, but its synergism with rifampicin was crucial to shortening tuberculosis treatment duration to six months (British Medical Research Council, 1981). MARS analysis methodology was applied to PK-PD data from a study conducted in South Africa and the authors reported that the sterilising activity was driven mainly by isoniazid and ethambutol in patients who had low rifampicin exposure (Chigutsa *et al.*, 2015). The same authors also reported that in patients with rifampicin C_{max} > 8.2 mg/L, the sterilising activity was determined by the synergistic interaction of rifampicin and pyrazinamide ($AUC_{0–24}$/MIC ratio of 11.3). Concentration-dependent antagonism of isoniazid vs rifampicin and pyrazinamide was reported in Indian children with pulmonary tuberculosis. The proportion of poor treatment outcomes was higher in children who had isoniazid $AUC_{0–24}$ > 31.8 mg·h/L, pyrazinamide C_{max} ≤ 38.1 mg/L, and rifampicin C_{max} ≤ 6.2 mg/L. Chigutsa *et al*. also reported the antagonism of isoniazid on sterilising activities of rifampicin and pyrazinamide in patients with low ($AUC_{0–24}$ < 35.4 mg·h/L) rifampicin exposure. Using MARS analysis, isoniazid (C_{max} < 4.6 mg/L) was reported to have an antagonistic effect on culture conversion in patients who had rifampicin C_{max}/MIC < 28 (Rockwood *et al.*, 2017). Treatment of TB/HIV coinfected patients is complicated by multidrug nature of both tuberculosis and HIV therapy, and there could be potential pharmacokinetic drug-drug interactions. The effect of antituberculosis drugs especially rifampicin on antiretroviral therapy has been well studied (Lalloo, 2009; McIlleron, Meintjes, Burman, *et al.*, 2007; Semvua *et al.*, 2015), but few studies have evaluated the impart of ART on pharmacokinetics of first-line antituberculosis drugs

(Bhatt *et al.*, 2014; Naidoo *et al.*, 2017). Identifying PK-PD relationships is challenging due to variability in drug exposure caused by factors that include drug-drug interaction, genetic mutations, disease status, poor quality formulations, and drug stability in different environments.

1.6 Tuberculosis treatment outcomes

The evaluation of test regimens for the treatment of tuberculosis requires well-defined endpoints. The time at which an event occurs, such as time-to-stable culture conversion (TSCC), time-to-death on or after treatment, or time-to-relapse all provide rich quantitative information compared to the qualitative positive/negative status at a time point e.g. two-month culture results. (Chigutsa *et al.*, 2013; García-García *et al.*, 2002; Gillespie *et al.*, 2014; Pasipanodya *et al.*, 2013; Smythe, 2016; Svensson & Karlsson, 2017). TSCC is defined by two consecutive culture negative results at visits separated by a week, two weeks, or a month. The date of culture conversion is then defined as the date of the first negative culture result (Gillespie *et al.*, 2014; Wallis *et al.*, 2009). Relapse is defined as the presence of microbiologically confirmed tuberculosis in patients who successfully completed treatment with negative culture results. In tuberculosis control programmes, any deaths during the course of tuberculosis treatment are classified as tuberculosis related (World Health Organization, International Union Against Tuberculosis and Lung Disease, & Royal Netherlands Tuberculosis Association, 2001). In clinical trials, patients could be monitored for longer than the treatment duration and any deaths are also classified as tuberculosis related.

The drug related factors described in sections 1.4 and 1.5 contribute to overall tuberculosis treatment outcomes, but disease factors and patient characteristics also influence treatment success. Presence of cavitation has been reported to delay time-to-culture conversion (Dorman *et al.*, 2009; Güler, Ünsal, Dursun, *et al.*, 2006; Telzak *et al.*, 1997; Visser *et al.*, 2012) and is also associated with treatment failure or relapse (Benator *et al.*, 2002). Visser et al. also reported that shorter baseline time-to-positivity was associated with delayed time-to-sputum culture conversion (Visser *et al.*, 2012). Time-to-culture or smear conversion is also correlated with patient's sex: male patients generally convert at a later stage than females (Banu Rekha *et al.*, 2007; Caetano Mota, Carvalho, Valente, Braga, & Duarte, 2012; Hesseling *et al.*, 2010). The results of a pooled analysis reported by Banu Rekha *et al*. also showed that

higher number of chest X-ray zones affected was associated with delayed culture conversion (Banu Rekha *et al.*, 2007). In TB/HIV coinfected patients, relapse was reported to be high in patients with $CD4^+$ count < 100 cells/µL (Pulido *et al.*, 1997). Patients with low BMI are reported to have increased chances of poor long term treatment outcomes including death and relapse (Hanrahan *et al.*, 2010; Hesseling *et al.*, 2010; Mupere *et al.*, 2012; Yen *et al.*, 2016; Zachariah, Spielmann, Harries, *et al.*, 2002).

1.7 Pharmacometrics

Pharmacometrics is the science of developing and applying mathematical and statistical methods to characterise, understand, and predict pharmacokinetics, pharmacodynamics, and disease progression (Williams & Ette, 2007). Pharmacokinetics describes the time course of drug concentration in different body spaces such as plasma, blood, urine and tissues (Gabrielsson & Weiner, 2007). It covers the process of absorption, distribution, metabolism, and excretion. Pharmacodynamics is the study of the time course of biological effects of drugs, and the relationship of these effects with drug exposure (Gabrielsson & Weiner, 2007).

The biological processes linked to pharmacokinetics are complex and usually simplified using compartmental models: the body is described by a series of compartments in which the drug is distributed (Lavielle, 2014). The link between the compartments can be turned into a mathematical model by using differential equations and the differential equations are used to capture the changes in drug concentrations over time. Population pharmacokinetics is then the application of mathematical and statistical models to a cohort of patients in a study, considering the different levels of variability (between patient and within patient/between occasion). Application of population modelling comes with some advantages over traditional noncompartmental analysis: inclusion of sparse data, integrating data from different studies, the inclusion of prior knowledge, higher statistical power, and suitability for dose individualisation (Bonate, 2011).

Data collected for pharmacokinetic analysis usually involves several measurements such as drug concentrations from the same subject following single or multiple doses. These measurements are correlated and classical analysis methods that assume independence of measurements lead to invalid inferences. Population modelling/mixed-effects modelling allows estimation of individual pharmacokinetic parameters via the inclusion of random effects to

account for the correlation between measurements from the same subject. In pharmacokinetics, the relationship between drug concentrations and parameters is usually nonlinear hence population modelling is also called nonlinear mixed-effects modelling. More formally, nonlinear mixed-effects models consist of two components: a structural model and a stochastic model. The structural model is a function that describes the average time course of measured concentrations and may include covariates. The stochastic model includes between/within-subject variability of the model's parameters and residual unexplained variability (Upton & Mould, 2014).

To formalise these concepts mathematically, let us take the response variable **Y**, which consists of measurements, e.g. drug concentrations measured from *n* subjects with each i^{th} subject contributing n_i measurements at different time points $t_{i1}, t_{i2}, \cdots, t_{in_i}$. The vector of the observed measurements becomes $Y = \{Y_{1,1}, Y_{1,2}, \cdots, Y_{n,1}, Y_{n,2}, \cdots, Y_{n,n_i}\}^T$. The j^{th} measurement of subject *i* can be described as

$$y_{ij} = f(\mathbf{x_{ij}};\ \mathbf{\Theta_i}) + \varepsilon_{ij} \tag{1.1}$$

Where $f(\cdot)$ is the individual prediction described by a nonlinear function with parameter vector $\mathbf{\Theta_i}$ and independent variables (time, dose and covariates). ε_{ij} is the residual unexplained variability describing the deviation of the individual prediction from the observed value and is assumed to follow a gaussian distribution with mean of zero and estimated variance of σ^2. The individual parameters (e.g. clearance) are positive and often right skewed hence a log-normal distribution is assumed as shown in equation 1.2.

$$p_{k_i} = \theta_k \cdot e^{\eta_{k_i}} \tag{1.2}$$

Where p_{k_i} is the individual value for the i^{th} subject of the k^{th} parameter in $\boldsymbol{\Theta_i}$ and θ_k is the typical/population value of p_{k_i}. The random effect η_{k_i} describes the random deviation between

the i^{th} individual parameter value and the typical parameter value (population parameter value), and it is assumed to follow a gaussian distribution with mean zero and estimated variance of ω_k^2. A variance-covariance matrix for all the random effects (etas) is then estimated. The effect of covariates on the typical parameters can also be estimated as an additional fixed effect. Variability in individual parameters over time can be estimated as another level of random effects and this level of variability is called within-subject variability or between-occasion variability, with an occasion usually defined as a collection of measurements following a dose (Ette & Williams, 2004; Karlsson & Sheiner, 1993).

Methods to describe the exposure-response relationship are available, and the choice of the method for analysis is guided by the type of the data available. As explained in section 1.6, time to a specific event is often used as a response variable for tuberculosis treatment outcome. For time-to-event (TTE) data, the time of an event is observed for the subject that experience the event during the observation period, while it may never occur during the observation period in others, in which case it is considered right-censored, meaning that it is unknown if and when the event may have happened after the end of the observation period. One could use the Cox proportional hazard regression model or parametric models, such as exponential, Weibull, Gompertz, and surge functions (Charles, Touitou, & Selmaoui, 2009; Holford, 2013). If the time between outcome measurements is long, it is recommended to apply methods that account for the fact that the event occurred between the first positive observation and the previous negative one (interval censoring). Assuming the event of interest occurred at the time of observation would lead to incorrect conclusions about the estimated survival curves and the effects of covariates on time (Radke, 2003). In TTE modelling with only a single event, the outcome/event is modelled using the instantaneous hazard $h(t)$ of an event occurring at time *t*:

$$h(t) = \lim_{\delta t \to 0} \frac{Pr(t \leq T < (t + \delta t) \mid T \geq t)}{\delta t} \tag{1.3}$$

The effect of individual covariates can be included on the hazard of the event occurring. Related to the hazard function is the probability of an event occurring to individual after time $t > \tau$, called the survivor function

$$S(t) = e^{-\int_0^t f(u)\cdot du} \tag{1.4}$$

With time-to-event data, three scenarios are possible:

a) The event occurs at time *t* with probability: $f(t) = S(t) \cdot h(t)$
b) The event occurs in interval $a < T \leq b$ with probability:
   $f(t) = S(t_0, t_a) \cdot \big(1 - S(t_a, t_b)\big)$ were $S(t_0, t_a)$ is the survival function from entry to time *t*=a and $S(t_a, t_b)$ is the survivor function in the interval when the event occurred.
c) The event is right-censored/ not observed with probability: $f(t) = S(t_0, t_{end})$

The parametric methods described in the previous paragraph are powerful, but have some limitations: (1) they force a specific link between the response and covariates and (2) do not allow data driven covariate interactions (Bou-Hamad, Larocque, & Ben-Ameur, 2011). Recursive partitioning methods offer an alternative to conventional time-to-event analysis methods. The methods involve stratifying and segmenting the covariate space into nonoverlapping regions/nodes by applying a binary split to covariates in a stepwise manner (James, Witten, Hastie, *et al.*, 2013). The final product of the analysis is presented as a tree diagram, and at the top of the tree is the root node which contains all the data. The subsequent nodes are either internal nodes (those that are further split) or terminal nodes. Recursive methods are flexible, require fewer assumptions and can handle nonstandard and nonlinear data structures efficiently (De Rose & Pallara, 1997).

The idea behind the stratification and segmentation is to force each node to become more homogeneous using a splitting criterion. Ciampi et al. suggested the use of a log-rank statistic to determine the best split, and it leads to a split that assures the best separation of the median time-to-event in two children nodes (Ciampi, Thiffault, Nakache, *et al.*, 1986). This method and many others (Davis & Anderson, 1989; Gordon & Olshen, 1985; Segal, 1988) fail to recognise the two steps involved in developing the tree: (1) selection of splitting variable and (2) selection of splitting point. These methods then tend to favour covariates that have many possible splitting points. Hothorn et al. developed an unbiased conditional inference tree algorithm for right censored data to address the problem by separating the selection of splitting variable and the splitting point (Hothorn, Hornik, & Zeileis, 2006). The method was further developed to account for interval-censored data, and variable selection by the method is unbiased. The method was also shown to be able to recover the correct tree structure and has good predictive performance (Fu & Simonoff, 2017). A permutation test is applied to select a variable to split on using the log-rank score as the test statistic and a predefined level of significance α. The test is applied under the null hypothesis of no relationship between the response and any covariate by fixing the covariates and conditioning on all possible permutations of the response. If no covariate is significant, the procedure stops, otherwise the next step will be to select the splitting point. The permutation test framework is also applied to find the optimal binary split for the selected covariate. A description of the methods of handling missing covariate data has been reported (Hothorn, Hornik, & Zeileis, 2006).

1.8 Study justification

Efforts to reduce mortality in TB/HIV co-infected patients are focussing on early introduction of antiretroviral therapy (Abdool Karim *et al.*, 2010). Other recent studies are focussing on increasing the doses of rifampicin, but the inclusion criteria exclude HIV-positive patients with low CD4+ count (< 350 cells/µL) (Boeree *et al.*, 2015). It is important to characterise pharmacokinetic variability of tuberculosis treatment in TB/HIV co-infected patients including those that have low CD4+ count. The relationship between drug exposure and treatment outcomes in patients with low CD4+ count might differ from those with a CD4+ count of at least 350 cells/µL hence the need to describe the PK-PD relationship in this specific population.

Rifampicin induces its own metabolism (autoinduction) and doses of at least 450 mg show saturable pharmacokinetics. Smythe et al. described the autoinduction process using pharmacokinetic data collected only on two occasions, and each patient contributed three samples hence these data might not accurately describe the change in exposure to rifampicin over time (Smythe *et al.*, 2012). In the current body of work, nonlinear mixed-effects modelling was applied to a rich rifampicin pharmacokinetic dataset with repeated intensive sampling over four occasions during the first four weeks of treatment. Pharmacokinetic data were obtained from 60 patients spanning a range of doses: 300 mg to 750 mg. Through the application of semimechanistic modelling techniques, the data could be expected to contribute towards the understanding of the duration and extent of autoinduction. The range of doses is also important for describing the nonlinear pharmacokinetics of rifampicin: increase in dose results in more than proportional increase in exposure to rifampicin as a result of saturable pharmacokinetics. Pharmacokinetic data for desacetyl-rifampicin together with increased rifampicin doses of up to 15 mg/kg is important for separating metabolic pathways and identifying the saturable pathway(s). In addition, joint modelling of rifampicin and desacetyl-rifampicin helps identify correlations between the parent drug and metabolite. Subsequent to

the publication of results from this thesis, Svensson et al. also reported on autoinduction of rifampicin and its saturable pharmacokinetics using pharmacokinetic data of rifampicin with doses up to 40 mg/kg (Svensson, Aarnoutse, *et al.*, 2017). However, at the time of working on chapter 3, this was not known. In their study, pharmacokinetic data was collected in the first two week of treatment which is less than the four weeks in our first study (chapter 3) and did not quantify metabolite pharmacokinetic data included in our second study (chapter 6).

Pyrazinamide is used for the treatment of drug-susceptible and -resistant tuberculosis. Changes in clearance of pyrazinamide during treatment are documented in patients from Tanzania and West Africa (Denti, Jeremiah, *et al.*, 2015; Smythe, 2016). The increase has not been reported in South African patients or more importantly in TB/HIV co-infected patients, and its effect on drug exposure. The currently recommended dose of pyrazinamide achieves low exposure in males who have low weight (McIlleron *et al.*, 2012). A proposal was put forward for a 1500 mg of pyrazinamide for all patients, but this is unfeasible with the current FDC treatment regimen (Sahota & Della Pasqua, 2012). A dosing regimen that fits into the current FDC treatment regimen would be much preferable and could be acceptable to the community working on tuberculosis treatment. There are currently no reports on the evaluation of exposure to pyrazinamide in patients with drug-resistant tuberculosis regarding whether the dose administered achieve therapeutic targets and if the patients in different weight bands achieve comparable exposure levels.

Co-administration of antituberculosis and antiretroviral drugs results in potential drug-drug interaction. Researchers are focussing on the effect of rifampicin on exposure to antiretroviral drugs (Semvua *et al.*, 2015). Antiretroviral drugs could also affect the pharmacokinetics of antituberculosis drugs. Results of a non-compartmental analysis showed that concomitant intake of efavirenz-based antiretroviral therapy was associated with a 29% reduction in

isoniazid AUC (Bhatt *et al.*, 2014). However, the cohort in that study was small and the difference in metabolism due acetylator phenotype was not considered. In the present study, we used nonlinear mixed-effects modelling to describe jointly, the pharmacokinetics pf isoniazid and acetyl-isoniazid hence shared information (correlations) between the pharmacokinetics of parent and metabolite data can be incorporated. In the absence of acetylator status of patients, mixture modelling applied in the analysis is a powerful tool to differentiate pharmacokinetic parameters of patients belonging to different acetylator status. By including metabolite data and separating metabolic pathways, it is possible to determine whether covariates affect one or both pathways and if the effect is similar between fast and slow acetylators. In the cohort of TB/HIV co-infected patients receiving efavirenz based ART, it is possible to evaluate the effect of reduced exposure on attaining therapeutic targets.

With the current efforts on increasing the dose of rifampicin and early introduction of ART in TB/HIV co-infected patients, the relationship between antituberculosis drug exposure and treatment outcomes still needs investigation. PK-PD analysis helps determine the effects of drug exposure observed under different treatment strategies, and of clinical markers on treatment outcomes. It also provides evidence for or against dose adjustment and/or policy change. Early results of the RAFA clinical trial showed improved survival in patients who received 50% increased dose of rifampicin only in patients with $CD4^{\cdot}$ <100 cells/µL. The strengths of the PK-PD analysis in this report are: availability of rich pharmacokinetic data with all the four first-line antituberculosis drugs, data were collected from a well characterised clinical cohort of patient participating in a randomised clinical trial, data includes serial culture results collected during the treatment as opposed to single time point (e.g. two-month) culture, a wider range of rifampicin concentrations in one arm, and patients were followed up for 18 months after the end of treatment. The use of data mining techniques (classification and regression trees in particular) to determine the association between drug exposure and tuberculosis treatment outcomes is increasing (Pasipanodya *et al.*, 2013; Smythe, 2016).

These methods are effective in identifying nonlinear relationships between drug exposure and tuberculosis outcomes. However, the methods tend to favour covariates measured on a continuous scale, and even with high variability associated with the pharmacokinetics of antituberculosis drugs (Devaleenal Daniel, Ramachandran, & Swaminathan, 2017), the techniques would identify the effect of continuous covariates. The conditional inference framework applied to PK-PD modelling in this thesis eliminates the bias towards selection of continuous covariates. In addition, the methods apply nonparametric statistical significance testing for inclusion of covariates hence is able to handle small sample sizes.

1.9 Objectives

The purpose of the research was:

1. To describe the population pharmacokinetics of rifampicin and pyrazinamide in patients from South Africa, quantify the changes in parameters in the first month of treatment and determine factors contributing to variability between patients using nonlinear mixed-effects modelling techniques. The models developed will be used to evaluated exposure levels achieved by the patients against known therapeutic targets to provide evidence for dose adjustments.

2. To describe the population pharmacokinetics of rifampicin, isoniazid, pyrazinamide, ethambutol, desacetyl-rifampicin, and acetyl-isoniazid in West African patients and apply nonlinear mixed-effects modelling methods to evaluate the effect of concomitant intake of efavirenz-based antiretroviral therapy and a range of rifampicin doses up to 50% higher than the standard on pharmacokinetics on pharmacokinetics of companion drugs.

3. To characterise the impact of pharmacokinetics of first-line antituberculosis drugs, and tuberculosis and HIV disease markers on tuberculosis treatment outcomes (time-to-stable culture conversion, relapse, and death)

Chapter 2: Methodology

2.1 Study designs and data description

2.1.1 TB-HAART Study

HIV-1 infected and treatment naïve patients aged 18 to 65 years were recruited for the study between March 2007 and April 2008. Recruitment was done at primary health care centres in and around Durban, South Africa. Patients were included in the study if they had no history of previous antituberculosis treatment in the 24 months before the study, were not currently enrolled in a drug or treatment trial, and provided informed consent to participate in the trial, were willing to undergo HIV testing and provide blood samples for pharmacokinetics. A female patient was recruited if she had been post-menopausal for at least 12 months or was surgically incapable of bearing children. A female of childbearing potential was recruited provided that she had a confirmed negative pregnancy test, and agreed to use an accepted method of contraception for the duration of the study. Patients were excluded if there was evidence of pre-existing non-tuberculosis disease likely to affect response to or assessment of treatment effects. Patients with mental illness, WHO stage IV disease requiring drugs that would potentially interact with study drugs, weighing below 30 kg and who had clinical evidence of severe illness were also excluded. Having a history of drug abuse in the six months before the study, history of high daily alcohol intake (>0.5 L) and history of multi-drug resistant tuberculosis would make an individual ineligible for the study.

The main study was a six-arm clinical trial to investigate the bioavailability of rifampicin, isoniazid, zidovudine, lamivudine and efavirenz. The results presented in chapter three and four are based on data from patients recruited in treatment arms 1 to 5 shown in Table 1. Patients in arms 1, 2 and 3 were started on antiretroviral therapy after day 14 of treatment initiation. Each patient took a dose of antiretroviral therapy consisting of 600 mg of efavirenz daily, 150 mg of lamivudine twice daily and 300 mg of zidovudine twice a day. Patients in

treatment arms 4 and 5 received antiretroviral therapy upon completion of antituberculosis treatment.

Table 2.1 Study design for TB-HAART study

CD4+ count	**Group 1** **TB/HIV**	**Group 2** **TB/HIV**	**Group 1** **HIV (non-TB)**
350 – 500 cells/µL	Arm 1: HAART + ATT	Arm 4: ATT	
220 – 349 cells/µL	Arm 2: HAART + ATT	Arm 5: ATT	
< 200 cells/µL	Arm 3: HAART + ATT		Arm 6: HAART

HAART: Highly Active Antiretroviral therapy, ATT: Antituberculosis treatment

The National Tuberculosis Control Programme supplied the 4-drug FDC (Rifafour e-275 [Sanofi-Aventis, South Africa] and Antib-4 [Rusan Pharma, India]) used in the study. Each tablet contained rifampicin (150 mg), isoniazid (75 mg), pyrazinamide (400 mg) and ethambutol (275 mg). Patients were administered weight-adjusted doses of the FDC according to the WHO guidelines at the time of the study (World Health Organization, 2003). Patients weighing 30 to 37 kg received two tablets and those weighing 38 to 54 kg, 55 to 70 kg and >70 kg received 3, 4 and 5 tablets respectively. Antituberculosis treatment was administered on weekdays (Monday to Friday) except in 10 patients recruited after a change of dosing policy who received daily doses of the treatment.

Patients were admitted on the afternoon before the pharmacokinetic assessment on the 1st, 8th, 15th and 29th day of treatment. Patients fasted from midnight after an evening meal and a 22h00 snack. On the pharmacokinetic sampling day, 10 mL of blood was collected prior to dose intake which was observed by a study team member and at 1, 2, 3, 4, 6, 8 and 12 hours post-dose. Blood specimens were immediately placed on ice and plasma separated by centrifugation within 30 minutes before storage at -80^{o}C. The clinical analysis of the plasma

sample was conducted by the analytical laboratory at the Division of Clinical Pharmacology, University of Cape Town. Plasma drug concentrations for rifampicin and pyrazinamide were quantified by tandem HPLC mass spectrometry (Applied Biosystems API 200) as previously described (McIlleron *et al.*, 2007).

2.1.2 RAFA Study

Patients were recruited at tuberculosis centres in three countries in West Africa: Benin, Guinea, and Senegal. For the pharmacokinetic sub-study, only patients recruited in Benin and Guinea were considered. Patients were included in the study if all the following criteria are fulfilled: aged above 18 years, had positive HIV test result, had CD4+ lymphocyte count of at least 50 cells/µL, had recent positive acid-fast bacilli on any smear or molecular test, naïve to antiretroviral therapy and had voluntarily signed informed consent to participate in the study. Patients who met any of the following conditions were excluded from the study: pregnant women, lactating women, women who are unwilling to use contraception, HIV-2 infected, use of recreational drugs or alcohol that could prejudice the conduct of the study, AST or ALT greater than five times the normal value and unable to provide informed consent.

The RAFA study was a three-treatment arm study defined by the timing of introduction of antiretroviral therapy and rifampicin dose as shown in Figure 3. Patients in arm A received efavirenz-based antiretroviral therapy at two weeks post antituberculosis treatment initiation, and in arm B, antiretroviral therapy was delayed by two months. Patients in arm C received a higher dose of rifampicin (+50%) in the intensive phase of treatment and started antiretroviral therapy in the continuation phase of antituberculosis treatment. Patients received 600 mg of efavirenz regardless of body weight.

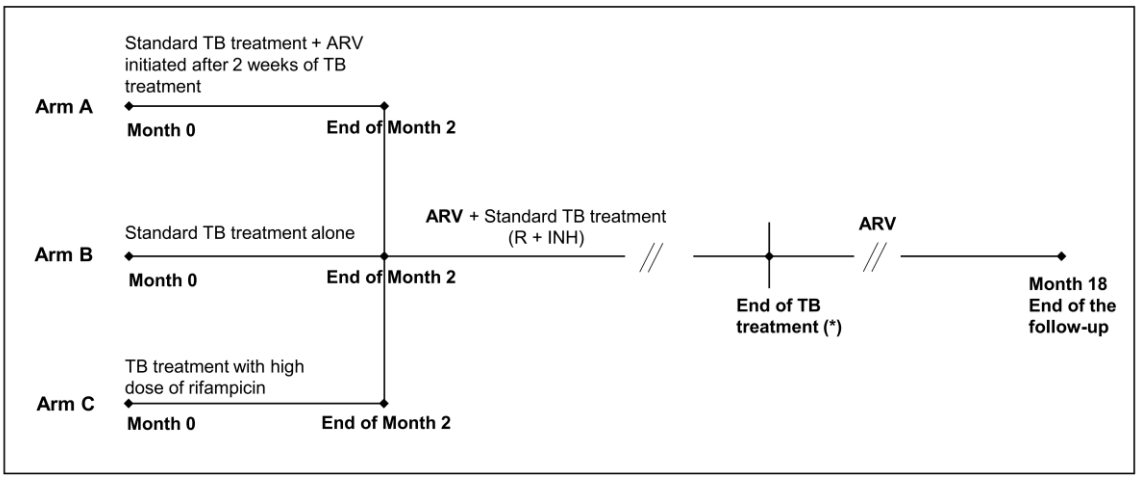

Figure 2.1 Treatment schedule for the RAFA study [4]

The FDC treatment dispensed in the trial was made available by the National Tuberculosis and HIV programmes in each country. Extra rifampicin tablets administered to patients in arm C were purchased for the trial. Patients took weight-adjusted daily doses of the FDC containing rifampicin, isoniazid, pyrazinamide, and ethambutol, and those in arm C took additional tablets containing rifampicin only to achieve a dose of approximately 15 mg/kg of body weight.

Patients who were recruited into the pharmacokinetic sub-study had pharmacokinetic sampling performed at a visit after one month and before two months of antituberculosis treatment. On the pharmacokinetic sampling day, patients took an observed dose of antituberculosis treatment after an overnight fast. Five serial blood samples were collected at approximately 15 minutes before the dose and 2, 3, 6 and 10 hours after the dose. Blood samples were processed, and plasma stored immediately at -80^{o}C before transfer to the analytical laboratory at the Division of clinical pharmacology, University of Cape Town. Concentrations of rifampicin, isoniazid, pyrazinamide and ethambutol were determined using

[4] Reprinted from A randomised controlled trial of 3 strategies for the treatment of ART-naive HIV infected patients with tuberculosis - RAFA Trial – Clinical trial protocol

validated tandem mass spectrometry high-performance liquid chromatography (LC-MS/MS) methods. The concentration ranges, mean percentage accuracies during inter-day sample analysis and precision coefficient of variation for rifampicin, isoniazid, pyrazinamide and ethambutol have been previously described (Denti, Jeremiah, *et al.*, 2015; Kwara *et al.*, 2016). Desacetyl-rifampicin was validated over the range 0.0391–10 mg/L. The mean percentage accuracies during inter-day sample analysis at low, medium and high-quality control levels were 99.4%, 97.6% and 101.8% respectively. The precision coefficient of variation for determination at low, medium and high-quality control levels were 11.4%, 6.8% and 9.3% respectively.

2.2 Software

Pharmacokinetic analyses were performed in NONMEM 7.3, using the first-order conditional inference with eta-epsilon interaction (FOCE-I) (Beal, Sheiner, Boeckmann, & Bauer, 2013). Perl-speaks-NONMEM (versions 3.7.6–4.7.0) were used to aid model development and evaluation (Lindbom, Pihlgren, & Jonsson, 2005). Model tracking and documentation were done in Pirana versions 2.8.1–2.9.6 (Keizer, Karlsson, & Hooker, 2013). Time-to-event modelling was implemented in Monolix Suite 2016 (Monolix version 2016R1, 2016). Time-to-event classification and regression trees analysis was performed in R (versions 3.0.1–3.4.3) via RStudio interface (versions 0.97.551–1.1383). Data management, post modelling processing of data and graphical analysis were done in R via RStudio interface (R Core Team, 2017; RStudio, 2014).

2.3 Pharmacokinetic modelling approach

The model development procedure generally started with a simple one-compartment structural model with first-order absorption and elimination, and based on scientific plausibility and physiological rationale, the model was made more complex by adding, for example two-

compartment disposition, a more flexible absorption framework, saturable clearance, or more semimechanistic models. The statistical model included between-subject and -occasion variability assumed to follow log-normal distribution and residual unexplained variability which comprised of additive and proportional components. Allometric scaling was applied in the early phases of model development using either total body weight or fat-free mass. Use of priors to stabilise models utilising sparse data was explored. The modelling process was guided by change in objective function value (OFV, -2 times the log-likelihood), the standard goodness of fit plots (and visual predictive checks (VPCs). In cases where modelling involved parent drug and metabolite, a model for the parent drug was first developed and, once deemed sufficient, metabolite data was then included. The inclusion of patient covariates was guided by biological plausibility and statistical significance based on 5% level of significance in the forward step of covariate selection and 1% in backward elimination. Parameter uncertainty was assessed via the nonparametric bootstrap method.

2.4 PK-PD analysis approach

The PK-PD analysis was split into parts: analysis of time-to-stable culture conversion and analysis of long-term tuberculosis treatment outcomes (relapse and death). Time-to-stable culture conversion was defined as the time when a negative culture result was obtained and confirmed at the next follow-up visit. Tuberculosis diagnosis was based on smear results and clinical assessments. Time-to-event analysis with interval censoring methodology was applied to the data. The association between time-to-stable culture conversion vs drug exposure and patient characteristics including disease burden was assessed using a two-stage approach. Firstly, a time-to-event structural model was determined in Monolix. Constant, Weibull, Gompertz, and three-parameter surge function hazard structural models were evaluated. The best model was selected based on lowest AIC value, and predictive ability using visual predictive checks.

In the second stage, time-to-event CART analysis in the conditional framework was applied to identify the most promising covariates effects that are predictive of time-to-stable culture conversion and the interactions between these covariates. The analysis produces a tree like structure with binary splits and the root node represents the most significant predictor. Additional significant covariates are added as daughter nodes in order of importance using a predefined statistical significance criterion (5% level of significance). The permutation test is applied at each level to determine the most significant covariate to be included as a node. The procedure ensures that patients in each terminal node are as homogenious as possible.The terminal nodes of the final tree were used to define a single categorical covariate for further testing taking the best time-to-event structural model identified in Monolix as the base model. Two categories were combined if the model with one less parameter did not result in a worse fit (ΔOFV < 3.84 points). Predictors of long-term treatment outcomes were identified using binary CART in the conditional inference framework.

Chapter 3: Model-based evaluation of higher doses of rifampicin using a semimechanistic model incorporating autoinduction and saturation of hepatic extraction

3.1 Abstract

Rifampicin is a key sterilizing drug in the treatment of tuberculosis (TB). It induces its own metabolism, but neither the onset nor the extent of autoinduction has been adequately described. Currently, the World Health Organization recommends a rifampicin dose of 8 to 12 mg/kg of body weight, which is believed to be suboptimal, and higher doses may potentially improve treatment outcomes. However, a nonlinear increase in exposure may be observed because of saturation of hepatic extraction and hence this should be taken into consideration when a dose increase is implemented. Intensive pharmacokinetic (PK) data from 61 HIV-TB co-infected patients in South Africa were collected at four visits, on days 1, 8, 15, and 29, after initiation of treatment. Data were analysed by population nonlinear mixed-effects modelling. Rifampicin PK were best described by using a transit compartment absorption and a well-stirred liver model with saturation of hepatic extraction, including a first-pass effect. Autoinduction was characterized by using an exponential-maturation model: hepatic clearance almost doubled from the baseline to steady state, with a half-life of around 4.5 days. The model predicts that increases in the dose of rifampicin result in more-than-linear drug exposure increases as measured by the 24-h area under the concentration-time curve. Simulations with doses of up to 35 mg/kg produced results closely in line with those of clinical trials.

3.2 Introduction

Rifampicin is a key drug in the treatment of tuberculosis (TB), and the World Health Organization (WHO) currently recommends weight-adjusted doses of 8 to 12 mg/kg daily. Despite its being used in the treatment of TB for nearly 50 years, there is evidence that current rifampicin exposures may be suboptimal. Rifampicin's efficacy is exposure dependent (Gumbo, Louie, Deziel, *et al.*, 2007; Mehta *et al.*, 2001; Steingart *et al.*, 2011); therefore, the efficacy and toxicity of higher doses are under investigation. Recent reports show that larger doses of rifampicin are well tolerated by humans (Boeree *et al.*, 2015) and may improve treatment outcomes, as well as reduce the treatment duration from the current 6 months (de Steenwinkel *et al.*, 2013; Jayaram *et al.*, 2003).

Rifampicin is mainly hepatically cleared, and it undergoes extensive first-pass metabolism (Loos *et al.*, 1985), whose saturation with higher doses has been reported since early pharmacokinetic (PK) studies (Acocella, 1978). Thus, when the rifampicin dose is increased above a certain level, a more-than-proportional increase in the plasma rifampicin concentration results. Rifampicin also induces its own metabolism via the pregnane X receptor (Chen & Raymond, 2006), a phenomenon known as clearance autoinduction, resulting in less exposure at steady state than after a single dose.

Previous studies have proposed rifampicin PK models (Wilkins *et al.*, 2008), but those trying to characterize clearance autoinduction have done so mostly by relying on only two PK sampling occasions (Smythe *et al.*, 2012), which limited their ability to characterize the process. Nonlinearity in a dose-exposure relationship suggesting saturation of rifampicin clearance has been reported (Acocella, 1978). However, a population PK model has not jointly described the autoinduction and hepatic extraction (E_H) of rifampicin. In this study, we analysed rich data from an intensive sampling scheme to develop a rifampicin PK model for

TB patients that accounts for both clearance autoinduction and saturation of E_H. This model was then employed to explore changes in rifampicin exposure when doses are increased beyond the currently recommended range.

3.3 Methodology

Study design and patient selection

Extensive details of this study, including design, patient selection, and dose administration, have been reported before (McIlleron *et al.*, 2012). Two four-drug fixed-dose combinations (FDCs) were administered; each tablet contained 150 mg of rifampicin, 75 mg of isoniazid, 400 mg of pyrazinamide, and 275 mg of ethambutol. Patients received weight-adjusted doses for 5 days a week, from Monday to Friday, according to WHO guidelines (World Health Organization, 2003), except 10 patients who received medication for 7 days a week. Thus, patients weighing 30 to 37 kg at the start of treatment received two FDC tablets per dose, while those weighing 38 to 54, 55 to 70, or 70 kg received three, four, or five FDC tablets, respectively. Efavirenz (EFV)-based antiretroviral therapy (ART) was initiated in two-thirds of the patients on day 15 after the start of TB treatment. Patients were excluded if they had evidence of a pre-existing disease likely to affect the response to or assessment of treatment effects or represent contraindications to the study medication.

Specimen collection and drug quantitation.

Participants were admitted for PK blood sampling on the 1st, 8th, 15th, and 29th days of TB treatment after an overnight fast. Blood samples were taken immediately before dosing and 1, 2, 4, 6, 8, and 12 h after dose administration. Additionally, a sample was collected at approximately 12h before the 15th dose. Details of plasma separation and storage and quantitation of drug concentrations were as reported before (McIlleron *et al.*, 2012). The lower limit of quantitation was 0.1 mg/L.

Pharmacokinetic analysis

Population PK analysis was used to describe the concentration data in NONMEM version 7.3 software (Beal, Sheiner, Boeckmann, & Bauer, 2013) by using the algorithm first-order conditional estimation with eta-epsilon interaction (FOCE-I). Perl-speaks-NONMEM, Xpose4,

and Pirana were used for model diagnostics and to track model development (Keizer, Karlsson, & Hooker, 2013). Additional diagnostic plots and post-modelling analysis were performed with R version 3.1.2 (R Core Team, 2017) via RStudio version 0.98.1091 (RStudio, 2014).

Several disposition models were evaluated, including one-compartment first-order elimination and a well-stirred liver model, with and without saturation of E_H (Gordi *et al.*, 2005) characterized by Michaelis-Menten parameterization. To characterize rifampicin absorption, a first-order model with and without lag time and a chain of transit compartments were assessed (Savic, Jonker, Kerbusch, *et al.*, 2007). Different approaches were used to describe autoinduction of rifampicin: estimating a different clearance value at each PK sampling occasion, using an enzyme induction model (Smythe *et al.*, 2012), or using an exponential maturation model with clearance increasing with time on treatment (Denti *et al.*, 2010).

Between-subject variability (BSV) and between-occasion variability (BOV) were assumed to follow a log-normal distribution. A PK profile was treated as a separate occasion: four sampling occasions with intensive sampling and three catering for concentrations obtained prior to dosing on days 8, 15, and 29. Allometric scaling was applied to all disposition parameters, with allometric exponents fixed to 0.75 for clearance parameters and 1 for volume parameters, as described by Anderson and Holford (Anderson & Holford, 2008). Total body weight (TBW) and fat-free mass (FFM) were evaluated on each of these parameters. All samples (including pre-dose after day 1) with concentrations below the limit of quantitation (BLQ) were handled by the M6 method (Beal, 2001). This means that they were replaced with half the lower limit of quantitation (LLQ), except for consecutive values in a series, for which the trailing BLQ values were ignored for the fit but included in the diagnostic plots. Pre-dose concentrations from day 1 were excluded from the fit after it was verified that they were BLQ, as expected. Overall, a combined additive and proportional error model was used to describe unexplained residual variability. The effect of covariates on PK parameters was assessed by exploring

proportional changes with a linear model for continuous variables and additive covariate model for categorical variables (Bonate, 2011).

Model building was guided by change in the objective function value (OFV, assumed to be approximately χ^2 distributed), inspection of diagnostic plots including a prediction-corrected visual predictive check (VPC) (Bergstrand, Hooker, Wallin, *et al.*, 2011), and physiological plausibility. The final model was used to simulate larger doses of rifampicin in a reference cohort of *in silico* TB patients created with demographic data of 870 TB patients in South Africa and West Africa (200 repetitions). With the same weight bands as described above and a tablet strength of 150 mg of rifampicin, daily doses of 15, 20, 25, 30, and 35 mg/kg were evaluated, assuming drug administration every day of the week. The model-based 24-h area under the concentration-time curve ($AUC_{0–24}$) and maximum concentration (C_{max}) were derived at the first dose and at steady state. The probability of target attainment (PTA) for each rifampicin daily dose at each specific MIC was calculated as the proportion of simulated patients with a steady-state $AUC_{0–24}$/MIC ratio of at least 271, a cut-off value that has been shown to correlate well with the bactericidal activity of rifampicin against *Mycobacterium tuberculosis* (Jayaram *et al.*, 2003). The MICs were derived from the distribution of *M. tuberculosis* MICs in South African isolates (Chigutsa *et al.*, 2015). The selected PTA was plotted against the range of MICs to describe the killing effects of different doses of rifampicin. The cumulative fraction of response (CFR) was computed by using equation 5 for the reference MIC distribution and expressed as a percentage to assess the overall PTA for each dose (Mouton, Dudley, Cars, *et al.*, 2005).

$$CFR_{dose} = \sum_{i=1}^{n} PTA_i \cdot F_i \qquad (5)$$

The subscript *i* shows the MICs ranked from the lowest to the highest for the population of microorganisms. PTA_i is the PTA for each MIC, and F_i is the fraction of the population of

microorganisms at each MIC. Simulations were also used to explore changes in 24-h trough levels associated with higher doses of rifampicin.

3.4 Results

Demographics

In total, 61 patients were recruited into the study. Their baseline characteristics are presented in Table 3.1, and further information can be found in the previous report (McIlleron *et al.*, 2012). The median weight, FFM, and height were 55.2 kg, 42.2 kg, and 1.59 m, respectively. The median age of the patients was 32 years, and their ages ranged from 18 to 47 years. Rifampicin concentrations in 1,342 plasma samples were included in the analysis, and 140 (10%) of these, mostly in pre-dose samples, were below the limit of quantitation. Of the 61 patients, 41 started EFV-based ART on day 15.

Table 3.1 Baseline characteristics of patients in TB-HAART (rifampicin model)

Characteristic	Value
N	61
No. (%) of females	33 (54%)
No. (%) undergoing ART	41 (67%)
No. (%) treated 5 days/wk	51 (84%)
Median age, yr (range)	32 (18–47)
Median wt, kg (range)	55.2 (34.4–98.7)
Median ht, m (range)	1.59 (1.41–1.81)
Median FFM, kg (range)	42.2 (28.0–57.6)
Median albumin level, g/liter (range)	26 (15–43)
Median creatinine level, μmol/liter (range)	74 (53–155)
Median viral load, 10^3 copies/ml (range)	86 (0.05–13000)
Median no. of $CD4^+$ cells/μl of blood (range)	254 (12–500)

Structural model

Rifampicin PK were best characterized by a well-stirred liver model, with absorption through a chain of transit compartments. A schematic diagram of the final model is shown in Figure 3.1. Inclusion of saturation of E_H further improved the model (a 216-point drop in the OFV, 1 degree of freedom, $P < 0.001$). In the final model, rifampicin clearance and bioavailability are

both dependent on E_H. E_H is influenced by the unbound fraction of rifampicin (f_u), hepatic plasma flow rate (Q_H), and intrinsic clearance (CL_{int}), which changes with time on treatment because of autoinduction. CL_{int} was saturable and followed Michaelis-Menten kinetics; that is, the rate of elimination had a maximum saturation value ($CL_{int,max}$) dependent on the Michaelis constant (K_m). More details of the model, including all of the equations describing saturable elimination, are included in the Appendix.

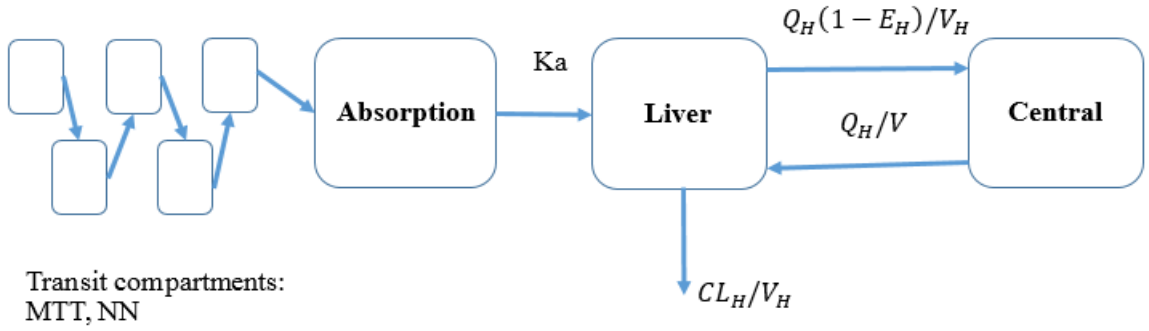

Figure 3.1 Schematic diagram of the final model for rifampicin (TB-HAART study)
V is the volume of the observation/central compartment, and NN is number of absorption transit compartments.

Rifampicin autoinduction was characterized by applying an exponential-maturation model to $CL_{int,max}$ so that this increased with time on treatment from a baseline value of $CL^0_{int,max}$ to a steady-state value of $CL^{ss}_{int,max}$ as follows:

$$CL_{int,max} = CL^0_{int,max} + \left(CL^{SS}_{int,max} - CL^0_{int,max}\right) \cdot \left(1 - e^{-\frac{ln(2)}{t_{\frac{1}{2}ind}} \cdot t}\right) \quad (3.1)$$

The model was used to estimate the half-life of the induction process ($t_{½ind}$). The typical value of prehepatic bioavailability (F_{prehep}) was fixed to a reference value of 1 and allowed to vary between occasions. Typical values of the volume of the liver (V_H) and hepatic plasma flow (Q_H) were fixed to 1 liter and 50 liters/h, respectively, and allometric scaling was included to account for size differences. The fraction of unbound rifampicin (f_u) was fixed to 20% (Acocella,

1978). Different typical values of V_H, Q_H, and f_u were explored by sensitivity analysis, and the model was found to be robust.

Allometric scaling of all disposition parameters, including those for the well-stirred hepatic model (CL_{int}, hepatic plasma flow, volume of the liver and the central compartment), was best characterized by using fat-free mass (FFM) compared to TBW (a 40-point decrease in the Akaike information criterion [AIC]) in addition to a 27-point drop in the AIC when allometric scaling was applied by using TBW. The median FFM of 42 kg was used as a reference. EFV co-administration was not found to affect rifampicin PK.

Parameter estimates of the final model

A VPC provided in Figure 3.2 shows that the simulated concentrations mirror the observed values well and that the model correctly captures the decrease in rifampicin exposure with time on treatment because of autoinduction.

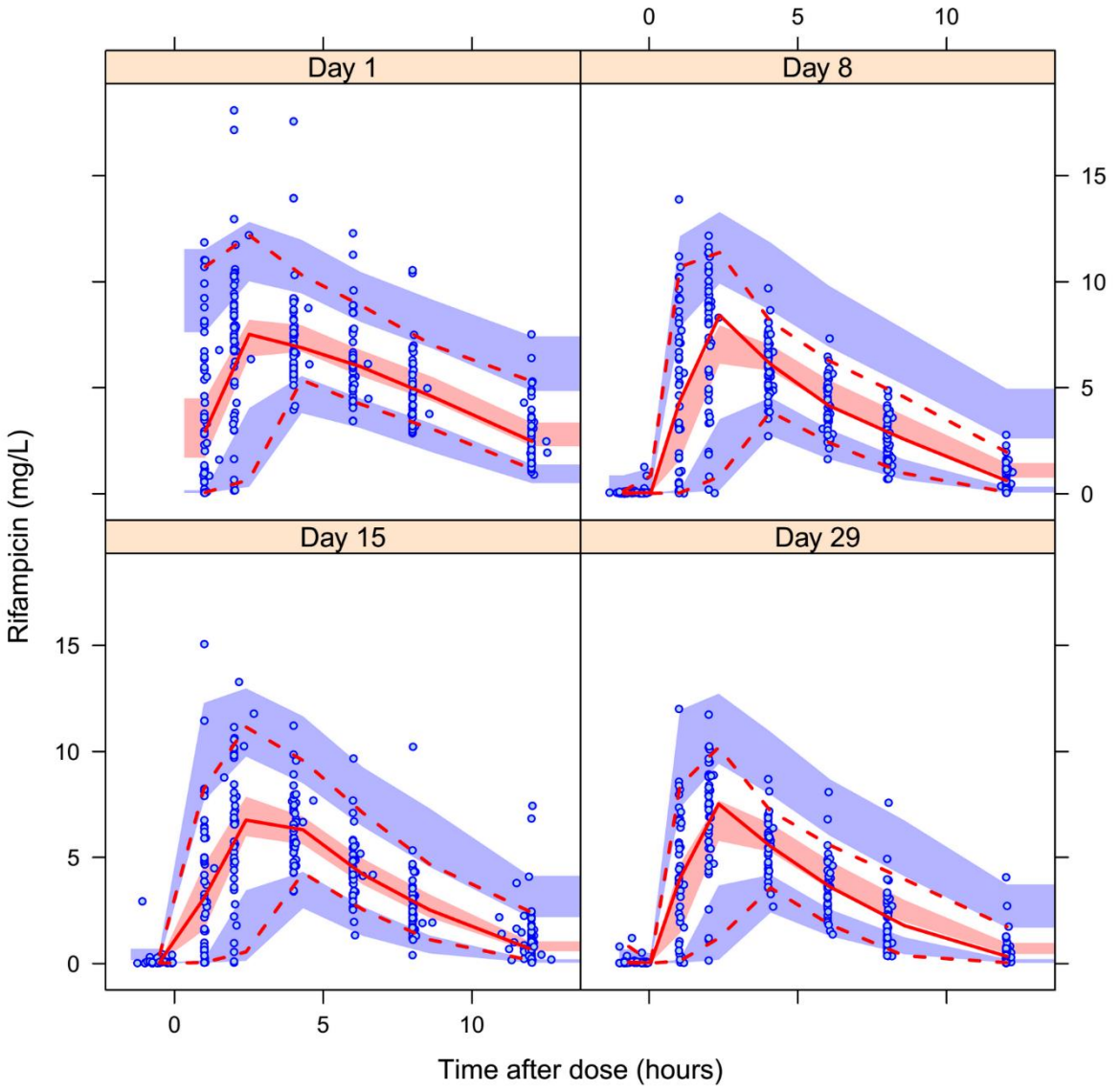

Figure 3.2 Prediction-corrected VPC for rifampicin model (TB-HAART study) stratified by day after treatment initiation Open circles are the observed concentrations. The middle continuous line is the 50th percentile of the observed data, and the upper and lower dashed lines are the 95th and 5th percentiles of the observed data, respectively. The shaded regions represent the 95% prediction intervals of the 5th, 50th, and 95th percentiles.

The parameter estimates of the final model and their precision obtained with a 200-sample nonparametric bootstrap with replacement are presented in Table 3.2. The maximum CL_{int} almost doubled from the first day of treatment to steady state; for a typical individual, it increased from 93 to 176 liters/h. The half-life of the induction process was estimated to be

4.5 days. The model estimated that a K_m concentration (bound plus unbound) of 3.4 mg/liter will result in half the maximum CL_{int}. The final model included BSV in clearance (23%) and the volume of the observation compartment (14%) and included BOV in clearance (22%), bioavailability (11%), the absorption rate constant (K_a) (81%), and the mean transit time (MTT) (63%). A combined additive (0.07 mg/liter) plus proportional (11%) error model was supported by the data.

Table 3.2 Values estimated by the final model

Parameter	Estimate	Bootstrap 90% CI[a]
$CL^{0}_{int,max}$ (L/h)[b]	93.2	83.7–108.1
V (L)[b]	50.1	47.7–52.8
K_a (/h)	1.96	1.7–2.2
MTT (h)	0.71	0.67–0.78
NN[c]	19.3	18.1–22.2
F[d]	1 FIXED	
$CL^{SS}_{int,max}$ (L/h)[b]	176	159–210
$t_{1/2_{ind}}$ (days)	4.5	4.1–4.9
V_H (L)[b]	1 FIXED	
Q_H (L/h)[b]	50 FIXED	
f_u	0.2 FIXED	
K_m (mg/L)[e]	3.35	3.0–3.56
Between subject variability (%)		
CL	22.5	19.1–26.1
V	14.2	11.5–16.2
Between occasion variability (%)		
CL	21.9	18.3–25.7
F	11.0	9.6–13.6
K_a	81.2	72.8–88.4
MTT	62.7	57.0–75.4
Error		
Additive (mg/L)	0.064	0.059–0.07
Coefficient of variation (%)	10.8	10.0–12.8

[a] CI, confidence interval.
[b] This parameter has been adjusted by allometric scaling, and the values reported refer to a subject with an FFM of 42 kg (the median value of the cohort).
[c] NN, number of absorption transit compartments.
[d] F, bioavailability.
[e] Total concentration (bound plus unbound).

Simulations

Model-simulated rifampicin exposures on days 1 and 29 after TB treatment initiation for our reference cohort of 870 TB patients are shown in Table 3.3.

Table 3.3 Simulated exposures at first dose and steady state by dose[a]

Dose	First dose		Steady-state dose		
	C_{max} (mg/L)	$AUC_{0–24}$ (mg·h/L)	C_{min} (mg/L)	C_{max} (mg/L)	$AUC_{0–24}$ mg·h/L)
10 mg/kg	8.0 (4.7–12.6)	71.1 (35.1–140.3)	0.005 (0.0001–0.13)	6.9 (3.6–11.6)	39.3 (19.0–81.3)
15 mg/kg	13.5 (8.2–20.9)	150 (74.0–282.3)	0.023 (0.0003–0.78)	12.1 (6.7–19.7)	84.6 (40.0–180.5)
20 mg/kg	17.4 (10.8–27.0)	217.1 (107.1–403.5)	0.06 (0.001–2.67)	16.1 (9.0–26.8)	127.0 (58.3–298.0)
25 mg/kg	23.2 (14.7–35.3)	326.3 (166.7–573.8)	0.26 (0.002–15.78)	22.3 (12.8–46.9)	207.0 (92.7–735.8)
30 mg/kg	27.2 (17.2–41.7)	407.9 (211.0–709.1)	0.72 (0.005–86.82)	27.3 (15.5–123.2)	280.6 (119.3–2543.5)
35 mg/kg	33.1 (21.3–50.1)	531.1 (287.0–893.2)	2.96 (0.015–251.8)	35.8 (19.9–291.1)	425.2 (169.5–6532.5)

[a] Data are medians (90% ranges)

Changes in the $AUC_{0–24}$ from the first day of treatment due to autoinduction for a reference male in the data set (median weight of 55 kg and height of 1.65 m) are presented in Figure 3.3a for the current 10-mg/kg dose and larger doses of up to 35 mg/kg. Figure 3.3b shows the concentration-time PK profiles for the same male patient at full induction. As expected, a nonlinear increase in exposure with increasing doses is predicted. At steady state, with the currently recommended dose of 10 mg/kg as the reference, increases in exposure were 2.2-fold for 15 mg/kg, 3.2-fold for 20 mg/kg, 5.3-fold for 25 mg/kg, 7.1-fold for 30 mg/kg, and 10.8-fold for 35 mg/kg. At a dose of ≥ 25 mg/kg, the simulations predict a median trough concentration (C_{min}) of 0.3 mg/liter, higher than the LLQ of 0.1 mg/liter in this study. The changes in exposure during the first days of treatment are a result of the balance between the effect of autoinduction and that of accumulation after multiple consecutive doses. Our model predicts that, for doses of > 20 mg/kg, the daily exposures from the first dose on will

significantly increase during the first days and then decrease to levels lower than that of the first day because of autoinduction.

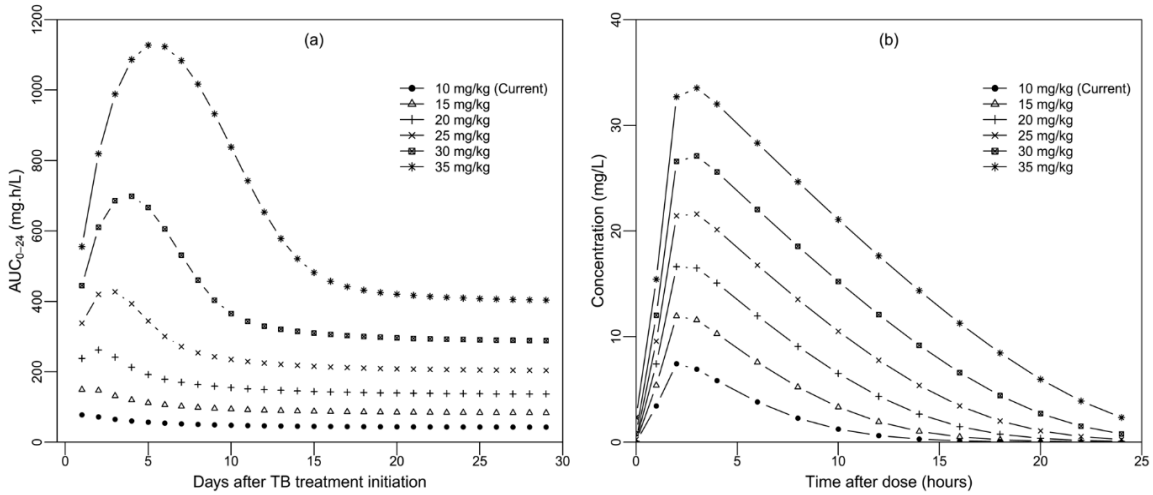

Figure 3.3 Change in AUC_{0-24} over time and simulated day 29 concentrations for doses of 10 mg/kg to 35 mg/kg (a) Change in the AUC_{0-24} from the first day of treatment to day 29 for a typical male patient (median weight of 55 kg and height of 1.65 m) daily administered 600 mg and larger doses of up to 2,100 mg (3.5 times larger) (b) Simulated concentration-time profile on day 29 after TB treatment initiation for a typical male patient.

Moreover, with the current dosing recommendations based on total weight, the model predicts that patients in lower-weight bands are exposed to lower drug levels, as shown in Figure 3.4. In the TB patient population used in our simulation, subjects with weights of 30 to 37 kg had, on average, 44% less rifampicin exposure than those with weights of > 70 kg.

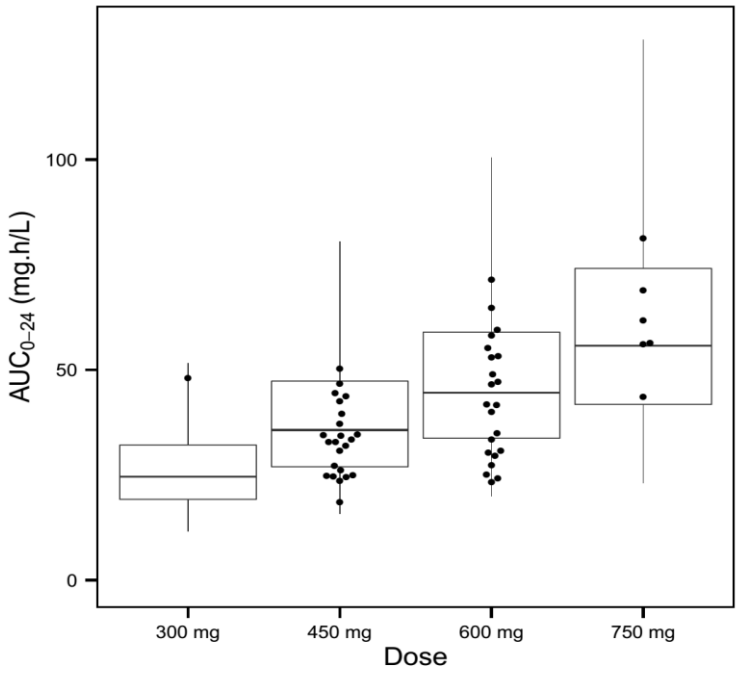

Figure 3.4 Distribution of exposures ($AUC_{0–24}$) at steady state (day 29) based on the currently recommended doses The simulated exposures are shown in box plots with the individual values observed in the present study superimposed in closed circles.

The PTA results are shown in Figure 3.5. At the current MICs prevalent in the South African population of drug-sensitive TB patients (0.016 to 0.5 mg/liter), the current rifampicin dose of 10 mg/kg alone is predicted to have a PTA of slightly above 60% for a median MIC of 0.125 mg/liter, so larger doses of rifampicin are likely to be more effective. For *M. tuberculosis* strains with higher MICs, the currently recommended doses are predicted to be ineffective. The predicted CFR for a daily dose of 10 mg/kg was 65%, and increasing the dose to 15 mg/kg achieves a CFR of 90%. A further increase to 20 mg/kg will result in a CFR of 96%. Doses of at least 25 mg/kg will achieve an overall PTA of > 99%.

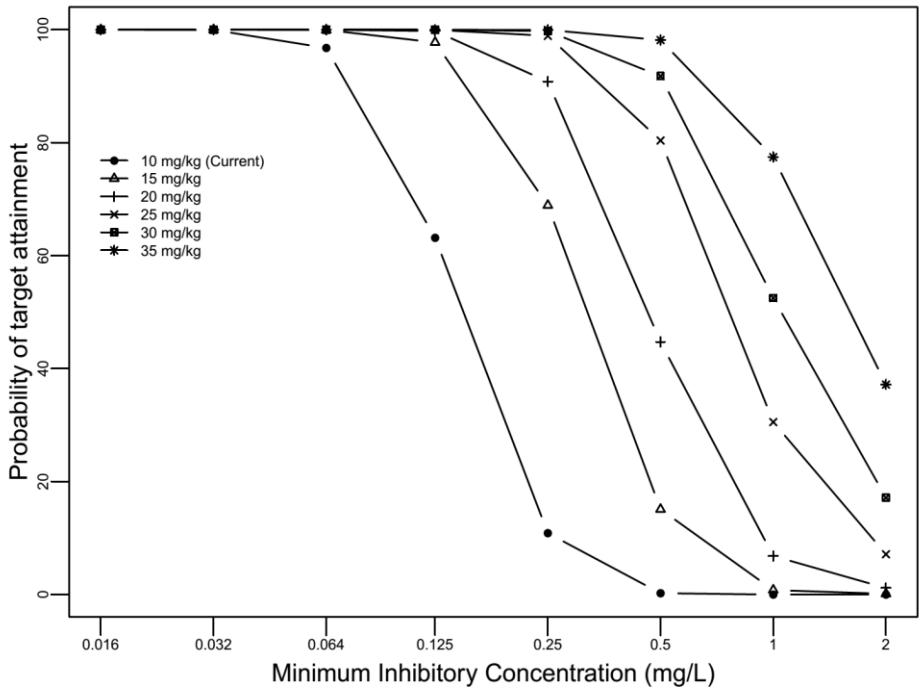

Figure 3.5 Probabilities of target (steady-state AUC_{0-24}/MIC ratio of 271) attainment over a range of MICs (plotted on a $\log_2$ scale) with different doses in milligrams per kilogram of body weight

3.5 Discussion

A population PK model of rifampicin describing autoinduction and saturation of E_H was developed and used to simulate larger doses of rifampicin of up to 35 mg/kg of body weight. Autoinduction of rifampicin clearance has been previously described on the basis of results of both traditional noncompartmental analysis (NCA) (Acocella, Lamarina, Nicolis, *et al.*, 1972; Loos *et al.*, 1985) and population PK (Smythe *et al.*, 2012). To our knowledge, previous reports were based on two sampling occasions (first dose and steady state), while our data comprised four sampling occasions starting from treatment initiation and we could characterize rifampicin autoinduction by using an exponential-maturation model, enabling us to estimate the half-life of the process. The model suggests that, on average, clearance of rifampicin almost doubles from the first day of treatment to steady state, and the induction process takes around 2 weeks to reach 90% of the fully induced state. The duration of the process differs from that reported in other studies, possibly because of the richness of data and the dosing strategies used (daily versus intermittent dosing) (Acocella, Pagani, Marchetti, Baroni, & Nicolis, 1971; Smythe *et al.*, 2012). Though the induction half-life estimated by our model is shorter than that reported by Smythe et al., the extent of the autoinduction effect on clearance is roughly the same.

E_H was described by using a well-stirred liver model, and its saturation was characterized by using Michaelis-Menten kinetics. This model confirms findings of previous studies showing saturation of rifampicin clearance already at doses of about ≥ 450 mg (Acocella, 1978, 1983; Gumbo, Louie, Deziel, *et al.*, 2007). The proposed PK model with saturable E_H could mechanistically explain three different phenomena seen in the present data and/or previously reported in other studies: nonlinearity of rifampicin exposure with dose, underexposure of lower-weight patients by the current weight band approach, and a correlation between faster rifampicin absorption and greater bioavailability.

Previous studies and recent clinical trials show the nonproportionality of the dose-exposure relationship (Mouton, Mattie, Swart, *et al.*, 1979; Pargal & Rani, 2001). This means that the rifampicin exposure level for doses larger than the current recommendation is greater than that expected if the dose-exposure relationship were linear. Our model mechanistically explains this nonproportionality by using saturable E_H. For example, simulations based on our model show that doubling of the dose is associated with more than double the exposure. This could be explained by saturation of the beta-esterase metabolizing enzymes and/or p-glycoprotein after oral administration with a reduction in the first-pass effect and increased bioavailability. With the currently used doses, the effect of -saturation is evident only on first-pass metabolism and not on systemic clearance. With larger doses, however, our model predicts that systemic clearance will also be affected by the saturation effect, resulting in, *inter alia*, nonnegligible accumulation of rifampicin between consecutive doses. Our results showing nonproportionality of the dose-exposure relationship are in line with previous studies evaluating doses of rifampicin of 15 to 20 mg/kg (Acocella, 1983; Ruslami *et al.*, 2007) and more recently up to 35 mg/kg (Boeree *et al.*, 2015). Ruslami et al. predicted a 65% larger AUC0 –24 for patients receiving 13 mg/kg than for those receiving 10 mg/kg (Ruslami *et al.*, 2007), and Boeree et al. recently showed that increasing the dose to 35 mg/kg results in a 10-fold increase in the AUC_{0-24} (Boeree *et al.*, 2015). Simulations based on our model closely mirror the exposures detected by Boeree et al., as shown in Figure 3.6, which provides a visual comparison of the C_{max} and AUC_{0-24} on day 14.

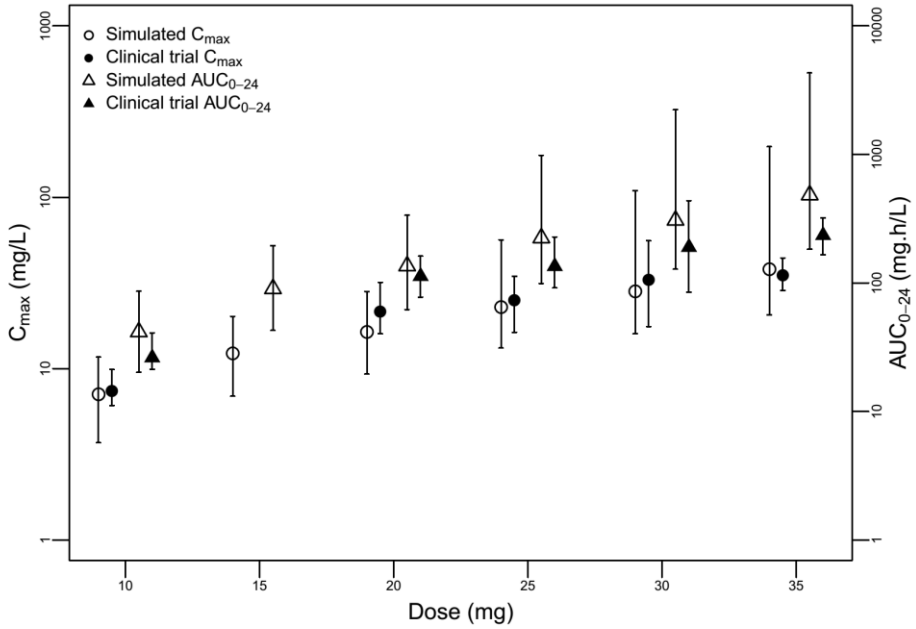

Figure 3.6 Comparison of simulated exposure (C_{max} and $AUC_{0–24}$, median and 90% range) on day 14 after TB treatment initiation and exposure (C_{max} and $AUC_{0–24}$, geometric mean and range) obtained from Boeree et al. (Boeree *et al.*, 2015)

Although our model predictions for larger rifampicin doses closely mirror the median exposure values observed in recent trials, the simulations for 30 and 35 mg/kg showed alarmingly large variability and predictions of extremely high values in some individuals (Table 3.3). These results could be due to the limits of the extrapolation capability of our model, since it was developed on the basis of data obtained with a 10-mg/kg dose. Despite this caveat, greater variability in exposure is to be expected when increasing the dose of a drug that exhibits saturation kinetics, because relatively small changes in the dose may be enough to reach the "tipping point" for some patients but not for others. Boeree et al. also reported increased variability in exposure with larger doses (Boeree *et al.*, 2015), although not to the extent that our model predicted. It is interesting that in our simulations, the patients with extremely high exposure values were mostly women with high body weights, whom our model found to be relatively overexposed even on the basis of the current guidelines, as discussed below. In the present simulations, it was assumed that the level of autoinduction remains the same even at

higher rifampicin concentrations. The consistency of our predictions with the values observed in clinical trials supports this assumption.

Before the inclusion of saturable E_H, the model detected a positive effect of the total dose on bioavailability; that is, patients in the higher-weight bands receiving larger absolute doses had greater bioavailability than patients in the lower-weight bands. This suggests that doses intended to achieve the same dose in milligrams per kilogram of body weight across weight bands are not appropriate and lower-weight patients should be prescribed larger doses. This finding is driven by saturation of first-pass metabolism, which was more evident for patients in the highest weight band, the relatively increased clearance per unit of body size described by allometric scaling theory, and FFM being the most appropriate body size descriptor for scaling of clearance, which is consistent with previous evidence (Jeremiah *et al.*, 2014; Smythe *et al.*, 2012). Geiseler et al. showed that daily dosing of a number of anti-TB drugs, including rifampicin, should be based on the ideal body weight rather than the TBW (Geiseler, Manis, & Maddux, 1985). This argument has implications in settings where a significant proportion of the population is overweight, and it could cause differences in exposure among patients receiving the same dose (milligrams per kilogram) in different weight bands. This was indeed the case in our study cohort, which contained several women with high body mass indexes who were found to achieve greater exposures. This is in keeping with previous NCA results based on the same data set (McIlleron *et al.*, 2012), which showed that patients in the lower-weight bands, as well as males, have lower drug exposure levels than other patients do.

Similar to findings described by Jeremiah et al. (Jeremiah *et al.*, 2014), a negative correlation between absorption MTT and bioavailability was observed, so that faster absorption was associated with increased bioavailability. Upon inclusion of the saturable E_H model, this phenomenon could be explained mechanistically as follows: higher absorption rates achieve

higher rifampicin concentrations in the liver, thus saturating the clearance and reducing the extent of first-pass extraction, resulting in greater exposure. Rifampicin exposure levels greater than those achieved with the current dosing have been shown to correlate with better treatment outcomes (Long, Snider, & Farer, 1979; Pasipanodya *et al.*, 2013); hence, the increased rifampicin exposure due to saturation is likely to be beneficial to patients. On the basis of the range of MICs obtained from a South African study (Chigutsa *et al.*, 2015), our simulation suggests that the currently recommended dose may not be adequate for some patients. The PTA for the currently recommended dose was 63% for a median MIC of 0.125 mg/liter. This result corroborates the notion that increasing rifampicin doses is likely to result in improved responses to treatment, which might allow shorter treatment times. On the basis of Monte Carlo simulations of exposure with the current weight and dosing and the reported MICs, a dose of 20 mg/kg is expected to achieve a CFR of >95%.

The model presented here has some limitations. It was developed on the basis of data obtained only with a 10-mg/kg dose, so the extrapolation becomes less reliable as our simulations explore much larger doses such as 30 or 35 mg/kg. Though we could not establish a relationship between autoinduction and the administration schedule (5 versus 7 days/week), there is no guarantee that the extent of autoinduction will be similar for other intermittent dosing schedules, for example, dosing two or three times a week. Similarly, our data could not be used to predict whether larger doses of rifampicin will result in higher levels of autoinduction. Predicted PTAs should be interpreted while keeping in mind that the cut-off values used for PTA determination were obtained from a murine model (Jayaram *et al.*, 2003) and extrapolation to humans may not be accurate for a number of factors, including differences in the lesions: more granuloma as well as cavity formations in humans (Capuano *et al.*, 2003; Rhoades, Frank, & Orme, 1997).

In conclusion, the model developed here describes autoinduction of clearance and saturation of E_H of rifampicin. The model was used to simulate doses larger than those currently recommended, and a more-than-proportional increase in exposure in relation to the dose was observed. Doses larger than those currently recommended are likely to be more effective against the *M. tuberculosis* strains considered in this study. Since it was not possible to characterize whether higher rifampicin concentrations may affect the extent of autoinduction, further research is necessary to address this question. Moreover, the effect of increased rifampicin exposure on the PK of co-administered drugs, in particular, the companion anti-TB and antiretroviral drugs, would need to be assessed. Alternative dosing strategies based on FFM need to be explored to reduce differences in exposure among TB patients, and this is likely to become even more critical with higher doses, with which even greater variability is expected.

3.6 Appendix

Structural model with saturable E_H

The model structure depicted in Figure 3.1 is explained in detail below. Upon oral administration, rifampicin is transferred into the absorption compartment via transit compartments, and from there, it reaches the liver, where it is subjected to first-pass metabolism. It is then transferred into the central compartment, from which it recirculates to the liver because of blood circulation. The site of drug clearance, characterized with a well-stirred model, is the liver. Clearance is determined by hepatic plasma flow (Q_H) and the E_H ratio as follows:

$$CL_H = Q_H \cdot E_H \tag{3.2}$$

The E_H ratio is defined as follows:

$$E_H = \frac{CL_{int} \cdot f_u}{CL_{int} \cdot f_u + Q_H} \tag{3.3}$$

where CL_H is the saturable intrinsic hepatic clearance and f_u is the unbound fraction of rifampicin. Saturable CL_{int} is defined by Michaelis-Menten parameterization as follows:

$$CL_{int} = \frac{CL_{int,max} \cdot K_m}{C_H + K_m} \tag{3.4}$$

where $CL_{int,max}$ is the maximum CL_{int}, C_H is the concentration of rifampicin in the liver, and K_m is the Michaelis constant, a parameter that governs saturable hepatic elimination and denotes the rifampicin concentration at which the CL_{int} is half its maximal value. To stabilize the model during estimation of K_m, the parameter was estimated on a log scale. $CL_{int,max}$ was autoinduced in accordance with equation 3.1.

Chapter 4: Pharmacokinetics of pyrazinamide and optimal dosing regimens for drug-sensitive and -resistant tuberculosis

4.1 Abstract

Pyrazinamide is used in the treatment of tuberculosis (TB) because its sterilizing effect against tubercle bacilli allows the shortening of treatment. It is part of standard treatment for drug-susceptible and drug-resistant TB, and it is being considered as a companion drug in novel regimens. The aim of this analysis was to characterize factors contributing to the variability in exposure and to evaluate drug exposures using alternative doses, thus providing evidence to support revised dosing recommendations for drug-susceptible and multidrug-resistant tuberculosis (MDR-TB). Pyrazinamide pharmacokinetic (PK) data from 61 HIV/TB-coinfected patients in South Africa were used in the analysis. The patients were administered weight-adjusted doses of pyrazinamide, rifampicin, isoniazid, and ethambutol in fixed-dose combination tablets according to WHO guidelines and underwent intensive PK sampling on days 1, 8, 15, and 29. The data were interpreted using nonlinear mixed-effects modelling. PK profiles were best described using a one-compartment model with first-order elimination. Allometric scaling was applied to disposition parameters using fat-free mass. Clearance increased by 14% from the 1st day to the 29th day of treatment. More than 50% of patients with weight less than 55 kg achieved lower pyrazinamide exposures at steady state than the targeted area under the concentration-time curve from 0 to 24 h of 363 mg h/liter. Among patients with drug-susceptible TB, adding 400 mg to the dose for those weighing 30 to 54 kg improved exposure. Average pyrazinamide exposure in different weight bands among patients with MDR-TB could be matched by administering 1,500 mg, 1,750 mg, and 2,000 mg to patients in the 33-to 50-kg, 51- to 70-kg, and greater than 70-kg weight bands, respectively.

4.2 Introduction

Pyrazinamide is a prodrug converted to its active form, pyrazinoic acid, by hepatic microsomal deamidase (Konno, Feldmann, & McDermott, 1967) and is active against dormant and semi-dormant *Mycobacterium tuberculosis* bacilli, especially in acidic environments (Mitchison, 1985; Steele & Des Prez, 1988). It is currently part of a four-drug fixed-dose combination (FDC), which includes isoniazid, ethambutol, and rifampicin, an inducer of a number of cytochrome P450 enzymes via the pregnane X receptor (PXR) (Chen & Raymond, 2006). Pyrazinamide is currently being considered as a companion drug in novel tuberculosis (TB) treatment regimens for drug-susceptible and -resistant TB (Diacon *et al.*, 2012; Mitchison & Fourie, 2010; Pasipanodya *et al.*, 2013).

Interest in the drug derives from its potent sterilizing activity, which confers the ability to shorten treatment duration. Pyrazinamide exposures have been correlated with favourable treatment outcomes in patients on standard doses (Chideya *et al.*, 2009; Chigutsa *et al.*, 2015; Gumbo *et al.*, 2014; Heifets & Lindholm-Levy, 1992; Mitchison, 2005; Pasipanodya *et al.*, 2013; Zhang & Mitchison, 2003). A pyrazinamide area under the concentration-time curve from 0 to 24 h ($AUC_{0–24}$) of at least 363 mg·h/liter has been associated with long-term TB treatment outcomes among patients with drug-susceptible TB and could be targeted for treatment optimization (Pasipanodya *et al.*, 2013). The current recommended weight-adjusted daily dose of pyrazinamide for treatment of drug-susceptible TB is approximately 25 (range, 20 to 30) mg/kg of body weight (World Health Organization, 2003), while that for treatment of MDR-TB is about 35 (range, 30 to 40) mg/kg (World Health Organization, 2009). Doses higher than those currently recommended may result in high levels of 5-hydroxypyrazinoic acid, which is responsible for pyrazinamide induced hepatotoxicity (Shih *et al.*, 2013). On the other hand, there exist discrepancies in exposure between the weight bands; patients in the lower weight bands achieve lower drug exposures (McIlleron *et al.*, 2012; Sahota & Della Pasqua, 2012).

Despite interest in pyrazinamide, relatively few studies have described its pharmacokinetics (PK) longitudinally (Chigutsa, McIlleron, & Holford, 2010; Peloquin *et al.*, 1998; Wilkins *et al.*, 2006; Zhu *et al.*, 2002). We previously reported PK exposures of pyrazinamide in this cohort of HIV/TB-coinfected patients (McIlleron *et al.*, 2012). Here, we use a population modelling approach to describe changes in PK parameters during the first month of treatment and identify other factors affecting the PK. We then used parameter estimates of the final model to simulate exposures associated with a range of feasible doses for treatment of drug-susceptible TB and MDR-TB

4.3 Methodology

This report is a model-based secondary analysis of a study described before. The original report includes a detailed description of the study design, including patient selection, inclusion and exclusion criteria, informed consent, adherence monitoring, and blood sample collection (McIlleron *et al.*, 2012). Briefly, patients were administered 4-drug FDC tablets, each containing 150 mg of rifampicin, 75 mg of isoniazid, 400 mg of pyrazinamide, and 275 mg of ethambutol. Individual doses were adjusted based on body weight according to WHO guidelines (World Health Organization, 2003), with 51/61 patients receiving the medications daily from Monday to Friday and the remaining 10 every day of the week.

Pharmacokinetic blood sampling was performed on the 1st, 8th, 15th, and 29th day of TB treatment after an overnight fast. Samples were collected immediately before the dose and at 1, 2, 4, 6, 8, and 12 h post-dose. An additional sample was collected at approximately 12 h before the dose administered on the 15th day. Details of procedure and methods used for separation of plasma, storage of samples, and quantification of drug concentrations were as described in a previous report (McIlleron *et al.*, 2012). The lower limit of quantification for the assay was 0.2 mg/liter.

Pyrazinamide concentrations were described using nonlinear mixed-effects modelling using the software NONMEM 7.3 (Beal, Sheiner, Boeckmann, & Bauer, 2013) and the first-order conditional estimation method with eta-epsilon interaction (FOCE-I). Model diagnostics and documentation of model development were performed using Perl-speaks-NONMEM (PsN) version 3.7.6, Pirana version 2.9.2, and Xpose4 (R package) (Keizer, Karlsson, & Hooker, 2013). Additional plots were generated using R, version 3.2.1 (R Core Team, 2017), via RStudio, version 0.98.1091 (RStudio, 2014).

Model development

One- and two-compartment disposition models with first-order elimination and different absorption models, including first-order absorption with and without lag time and a more flexible transit compartment absorption (Savic, Jonker, Kerbusch, & Karlsson, 2007), were assessed. Plots of random effects of PK parameters were generated to identify trends in pharmacokinetic parameters with time on treatment. Three approaches to characterize the change in clearance over time were explored: estimating a separate value of clearance at each sampling day, an exponential increase in clearance from the first day to day 29 (exponential induction model), and linear increase in clearance from day 1 to day 29. The exponential induction model characterizing clearance on each day was parameterized using clearance on the first day ($CL_{day\ 1}$), change in clearance at day 29 ($\Delta CL_{day\ 29}$), and a half-life of the exponential process (t_{50}), as in equation 4.1. In the equation, the time variable for days on treatment went from 0 (day 1) to 28 (day 29).

$$\mathrm{CL_{day}} = \mathrm{CL_{day1}} + \left(\mathrm{CL_{day29}} - \mathrm{CL_{day1}}\right) \cdot \left(\frac{1 - \mathrm{e}^{\frac{-\ln(2)\cdot \mathrm{time}}{\mathrm{t_{50}}}}}{1 - \mathrm{e}^{\frac{-\ln(2)\cdot 28}{\mathrm{t_{50}}}}} \right) \tag{4.1}$$

The model with a linear increase in clearance was parameterized using clearance at baseline (day 1) and change in clearance on day 29 ($\Delta CL_{day\ 29}$), and the relationship is shown in equation 4.2. Similar to the exponential induction model, time on treatment was recorded from day 0 (day 1) to 28 (day 29).

$$\mathrm{CL_{day}} = \mathrm{CL_{day1}} + \left(\mathrm{CL_{day29}} - \mathrm{CL_{day1}}\right) \cdot \frac{\mathrm{time}}{28} \tag{4.2}$$

Allometric scaling was applied testing either total body weight (TBW) or fat-free mass (FFM) as a body size descriptor. The allometry exponents were either estimated or fixed to 0.75 for CL and 1 for V, as suggested by Anderson and Holford (Anderson & Holford, 2008). Individual values of FFM (FFM_i) were calculated using the following formula:

$$\mathrm{FFM_i} = \frac{\mathrm{WHS_{max}} \cdot \mathrm{Height}^2 \cdot \mathrm{Weight}}{\mathrm{WHS_{50}} \cdot \mathrm{Height}^2 + \mathrm{Weight}} \quad (4.3)$$

The maximal weight height squared (WHS_{max}) is 42.92 kg/m^2 for males and 37.99 kg/m^2 for females. The WHS_{50} has values of 30.93 kg/m^2 for males and 35.98 kg/m^2 for females (Janmahasatian *et al.*, 2005).

The typical value of bioavailability was fixed to a reference value of 1. Between-subject variability (BSV) and between-occasion variability (BOV) in the PK parameters were explored assuming log-normal distribution. An error model with both additive and proportional components was used to describe residual unexplained variability. Model building was guided by a change in objective function value (ΔOFV; assumed to be approximately χ^2 distributed), inspection of diagnostic plots, including prediction-corrected visual predictive check (PcVPC) (Bergstrand, Hooker, Wallin, & Karlsson, 2011), and physiological plausibility. The effect of $CD4^+$ count, viral load, early antiretroviral therapy (ART) initiation, alanine transaminase (ALT), albumin, creatinine clearance, and formulation on PK parameters was assessed by exploring proportional changes in parameter estimates per unit of difference from the median for continuous covariates or relative changes from a reference category for categorical variables as described by Mould and Upton (Mould & Upton, 2013). Creatinine clearance was calculated from serum creatinine using the Cockroft-Gault equation (Cockcroft & Gault, 1976). The precision of parameter estimates of the final model was evaluated using a nonparametric bootstrap method with replacement (n = 200).

The final PK model was then used to simulate steady-state pyrazinamide concentrations achieved during the treatment of drug-susceptible TB and MDR-TB after administration of feasible doses based on WHO-defined weight bands. Simulations (1,000 repetitions) were performed using demographic data of 870 tuberculosis patients obtained from PK studies

conducted in South Africa and West Africa (Chigutsa *et al.*, 2011; Diacon *et al.*, 2007; McIlleron *et al.*, 2012; Pepper *et al.*, 2010; Smythe, 2016; Wilkins *et al.*, 2008). For drug-susceptible TB, dosing strategies were assessed using the current weight bands and currently available FDC tablet sizes or additional 400-mg pyrazinamide tablets. For each dosing strategy, the proportion of patients achieving a target $AUC_{0–24}$ of 363 mg · h/liter in each weight band was determined (Pasipanodya *et al.*, 2013). In the simulations for MDR-TB, we used estimated PK parameters for day 1 of treatment to explore exposure associated with currently recommended doses: patients with between 33 and 50 kg receive 1,000 to 1,500 mg, while patients with weight between 51 and 70 kg and those above 70 kg receive 1,750 mg and 2,000 to 2,500 mg, respectively (World Health Organization, 2009). Using the same weight bands and available single-dose tablet sizes of 400 mg, 500 mg, and 750 mg, we explored exposure obtained under different dosing strategies and identified the dose at which comparable exposure is attained in the different weight bands. Additionally, the proportion of patients achieving an $AUC_{0–24}$ of 363 mg · h/liter was evaluated, since there is limited information on AUC/MIC pharmacodynamic index for MDR-TB. However, the MIC distributions for pyrazinamide do not seem highly variable between patients with drug-susceptible or MDR-TB. Zheng et al. reported MIC values ranging from 6.2 mg/liter to 400 mg/liter among MDR-TB patients, and among patients with drug-susceptible tuberculosis, Chigutsa et al. reported MIC values from 12.5 mg/liter to >100 mg/liter (Chigutsa *et al.*, 2015; Zheng *et al.*, 2016). Furthermore, using the clinical breakpoints suggested by Zheng et al. of 18.75 mg/liter and 37.5 mg/liter, associated with 4-month culture conversion and treatment success, respectively (Zheng *et al.*, 2016), and an $AUC_{0–24}$ of 363 mg · h/liter, the calculated AUC/MIC values are close to 11.3, as reported by Chigutsa et al. (Chigutsa *et al.*, 2015).

4.4 Results

Demographic characteristics. Pyrazinamide concentration data for 61 HIV/TB co-infected patients were available for analysis. Demographic characteristics of these patients have been reported previously (McIlleron *et al.*, 2012), and a summary is provided in Table 4.1. A total of 1,342 plasma samples were included in the analysis. One sample had a concentration below the lower limit of quantification and was discarded.

Table 4.1 Baseline characteristics of patients in TB-HAART (pyrazinamide model)

Characteristic or parameter	**Value**
Total no.	61
Females, *n* (%)	33 (54)
Receiving ART, *n* (%)	41 (67)
Treatment 5 days/week, *n* (%)	51 (84)
Age (yr)	32 (18–47)
Weight (kg)	55.2 (34.4–98.7)
Height (m)	1.59 (1.41–1.81)
FFM (kg)	42.2 (28.0–57.6)
Albumin (g/liter)	26 (15–43)
ALT (U/liter)	16 (5–44)
Creatinine (mol/liter)	74 (53–155)
Viral load (1,000) (copies/ml)	86 (0.05–13,000)
CD4 count (cells/liter)	254 (12–500)

[a] Values are expressed as median (range) unless otherwise specified.

Structural model and parameter estimates

Pyrazinamide pharmacokinetics was best described by a one-compartmental model with first-order elimination and transit compartment absorption. Table 4.2 shows the parameter estimates of the final model and their 95% bootstrap confidence interval. Clearance (CL) was found to increase by 14% on day 29 from a typical value of 3.35 liters/h on day 1, thus, day 29 clearance would be estimated at 3.83 liters/h (change in objective function value [ΔOFV] of -21 compared to a model with one estimate for clearance, 1 degree of freedom [df], and a P value of <0.001). This process was best described using a linear model, which was more parsimonious than estimating separate values of CL. The clearance estimates for day 1 and day 29 obtained using a linear model were similar to the ones obtained by estimating separate clearance values on the 4 days. The latter model estimated clearance values of 3.35 liters/h on day 1, 3.46 liters/h on day 8, 3.66 liters/h on day 15, and 3.82 liters/h on day 29. Using the arguably more biologically plausible exponential model did not significantly improve the fit and could not provide a robust estimate of the half-life of the induction, sometimes producing implausible results in the bootstrap analysis. The absorption process was best characterized using the transit compartment absorption, which provided significant improvement compared to simple first-order absorption with a delay using a lag (ΔOFV of -37, 1 df, P value of <0.001). On average, the time from drug ingestion to absorption is around half an hour and then is followed by very fast absorption. Large variability (>50%) in absorption between occasions was observed. The model also identified between-subject variability in clearance and bioavailability as well as between-occasion variability in clearance, bioavailability, and absorption mean transit time.

Table 4.2 Estimated parameter values from the final model for pyrazinamide (TB-HAART study)

Parameter	Estimate	Bootstrap 95% CI[a]	Shrinkage (%)
$CL/F_{day\ 1}$[b] (liter/h)	3.35	3.11–3.56	
$\Delta CL/F_{day\ 29}$ (%)	14.3	6.0–25.8	
V/F[b] (liter)	43.2	41.5–44.7	
k_a[e] (h^{-1})	3.54	3.0–4.27	
MTT[f] (h)	0.542	0.47–0.61	
NN[c]	28	7–52	
F[d]	1 fixed		
Between-subject variability (%)			
CL	16.3	11.0–20.0	12.8
F	10.7	7.6–13.2	18.5
Between-occasion variability (%)			
CL	13.3	10.0–15.4	31.5
F	11.9	8.5–15.5	13.5
k_a	84.0	79.7–97.5	30.3
MTT	52.9	40.1–68.7	39.9
Error			
Additive (mg/liter)	1.23	0.85–1.57	
Coefficient of variation (%)	4.4	2.8–5.4	

[a]CI, confidence interval.
[b]This parameter has been adjusted by allometric scaling, and the values reported refer to a subject with FFM of 42 kg (the median value of the cohort). The individual estimates for clearance and volume parameters were defined as $CL_i = \theta_{CL}(FFM_i/42)^{0.75} \cdot e^{(BSVCL\ +\ BOVCL)}$ and $V_i = \theta_v(FFM_i/42)^1$, respectively. θ_{CL} is the typical values for clearance and θ_v is the typical value for volume of distribution.
[c]NN, number of absorption transit compartments.
[d]F, bioavailability.
[e]k_a, absorption rate constant.
[f]MTT, mean transit time.

Inclusion of allometric scaling on CL and volume of distribution (V) using total body weight (TBW) improved the fit (ΔOFV of -13), but the better predictor to adjust PK for body size was fat-free mass (FFM), which dramatically reduced the OFV further when changed to FFM (ΔOFV of -37). Estimating allometry exponents did not result in a significant improvement in OFV and the estimated values were close to 0.75 for CL and 1 for V, hence the exponents were fixed to these literature values. After the inclusion of allometric scaling, the model could not detect any additional effect of $CD4^+$ count, viral load, early antiretroviral therapy (ART) initiation, alanine transaminase (ALT), albumin, creatinine clearance, and formulation. The

visual predictive check plot in Figure 9 shows that our model correctly describes the observed concentrations and captures the change in clearance over time.

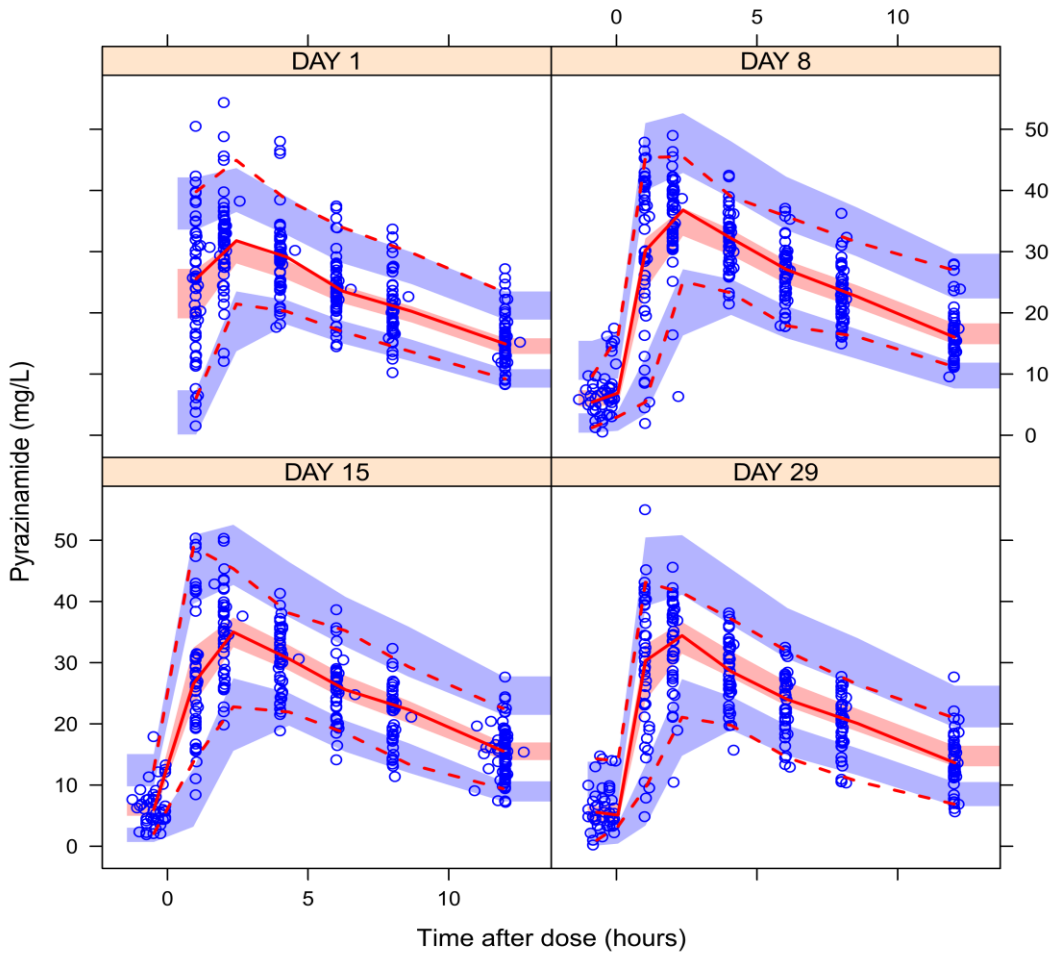

Figure 4.1 Visual predictive check for pyrazinamide model (TB-HAART study) stratified by treatment day Open circles are the observed concentrations. The middle continuous line is the 50th percentile of the observed data, and upper and lower dashed lines are the 97.5th and 2.5th percentiles of the observed data, respectively. The shaded regions represent the 95th prediction interval of the 2.5th, 50th, and 97.5th percentiles.

Monte Carlo simulations

The median weight, height, and FFM of the 870 patients with drug-susceptible TB were 53 kg (range, 30 to 102 kg), 1.65 m (range, 1.35 to 1.98 m), and 40.7 kg (range, 25.3 to 71.7 kg), respectively, with 45% being female. Figure 4.2 shows the simulated exposures at day 29 of treatment achieved under dosing strategies for the treatment of drug-susceptible TB. With the currently recommended weight-adjusted dose, patients in the lower weight bands are exposed to much lower levels of pyrazinamide, with patients of <38 kg being exposed to 42% lower $AUC_{0–24}$ than those weighing >70 kg.

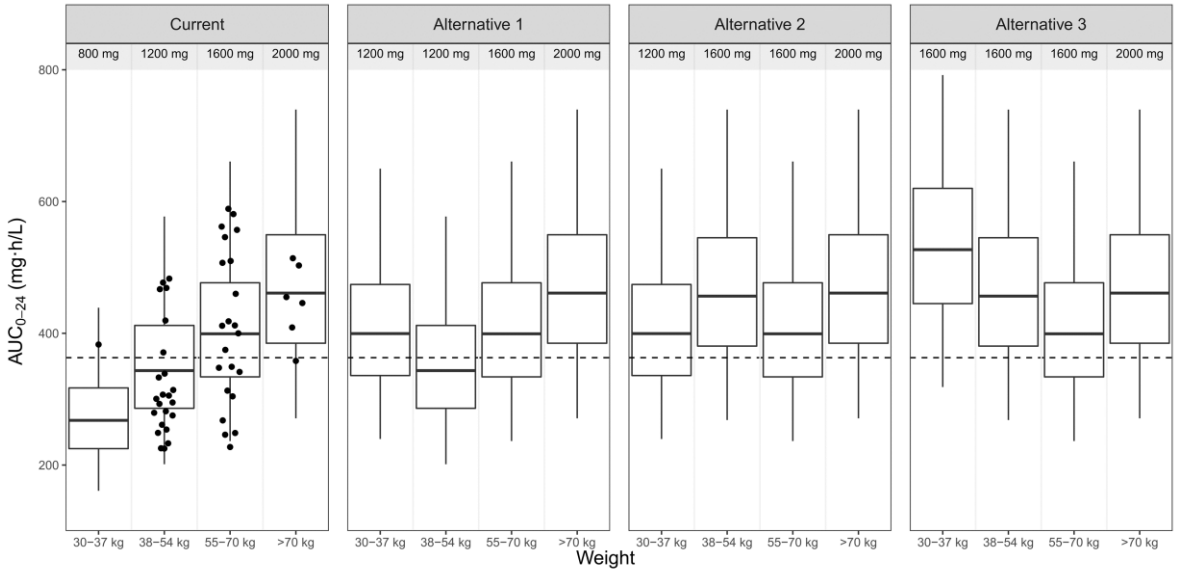

Figure 4.2 Box plots of simulated $AUC_{0–24}$ for currently recommended doses for drug-susceptible TB and 3 alternative dosing strategies, stratified by weight band (World Health Organization, 2003) Dots are the observed $AUC_{0–24}$ on day 29 of treatment. The dashed line represents an $AUC_{0–24}$ of 363 mg·h/liter. The dosing strategies used for the 30- to 37-, 38- to 54-, 55- to 70-, and >70-kg weight bands are 800 mg, 1,200 mg, 1,600 mg, and 2,000 mg for current doses. For alternative dosing strategy 1, patients weighing 30 to 37 kg receive 1,200 mg, while the doses for patients in the other weight bands are unchanged. For alternative 2, 1,200-mg and 1,600-mg doses are administered to patients weighing 30 to 37 kg and 38 to 54 kg, respectively, while other patients' dosing is unchanged. For alternative 3 dosing, 1,600 mg is administered to patients weighing 30 to 54 kg and dosing for other patients is unchanged.

The proportion of patients achieving a target $AUC_{0–24}$ of 363 mg h/liter in each weight band is presented in Table 4.3. The model predicts that at the current dose, only around 10% of the patients in the 30- to 37-kg weight band and 40% in the 38- to 55-kg weight band achieve the target exposure. Alternative dosing approaches minimizing the difference in exposure between weight bands without changing the weight bands are depicted in Figure 4.2. In the most balanced alternative, alternative 2 (administering 1,200 mg to patients in the 30- to 37-kg weight band and 1,600 mg to those in the 38- to 54-kg weight band; other patients' dosing remained unchanged), the highest median exposure would be in the >70-kg weight band while the lowest will be in the 55- to 70-kg weight band, resulting in a maximum difference in exposure of 16%. The simulations show that overall, 73% of the patients will achieve target exposure with alternative 2 dosing strategies compared to 51.5% for the current dosing strategy.

Table 4.3 Proportion of simulated patients with drug-susceptible TB achieving a target AUC_{0-24} of 363 mg·h/liter

Dose (mg)	Weight (kg)	Proportion (%)
800	30–37	11.4
1,200	30–37	64.6
	38–54	41.9
1,600	30–37	93.4
	38–54	80.4
	55–70	64.1
2,000	>70	81.5

Figure 4.3a and b show simulated concentrations for two typical male patients of weights of 34 kg and 46 kg achieved with the current dose and alternative dosing strategy 2. The two typical patients attain a maximum concentration of drug in serum (C_{max}) of at least 35 mg/liter when dosing is administered per alternative strategy 2. As shown in Figure 4.2, alternative dosing strategies 1 and 3 do not seem to minimize differences in exposure between weight

bands, and some patients in the lower weight bands would achieve extremely high exposure when dosed using the alternative strategy 3.

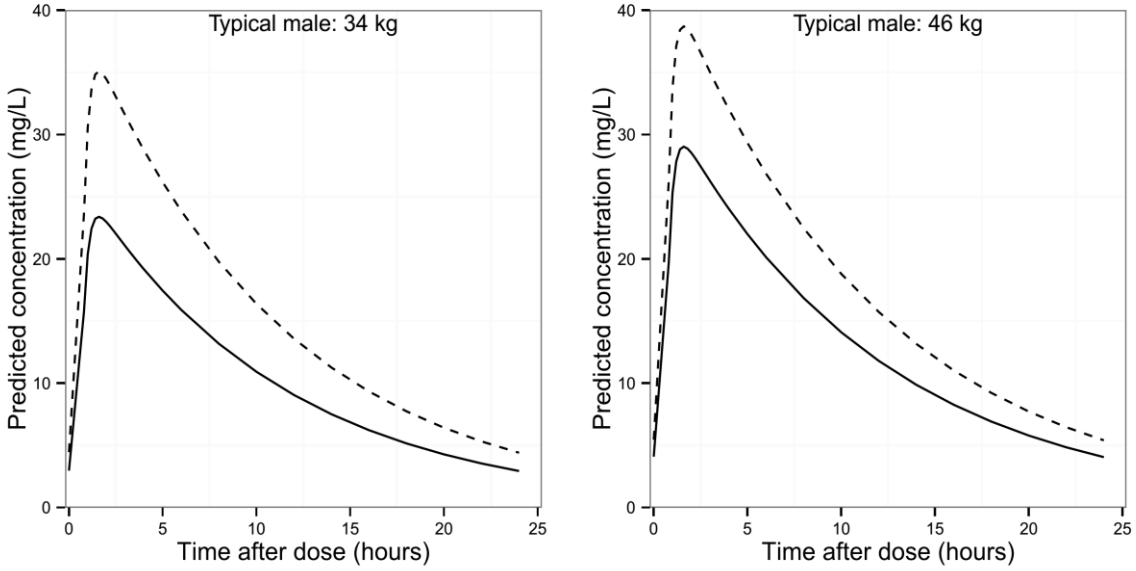

Figure 4.3 Predicted concentrations for typical male patients weighing 34 kg and 46 kg (a) Predicted concentrations for a typical male patient weighing 34 kg, receiving 800 mg (solid line) and 1,200 mg (dashed line). (b) Predicted concentrations for a typical male patient weighing 46 kg, receiving 1,200 mg (solid line) and 1,600 mg (dashed line)

Figure 4.4 shows simulated steady-state pyrazinamide $AUC_{0–24}$ achieved with doses within the recommended range of 1,000 mg to 2,500 mg for the treatment of MDR-TB. Simulations were performed using estimated PK parameters for day 1 without the increase in clearance, which may be due to co-administration with rifampicin. Pyrazinamide exposure associated with the currently recommended dose is only comparable if patients in the 33- to 50-kg weight band are administered 1,500 mg, while patients in the 51- to 70-kg and >70-kg bands receive 1,750-mg and 2,000-mg doses, respectively. These doses ensure that on average, at least 90% of patients in the three weight bands achieve an $AUC_{0–24}$ of at least 363 mg · h/liter. On the other hand, administering 1,000 mg or 1,200 mg to patients in the 33- to 50-kg weight band results in only 41% and 68% of them attaining an $AUC_{0–24}$ of 363 mg·h/liter.

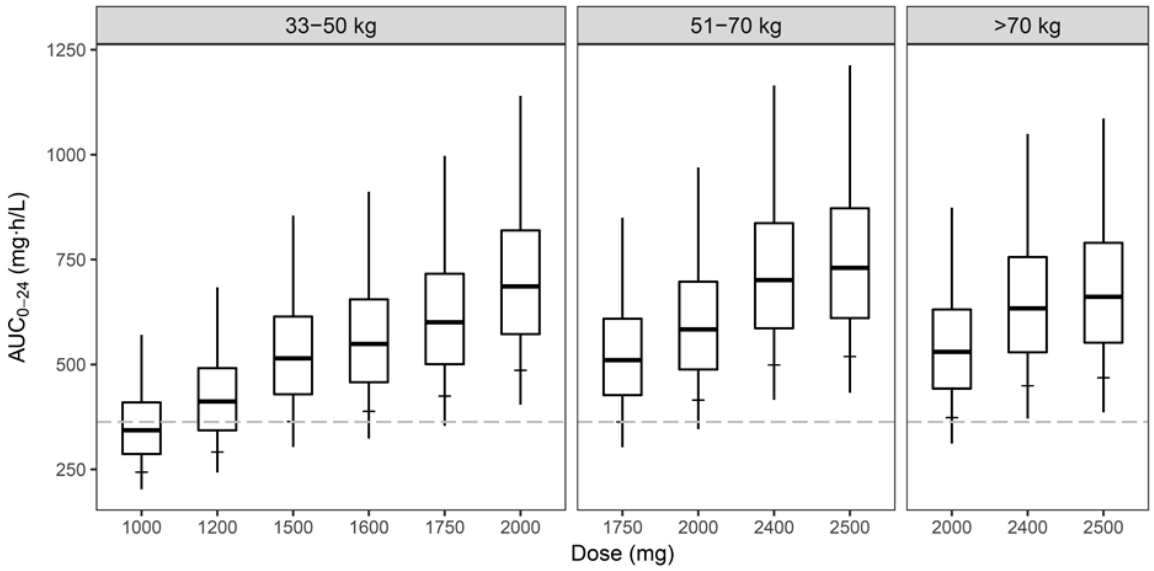

Figure 4.4 Box plots of simulated $AUC_{0–24}$ achieved during treatment of MDR-TB using the model without the increase in clearance over time, stratified by weight band and dose administered. Single-dose tablets of pyrazinamide were used in the simulations, with each tablet containing either 400 mg, 500 mg, or 700 mg. The minimum and maximum values of the box plots are the 2.5^{th} and 97.5^{th} percentiles, and the horizontal tick mark on each box plot shows the 10th percentile. The dashed line represents the $AUC_{0–24}$ of 363 mg·h/liter.

4.5 Discussion

We described the population pharmacokinetics of pyrazinamide among HIV/TB co-infected patients during the first month of treatment using nonlinear mixed-effects modelling. The model described an increase in pyrazinamide clearance with days on treatment (from day 1 to day 29) and identified FFM as the best predictor of the effect of body size on exposure compared to total body weight. Simulations were used to explore pyrazinamide exposure achieved with different dosing strategies for the treatment of drug-susceptible and multidrug-resistant TB.

FFM is calculated based on weight, height, and sex and was found to be superior to total body weight when included in the model via allometric scaling to capture the effect of body size on differences in CL/F and V/F (Anderson & Holford, 2008). Some previously proposed population PK models of pyrazinamide do not account for the effect of body size using allometric scaling (Wilkins *et al.*, 2006; Zhu *et al.*, 2002). One of these, by Wilkins et al. (Wilkins *et al.*, 2006), described a linear effect of weight on both CL/F and V/F and also reported higher V/F in males than females (16% more). More recently, Chigutsa et al. (Chigutsa, McIlleron, & Holford, 2010) proposed a model incorporating allometric scaling using total body weight and reported larger bioavailability in women. When we accounted for body size using total body weight instead of FFM, the model estimated bioavailability among females to be 26% higher, the same effect observed by Chigutsa et al. Both results discussed above are consistent with ours, although the covariate effects were accounted for differently. By using allometric scaling to explain variability in body size, we apply a well-known concept without estimating any additional parameters (Anderson & Holford, 2008). We believe that this strategy, also applied by Denti et al. (Denti, Jeremiah, *et al.*, 2015) and Rockwood et al. (Rockwood *et al.*, 2016), of describing the differences as being due to differences in size and body composition is both more parsimonious and physiologically plausible. Furthermore, this strategy has also been reported for other drugs in the FDC (Chirehwa *et al.*, 2016; Denti, Jeremiah, *et al.*, 2015;

Geiseler, Manis, & Maddux, 1985; Rockwood *et al.*, 2016; Smythe *et al.*, 2012); hence, dosing regimens using current FDCs could be modified to take into account the variability in body size and composition.

Clearance of pyrazinamide was found to increase from the first day to day 29. The increase in clearance with time on treatment has been described by Smythe and Denti et al., with a later report of a 16% increase among Tanzanian patients, which is close to our 14% (Denti, Jeremiah, *et al.*, 2015; Smythe, 2016). Smythe reported a higher increase (30%) in clearance from the first day to steady state in a cohort of TB patients from West Africa. The exact mechanism driving this change needs further investigation, and a number of reasons might explain this. Rifampicin is a potent inducer of a large number of metabolic pathways via PXR (Chen & Raymond, 2006). Induction of microsomal deamidase and xanthine oxidase enzymes responsible for pyrazinamide metabolism by rifampicin might explain the observed result. Tuberculosis has been reported to lower drug-metabolizing capacity in animals (Batra, Venkitasubramanian, & Raj, 1987), hence, treatment and improvement of the disease symptoms may enhance drug metabolism and other body functions, consistent with the observed increase in pyrazinamide clearance. Our estimated value of CL/F on day 29 is comparable to those reported in other studies, conducted in healthy volunteers, TB patients, and HIV/TB-coinfected patients (Peloquin *et al.*, 1997; Wilkins *et al.*, 2006; Zhu *et al.*, 2002). However, when predicting appropriate doses for patients with MDR-TB, we assumed a constant clearance over time, as the regimens used do not contain Rifampicin and the response to treatment is generally more gradual with the weaker second-line regimens than for patients with drug-susceptible TB.

Parameter estimates of the final model were used to simulate pyrazinamide exposure under different dosing schemes so as to achieve comparable $AUC_{0–24}$ values across weight bands.

Consistent with the previous noncompartmental analysis (NCA) of the data (McIlleron *et al.*, 2012), our model predicted that patients in lower weight bands attain lower drug exposures than those in the 55- to 70-kg weight band despite administering similar weight-adjusted doses. Disease severity is associated with low body mass index (Van Lettow *et al.*, 2004). Lower pyrazinamide exposure among these patients is likely to be even more critical and is associated with poor treatment outcomes (Chideya *et al.*, 2009; Pasipanodya *et al.*, 2013). Alternative doses for the treatment of drug-susceptible TB suggested in this report are based on the current weight bands and available FDC tablet sizes or single pyrazinamide tablets, each at a strength of 400 mg. Implementation of a fixed pyrazinamide dose of 1,500 mg as proposed by Sahota and Della Pasqua might be challenging under the current FDC therapy. Moreover, while desirable in terms of simplification, it implies reducing exposures of pyrazinamide and other drugs among patients with weight greater than 54 kg, thereby increasing the risks of poor treatment outcomes (Sahota & Della Pasqua, 2012). The distribution of model predicted $AUC_{0–24}$ suggests that adding 400 mg of pyrazinamide to the current FDC for patients with weights less than 55 kg (alternative dosing strategy 2) would achieve more uniform exposures across weight bands and increase the proportion of patients attaining an $AUC_{0–24}$ of 363 mg·h/liter. The same dosing strategy will result in the majority of patients attaining a C_{max} of 35 mg/liter, which was found to be associated with favourable treatment outcomes (Chideya *et al.*, 2009). McIlleron et al. reported reduced exposure to drugs in FDC among patients who are male or with low weight (McIlleron *et al.*, 2012), hence our proposed optimal dosing strategy could be transferable to other drugs of the FDC. Another advantage of the proposed dosing strategy is the reduction of weight bands from 4 to 3, where the 38- to 54-kg and 55- to 70-kg weight bands are combined. There would be a slight gain in the proportion of patients achieving the target $AUC_{0–24}$ overall under the alternative dosing strategy 3 compared to alternative 2, but the risk of hepatotoxicity could be elevated for patients in the 30- to 37-kg weight band treated under the alternative dosing strategy 3, who would be administered between 42 and 53 mg/kg doses (US Public Health Service, 1959).

The currently recommended pyrazinamide dose of 30 to 40 mg/kg results in disparate exposure among patients with MDR-TB (World Health Organization, 2009). Moreover, a significant proportion of patients treated according to the recommended dose do not achieve the therapeutic $AUC_{0–24}$ of 363 mg·h/liter identified for drug-susceptible TB. Assuming availability of 400-, 500-, and 750-mg tablet sizes, our simulations predict that prescription of doses at the higher end of the recommended range for low-weight patients will help minimize the differences in exposure between weight bands. Our proposed optimal dosing strategy of 1,500 mg for patients in the 33- to 50-kg weight band, 1,750 mg for patients weighing up to 70 kg, and 2,000 mg for heavier patients ensures that exposures between weight bands are comparable. Furthermore, the strategy guarantees that 90% of MDR-TB patients achieve exposures of >363 mg·h/liter.

The model presented here has some limitations. A simple linear change in clearance over time from initiation of treatment was assumed, hence limiting our capacity to extrapolate from our results beyond those observed on day 29. On the other hand, since the values of CL on day 29 are similar to those of prior reports, one can speculate that the change in clearance after the first month is not as large as the one observed in the first month of treatment. Our simulations were based on the assumption of first-order elimination. Since pyrazinamide is eliminated mainly as metabolites through multiple pathways (Chigutsa, McIlleron, & Holford, 2010; Lacroix, Tranvouez, Phan Hoang, *et al.*, 1990), if one or more of these pathways were to saturate at higher doses, the model may be underpredicting exposure in lower weight bands. The model developed was based on PK from a single study population. However, demographic characteristics broadly representing an African population were used in the simulations to account for a key covariate effect (FFM) during simulations, hence the use of FFM values outside the range that was used to optimize parameter estimates of the model. The demographic characteristics of patients with drug-susceptible TB were assumed to be similar to those of MDR-TB patients in the simulations, but there could be differences between

the two groups of patients in terms of disease chronicity and severity that may influence pharmacokinetics and pharmacokinetic targets. Another limitation of the study is the nonavailability of MIC distribution for calculation of AUC/MIC ratio as a pharmacodynamic index. However, the range of MICs for drug-susceptible and MDR-TB are comparable as reported by Chigutsa et al. and Zheng et al., respectively (Chigutsa *et al.*, 2015; Zheng *et al.*, 2016). Regardless of the therapeutic index used (AUC or AUC/MIC), the target will be affected by activity of concomitant drugs as well as the synergy or antagonism with pyrazinamide, demonstrated with rifampicin and bedaquiline (Chigutsa *et al.*, 2015; Field, 2015).

In conclusion, our data in patients on the standard rifampicin-based first-line regimen suggest that there is an increase in clearance of pyrazinamide during the first month of treatment. The currently recommended doses of pyrazinamide result in different levels of exposure among patients in the different weight bands. More uniform exposures with more patients attaining target exposures would be achieved by adding 400 mg to the dose for patients weighing between 30 and 54 kg. Reduced exposure to other drugs of the FDC has been reported among patients with low weight; hence, alternative 2 dosing strategy could be applied to all four drugs by adding one FDC tablet. While it is necessary to confirm our findings in patients with MDR-TB, our analysis suggests that average pyrazinamide exposure in different weight bands could be made uniform by administering 1,500 mg to those with weights of at most 50 kg and 1,750 mg and 2,000 mg to those in the 51- to 70-kg and >70-kg weight bands, respectively.

Chapter 5: Effect of efavirenz-based antiretroviral therapy on pharmacokinetics of isoniazid and acetyl-isoniazid

5.1 Abstract

Objectives

To describe the pharmacokinetics of isoniazid and acetyl-isoniazid in TB/HIV co-infected patients, and assess the effect of efavirenz co-administration and a 50% increase in dose of rifampicin on pharmacokinetic parameters.

Methods

TB/HIV co-infected patients participating in the three-treatment arm RAFA randomised controlled trial conducted in West Africa were recruited into the pharmacokinetic sub study. Five serial blood samples were collected on a single visit at between four and eight weeks after initiation of antituberculosis treatment. Concentration-time data for isoniazid and acetyl-isoniazid were analysed using nonlinear mixed-effect modelling.

Results

Isoniazid concentrations from 150 patients were available for analysis, and 79 of these (53%) also had concentrations of acetyl-isoniazid. Isoniazid pharmacokinetics was best described using a two-compartment disposition model with first-order absorption and elimination using a semi-mechanistic model describing hepatic extraction. The model could identify two elimination pathways, separating formation of acetyl-isoniazid from other routes of metabolism. The elimination route for the formation of acetyl-isoniazid was best described using a mixture model with fast and slow acetylator status. In patients classified as fast acetylators who started efavirenz-based antiretroviral therapy at two weeks after antituberculosis treatment initiation, clearance of isoniazid was increased by 54%.

Conclusions

Co-administration of isoniazid and efavirenz-based antiretroviral therapy results in reduced exposure to isoniazid. Efavirenz-based antiretroviral therapy affects the acetylation metabolic pathway, and the mechanism of action will require further investigation. Pharmacokinetics of isoniazid and acetyl-isoniazid were not influenced by a 50% higher dose of rifampicin.

5.2 Introduction

Isoniazid is part of a four-drug Fixed-Dose Combination (FDC) for the treatment of drug-susceptible tuberculosis (TB) which also includes rifampicin, pyrazinamide and ethambutol (World Health Organization, 2003). The currently recommended daily dose of isoniazid is 5 mg/kg (4–6 mg/kg)(World Health Organization, 2010c), administered with the aim of achieving maximum concentrations of 3 to 6 mg/L (Alsultan & Peloquin, 2014b). The drug has excellent early bactericidal activity (EBA) mostly against rapidly metabolising and replicating bacilli (Donald *et al.*, 1997). In an EBA study, a steady-state area under the concentration-time curve (AUC) of 10.52 mg·h/L achieved 90% of the maximum bactericidal activity (Donald *et al.*, 2007). In addition, isoniazid is also effective in preventing resistance to companion drugs in the FDC (Donald & Schaaf, 2011; Mitchison, 2000).

The major metabolic pathways for isoniazid include acetylation via the N-acetyltransferase 2 (NAT2) pathway to form acetyl-isoniazid, and hydrolysis to produce isonicotinic acid (Ellard, 1976; Ellard & Gammon, 1976). Polymorphisms in NAT2 confer high interindividual variability in isoniazid exposure and are associated with fast, intermediate and slow phenotypes (Parkin *et al.*, 1997). Exposure among fast acetylators is on average between 5-6 times lower than slow acetylators (Ellard & Gammon, 1976). Information on acetylator genotype is not always available, and mixture models are often used to classify patients into the different metabolic groups (Wilkins *et al.*, 2011). Interindividual variability in isoniazid due to NAT2 polymorphisms may be associated with the emergence of multi-drug resistant tuberculosis, treatment failure or relapse and reduced bactericidal activity (Donald *et al.*, 2004; Pasipanodya, Srivastava, & Gumbo, 2012). Regardless of the acetylator status, variability in isoniazid pharmacokinetics is also attributed to drug-drug interactions, weight, sex, health conditions, and formulation (Babalik *et al.*, 2013; Bhatt *et al.*, 2014; McIlleron *et al.*, 2012; Wilkins *et al.*, 2011). TB/HIV co-infected patients receiving antituberculosis therapy and antiretroviral therapy (ART) are at risk of drug-drug interactions, and results of a non-compartmental analysis of a study conducted

in Mozambique showed a 29% reduction in isoniazid exposure when co-administered with efavirenz based ART (Bhatt *et al.*, 2014).

We have found only one publication describing the integrated population pharmacokinetics of isoniazid and acetyl-isoniazid. However, the study was conducted among healthy volunteers who may have different absorption and distribution profile compared to tuberculosis patients with or without HIV (Seng *et al.*, 2015a). In this study, we describe the pharmacokinetics of isoniazid and acetyl-isoniazid among TB/HIV co-infected patients recruited in a trial that mimicked a routine clinical setting and evaluated the effect of efavirenz-based ART and a 50% increase in dose of rifampicin.

5.3 Methods

Study design and patient selection

The RAFA study was a three-arm randomised controlled study designed to assess the effect of timing of antiretroviral therapy and high dose (+50%) of rifampicin on patient survival and tuberculosis treatment outcomes among TB/HIV co-infected and treatment naïve patients. Patients in arm A started efavirenz-based ART at two weeks after initiating antituberculosis treatment whereas those in arm B and C started antiretroviral therapy after eight weeks of TB treatment. Patients in arm C received a 50% higher dose of rifampicin in the first eight weeks of TB treatment. Patients were included in the study if they were aged 18 or above, had a positive HIV test result, had a CD4+ lymphocyte count of at least 50 cells/µL, had recently been diagnosed with tuberculosis (with bacteriological or molecular evidence) and were ART naïve. Women were excluded from the study if they were pregnant, lactating, or unwilling to use contraception. Other criteria used for exclusion include HIV-2 infection, recreational drug and alcohol abuse, and laboratory values outside the normal ranges defined by the National Institutes of Health, excluding patients with up to grade three anemia (National Institute of Allegy and Infectious Diseases, 2001).

Antituberculosis treatment was administered as a four-drug FDC according to WHO weight band-based guidelines (World Health Organization, 2010c). Each tablet contained 75 mg of isoniazid, 150 mg of rifampicin, 400 mg of pyrazinamide and 275 mg of ethambutol. Patients in arm C received additional 150 mg single dose tablet(s) of rifampicin together with the standard dose of FDC tablets to attain a dose of 15 mg/kg of body weight. A dose of 600 mg of efavirenz was administered to patients regardless of body weight. All patients received co-trimoxazole preventive therapy at the start of TB treatment as recommended by WHO (World Health Organization, 2010a).

Specimen collection and drug quantification

Between four and eight weeks after antituberculosis treatment initiation, patients were admitted overnight before PK sampling. Five serial blood samples were drawn pre-dose (approximately 15 mins before a dose), and at 2, 3, 6, and 10 hours post-dose. Blood samples were processed and plasma stored immediately at -80°C before transfer on ice to the analytical laboratory (Division of Clinical Pharmacology, University of Cape Town, South Africa) for analysis. Isoniazid and acetyl-isoniazid were analysed with a validated liquid chromatography tandem mass spectrometry assay developed at the laboratory. Samples were processed with a protein precipitation extraction method using isoniazid-d4 and acetyl-isoniazid-d4 as internal standards, followed by high-performance liquid chromatography with MS/MS detection using an AB SCIEX API 3000 instrument. The analyte, metabolite, and internal standards were monitored at mass transitions of the protonated precursor ions m/z 138.11, m/z 180.16, m/z 142.21 and m/z 184.21 to the product ions m/z 79.10, m/z 121.10, m/z 83.10 and m/z 83.20 for isoniazid, acetyl-isoniazid, isoniazid-d4 and acetyl-isoniazid-d4, respectively. The calibration curves fitted quadratic (weighted by 1/concentration) regressions over the ranges 0.102 to 26.0 mg/L for isoniazid and 0.0501 to 25.6 mg/L for acetyl-isoniazid. The combined accuracy (%Nom) and precision (%CV) statistics of the limit of quantification, low, medium, and high-quality controls (3 validation batches, N=18) of the analyte and metabolite were between 92.2% and 107%, and 2.9% and 10.9%, respectively.

Pharmacokinetic data analysis

Isoniazid and acetyl-isoniazid pharmacokinetic data were interpreted using nonlinear mixed-effects modelling in the software NONMEM version 7.3 and the algorithm First-Order Conditional Estimation with eta-epsilon interaction (FOCE-I)(Beal, Sheiner, Boeckmann, & Bauer, 2013). Pearl-Speaks-NONMEM (PSN) version 3.7.6, Pirana version 2.9.6, and R (Xpose4 package) software were used to interact with NONMEM, track model development, and evaluate model diagnostics, respectively (Keizer, Karlsson, & Hooker, 2013). R version

3.2.3 was used for data manipulation, generating additional plots and post-modelling analysis using RStudio interface version 0.99.903 (R Core Team, 2017; RStudio, 2014).

Model development was performed in a stepwise manner, starting with the structural pharmacokinetic model for isoniazid and then incorporating the pharmacokinetic model for acetyl-isoniazid. One- and two-compartment disposition models together with a liver compartment to capture the first-pass effect were explored to describe the pharmacokinetics of isoniazid (Gordi *et al.*, 2005). Information on each patient's acetylator genotype was not available, and a mixture model with two or three sub-populations was investigated to classify patients into different acetylator phenotypes (Frame, 2007). Allometric scaling was applied to all clearance and volume of distribution parameters (exponent fixed to 0.75 for clearance and 1 for volume) for both isoniazid and acetyl-isoniazid to account for the effect of body size using either total body weight (TBW), fat-free mass (FFM) or body fat (Anderson & Holford, 2008). Both the mixture model on clearance of isoniazid and allometric scaling were included since the early phases of model development, as there is strong evidence supporting their effect on the pharmacokinetics of isoniazid (Denti, Jeremiah, *et al.*, 2015; Parkin *et al.*, 1997). Absorption of isoniazid was described using a first-order absorption model, with or without a delay using a lag time or a chain of transit compartments (Savic, Jonker, Kerbusch, & Karlsson, 2007). Bioavailability of isoniazid was fixed to a reference value of 1 and variability was included. Clearance of isoniazid was assumed to be either via a single metabolic pathway or two metabolic pathways, with one being responsible for the formation of acetyl-isoniazid. The pharmacokinetics of acetyl-isoniazid were described using either a one- or two-compartment disposition model and first-order elimination from the central compartment. Concentrations of isoniazid and acetyl-isoniazid were measured in mg/L, and a correction factor was included to adjust for differences in molecular weight at the formation of acetyl-isoniazid (179.18 g/mol for acetyl-isoniazid vs. 137.139 g/mol for isoniazid) (Zannikos & Argenti, 2004).

A log-normal distribution was assumed for the between-subject variability (BSV) and between-occasion variability (BOV) of the pharmacokinetic parameters. To account for the uncertainty in reported dosing time for the dose administered the day before PK sampling, inclusion of a scaling parameter on BOV in bioavailability was investigated. Residual unexplained variability defined separately for isoniazid and acetyl-isoniazid comprised both additive and proportional components. Concentrations below the lower limit of quantification (LLOQ) for both isoniazid and acetyl-isoniazid were provided by the laboratory and included in the analysis. Undetectable concentrations of isoniazid and those below 0.01 mg/L, which corresponds to 10% of the LLOQ value, were censored at 10% of the LLOQ, and half the censoring value was imputed as suggested by Beal 2001 (Beal, 2001). A similar approach was applied to undetectable concentrations of acetyl-isoniazid and those below 0.005 mg/L. The minimum value of the additive error for both isoniazid and acetyl-isoniazid was fixed to 20% of the respective LLOQ value.

The effects of physiologically plausible covariates including early initiation of ART, high dose rifampicin, creatinine clearance, drug batch of FDC tablets, alanine transaminase (ALT), and study site on the PK parameters were investigated in the model. Covariate effects resulting in a significant drop in objective function value (OFV) and improvement in goodness of fit (GOF) plots, were retained in the model. A drop in OFV of 3.84 associated with 1 degree of freedom for a chi-squared distribution was considered for statistical significance. A nonparametric bootstrap (n=300, with replacement) was applied to evaluate the robustness of the parameter estimates by computing the 95% confidence intervals. Model derived individual exposures were extracted from the final model and presented for different strata of significant covariates including metabolic status.

Ethics

Ethics approval for the study was provided by the University of Cape Town in South Africa, London School of Hygiene and Tropical Medicine, and the national ethical commitees of Benin and Guinea.

5.4 Results

Patient characteristics

A total of 222 patients were recruited for the pharmacokinetic sub-study of the RAFA randomised controlled trial in Benin and Guinea. Plasma samples from 72 patients were temporarily thawed due to a freezer failure, and stability tests showed that isoniazid concentrations could not be reliably quantified in these samples. Thus, only data from the remaning 150 patients were included in the analysis. Table 5.1 shows the baseline characteristics of the 150 patients. The median weight, height and FFM were 52 kg, 1.7 m and 43.5 kg respectively. Of the 150 patients, 40 (26%) started ART at two weeks after initiating antituberculosis treatment, and 79 (53%) were randomised to high dose rifampicin. A total of 745 plasma isoniazid concentrations and 390 plasma acetyl-isoniazid concentrations from the 150 patients were included in the PK analysis. Concentration of isoniazid could not be detected in 12% of the plasma samples (concentrations were less than the sensitivity of the spectrometer), and 83% of these were pre-dose whereas acetyl-isoniazid was detected in all samples.

Table 5.1 Baseline characteristics of patients with isoniazid concentrations (RAFA study)

Characteristic	Value[a]
Total No.	150
No. (%) of females	56 (37.3)
No. (%) in early ART arm	40 (26.7)
No. (%) in high dose rifampicin arm	70 (46.7)
Weight, kg	51 (33–87)
Height, m	1.7 (1.4–1.94)
FFM, kg	43.3 (24.8–65.3)
Age, years	38 (19–65)
$CD4^+$ cells/µL	167 (51–772)
Viral load, copies/mL ($x10^3$)	150 (0.08–10000)
Serum creatinine, µmol/L	89 (23–212)
Haemoglobin level, g/dL	9.35 (5.2–15.9)
ALT, units/L	26 (3–97)
White blood cells, $x10^9$/L	7 (2.6–26.2)
Platelets, $x10^9$/L	339 (124–832)

[a] Unless otherwise indicated, the median (range) values are presented.

Isoniazid and acetyl-isoniazid pharmacokinetics

Figure 5.1 shows the schematic diagram of the final integrated model for isoniazid and acetyl-isoniazid pharmacokinetics. Isoniazid pharmacokinetics was best described using a two-compartment disposition model. A mixture model was incorporated in the base model to describe the multimodal distribution of isoniazid clearance. Our model could only separate fast and slow acetylator status and estimated the proportion of fast acetylators to be 50%. A mixture model with three sub-populations for isoniazid clearance was not significantly different from the one with two sub-populations. The

inclusion of a liver compartment to capture hepatic extraction including first-pass effect improved the model (ΔOFV= -9, no extra parameter was estimated). The model could also separate acetylation, which leads to the formation of acetyl-isoniazid, from other routes of elimination (OFV= -143, one additional parameter, p-value<0.001). The pharmacokinetics of acetyl-isoniazid followed a two-compartment disposition model with first-order elimination.

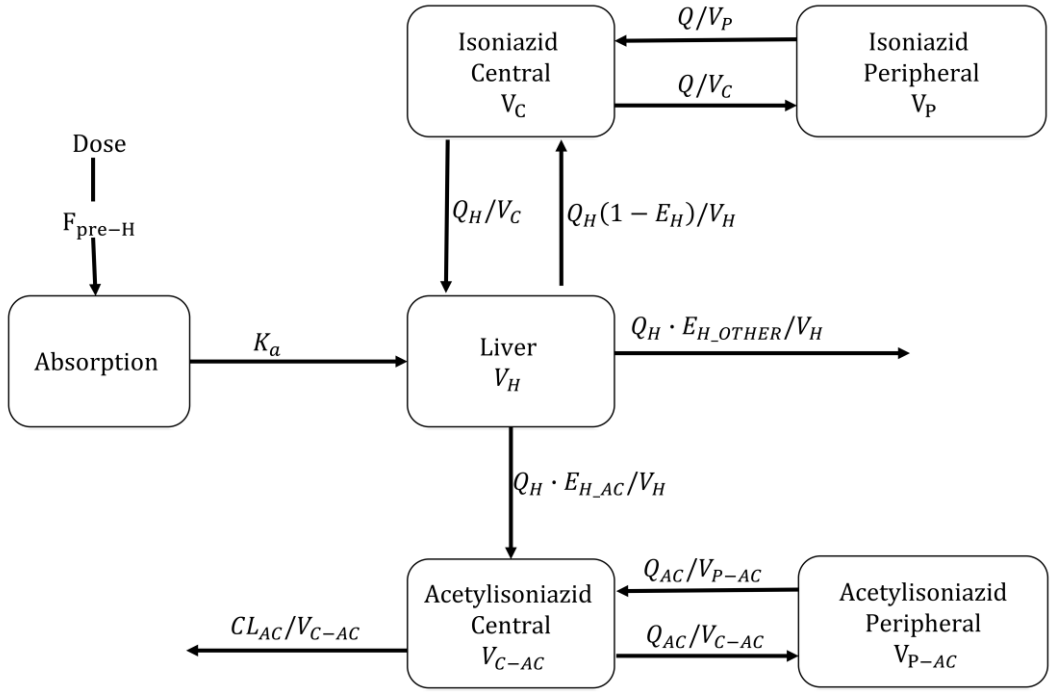

Figure 5.1 Schematic diagram of the model describing the pharmacokinetics of isoniazid and acetyl-isoniazid F_{pre-H}, pre-hepatic bioavailability; Ka, absorption rate constant; E_H, hepatic extraction; E_{H_AC}, hepatic extraction to acetyl-isoniazid via acetylation; E_{H_OTHER}, hepatic extraction to via other routes of metabolism; V_C, volume of central compartment for isoniazid; V_P, volume of peripheral compartment for isoniazid; V_{C-AC}, volume of central compartment for acetyl-isoniazid; V_{P-AC}, volume of peripheral compartment for acetyl-isoniazid; V_H, volume of liver; Q, inter-compartmental clearance for isoniazid; Q_{AC}, inter-compartmental clearance for acetyl-isoniazid; Q_H, hepatic plasma flow; CL_{AC}, clearance for acetyl-isoniazid.

Pre-hepatic bioavailability was fixed to a reference value of 1 for a typical individual and varied between the two occasions in the dataset (one occasion for pre-dose

samples and another for post-dose samples). The typical values for the volume of the liver and hepatic plasma flow were fixed to 1 L and 50 L/h respectively, and the unbound fraction of isoniazid was fixed to 95% (Clemmesen, Tygstrup, & Ott, 1998; Sturkenboom *et al.*, 2015). Sensitivity analysis was performed on the values for liver plasma flow and unbound fraction to assess their effect on overall conclusion. Allometric scaling was applied to all clearance and volume parameters including that of the liver and peripheral compartments using FFM, which was superior to total body weight (ΔOFV= -14, no extra parameter was estimated). All typical values for clearance and volume parameters refer to a patient with FFM of 43 kg, the median value in the cohort.

Table 5.2 shows the parameter estimates from the final model and the associated precision obtained using a 300-sample nonparametric bootstrap. The visual predictive check displayed in Figure 5.2 provides evidence that the model describes the observed data adequately. The model estimated that the average intrinsic clearance via acetylation was around 6-fold higher for fast compared to slow metabolisers. Acetylation is the major route of elimination for the fast metabolisers contributing about 75% of the total clearance, while around a third of the clearance among slow metabolisers is due to acetylation. Patients classified as fast acetylators and receiving efavirenz-based ART at two weeks after initiation of antituberculosis treatment had 54% higher intrinsic clearance compared to ART naïve patients for the pathway associated with the formation of acetyl-isoniazid (ΔOFV= -9, one additional parameter, p-value<0.002). The effect of efavirenz-based ART on clearance of isoniazid via acetylation in patients classified as slow acetylators was not supported in the model and clinically insignificant (p-value>0.05, 5% increase in clearance). There was no

effect of efavirenz-based ART on the clearance component not associated with acetylation. While the increased dose of rifampicin did not affect isoniazid PK, our model detected a 61.6% reduced bioavailability in all 28 patients who were treated with two of the drug batches (ΔOFV= -106, one additional parameter, p-value<0.001). Of these patients, 70% were in the high-dose rifampicin treatment arm whereas, 11% and 18% were in the early ART and standard treatment arms, respectively. The proportion of patients who received tablets from the two batches did not differ by acetylator status (20% and 18% among slow and fast acetylators respectively). Regardless of acetylator status and whether patients received tablets for batches with reduced bioavailability, the distribution of clearance due to acetylation and that of other metabolic pathways was similar.

Table 5.2 Parameter estimates of the final model for isoniazid and acetyl-isoniazid

Parameter	Estimate (95% CI)[a]	Variability (BSV)
Isoniazid		
Clearance (L/h)		
Acetylation: Fast[b,c]	35.9 (30.1; 45.1)	35.6 (28.6; 41.8)
Acetylation: Slow[b,c]	6.64 (5.55; 8.39)	35.6 (28.6; 41.8)
Other pathways[c]	11.4 (9.11; 13.3)	34.6 (17.7; 45.4)
Central volume (L)[c]	47.7 (40.8; 56.3)	18.9 (8.29; 27.7)
Inter-compartmental clearance (L/h) [c]	4.8 (0.73; 11.5)	
Peripheral volume (L) [c]	8.14 (5.06; 247)	
Absorption constant (/h)	1.59 (1.36; 2.09)	36.7 (22.9; 54.3)
Absorption lag (h)	0.287 (0.202; 0.59)	
Pre-hepatic bioavailability[d]	1 FIXED	16.9 (12.4; 22.8)[e]
Proportion of fast acetylator (%)	50.1 (40.5; 59.0)	
Efavirenz effect on acetylation clearance in fast acetylors (%)	54.1 (23.2; 97.8)	
Drug batch effect on bioavailability (%)	-62.1 (-66.7; -57.0)	
Proportional error (%)	11.2 (9.55; 12.6)	
Additive error (mg/L)	0.02 FIXED	
Acetyl-isoniazid		
Clearance (L/h) [c]	6.77 (5.78; 7.87)	17.5 (13.9; 21.3)
Central volume (L) [c]	34.4 (30.5; 40.1)	
Inter compartmental clearance (L/h) c	0.506 (0.323; 1.42)	
Peripheral volume (L) c	81.4 (19.8; 991)	
Proportional error (%)	5.25 (3.9; 6.49)	
Additive error (mg/L)	0.013 (0.01; 0.019)	

[a]Obtained with a non-parametric bootstrap (n=300).

[b]Intrinsic CL of isoniazid when given without efavirenz.

[c]All CL and volume parameters have been allometrically scaled with FFM, and the typical values reported here refer to the typical patient, with FFM of 43.5 kg.

[d]Pre-hepatic bioavailability is the fraction of the drug that is absorbed, crosses the gut wall unchanged, thus entering the portal vein and reaching the liver.

[e]Between occasion variability (BOV)

Between-subject variability in clearance attributed to acetylation was slightly higher compared to other routes of metabolism. A large improvement in model fit (ΔOFV= -37, one additional parameter, p-value<0.001) was observed after separating between-subject variability by the route of metabolism. Inclusion of the effect of the high-dose rifampicin arm on pharmacokinetics of isoniazid was not significant and did not improve the model fit.

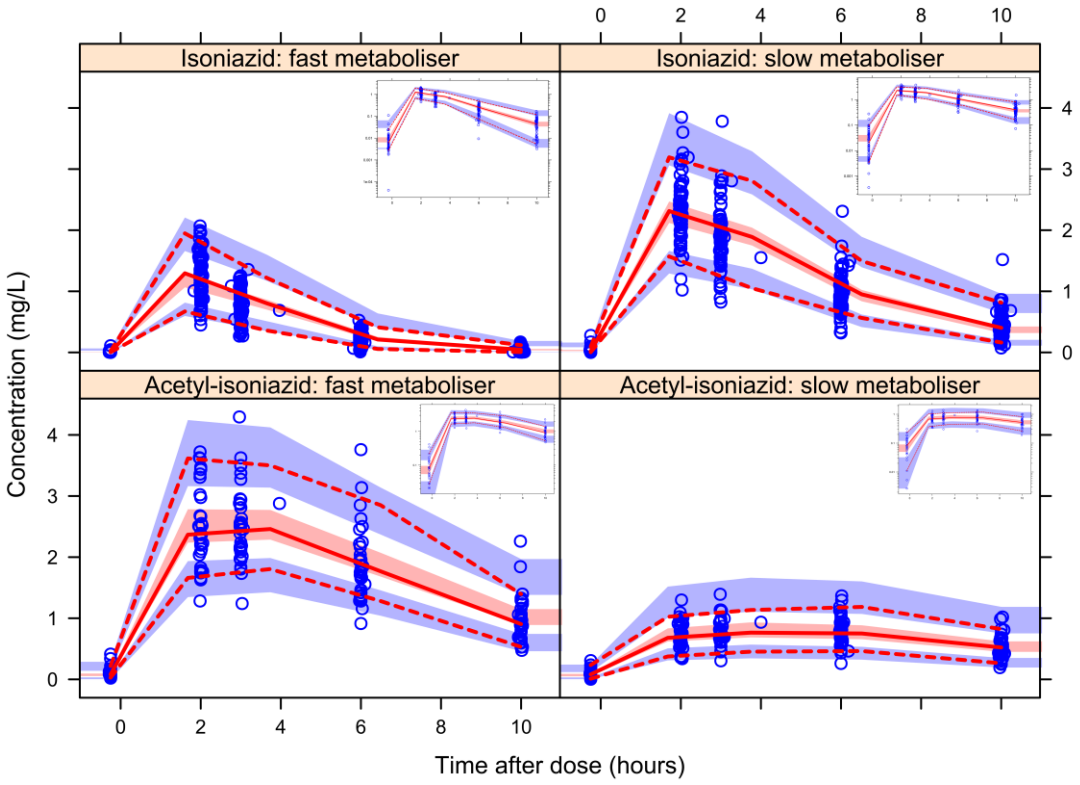

Figure 5.2 Visual predictive checks for isoniazid and acetyl-isoniazid stratified by metabolic status The lines represent the 2.5th, 50th and 97.5th percentile of the observed concentrations (hollow circles). The shaded regions are the 95% prediction intervals for the 2.5th, 50th and 97.5th percentiles. The sub-plot in each stratum shows the same VPC with a logarithmic transformation applied to the y-axis.

Model derived steady-state individual estimates of $AUC_{0–24}$ and C_{max} were obtained from the final model. $AUC_{0–24}$ and C_{max} estimates for 28 patients who were administered tablets from the two batches with reduced bioavailability are not presented in Figure 5.3 and 5.4, hence the results in the plots shows what would

normally be observed if the bioavailability is not significantly reduced. Figure 5.3 shows the model-derived steady-state $AUC_{0–24}$ for isoniazid and acetyl-isoniazid, stratified by acetylator status and co-administration with efavirenz. Among the patients classified as fast acetylators by the model, the median $AUC_{0–24}$ in those who were not receiving ART was 56% higher than those who had started ART two weeks after antituberculosis treatment start. Regardless of the timing of ART initiation, slow acetylators had 3.6 and 2.3 times higher $AUC_{0–24}$ compared to fast acetylators who did and did not receive ART, respectively. None of the patients classified as fast acetylators achieved the $AUC_{0–24}$ of 10.52 mg·h/L associated with early bactericidal activity, whereas more than 75% of slow acetylators achieved this exposure level. As expected, acetyl-isoniazid exposure was higher among fast acetylators compared to slow acetylators.

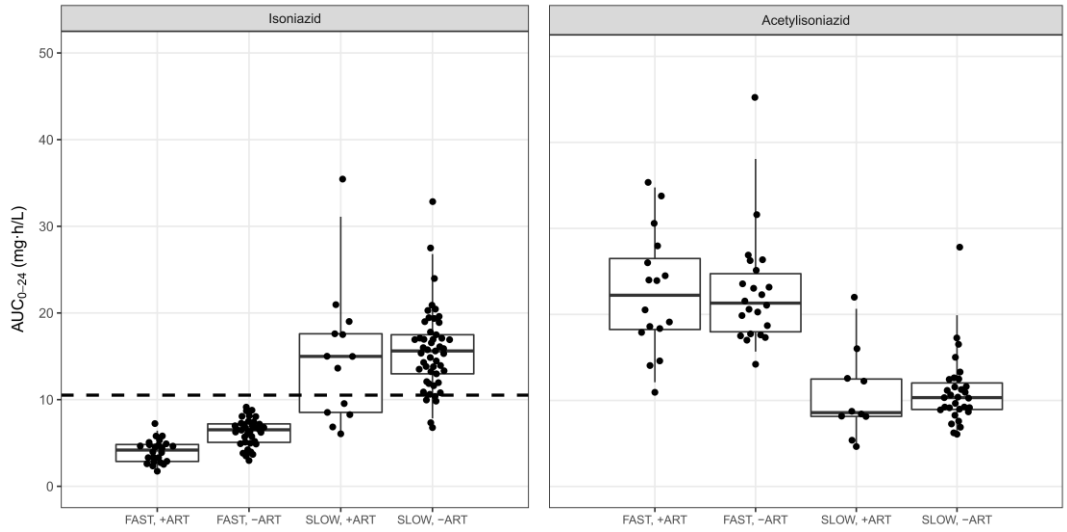

Figure 5.3 Boxplot of $AUC_{0–24}$ for isoniazid and acetyl-isoniazid stratified by treatment arm (receiving efavirenz based ART vs. no ART) and NAT2 metaboliser status. The dots are model-derived individual exposures (steady-state $AUC_{0–24}$). The dashed line represents the exposure ($AUC_{0–24}$=10.52 mg·h/L) associated with 90% of early bactericidal activity of isoniazid.(Donald *et al.*, 2007)

Figure 5.4 depicts the model-derived C_{max} on the pharmacokinetics sampling day (equivalent to steady state). Regardless of treatment arm, all patients classified as fast

acetylators had C_{max} below the range of 3–6 mg/L and more than 85% of the slow acetylators had C_{max} below the range.

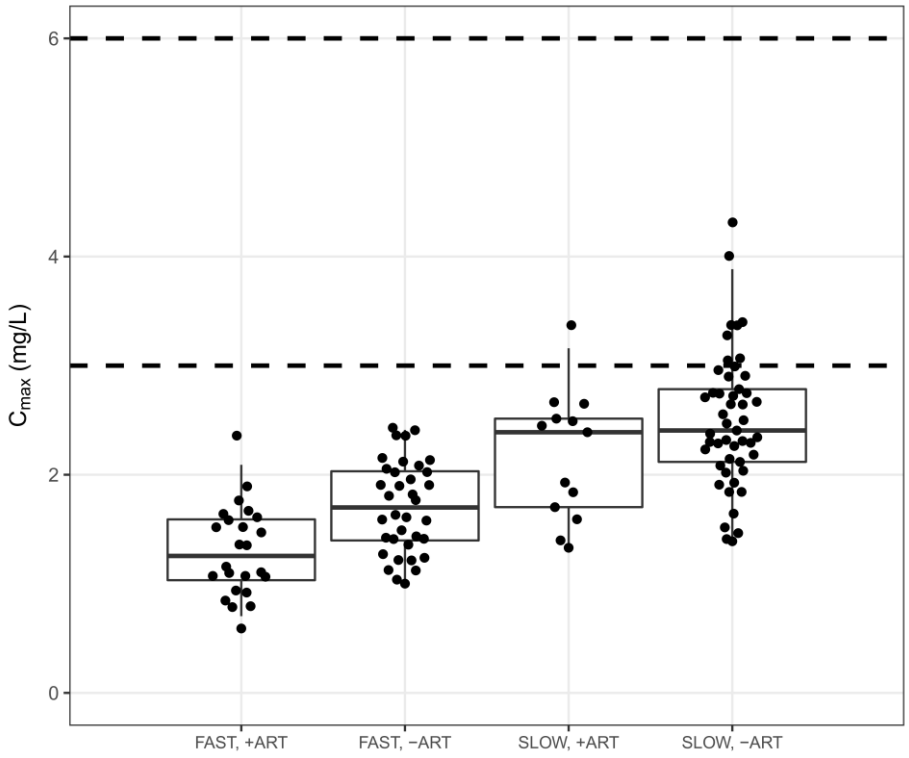

Figure 5.4 Boxplot of C_{max} for isoniazid stratified by treatment arm (receiving efavirenz based ART vs. no ART) and NAT2 acetylator status (fast or slow). Dashed line indicates the target minimum and maximum C_{max} concentrations for isoniazid.

5.5 Discussion

This study described the pharmacokinetics of isoniazid and acetyl-isoniazid in a cohort of TB/HIV co-infected patients. Using population pharmacokinetic modelling, we show that co-administration of isoniazid and efavirenz results in reduced exposure to isoniazid. This effect has also been reported in a study among TB/HIV-infected patients in Mozambique (Bhatt *et al.*, 2014), suggesting that the effect can be generalised to a wider population of TB/HIV co-infected patients on tuberculosis treatment and efavirenz-based ART. One difference with the Mozambican study is that Bhatt et al. reported the effect of efavirenz on isoniazid clearance regardless of the metabolic pathway whereas, in our study, the effect was supported on the acetylation metabolic pathway. Efavirenz has also been found to increase the clearance of *para*-aminosalicylic acid, a drug that is also metabolised by NAT1 and NAT2 enzymes (de Kock *et al.*, 2014). Efavirenz induces a number of enzymes in the cytochrome P450 family(Adkins & Noble, 1998), but to the best of our knowledge, nothing has been reported on the effect of efavirenz on the activity of NAT2. Our results, that of Bhatt et al., and de Kock et al., suggest that efavirenz could modulate the activity of NAT2.

The 6-fold higher intrinsic clearance via acetylation for fast compared to slow acetylators observed in our study is within the range previously reported (Ellard, 1984; Seng *et al.*, 2015a). Slow acetylators lack functional NAT2 enzyme (Hein *et al.*, 2000), and our results show that the clearance reported in other studies for slow acetylators is driven largely by metabolic pathways other than acetylation. Furthermore, since the NAT2 enzymes are predominantly hepatic, the higher exposure among slow acetylators would be a result of reduced clearance rather than higher pre-hepatic bioavailability. Overlapping of exposure range between slow and fast acetylators is not unexpected since multiple slow acetylator phenotypes may lead to high pharmacokinetic variability (Chen, Li, Xu, *et al.*, 2006; Fretland, Leff, Doll, *et al.*, 2001; Leff, Fretland, Doll, *et al.*, 1999).

Adequacy of exposure to isoniazid is evaluated against target $AUC_{0–24}$ or C_{max}. The C_{max} range of 3–6 mg/L was suggested based on concentrations observed in healthy volunteers recruited under controlled phase I studies (Peloquin, 2002). However, the C_{max} observed in patients could be lower than these and a weakness of using the C_{max} is that it could be affected by high variability in the absorption process (Devaleenal Daniel, Ramachandran, & Swaminathan, 2017). On the other hand, steady-state $AUC_{0–24}$ is a more stable exposure index with a value >10.52 mg·h/L being associated with 90% of the maximum early bactericidal activity of isoniazid (Donald *et al.*, 2007). All patients classified as fast acetylators had $AUC_{0–24}$, of less than 10.52 mg·h/L, and this reflects the extent of metabolism due to NAT2 activity in fast compared to slow acetylators and its overall effect on exposure. This results in widely varying exposure levels between fast and slow acetylators, thereby contributing to differences in treatment outcomes and toxicity. To quantify the effect of increased exposure in slow acetylators, Azuma et al. compared the currently recommended dose of 5 mg/kg to a NAT2 adjusted dose (2.5 mg/kg for slow acetylators and 7.5 mg/kg for fast acetylators). The risk of drug-induced liver injury was 78% in the standard treatment group compared to none in the NAT2 adjusted dose group. Among fast acetylators, early treatment failure in the standard dose arm was double that of the NAT2 adjusted dose arm (Azuma *et al.*, 2013). Reduced isoniazid exposure could imply an innapropriate continuation phase TB drug regimen with patients being almost only on monotherapy with rifampicin. This might increase the risk of emergence of drug resistance. Along with other factors, this could explain the increased risk of MDR-TB in HIV patients (Mesfin, Hailemariam, Biadgilign, *et al.*, 2014).

While genotyping is expensive in a resource-limited setting, other approaches could be used to classifying patients according to acetylator status. Collecting and quantifying isoniazid and acetyl-isoniazid concentration from a single blood sample after dose administration, combined with the use of mixture models in population pharmacokinetics to determine the acetylator status could be useful to implementing therapeutic drug monitoring for tuberculosis treatment.

The result that a 50% increase in rifampicin dose does not influence the pharmacokinetics of isoniazid is in line with reports by Boeree et al., who investigated the effect of higher dose of rifampicin of up to 35 mg/kg (3.5 fold increase) on pharmacokinetics of the other drug in the FDC and did not find any difference in AUC of the co-administered drugs between the standard dose rifampicin arm and higher dose arms (Boeree *et al.*, 2017). Based on these results, we can conclude that doses higher than the current dose of rifampicin are less likely to affect isoniazid exposure.

Our finding showing reduced bioavailability in two of the drug batches of the same formulation used in the study shows the need for continuous quality control checks on batch-to-batch variability. This result also reflects the challenges associated with conducting clinical trials in routine clinical settings and, most importantly, it provides essential information for monitoring tuberculosis treatment programmes. An analysis of the drug content in a sample of tablets from the two batches with reduced bioavailability could have helped to explain if the quality of the tablets was unsatisfactory, but there were no remaining tablets at the end of the trial to conduct the tests. Fortunately, the demographic characteristics of the patients who received tablets from the two batches were not dissimilar from the rest of the cohort, and their distribution was comparable across treatment arms, so this finding is not expected to have any significant impact on the main study question.

Differences in body size and composition included in our model via allometric scaling using FFM also explain some variability in the pharmacokinetics of isoniazid in addition to acetylator status (Anderson, 2008). This combined effect of weight, height, and sex could explain the reported disparity in exposure among males and females (McIlleron *et al.*, 2012), since females usually have a larger proportion of body fat, which does not contribute to the size of other body organs such as the liver (Green & Duffull, 2004). Recent population pharmacokinetics models for the first-line antituberculosis drugs have shown that FFM is a better size descriptor for scaling clearance and volume compared to total body weight (Denti,

Jeremiah, *et al.*, 2015; Rockwood *et al.*, 2016; Smythe, 2016). The feasibility of introducing FFM based dosing with the current FDCs for the treatment of tuberculosis in the clinic setting could be investigated. We postulate that the implementation of FFM based dosing could reduce the variability in drug exposure usually observed among tuberculosis patients, which will translate to favourable treatment outcomes and reduced toxicity.

A limitation of our study is that no genotyping has been performed to identify the acetylator status of each patient but will be done in a future study using DNA samples from some patients. Without genetic information, it is difficult to separate homozygous fast and heterozygous fast acetylator status (Hickman & Sim, 1991). However, the proportion of fast acetylators (50%) in our model is not different from the ones that have been reported for African populations. and more closely to the 47% reported by Smythe (Ellard, 1984; Roy, Majumder, & Roy, 2008; Smythe, 2016).

In conclusion, we developed a population pharmacokinetic model for isoniazid and acetyl-isoniazid in a population of TB/HIV co-infected patients. The model could separate clearance due to acetylation and other routes of metabolism and showed reduced exposure to isoniazid among fast acetylators receiving efavirenz-based ART. A 50% increase in dose of rifampicin did not influence the pharmacokinetics of isoniazid and acetyl-isoniazid.

Acknowledgements

We wish to thank the participating patients and staff at the Benin and Guinea clinical trial sites, the London School of Hygiene, the University College London, Hopitaux de Paris and Tropical Institute of Antwerp. The Division of Clinical Pharmacology at the University of Cape Town gracefully acknowledges Novartis Pharma for support of the development of pharmacometric skills in Africa. M.T.C. is supported by the European & Developing Countries Clinical Trials Partnership (PACTR201105000291300). M.T.C. and H.M. are funded in part by the National Research Foundation of South Africa (grants 95106 and 90729). The drug assays were

supported in part by the National Institute of Allergy and Infectious Diseases of the National Institutes of Health (UM1AI068634, UM1 AI068636 and UM1AI106701, U01 AI068632), the Eunice Kennedy Shriver National Institute of Child Health and Human Development, and the National Institute of Mental Health (AI068632). Its contents are solely the responsibility of the authors and do not necessarily represent the official views of the government.

Funding

The RAFA clinical trial and its PK component were sponsored by the European & Developing Countries Clinical Trials Partnership (PACTR201105000291300).

Chapter 6: Pharmacokinetics of rifampicin, pyrazinamide, and ethambutol in patients recruited in the RAFA study

6.1 Introduction

Rifampicin is metabolised to desacetylrifampicin by liver esterase. It is also excreted in bile unchanged or as desacetylrifampicin (Acocella, 1983). The results in chapter three and other studies show that increase in dose of rifampicin yields a more than proportional increase in exposure due to saturation of transporters involved in the extraction of rifampicin in the liver (Boeree *et al.*, 2015; Chirehwa *et al.*, 2016; Svensson, Aarnoutse, *et al.*, 2017). The transporters responsible for the excretion of rifampicin are also involved in the excretion of desacetylrifampicin hence the concentrations of both substrates drive the saturation of the transporters (Acocella, 1983; Denti *et al.*, 2017). The pharmacokinetics of rifampicin has been described in tuberculosis patients receiving higher than the currently recommended 10 mg/kg dose of rifampicin (Boeree *et al.*, 2015), but the TB/HIV infected patients recruited in that study had a CD4+ count of greater than 350 cells/μL. It is important to describe the pharmacokinetics of rifampicin in TB/HIV infected patients including those low CD4+ count.

Pyrazinamide is included as part of the treatment for drug-sensitive and -resistance tuberculosis and is also being evaluated in some novel tuberculosis treatment regimens. It is active against dormant and semi-dormant M. tuberculosis bacilli in acidic environment (Mitchison, 1985). The currently recommended daily dose of pyrazinamide for the treatment of drug-susceptible tuberculosis is 25 (range: 20–30) mg/kg of body weight (World Health Organization, 2010b).

Ethambutol is a broad antimycobacterial agent which shows concentration dependent microbial killing and protect against rifampicin resistance in patients with known resistance to isoniazid (Srivastava et al., 2010). A 15 mg/kg daily dose of ethambutol is currently recommended together with rifampicin, isoniazid and pyrazinamide. The objective of the study

was to describe the pharmacokinetics of (1) rifampicin and desacetylrifampicin, (2) pyrazinamide, and (3) ethambutol. We also sought to determine the effect of a 50% increased dose of rifampicin on the pharmacokinetics of pyrazinamide and ethambutol. The effect of early introduction of efavirenz-based ART on the pharmacokinetics of rifampicin, pyrazinamide and ethambutol was also evaluated.

6.2 Methods

The details of the study design including patient recruitment and quantification of drug concentrations for the RAFA clinical trial is described in chapter 2. Concentration time data were described using nonlinear mixed-effects modelling and the software NONMEM 7.3 (Beal, Sheiner, Boeckmann, & Bauer, 2013) using the first-order conditional estimation method with eta-epsilon interaction (FOCE-I). Model diagnostics and documentation of model development were performed using Perl-speaks-NONMEM (PsN) version 3.6, Pirana version 2.9.0, and Xpose4 (R package) (Keizer, Karlsson, & Hooker, 2013). Additional plots were generated using R version 3.4.0 (R Core Team, 2017) via RStudio version 0.98.1091 (RStudio, 2014).The model building procedure was generally the same for rifampicin, pyrazinamide, and ethambutol. We started with a one-compartment model with first-order linear absorption and elimination. Between-subject variability was tested on all parameters of the model, while between-occasion variability was included on the bioavailability parameter to describe the difference in the bioavailability on the pharmacokinetic sampling day and dose administered the previous day. The model was further improved by inclusion of a delay in absorption by using a lag time or a chain of transit compartments. Allometric scaling based on total body weight or fat-free mass was included in the initial phase of model building using known allometric exponents of 0.75 for clearance and 1 for volume parameters (Anderson & Holford, 2008). Two-compartment disposition models were also evaluated to verify ether that the chosen one compartment model was sufficient to describe the pharmacokinetics of the drug or that a two-compartment was better than a one-compartment model.

For the joint model describing the pharmacokinetics of rifampicin and desacetylrifampicin, we first developed a model for rifampicin as described above and included the semi-mechanistic component describing saturation of hepatic extraction, as described in chapter 4. Concentration-time data for desacetylrifampicin were included in the model for rifampicin after the rifampicin model was deemed sufficient. We evaluated one- and two-compartment

disposition models including a liver compartment to describe the pharmacokinetics of desacetylrifampicin. A semi-mechanistic component to capture saturation of desacetylrifampicin elimination was also assessed. Since both rifampicin and desacetylrifampicin compete for the same transporters for excretion, an attempt was made to describe this process in a semi-mechanistic way. The difference in molecular weight of rifampicin and desacetylrifampicin was adjusted for in all models describing the pharmacokinetics of rifampicin and desacetylrifampicin jointly.

A physiologically plausible covariate was included and retained in the model if upon its inclusion, it resulted in a reduction in OFV of at least 3.84 points, corresponding to 5% level of significance for a chi-squared test. Model fit was evaluated by using a change in OFV and analysis of residuals, fitted values, and visual predictive checks.

6.3 Results

6.3.1 Pharmacokinetics of rifampicin and desacetyl-rifampicin

The RAFA study recruited 222 patients for the PK sub-study. Plasma samples of 19 patients were affected by a temporary change in temperature of the storage freezer and were deemed unreliable, hence rifampicin concentrations were not determined. After these exclusions, plasma samples of 203 patients were available for pharmacokinetics analysis. Desacetyl-rifampicin concentrations were quantified in plasma samples from 132 patients due to limited budget. Table 1 shows the baseline characteristics of the 203 patients included in the pharmacokinetic analysis. The distributions of the baseline characteristics closely mirror those reported in patients who had isoniazid concentrations reported in chapter 5.

Table 6.1 Baseline characteristics of patients with rifampicin concentrations (RAFA study)

Characteristic	Value
Total No.	203
No. (%) of females	80 (39.4)
No. (%) in early ART arm	55 (27.1)
No. (%) in high dose rifampicin arm	87 (42.3)
Weight, kg	51 (33–87)
Height, m	1.7 (1.4–1.94)
FFM, kg	42.9 (24.8–65.3)
Age, years	37 (19–69)
$CD4^+$ cells/µL	170 (51–772)
Viral load, copies/mL ($x10^3$)	150 (0.08–10000)
Serum creatinine, µmol/L	89 (23–212)
Haemoglobin level, g/dL	9.3 (5.2–15.9)
ALT, units/L	31 (3–97)
White blood cells, $x10^9$/L	7 (1.8–26.2)
Platelets, $x10^9$/L	337 (119–832)

A total of 1008 and 653 concentrations were available for analysis for rifampicin and desacetyl-rifampicin respectively. Values below the limit of quantification were released by the laboratory and available for analysis. However, rifampicin and desacetyl-rifampicin concentrations were not detected by the mass spectrometer in 59 and 92 plasma samples, respectively. Most of these were pre-dose samples, 92% and 96% for rifampicin and desacetyl-rifampicin, respectively. For these, we imputed a value equal to half of the lower limit of detection (defined as 10% of the LLOQ) as suggested by Keizer et al., (Keizer *et al.*, 2015).

Figure 6.1 shows the schematic diagram of the model for rifampicin and desacetyl-rifampicin. Pharmacokinetics of rifampicin were best described by a one-compartment disposition model linked to the liver compartment modelled with the well-stirred assumption (Gordi *et al.*, 2005) and a chain of transit compartment to capture the delay in absorption. The model could

estimate two clearance pathways from the liver compartment; one for the formation of desacetyl-rifampicin and another for excretion and other pathways. Desacetyl-rifampicin was described by a one-compartment disposition model attached to the liver compartment that is connected to the liver compartment of rifampicin. Elimination of desacetyl-rifampicin was via the hepatic route.

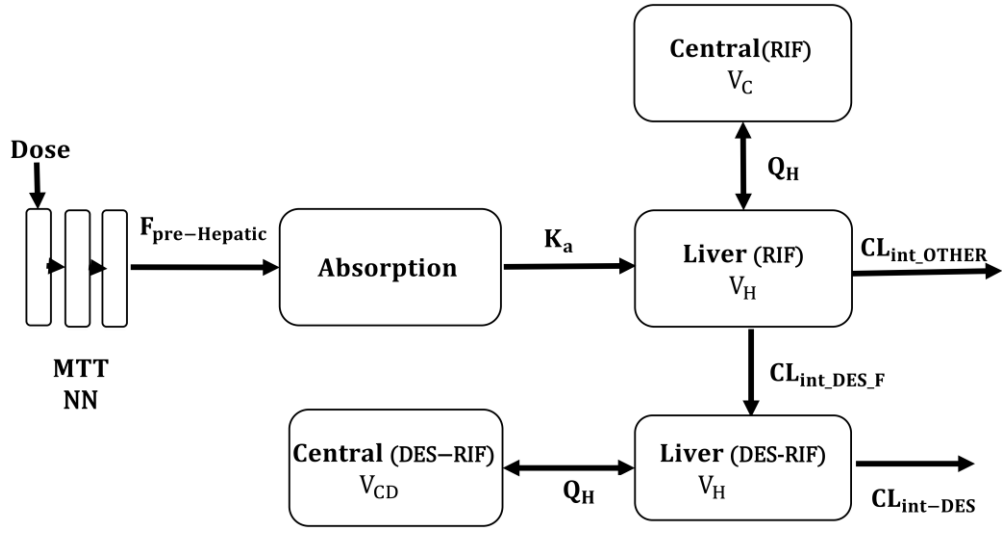

Figure 6.1 Schematic diagram of the semi-mechanistic model of rifampicin and desacetyl rifampicin in TB/HIV co-infected patients MTT, mean transit time; NN, number of transit compartments; $F_{pre\text{-}hepatic,}$ pre-hepatic bioavailability; K_a, absorption rate constant; V_H, volume of liver; Q_H, hepatic plasma flow; V_C, volume of central compartment for rifampicin; V_{CD}, volume of central compartment for desacetyl-rifampicin; CL_{int_OTHER}, intrinsic clearance of rifampicin to other metabolites; $CL_{int\_DES\_F}$, intrinsic clearance of rifampicin to desacetyl-rifampicin; $CL_{int\_DES\_}$, intrinsic clearance of desacetyl-rifampicin.

Table 6.2 shows the parameter estimates of the final model and the associated 95% confidence interval obtained from the SIR procedure with five iterations, as suggested in Dosne et al. (Dosne, Bergstrand, & Karlsson, 2017). The SIR procedure was used due to long model run times, and the nonparametric bootstrap method would have taken very long to complete. The absorption model with a chain of transit compartments was superior to a lag time and resulted in 126 points lower AIC value. The inclusion of allometric scaling using total

body weight improved the model fit (ΔAIC = -21), and a further improvement of 3 points in AIC was observed when FFM was used as size descriptor for allometric scaling. The model with hepatic extraction and saturation was superior to a simple one-compartment disposition model (ΔOFV = -32 points, 1 df, P value<0.0001). The typical values for the liver volume of distribution, hepatic plasma flow, and unbound fraction of rifampicin were fixed to 1 L, 50 L/h, and 0.2 respectively. Allometric scaling was also applied to the liver volume of distribution and hepatic plasma flow using fat-free mass. Sensitivity analysis was performed on the typical values of parameters for the well-stirred model, and the main conclusions were not affected. All typical values for clearance and volume parameters refer to a patient with FFM of 43 kg, the median value in the cohort. Upon inclusion of desacetyl-rifampicin data into the model, we discovered that the disappearance of rifampicin could be ascribed to two separate metabolic pathways: the first one non-saturable and responsible for the synthesis of desacetyl-rifampicin, and the second one not associated with desacetyl-rifampicin formation and displaying saturation. The elimination of desacetyl-rifampicin was also found to be saturable with a Michaelis-Menten constant that is lower than that of rifampicin (1.62 mg/L vs 2.32 mg/L). The intrinsic clearance of rifampicin not associated with the formation of desacetyl-rifampicin (excretion intrinsic clearance) was found to be correlated with the intrinsic clearance of desacetyl-rifampicin (55%). Since concentrations of rifampicin and desacetyl-rifampicin was measured in the same plasma sample, a component of the residual unexplained variability is common between the two measurements hence a correlation (78%) between the RUV was included in and supported by the model. The volume of distribution of the central compartment for desacetyl-rifampicin was defined to be the same as the volume of distribution of the central compartment for rifampicin to avoid overparameterisation. Two of the drug batches of the same formulation used in the study were found to have 62.5% reduced bioavailability. Finally, the variability in bioavailability was found to be 59% higher on the day before the pharmacokinetics sampling day. This parameter was included in the model to account for the uncertainty in the reported time of dose on the day before the PK sampling day.

Table 6.2 Parameter estimates of the final model for rifampicin and desacetyl-rifampicin (RAFA study)

Parameter	Estimate (SIR 95% CI[a])	BSV / BOV[+] (%) (SIR 95% CI[a])
Rifampicin		
$CL_{int,max,deac}$ (L/h)[b]	36.5 (34; 38.9)	19.8 (16.3; 23.6)
$CL_{int,max,other}$ (L/h)[b]	150 (120; 181)	64.3 (57.3; 72.5)
V (L)[b]	52.2 (49.5; 54.8)	
K_a (/h)	1.27 (1.04; 1.57)	67.3 (53.3; 77.1)
MTT (h)	0.515 (0.345; 0.682)	74.4 (52.6; 104)
NN[c]	3.76 (1.94; 7.09)	
F[d]	1 FIXED	23.5 (20.3; 26.9) [+]
K_m (mg/L)[e]	2.32 (1.69; 3.32)	
Covariates		
Batch on bioavailability (%)	-62.5 (-68.3; -55.2)	
Scaling factor for variability in bioavailability for unobserved doses (-fold)[f]	1.59 (1.09; 2.28)	
Error		
Additive (mg/L)[g]	0.0234 FIXED	
Proportional (%)	13.5 (12.4; 14.7)	
Desacetyl-rifampicin		
$CL_{int,max,des}$ (L/h)[b]	423 (390; 467)	27.7 (23.3; 31.5)
$K_{m,des}$ (mg/L)[e]	1.62 (1.27; 2.03)	
Error		
Additive (mg/L)[g]	0.00782 FIXED	
Proportional (%)	19.2 (17.5; 21.5)	
Correlations		
BSV $CL_{int,max,other}$ and BSV $CL_{int,max,des}$ (%)	55 (37.3; 72.7)	
Error component parent/metabolite (%)	78.2 (73.6; 82.2)	

[a] SIR 95% CI, Sampling Importance Resampling 95% confidence interval.

[b] This parameter has been adjusted by allometric scaling, and the values reported refer to a subject with an FFM of 43 kg (the median value of the cohort).

[c] NN, number of absorption transit compartments.

[d] F, bioavailability.

[e] Total concentration (bound plus unbound).

[f] The scaling factor modulate the magnitude of the between-occasion variability in pre-hepatic bioavailability for the unobserved doses.

[g] These parameters were fixed to 10% of the LLOQ

[h] The scaling factor modulates the magnitude of the between-subject variability in volume of distribution of desacetyl-rifampicin. A single parameter was estimated for the BSV in volume of distribution and BSV in clearance due to high correlation.

Figure 6.2 shows that the model adequately described the pharmacokinetics of rifampicin and desacetyl-rifampicin. The model was deemed acceptable for the purposes of the analysis as the main objective was to describe rifampicin concentrations and extract individual exposures for input into the PK/PD modelling described in chapter 7.

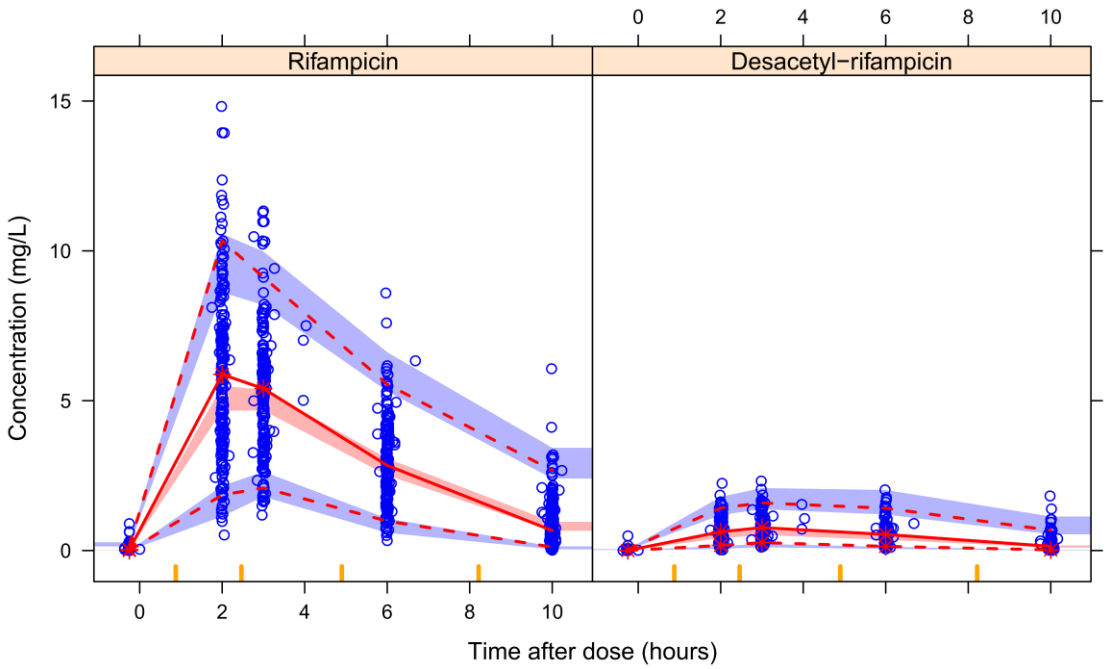

Figure 6.2 Prediction-corrected visual predictive check for a model describing the pharmacokinetics of rifampicin and desacetyl-rifampicin.

6.3.2 Pharmacokinetics of pyrazinamide

Pharmacokinetic modelling of pyrazinamide included 1103 plasma concentrations from 222 patients. Concentrations of pyrazinamide could not be detected in 11 plasma samples, and we imputed a value of half the lower limit of detection of the assay (defined as 10% of the LLOQ). The baseline characteristics of the 222 patients are in Table 6.3.

Table 6.3 Baseline characteristics of patients recruited in the pharmacokinetic sub-study and had pyrazinamide concentrations measured (RAFA study)

Characteristic	**Value**
Total No.	222
No. (%) of females	87 (39.2)
No. (%) in early ART arm	62 (27.9)
No. (%) in high dose rifampicin arm	97 (43.7)
Weight, kg	51 (33–87)
Height, m	1.7 (1.4–1.94)
FFM, kg	43.3 (24.8–65.3)
Age, years	37 (19–69)
$CD4^+$ cells/µL	171.5 (51–880)
Viral load, copies/mL ($x10^3$)	150 (0.08–10000)
Serum creatinine, µmol/L	89 (11–212)
Haemoglobin level, g/dL	9.2 (5.2–15.9)
ALT, units/L	31.5 (3–97)
White blood cells, $x10^9$/L	6.75 (1.8–26.2)
Platelets, $x10^9$/L	334 (103–832)

Pyrazinamide pharmacokinetics were best described by a one-compartment disposition model with first-order elimination and a transit compartment absorption model. The final parameter

estimates are presented in Table 6.4 and a prediction-corrected visual predictive check is shown in Figure 6.3. The model included two transits (NN=1) with no separate estimate of K_a value since it was more parsimonious and had comparable OFV to the model with separate estimate of K_a. The model was parameterised in such a way that K_a can be calculated from number of transit compartments and mean transit time as shown in equation 6.1

$$K_a = \left(\frac{NN + 1}{MTT}\right) \quad (6.1)$$

Table 6.4 Parameter estimates of the final model for pyrazinamide (RAFA study)

Parameter	**Estimate (95% CI)[a]**	**BSV/ BOV[+] (%) (95% CI)**
CL (L/h)	3.7 (3.45; 3.97)	27.2 (23; 31.2)
V (L)	35.1 (32.8; 36.4)	
MTT (h)	0.342 (0.00342; 0.428)	66.6 (49; 428)
NN	1 FIXED	
Bioavailability	1 FIXED	10 (0.571; 14.6)/ 12 (3.35; 16.4)[+]
Covariates		
Batch effect on bioavailability (%)	-19.5 (-24.9; -14.5)	
Guinea site effect on clearance (%)	-15.1 (-21.9; -7.46)	
Error		
Additive	0.892 (0.501; 1.29)	
Proportional (%)	10.9 (9.55; 12.1)	

[a]CI, confidence interval

Fat-free mass was the best size descriptor for allometric scaling of clearance and volume of distribution, and improved the model fit by 145.5 points in AIC (22.5 point better than using total body weight). Patients receiving tablets from the same two drug batches that were found to have low rifampicin and isoniazid bioavailability also had reduced pyrazinamide

bioavailability (-20%) (ΔOFV of 64.5 points, 1 df, p-value<0.001). In patients recruited in the Guinea site, clearance was reduced by 13% compared to those from Benin (ΔOFV of 10 points, 1 df, p-value=0.002). The model did not detect any effect of high dose (+50%) of rifampicin or efavirenz-based on the pharmacokinetics of pyrazinamide.

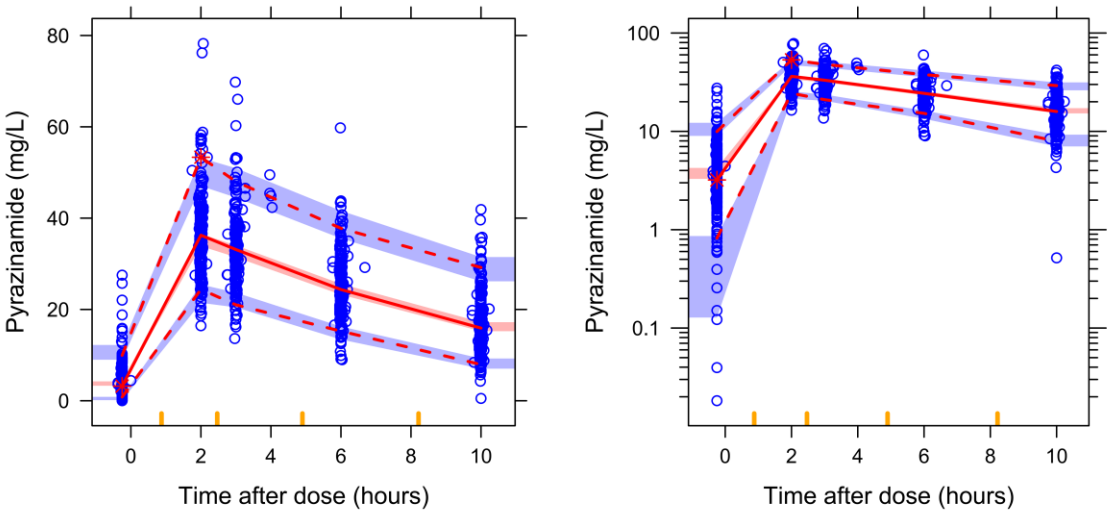

Figure 6.3 Prediction-corrected visual predictive check for a model describing the pharmacokinetics of pyrazinamide The left panel is the VPC in the normal scale and right panel in the VPC in the semi-log scale.

6.3.3 Pharmacokinetics of ethambutol

All 222 patients had concentrations of ethambutol measured and their baseline characteristics are presented in Table 6.3. Plasma concentrations were below the nominal limit of quantification in 16 of the 1103 samples, but the analytical laboratory released the values detected, and were included in the model. Ethambutol pharmacokinetics was best described by a two-compartment disposition model with first-order elimination, and absorption via a chain of transit compartments. The two-compartment model significantly improved the model fit compared to a one-compartment model (ΔOFV= -822, 2 df, p-value<0.001). The parameter estimates of the final model are presented in Table 6.5, and the prediction-corrected visual predictive check is shown in Figure 6.4.

Table 6.5 Parameter estimates of the final model for ethambutol (RAFA study)

Parameter	**Estimate (95% CI)[a]**	**BSV / BOV[+] (%) (95% CI)**
Non-renal clearance (L/h)	40.6 (32.7; 49.7)	15.4 (10.8; 19.8)
Glomerular filtration (L/h/ 75 mL/min CrCL)	12.9 (3.69; 21.8)	
$V_{central}$ (L/h)	225 (196; 245)	
K_a (h^{-1})	1.56 (1.17; 2.08)	84.7 (69.1; 97.5)
MTT (h)	1.25 (1.08; 1.4)	24.5 (14.1; 42.7)
NN	15.7 (3.42; 49.7)	
F	1 FIXED	21.7 (14.5; 27) / 17.5 (2.72; 23.9)[+]
$V_{peripheral}$ (L/h)	415 (376; 462)	
Q (L/h)	47.2 (43.3; 52.2)	
Covariates		
Batch effect on bioavailability (%)	-17.8 (-29.8; -3.43)	
Guinea site effect on clearance (%)	-13.7 (-18.8; -8.67)	
Error		
Additive (mg/L)	0.0224 (0.0062; 0.0396)	
Proportional (%)	13.8 (11.8; 15.7)	

[a]CI: Confidence interval;

Allometric scaling was applied to all clearance and volume parameters including that of the peripheral compartment using fat-free mass (40 points drop in AIC). Using total body weight

for allometric scaling did not result in a worse fit, but fat-free mass was used to maintain consistency with pharmacokinetic models for the co-administered drugs of the FDC. Clearance of ethambutol was separated between glomerular and extra glomerular pathways, and this was associated with a 12 points improvement in OFV (1 df, P value< 0.001) compared to using one clearance pathway. Parameter estimates of clearance (extra glomerular) and volume of distribution in Table 6.5 are reported for an individual with a fat-free mass of 43 kg. The glomerular filtration pathway was scaled by creatinine clearance, which was computed based on the Cockcroft and Gault formula. This route of elimination for an individual with a reference creatinine clearance of 75 mL/min was estimated to be 12.9 L/h. The model also estimated a 13% reduced clearance (both pathways) of ethambutol in patients recruited from Guinea (ΔOFV= -20.7, 1 df, p-value<0.001). Similar to other drugs in the FDC, patients who received tablets the two drug batches described before had lower estimated bioavailability (-18%) (ΔOFV= -10.8, 1 df, p-value=0.001). The inclusion of the effect of drug batch improved the model by 9 OFV points (1 df, P value= 0.003). There was no evidence of the influence of an increased dose of rifampicin nor efavirenz-based ART on the pharmacokinetics of ethambutol.

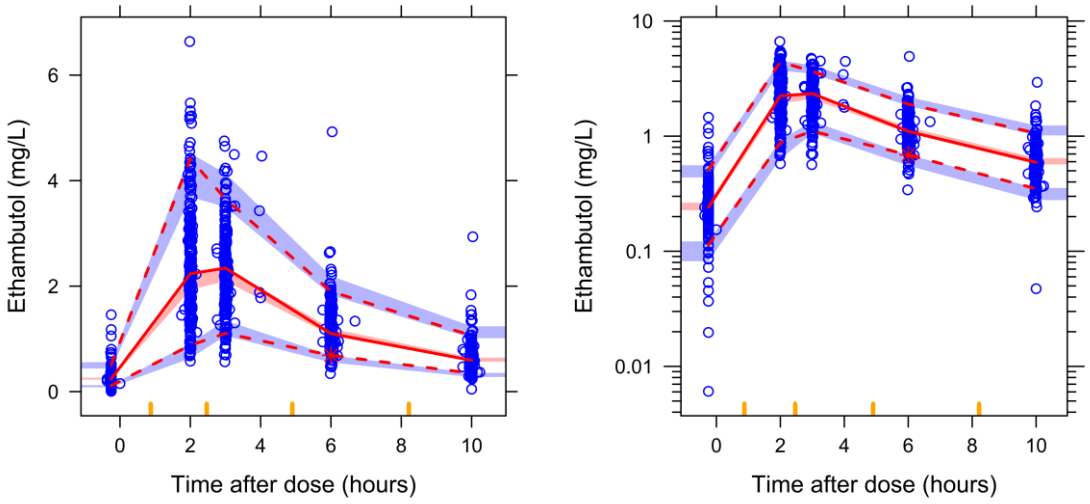

Figure 6.4 Prediction-corrected visual predictive check for a model describing the pharmacokinetics of ethambutol. The left panel is the VPC in the normal scale and right panel in the VPC in the semi-log scale.

6.3.4 Model-based steady-state individual exposure to rifampicin, pyrazinamide, and ethambutol

The parameter estimates of the final models for rifampicin, pyrazinamide, and ethambutol presented in sections 6.1.1 to 6.1.3 were used to derive steady-state individual estimates of AUC_{0-24} and C_{max}. These individual values are affected by covariates and are based on EBEs which are known to be influenced by shrinkage. The estimates for shrinkage in the models were below 40%. The AUC_{0-24} was obtained by integrating the concentration in the central compartment over a 24-hour period post-dose, and the C_{max} was obtained by following individual profile during numerical computation over time and identifying the maximum concentration in the central compartment. These exposures were stratified by the treatment arm and a reference line indicating the target exposure found in the literature for the different drugs (Alsultan & Peloquin, 2014a). The effect of arm was tested in the model and was not found to be significant hence any differences visible in the plots are either not significant or are ascribable to other factors already included in the models.

Figure 6.5 shows the steady-state AUC_{0-24} and C_{max} for rifampicin for the 203 patients who had rifampicin concentrations. As a consequence of the higher dose, patients who received 15 mg/kg rifampicin have slightly higher AUC_{0-24} and C_{max}. The median AUC_{0-24} in the high dose RIF arm was 73% higher than that of the standard 10 mg/kg dose which includes the early ART and delayed ART treatment arms (45.2 vs 26.1 mg·h/L). Overall, only 24% of the patients achieved the target rifampicin C_{max} of 8 mg/L and most (73%) of these were in the high-dose rifampicin arm. In this cohort of TB/HIV patients, there is large variability in exposure, especially in the treatment arm that received an increased dose of rifampicin.

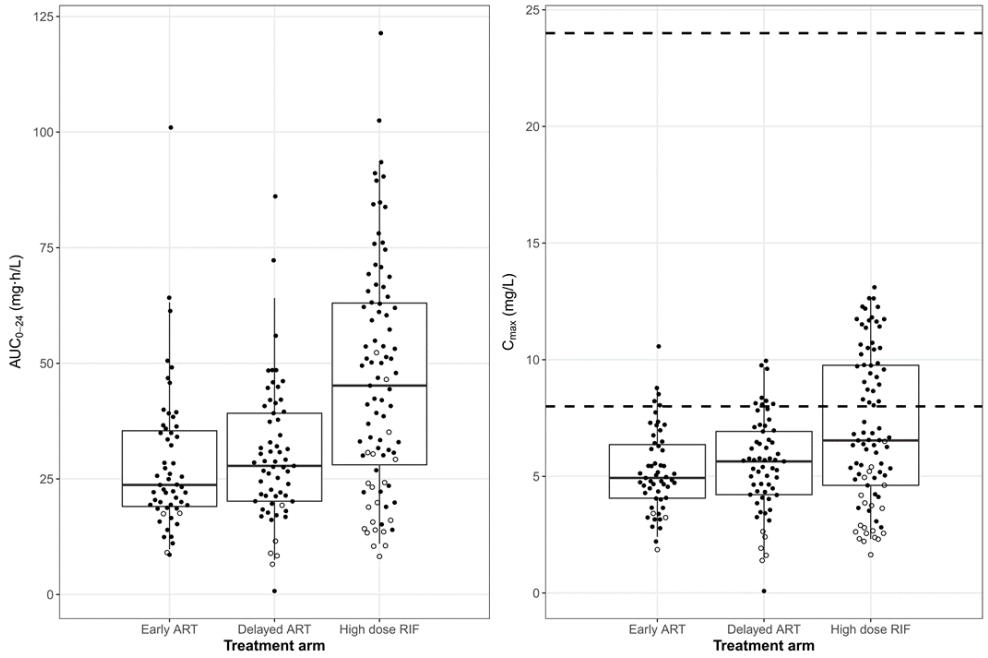

Figure 6.5 Steady-state AUC_{024} (left) and C_{max} (right) for rifampicin stratified by the treatment arm. The horizontal line C_{max} = 8 mg/L represents the suggested threshold for peak concentration of rifampicin. The hollow circles represent the exposure for patients who received tablets from the two drug batches found to have reduced bioavailability.

Steady-state pyrazinamide $AUC_{0–24}$ and C_{max} for the 222 patients recruited in the pharmacokinetic sub-study are shown in Figure 6.6. In most patients, the C_{max} lies within the target range of 20 – 50 mg/L except in two patients who had very low C_{max}. The plots also suggest that in patients who received a 50% higher dose of rifampicin, both $AUC_{0–24}$ and C_{max} are slightly reduced, although the effect was not significant when tested in the model. However, only 55% of the patients achieved an $AUC_{0–24}$ of at least 363 mg·h/L, which was previously found to be associated with long-term favourable treatment outcomes (Pasipanodya *et al.*, 2013). These results were not dissimilar when comparing the C_{max} to a target of 35 mg/L, also found to be associated with tuberculosis treatment outcomes.

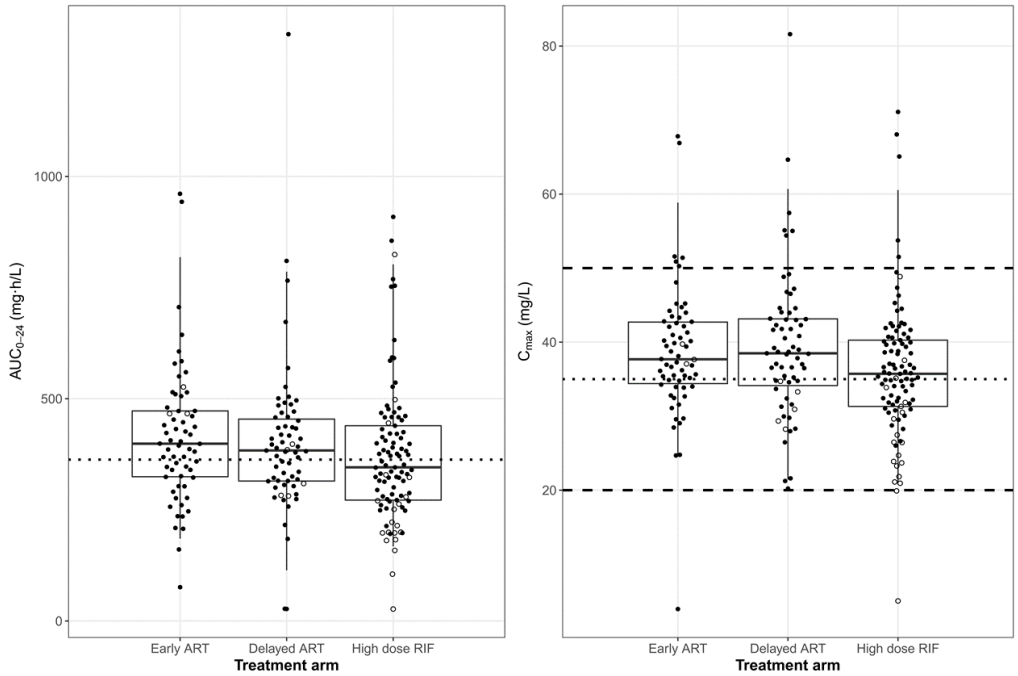

Figure 6.6 Steady-state $AUC_{0–24}$ (left) and C_{max} (right) for pyrazinamide stratified by the treatment arm. The dotted line in the left panel is the $AUC_{0–24}$ of 363 mg·h/L and the one in the right panel is a C_{max} of 35 mg/L. The dashed lines in the right panel show the target C_{max} range for pyrazinamide. The hollow circles represent the exposure for patients who received tablets from the two drug batches found to have reduced bioavailability.

Figure 6.7 shows the steady-state individual exposures to ethambutol for 222 patients in the cohort. Patients recruited into the high dose rifampicin arm had marginally reduced ethambutol exposure, but this was not statistically significant when tested in the model. Ethambutol C_{max} was below the target range in 26% of the patients overall, and this was more pronounced in patients who received an increased dose of rifampicin (40% of patients in the high dose rifampicin arm).

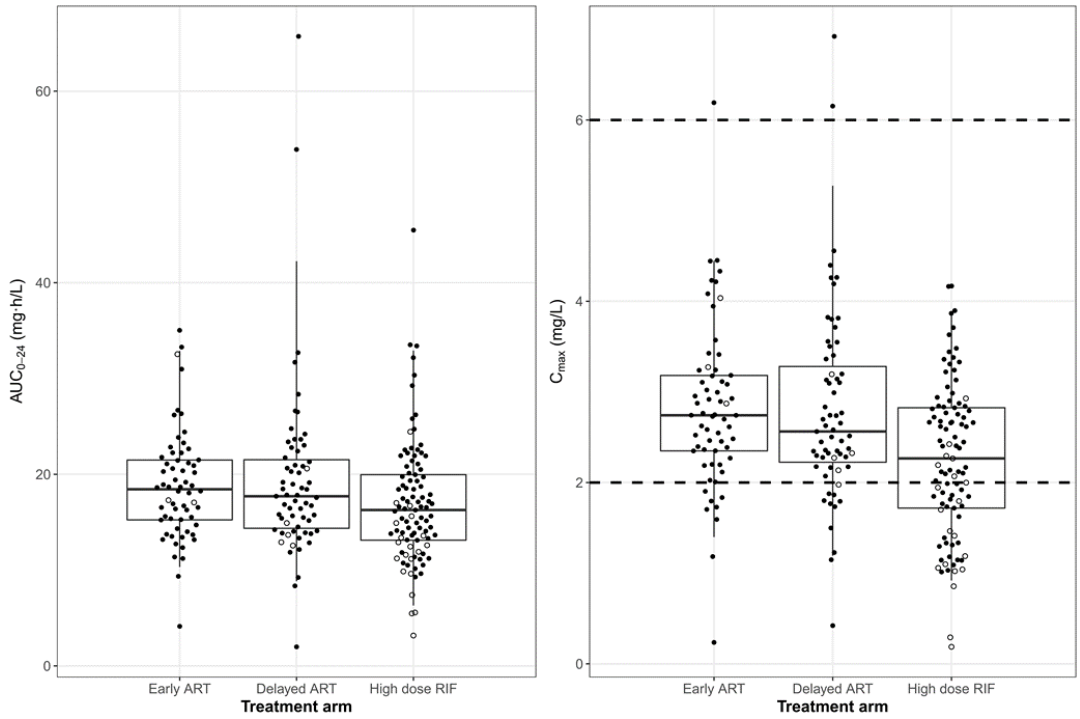

Figure 6.7 Steady-state $AUC_{0–24}$ (left) and C_{max} (right) for ethambutol stratified by the treatment arm The dashed lines in the right panel show the target range of C_{max} for ethambutol. The hollow circles represent the exposure for patients who received tablets from the two drug batches found to have reduced bioavailability.

6.4 Discussion

Population pharmacokinetics of rifampicin, desacetyl-rifampicin, pyrazinamide, and ethambutol were described in TB/HIV co-infected patients recruited in the pharmacokinetic sub-study of the RAFA randomised clinical trial. Model-based steady-state individual exposures were derived for rifampicin, pyrazinamide, and ethambutol and compared with target exposure based on PK-PD studies and “normal” concentrations observed after standard doses (Alsultan & Peloquin, 2014b).

The elimination of rifampicin was found to be saturable, due to the saturation of the pathway that is not linked to the formation of desacetyl-rifampicin. The total intrinsic clearance of 186.5 L/h reported here is close to the value of 176 L/h reported in chapter 3 (Chirehwa *et al.*, 2016). The results are in keeping with previous reports describing rifampicin elimination as mainly due to two processes: deacetylation and biliary excretion, and with the latter hypothesised to be saturating. (Acocella, 1978; Acocella, Pagani, Marchetti, Baroni, & Nicolis, 1971). A semimechanistic model describing the liver as a separate compartment explained the data significantly better than a traditional model with elimination from the central compartment (where the concentrations are observed).

The K_m for desacetyl-rifampicin was lower than for rifampicin. This phenomenon was reported by Acocella, who observed that the rate of transfer into bile of desacetyl-rifampicin was three times higher than that of rifampicin (Acocella, 1983). Denti et al. also reported a higher affinity for the metabolite than for the parent (Denti *et al.*, 2017). It is quite likely that rifampicin and desacetyl-rifampicin compete for the same transporters for excretion, and it we attempted to capture this by implementing saturation with competing substrates as described by Cornish-Bowden (Cornish-Bowden, 2015). However, this more complex model was not supported by our data, as the estimation was unstable and provided unrealistic values of K_m for both

rifampicin and desacetyl-rifampicin. The excretion intrinsic clearance of rifampicin was positively correlated (55%) with excretion clearance of desacetyl-rifampicin, and this shows that both rifampicin and desacetyl rifampicin are transferred into bile, but the strength of the correlation suggests different transfer rates.

The model describing the pharmacokinetics of pyrazinamide in TB/HIV co-infected patients presented here mirrors previous reports in TB infected and TB/HIV co-infected patients from Africa (Denti, Jeremiah, *et al.*, 2015; Smythe, 2016). However, the value clearance of 3.7 L/h detected here are much lower than those reported in a cohort of South African patients by Rockwood et al. (Rockwood *et al.*, 2016) and another study with patients from South Africa, Uganda, and United States (Alsultan *et al.*, 2017) where the clearance were 4.17 and 5.06, respectively. Further investigation suggests that this could be a bioavailability difference because the clearance is around 10% of the volume of distribution in all the three models. Chigutsa et al. described the elimination of pyrazinamide as a parallel first- and mixed-order process (Chigutsa, McIlleron, & Holford, 2010), but in our analysis simple first-order elimination fit the data suitably. Smythe reported lower concentration of pyrazinamide in the Benin site of their study and the effect was reportedly due to differences in bioavailability (Smythe, 2016). In our study, only a difference in clearance of pyrazinamide was observed between the two sites (Benin vs Guinea), but the difference in concentrations between the sites is in the same direction, in that Guinea patients have higher exposure than those from Benin. It could be speculated that there could be differences in expression of enzymes responsible for the metabolism of pyrazinamide in the two populations.

Pharmacokinetics of ethambutol has been previous reported to show a biphasic disappearance, which was also confirmed in this study. Population pharmacokinetics of ethambutol in African adult population has been reported in studies conducted in Benin,

Guinea, Senegal, South Africa and Tanzania (Denti, Jeremiah, *et al.*, 2015; Jönsson *et al.*, 2011; Smythe, 2016). The disposition parameters are closely in line with the parameters reported before among TB/HIV co-infected patients. In our model, we separated glomerular filtration from extra glomerular filtration clearance, since a significant proportion of ethambutol is eliminated renally. The effect of age on exposure to ethambutol reported by Denti et al. and McIlleron et al. in patients recruited from Tanzania and South Africa, respectively (Denti, Jeremiah, *et al.*, 2015; McIlleron *et al.*, 2006) is compatible with the effect of creatinine clearance on the glomerular filtration component of clearance in our model. However, this effect plays a significant role only if the age range of the study participants is wide and includes a significant proportion of older participants who are known to have reduced renal function.

The effect of body size on the disposition parameters was included via allometric scaling in all the three models. The World Health Organisation currently recommends weight-adjusted daily doses of antituberculosis drugs for the treatment of drug-susceptible tuberculosis (World Health Organization, 2010c). Despite patients being dosed based on their weight, disparities in exposure have been reported: reduced exposure to all drugs of the FDC in patients with lower weight who are males (McIlleron *et al.*, 2012), higher exposure to pyrazinamide in female patients (Chigutsa, McIlleron, & Holford, 2010; Wilkins *et al.*, 2006), and faster clearance of rifampicin in males (Sloan *et al.*, 2017). For the three drugs reported in this chapter, the effect of body size was best described using fat-free mass as opposed to total body weight except for the pharmacokinetic model for ethambutol where model diagnostics were comparable when either fat-free mass or total body weight was used. Developing and evaluating dosing guidelines based on fat-free mass could help reduce the disparities in exposure currently observed and attributed to the weight-adjusted dosing.

The variability in rifampicin exposure was found to be higher and more noticeable in patients who received the increased dose of rifampicin. With an increased dose of rifampicin, enzymes present in the gut wall and transporters such as P-glycoprotein may become saturated, and the level of saturation could differ in different patients (Prakash, Velpandian, Pande, *et al.*, 2003). Exposure to rifampicin achieved in patients recruited in the study is consistent with those reported in several studies despite one treatment arm receiving a 50% higher dose. The proportion of patients who did not attain a target C_{max} of 8 mg/L was 67%, and comparable to the OFLOTUB study (70%) also conducted in West Africa but also including a South African site (Smythe, 2016). Studies conducted in South Africa show that between 61–75% of patients receiving rifampicin fail to achieve a C_{max} of 8 mg/L (McIlleron *et al.*, 2006, 2012; Rockwood *et al.*, 2016). The proportion was higher in studies conducted in Botswana (78% and 84%)(Chideya *et al.*, 2009; Tappero *et al.*, 2005), Kenya (90%) (Choudhri *et al.*, 1997) and Burkina Faso (100% at 10 weeks)(Saleri *et al.*, 2012). The median C_{max} of rifampicin in patients from Malawi was much lower than the target (4.8 mg/L; range (1.4–10.9 mg/L))(Sloan *et al.*, 2017). Encouraging results were reported in patients from Uganda where the lowest proportion of patients not achieving the target was 54% (Wiltshire *et al.*, 2014). That our results show most of the patients who did not achieve the target C_{max} were in the treatment arms that received the standard 10 mg/kg dose is not surprising. However, increasing the dose by 50% might have been too conservative considering that recent studies have explored doses of up to 40 mg/kg (Boeree *et al.*, 2015; Svensson, Aarnoutse, *et al.*, 2017). Jeremiah et al. showed that in TB/HIV co-infected patients, nutritional supplementation improves the rifampicin exposure by around 14% and more research needs to be conducted to confirm the result and its implications for dosing (Jeremiah *et al.*, 2014).

Virtually all patients achieved a pyrazinamide C_{max} of 20 mg/L. However, only slightly more than half of the patients achieved a target C_{max} of 35 mg/L that was found to be associated with improved tuberculosis treatment outcomes (Chideya *et al.*, 2009). Variability in exposure

to pyrazinamide was not as large as that observed for rifampicin. This result has been previously reported and could be partly due to efficient absorption of pyrazinamide compared to rifampicin (Denti, Jeremiah, *et al.*, 2015; Tappero *et al.*, 2005).The target of 35 mg/L identified by Chideya et al. was derived by dichotomising the C_{max} prior to analysis based on the median dose of 35 mg/kg. Pasipanodya et al. applied CART methodology and reported that a target C_{max} of at least 58.3 mg/L was associated with 2-month culture conversion (Pasipanodya *et al.*, 2013). Less than 5% of the participants in the present study achieved the threshold. The C_{max} used by Pasipanodya et al. was derived from a cohort of TB patients with a TB/HIV co-infection rate of only 10% hence we could speculate that low C_{max} in the current research work might be due to malabsorption since all the patients were TB/HIV coinfected. Results of MARS analysis showed that pyrazinamide interacted synergistically with rifampicin where in patients with rifampicin C_{max} of at least 8.2 mg/L, having an $AUC_{0–24}$/MIC ratio of pyrazinamide > 11.3 was associated with enhanced sterilizing activity. Pasipanodya et al. reported that $AUC_{0–24}$ is associated with long-term tuberculosis treatment outcomes: favourable outcomes were observed in patients with $AUC_{0–24}$ of at least 363 mg·h/L. Only 55% of patients in our cohort achieved the target, and this could also be linked to lower drug exposure reported in TB/HIV co-infected patients. The small decrease in pyrazinamide exposure in patients who received an increased dose of rifampicin highlights the need to assess the effect of rifampicin exposure on co-administered drugs in studies evaluating high doses of rifampicin. Early introduction of ART does not seem to affect exposure to pyrazinamide.

Ethambutol C_{max} was below the target of 2 mg/L in 26% of the patients in the cohort. A similar proportion was reported among patients from Tanzania (Denti, Jeremiah, *et al.*, 2015). Our proportion and the one reported by Denti *et al*. was lower than the one reported in two studies conducted in Botswana (41% and 87%) (Chideya *et al.*, 2009; Tappero *et al.*, 2005). In a cohort from South Africa, McIlleron et al. reported a low proportion (12%) of patients who did

not attain the targeted 2 mg/L C_{max} of ethambutol (McIlleron *et al.*, 2012). Chigutsa et al. reported that the target therapeutic index (C_{max}/MIC > 0.46) associated with treatment outcomes for ethambutol, but our study did not measure MICs, and this association was only significant in patients with rifampicin AUC_{0-24} < 35.4 mg·h/L (Chigutsa *et al.*, 2015). Both C_{max} and AUC_{0-24} of ethambutol were marginally reduced in patients who received 15 mg/kg of rifampicin, but the effect of treatment arm was not significant hence the observed pattern could be a result of effects already in the model, and this should be investigated further with higher than 15 mg/kg doses of rifampicin. The effect of exposure to ethambutol has not received much attention until recently where ethambutol was found to accumulate in diseased tissues and penetrates into lesions (Zimmerman *et al.*, 2017).

The result showing reduced bioavailability in all four drugs used in the RAFA study shows the need to monitor the quality of FDC products including batch to batch variability. The reason for the reduced bioavailability is unclear, but we speculate that both the quality of products and variation in storage conditions such as temperature changes could have influenced the bioavailability (Hutchings, Monie, Spragg, *et al.*, 1983). Regular dissolution testing suggested by Ashokraj et al. could be implemented as part of tuberculosis treatment programmes (Ashokraj, Agrawal, & Panchagnula, 2008).

A limitation of this study is that the MICs of the isolates were not quantified which would have enabled further assessment of drug exposure against therapeutic indices (e.g. AUC_{0-24}/MIC) found to be associated with treatment outcomes. In addition, the target C_{max} values used in this study are average concentrations derived from studies conducted in volunteers and tuberculosis patients hence are higher than what would be observed in TB/HIV co-infected patients. Exposure reported in this thesis was measured on a single day therefore does not account for any fixed or random time effects.

In conclusion, we described the pharmacokinetics of rifampicin, desacetyl-rifampicin, pyrazinamide, and ethambutol in TB/HIV co-infected patients from Benin and Guinea. Exposure to the three drugs was generally consistent with what has been reported before, and a large proportion of the patients had reduced drug exposure.

6.3 Appendix

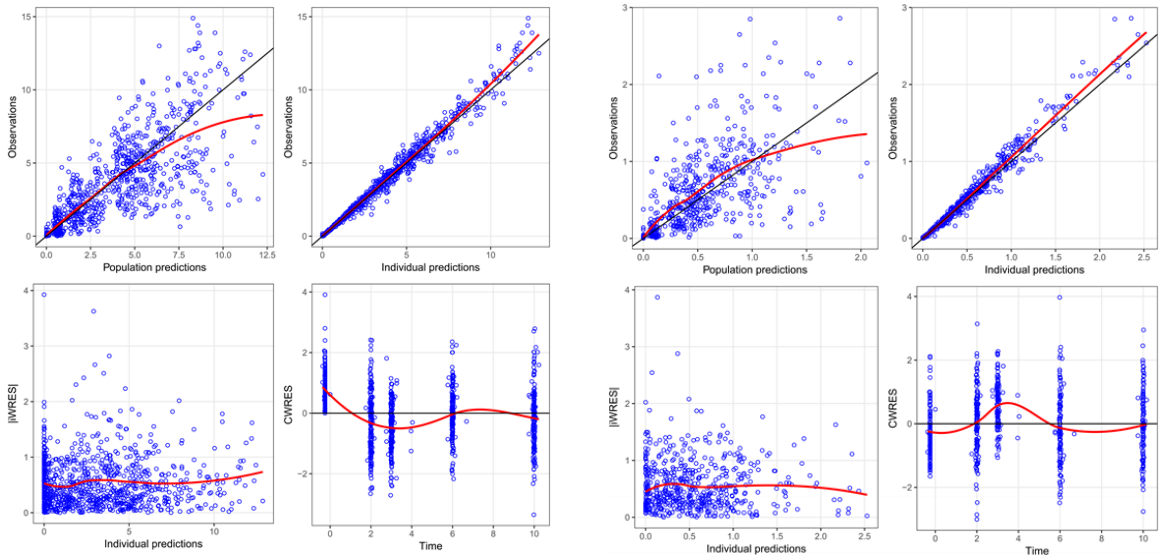

Figure 6.8 Goodness of fit plots for the model describing pharmacokinetics of rifampicin (left) and desacetyl-rifampicin (right)

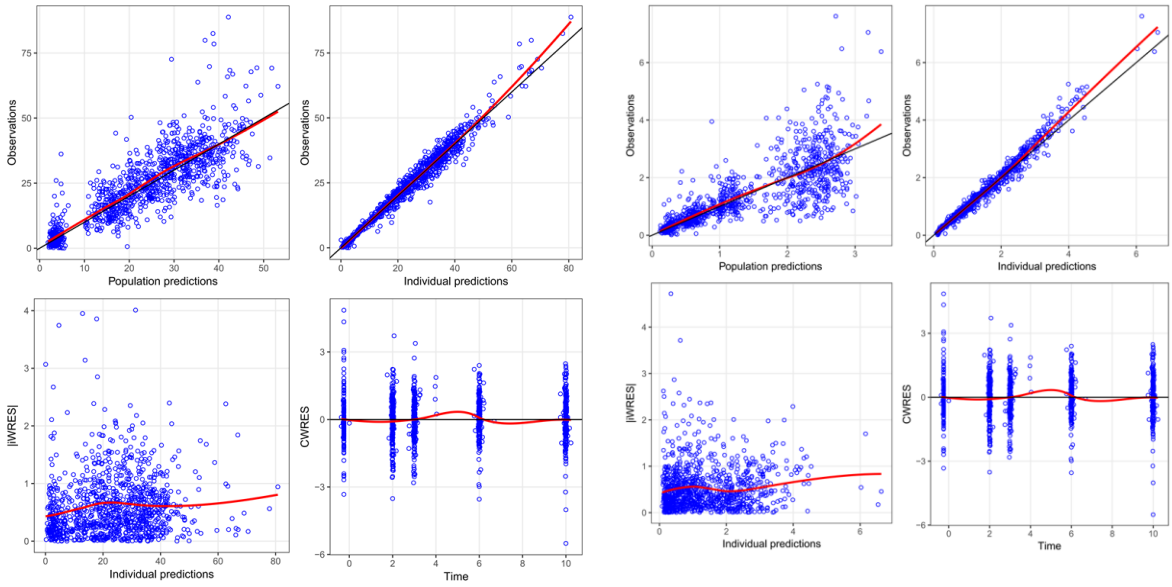

Figure 6.9 Goodness of fit plots for the model describing pharmacokinetics of pyrazinamide (left) and ethambutol (right)

Chapter 7: Correlates of tuberculosis treatment outcomes in a cohort of TB/HIV co-infected patients

7.1 Introduction

The long duration of therapy remains a challenge for the successful treatment of tuberculosis (TB). Response to tuberculosis treatment is monitored by the use of sputum cultures. Time-to-sputum culture conversion is an important measure of treatment response and is defined as the time in days from the start of treatment to the first negative sputum culture result which is confirmed at a follow-up visit after at least one week (Gillespie *et al.*, 2014; Wallis & Johnson, 2009). Time-to-culture conversion has been reported to be delayed in patients who have cavitation at baseline (Domínguez-Castellano *et al.*, 2003) and male patients (Hesseling *et al.*, 2010). Similarly, high bacillary load at baseline delays culture conversion (Caetano Mota, Carvalho, Valente, Braga, & Duarte, 2012). Hesseling et al. showed that baseline time to detection in liquid media is associated with month 2 culture conversion and relapse (Hesseling *et al.*, 2010). Month 2 culture result is a widely used measure of treatment bacteriologic response to therapy. Using CART methodology, peak concentrations of pyrazinamide, rifampicin and, isoniazid were found to be predictive of month 2 culture results in two separate studies conducted in South Africa and West Africa (Pasipanodya *et al.*, 2013; Smythe, 2016). The same authors also showed that the area under the concentration-time curve for pyrazinamide, rifampicin and isoniazid is related to long-term treatment outcomes. In patients with CD4+ count less than 100 cells/µL, the proportion of relapse was reportedly higher than those with CD4+ of at least 100 cells/µL (Pulido *et al.*, 1997). Poor long-term treatment outcome which include death and relapse is also more likely to be observed in patients with low BMI (Hanrahan *et al.*, 2010). The purpose of the PK-PD analysis was to determine factors including drug exposure that are correlated with time-to-sputum culture conversion and long-term treatment outcome (death or relapse).

7.2 Methods

Data used for the analysis presented in this chapter were collected in the RAFA clinical trial and the study design has been described in chapter 2 this report. The analysis approach for the PK-PD analysis is reported in section 2.4. In summary, the “best” hazard model describing the time-to-sputum culture conversion was determined using Monolix Suite R2016 based on the AIC values for the Weibull, Gompertz and three-parameter surge function time-to-event models. CART methodology was applied in the conditional inference framework to identify drug exposure, disease burden and patient characteristics predictive of time-to-sputum culture conversion (Fu & Simonoff, 2017). Patients were classified into different categories based to the terminal nodes of the derived regression tree and the difference in hazards of culture conversion between the groups was assessed in the time-to-event model. Binary CART methodology was used to determine drivers of long-term treatment outcome using ctree package (Hothorn, Hornik, & Zeileis, 2006) in R software version 3.4.0 (R Core Team, 2017). All statistical tests were performed at 5% level of significance.

7.3 Results

In this chapter, we sought to evaluate the effect of drug exposure, patients' characteristics, and disease burden on time-to-stable culture conversion (section 7.1.1) and the effect of these factors on relapse and death (section 7.1.2). For the PK-PD analysis, only the data from patients with exposure to all four drugs were considered, i.e. 150 subjects. Figure 7.1 shows histograms of drug exposure in these patients, while the patient characteristics before tuberculosis treatment initiation are presented in table 5.1.

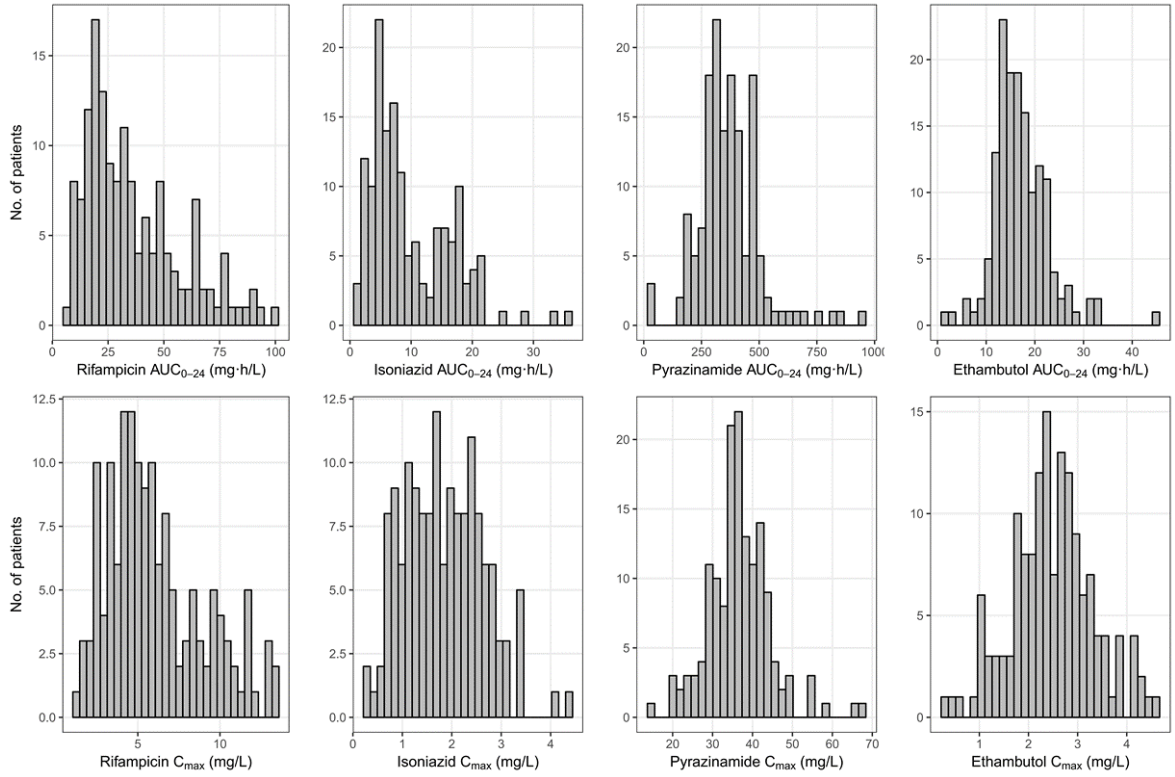

Figure 7.1 Steady-state $AUC_{0–24}$ and C_{max} for rifampicin, isoniazid, pyrazinamide and ethambutol used for the PK-PD analysis

7.3.1 Time-to-stable culture conversion

Three of the 150 patients had a negative culture result at the start of treatment and were excluded only for the time-to-event analysis, which describes the time-to-stable culture conversion and sought to identify factors modifying this measure of treatment response. The

Gompertz hazard model had the lowest AIC (9 points lower than the three-parameter surge function model). The predictive ability of the Gompertz and three parameter surge function were similar. The Gompertz hazard model was selected for inclusion of covariates. Figure 7.2 is the VPC for the Gompertz hazard model without the effects of covariates and suggests adequate fit to the data.

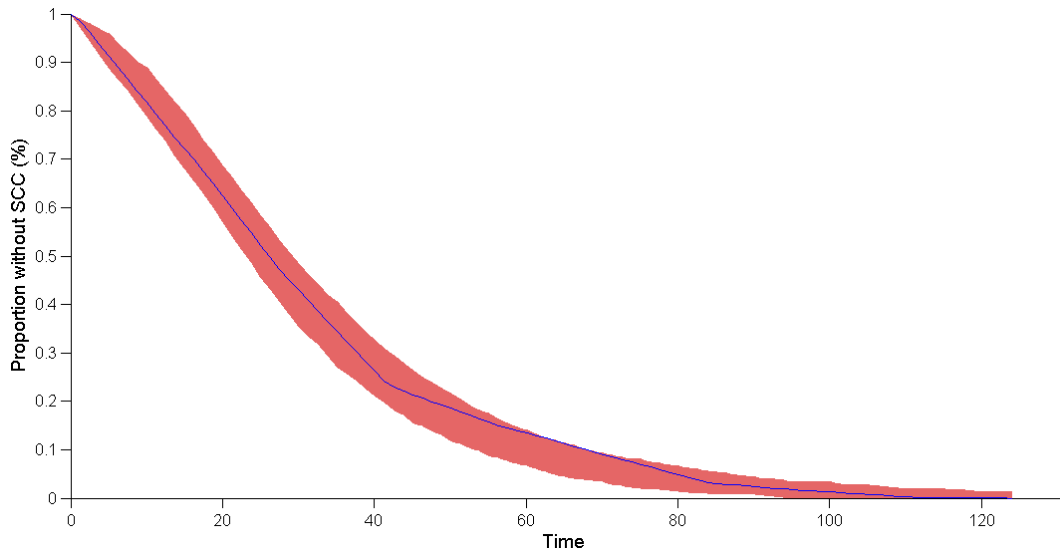

Figure 7.2 Visual predictive check of the time-to-stable culture conversion. The shaded area is the 95% prediction interval of the time-to-stable culture conversion profile, and the line is the empirical time-to-stable culture conversion.

Figure 7.3 shows the final time-to-event classification and regression tree with the selected covariates. The procedure identified X-ray grading as the most important covariate associated with time-to-stable culture conversion (P value= 0.004): patients with a normal, minor, and advanced X-ray grade were separated from those that had a very advanced X-ray grade. Among patients with very advanced X-ray reading, there was an association between HIV stage before tuberculosis diagnosis and time-to-stable culture conversion: patients who were in HIV stage 2 had faster time-to-stable culture conversion compared to those in stage 3 or 4 (P value= 0.048). Amongst the patients in HIV stage 3 or 4, those who initiated ART at two weeks had a faster time-to stable culture conversion compared to those who delayed ART regardless of the dose of rifampicin received (10 mg/kg or 15 mg/kg) (P value= 0.043). No

significant association between drug exposure as measured by AUC_{0-24} or C_{max} with time-to-stable culture conversion was observed.

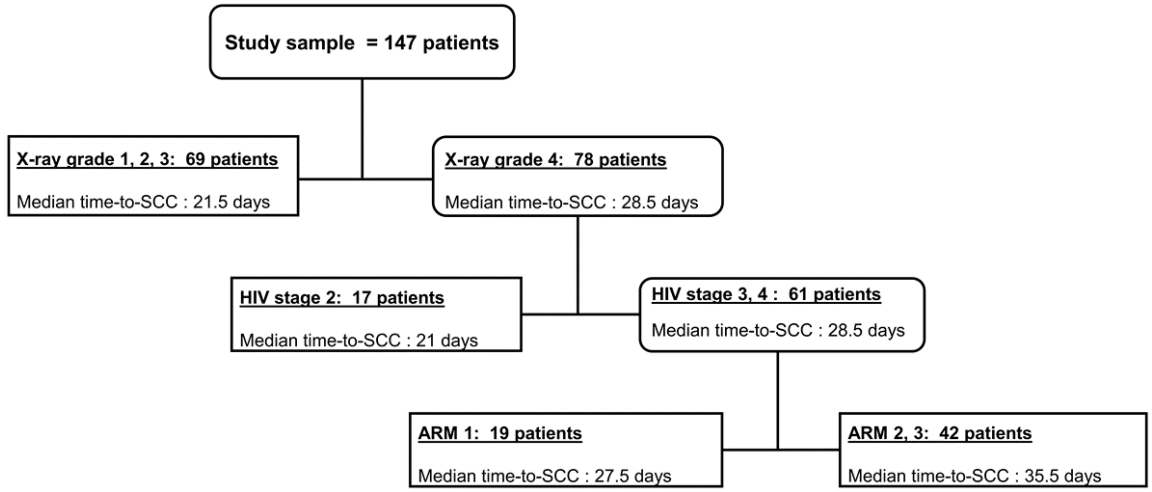

Figure 7.3 Variables predictive of time-to-stable culture conversion X-ray grading: 1, normal X-ray; 2, minor X-ray; 3, advanced X-ray; 4, very advanced X-ray. HIV stage is the WHO clinical staging of HIV at tuberculosis diagnosis. Treatment arm: 1, patients started ART at two weeks after tuberculosis treatment initiation; 2, patients started ART at two months after tuberculosis treatment initiation; 3, patient received increased dose of rifampicin (+50%) and started ART at two months after tuberculosis treatment initiation. SCC: stable culture conversion.

The four terminal nodes shown in Figure 7.3 were included in the time-to-event model in Monolix as a single categorical variable: each terminal node as a category of the new variable. The effect of the new variable representing the terminal nodes was evaluated on the scale parameter of the Gompertz model. The new variable was then simplified consistently with the statistical significance testing and the parameter estimates of the final model are shown in Table 7.1.

Table 7.1 Parameter estimates of the base and final model for time-to-stable culture conversion

Parameter	Estimate	RSE (%)
Base model		
Scale	0.0094	28
Shape	0.0574	29
Final model		
Scale [nodes 1-3][a]	0.0153	17
Scale [node 4][b]	0.00529	27
Shape	0.0512	16

[a]Nodes 1-3: node 1, patients with normal, minor, or advanced X-ray grade; node 2, patients with very advanced X-ray grade and in HIV stage 2 before tuberculosis infection; node 3, patients with very advanced X-ray grade, in HIV stage 3 or 4 before tuberculosis infection who started ART two weeks after initiation of tuberculosis treatment.

[b]Node 4, patients with very advanced X-ray grade and in HIV stage 3 or 4 before tuberculosis diagnosis who started ART eight weeks after initiation of tuberculosis treatment.

There were no significant differences between time-to-stable culture conversion of the first three nodes, so these were merged into one. Comparing the scale parameter of the first three nodes to the last node, time-to-stable culture conversion for the last node was significantly higher (P value< 0.001). The median time-to-stable culture conversion in for nodes 1–3 and node 7 was estimated to be 23 and 37 days respectively. Figure 7.4 shows a stratified VPC of the time-to- stable culture conversion for node 4 and other nodes in Figure 7.3.

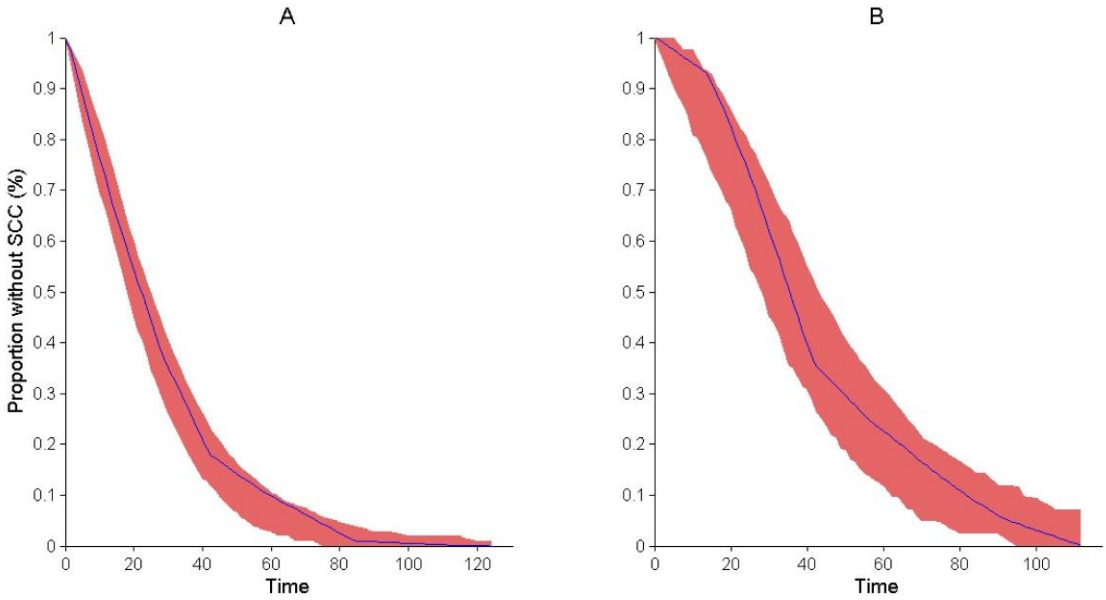

Figure 7.4 Visual predictive check of the time-to-stable culture stratified by patient characteristics. The left panel is a combined VPC for patients classified in nodes 1, 2 and 3, and the right panel is a VPC for patients classified into node 4 of figure 7.3.

7.3.2 Long-term treatment outcome

Long-term treatment outcome was defined as either relapse or death over 24 months of follow-up after tuberculosis treatment initiation. Of the 150 patients who had all tuberculosis drugs exposure data, 20 patients either had a relapse (13/20) or died (7/20). Patient characteristics of the 150 patients stratified by long-term outcome were comparable between the two groups, as shown in Table 7.2.

Table 7.2 Characteristics of patients with drug concentration for all four drugs stratified by long-term treatment outcome

Characteristic	Value[a]	
	Favourable outcome	Poor outcome
Total No.	130	20
No. (%) of females	50 (38%)	6 (30%)
No. (%) in early ART arm	32 (25%)	8 (40%)
No. (%) in high dose rifampicin arm	61 (47%)	9 (45%)
Weight, kg	51 (33–87)	54 (42–73)
Height, m	1.7 (1.4–1.9)	1.7 (1.6–1.9)
FFM, kg	43.3 (24.7–65.3)	44.0 (30.2–58.1)
Age, years	38 (19–64)	36 (23–65)
$CD4^+$ cells/µl	163.5 (51–772)	209 (51–512)
Viral load, copies/ml ($x10^3$)	150 (0.08–10000)	150 (4–500)
Serum creatinine, µmol/liter	89 (23–212)	89 (62–177)
Haemoglobin level, g/dl	9.4 (5.2–15.9)	9.0 (6.7–12.4)
ALT, units/liter	26 (5–71)	28 (3–97)
White blood cells, $x10^9$/L	7 (2.6–26.2)	6.9 (3.7–13.8)
Platelets, $x10^9$/L	343 (124–832)	327 (129–555)
Rifampicin $AUC_{0–24}$	29.4 (6.58–99.9)	35.4 (9.1–88)
Rifampicin C_{max}	5.43 (1.4–13.5)	5.26 (1.85–11.8)
Isoniazid $AUC_{0–24}$	7.66 (0.899–35.4)	6.85 (1.73–21.7)
Isoniazid C_{max}	1.8 (0.31–4.4)	1.56 (0.47–3.37)
Pyrazinamide $AUC_{0–24}$	343 (27.2–942)	410 (251–856)
Pyrazinamide C_{max}	36.1 (15.1–68)	37.7 (26.5–54)
Ethambutol $AUC_{0–24}$	16.5 (2.18–45.6)	16.5 (11.6–33.3)
Ethambutol C_{max}	2.44 (0.29–4.59)	2.41 (1.04–4.47)

[a] Median, minimum, and maximum value presented unless specified

Associations between tuberculosis treatment outcome vs. drug exposure, disease burden, and patient characteristics were assessed via CART in the conditional inference framework. CART identified the presence of cavities, the degree of patient's physical activity, and $CD4^+$ count as drivers of long-term treatment outcomes (Figure 7.5). Patients with lung cavitation were more likely to either relapse or die (25% vs. 13%, P value= 0.045). In patients who did not have lung cavitation, CART identified the degree of physical activity as predictive of the outcome. Patients were classified as not active if they were confined to bed before tuberculosis treatment initiation, otherwise they were categorised as active, regardless of TB symptoms. In patients who were confined to bed, 24% had poor outcome compared to 6% among those who were active (P value= 0.021). Patient's $CD4^+$ count was dichotomised as either below or above 100 cells/µL based on preliminary results of the main RAFA study, which will be discussed in the next section. The $CD4^+$ count was associated with treatment outcome in patients who did not present with lung cavitation and were active. A higher proportion of poor treatment outcome was observed in patients who had lower $CD4^+$ count (17% vs. 2%, P value= 0.006). Drug exposure was not found to be predictive of long-term tuberculosis treatment outcome.

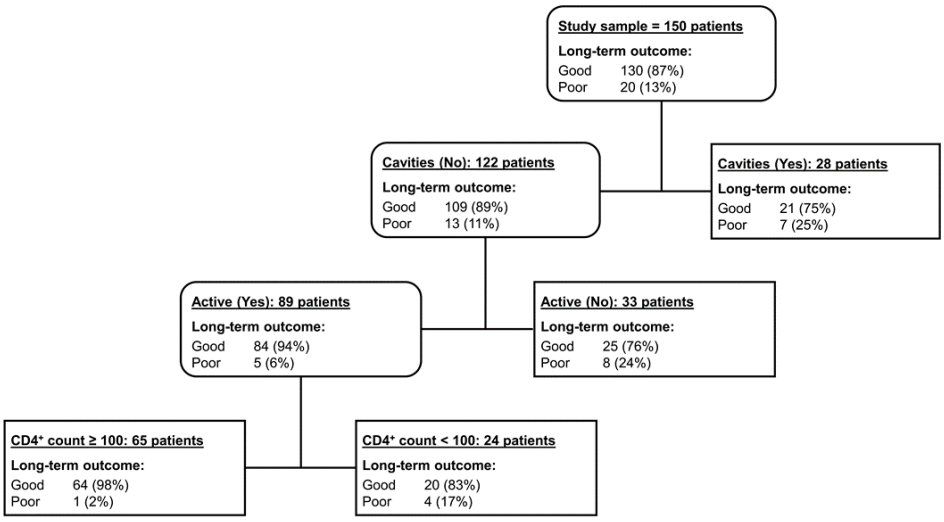

Figure 7.5 Variables predictive of long-term treatment outcomes in CART analysis

Table 7.3 provides the measure of association and the diagnostic accuracy measures for the identified predictors of poor long-term treatment outcome. The ability of the decision rules identified by the CART to correctly classify patients with poor long-term treatment outcome was low as measured by the sensitivity.

Table 7.3 Associations between derived cut-offs of predictors and poor long-term treatment outcome

Predictor	OR (95% CI)	Sensitivity % (95% CI)	Specificity % (95% CI)
Cavities (N=150)			
No	1		
Yes	2.8 (1.0–7.6)	25 (11–45)	89 (83–94)
Active (N=122)			
Yes	1		
No	5.4 (1.8–16.4)	24 (11–42)	94 (87–98)
$CD4^+$ count (N=89)			
≥ 100 cells/ µl	1		
< 100 cells/ µl	12.8 (2.1–80)	17 (5–37)	99 (92–100)
Overall classification (N=150)			
Favourable	1		
Poor	18.4 (3.9–86.1)	22.2 (14.0–32.7)	98.5 (91.7–100)

7.4 Discussion

The PK-PD analysis aimed to assess whether drug exposure, patient characteristics, and disease burden are associated with time-to-stable culture conversion and long-term poor treatment outcomes. We combined classical time-to-event modelling techniques, and time-to-event classification and regression trees to identify the factors and their interactions that contribute to time-to-stable culture conversion. Sputum culture results were determined bi-weekly in the first eight weeks of treatment and monthly thereafter, hence we applied interval censoring to handle the long gaps between observation of events.

Several factors could affect time-to-stable culture conversion, such as treatment, baseline bacterial load, the presence of cavitation, and baseline demographic characteristics (Güler, Ünsal, Dursun, AydIn, & Capan, 2006; Hesseling *et al.*, 2010; Visser *et al.*, 2012). We found disease-associated patient characteristics and treatment strategy as the main drivers of time-to-stable culture conversion. The X-ray grading reflects the extent of chest abnormality after tuberculosis infection (Ralph *et al.*, 2010). Patients with X-ray graded as advanced converted later than other patients. However, if these patients were in early-stage of HIV infection at time of tuberculosis diagnosis, the time-to-stable culture conversion was shorter. The last splitting variable of our regression tree shows the benefits of early initiation of ART in critically ill patients: those with very advanced X-ray abnormality and who were in the late-stage of HIV infection but started ART at two weeks after tuberculosis treatment initiation converted earlier than those who started ART at eight weeks after the start of tuberculosis treatment. Starting ART at two weeks has been shown to be associated with reduced mortality in TB/HIV co-infected (Abdool Karim *et al.*, 2010; Shastri, Naik, Shet, *et al.*, 2013), and our results show additional benefits among patients who present with severe tuberculosis and HIV infection.

The effects of drug exposure as measured by $AUC_{0–24}$ or C_{max} on time-to-stable culture conversion could not be detected in our study. Svensson et al. reported the significant effect of an increased dose of rifampicin on reducing the time-to-stable culture conversion (Svensson, Svensson, *et al.*, 2017), but their study observed a larger range of doses: 10 to 30 mg/kg compared to 10 to 15 mg/kg of body weight in our study. Pharmacokinetic sampling is usually performed on a single day during treatment, and with the variability associated with C_{max} (Endrenyi & Yan, 1993) the value may not be a true reflection of the overall C_{max} during treatment. Thus, if the variability between occasions is large then the relationship between exposure and treatment outcomes will not be accurately captured on a single occasion. In the absence of serial sputum culture results, which were available both in our study and that by Svensson et al., 2-months culture result is usually used as a marker of treatment success. At two months, Pasipanodya et al. identified peak concentrations of pyrazinamide, rifampicin, and isoniazid as drivers for culture conversion (Pasipanodya *et al.*, 2013). In a cohort from South Africa and West Africa, the peak concentration of rifampicin was associated with 2-months culture conversion (Smythe, 2016). Pasipanodya et al. and Smythe applied CART without permutation tests to identify the drivers of culture conversion. However, the method used in these two latter reports favours continuous variables that have many splits points and rarely identify ordinal or nominal variables. The effect of drug exposure on the time-to-stable culture conversion in the present study was further explored by classifying the C_{max} and $AUC_{0–24}$ into either quartiles, binary (above or below median) or using cut-off values based on population data in literature but PK-PD relationships could not be established (Alsultan & Peloquin, 2014a; Chideya *et al.*, 2009; Chigutsa *et al.*, 2015; Pasipanodya *et al.*, 2013).

Long-term treatment outcome was defined as relapse or death within 24 months after tuberculosis treatment initiation. We identified disease severity as primary drivers of long-term treatment outcome in the cohort of TB/HIV infected patients. This is different from some previous studies that identified drug exposures as primary drivers of long-term treatment

outcome (Pasipanodya *et al.*, 2013; Smythe, 2016; Swaminathan *et al.*, 2016). The association between cavitation and poor long-term treatment outcome could be a result of: (1) incomplete kill and then re-activation of previously dormant bacteria in cavities (Flynn & Chan, 2001), and (2) reduced distribution of drugs in cavities (Dartois, 2014). Our study recruited TB/HIV co-infected patients, and the level of physical activity identified in our analysis could be representing hidden disease severity of co-morbidities since all patients were in at least WHO stage 2 of HIV infection before tuberculosis diagnosis. Similarly, patients with $CD4^+$ count <100 cells/µL had poor long-term outcomes even if not presenting with cavities and physically active.

This study has several limitations. By measuring drug exposure on a single day of treatment, an assumption is that variability in exposure between different days over the duration of treatment is relatively low, but the assumption may be considered weak for C_{max} values. Multiple data imputation methods could have been used to impute exposure of patients with missing drug concentrations, especially for isoniazid that was the drug with most missing values, but this could result in less accurate exposure values due to the non-availability of acetylator status for isoniazid. The process would involve computing exposure assuming that the patient is a fast/ slow acetylator then adjust the exposure by the probability of a patient being a fast/slow acetylator. The exact date of culture conversion could not be accurately determined due to the long time period between follow-up visits, but time-to-event analysis with interval censoring applied in this thesis handles the problem well. Patients who relapsed and those who died could have different baseline characteristics, hence combining these due to small numbers could potentially mask some effects since death could be less likely related to drug exposure. The binary long-term outcome does not contain information on the time at which the event occurred, so we could not separate early and late treatment outcomes. Data on MICs of isolates were not available and this limited the analysis to PK-PD indices that are not adjusted for the level of resilience of the bacterial strain in each patient.

Chapter 8: Conclusions

Successful treatment of TB/HIV co-infected patients remains a challenge, and calls for research geared towards optimising the drugs in the currently recommended regimens. Limited information is available on the determinants of pharmacokinetic variability and the effects of variability on tuberculosis treatment outcomes. Strategies that are currently under investigation to improve the treatment of drug-susceptible tuberculosis include increasing the dose of rifamycins, aggressive management of HIV infection by early introduction of antiretroviral therapy, and repurposing of old anti-tuberculosis drugs. It is therefore pivotal to investigate the potential effect of these treatment changes on the pharmacokinetics of the currently recommended drugs as well as improve our understanding of the pharmacokinetics of antituberculosis drugs in TB/HIV co-infected patients in an African setting. Equally important is the need to identify and profile the drivers of successful tuberculosis treatment.

The research presented here contributes to the body of knowledge by describing the pharmacokinetics of first-line antituberculosis drugs in two cohorts of TB/HIV co-infected patients from South Africa and West Africa using nonlinear mixed-effects modelling techniques. While developing and refining the models, we chose to use a semi-mechanistic approach based on physiological plausibility and made possible by the availability of intensively-sampled pharmacokinetic data. Secondly, we sought to establish whether TB/HIV patients in the cohorts attain drug exposures with known associations with tuberculosis treatment success. HIV co-infection is expected to increase the variability in drug exposure due to possible drug-drug interactions between ART and TB medications and the previously reported effect of HIV infection on pharmacokinetics of tuberculosis drugs. Hence, another aim was to determine the drivers, including drug exposure, of successful treatment outcomes (time-to-stable culture conversion, and death or relapse). The main findings and their practical implications, together with limitations and suggestions for further research are discussed in the next sections.

8.1 Pharmacokinetics of rifampicin and desacetyl-rifampicin: increased dose, autoinduction and saturable pharmacokinetics

Increasing evidence points towards the possible benefits of increasing rifampicin dose within the 1st line regimen (Aarnoutse *et al.*, 2017; Boeree *et al.*, 2015, 2017; Diacon *et al.*, 2007). There has been further research on the pharmacokinetics of rifampicin since the publication of the manuscript on autoinduction of rifampicin and its saturable pharmacokinetics (chapter 3). It is reassuring that the recent publication by Svensson et al. confirms our results on the duration of autoinduction and saturable pharmacokinetics. In our study, autoinduction of rifampicin was estimated to be complete in three weeks, which is 50% longer than the two weeks previously reported in early pharmacokinetic studies of rifampicin (Acocella, 1978) but in line with the most recent results (Svensson, Aarnoutse, *et al.*, 2017). The longer duration of autoinduction implies exposures reported in pharmacokinetic studies at two weeks after initiation of daily rifampicin intake are relatively overestimated and would need to be adjusted to reflect the average exposure at the fully induced state. Overestimation of steady-state exposure becomes a challenge at a time when evaluation of doses higher than the currently recommended 10 mg/kg are ongoing and considering that the level of induction may increase with the larger administered dose (Svensson, Aarnoutse, *et al.*, 2017). The two models for rifampicin presented in chapter 3 and chapter 6 described the nonlinearity of the dose-exposure relationship due to the saturable pharmacokinetics of rifampicin. The inclusion of desacetyl-rifampicin data into the model for rifampicin helped separate deacetylation from other routes of metabolism, and the later shows saturable pharmacokinetics. Furthermore, the model presented in chapter 6 included the saturable pharmacokinetics of desacetyl-rifampicin and demonstrated that saturation occurs at lower concentrations than for rifampicin. Monte Carlo simulations of increased doses of up to 3.5 times higher mirrored the exposures reported in a clinical trial evaluating exposures achieved with increased doses of rifampicin. We also showed using simulations that a rifampicin dose of at least 25 mg/kg will be sufficient to reach an AUC_{0-24}/MIC ratio of 271 mg·h/L reportedly correlated with bactericidal activity of rifampicin

(Jayaram *et al.*, 2003). A recent clinical trial showed no improvement in bacteriological response with a 20 mg/kg dose compared to the currently recommended 10 mg/kg (Aarnoutse *et al.*, 2017) hence our simulations could have played a significant role in informing the doses for the clinical trial.

Our findings also showed that current weight band-adjusted dosing resulted in exposure disparities among patients in different weight bands: patients with lower weight have reduced exposure, a result also reported in a non-compartmental analysis of the TB-HAART study (McIlleron *et al.*, 2012). The difference in exposure is by and large driven by the saturable pharmacokinetics of rifampicin, and hence exposure to rifampicin in linked to the absolute dose of rifampicin rather than weight-adjusted dose. Additionally, the difference in exposure is also worsened by the result that fat-free mass was preferable to total body weight as the size descriptor for allometric scaling, and the relationship between weight and clearance is nonlinear. This difference becomes important in a population of tuberculosis patients with a wide range of body mass index or fat-free mass. Most importantly, low weight patients tend to be the ones with worse health status and may have lost weight because of tuberculosis, so it is even more crucial for them to achieve suitable drug concentrations.

The exponential model used to describe the autoinduction of rifampicin has a limitation that it cannot be used to simulate exposures associated with non-daily treatment. However, the rich data collected on days 1, 8, 15 and 29 was vital in describing the autoinduction process and was sufficient for estimation of the duration of autoinduction within the period when pharmacokinetic sampling was conducted. For the data used in the analysis reported in this thesis, the semimechanistic autoinduction model with an enzyme compartment did not perform significantly better than the one reported in chapter 3. The TB-HAART study implemented a 10 mg/kg dose hence we could not assess the effect of increased dose on extent and duration of autoinduction. This effect later evaluated by Svensson et al., but their study was did not have pharmacokinetic samples collected beyond two weeks after

tuberculosis treatment initiation (Svensson, Aarnoutse, *et al.*, 2017). SNPs such as SLCO1B1 rs4149032 have been suggested to be associated with the pharmacokinetics of rifampicin, but the effect needs to be reassessed in different patient populations. Data on genetic polymorphisms were not available at the time of this analysis but will be usefull to incorporate it in future projects linked to the RAFA study. This data might help explain the large between subject variability in rifampicin exposure observed in the RAFA study.

8.2 Pharmacokinetics of pyrazinamide and optimal doses for drug-susceptible and -resistant tuberculosis

The population pharmacokinetics of pyrazinamide was described in a cohort of TB/HIV co-infected patients from South Africa during the first month of tuberculosis treatment and a cohort of TB/HIV infected patients from West Africa between four and eight weeks after tuberculosis treatment initiation. The models for pyrazinamide presented in chapter 4 and 6 also supported the use of fat-free mass as the best body size descriptor for allometric scaling compared to total body weight. The result supports the hypothesis that hepatic function does not increase linearly with total body weight and that the contribution of fat mass to metabolic rate is minimal (Anderson & Holford, 2008). As reported for rifampicin, the implementation of a constant mg/kg dose based on total body weight in the study resulted in reduced exposure to pyrazinamide in lower-weight patients. Without modifying the boundaries of the currently used weight bands, we explored the doses of pyrazinamide required to achieve comparable exposure across the weight bands currently used for the treatment of drug-susceptible tuberculosis. Adding one tablet with 400 mg pyrazinamide to patients weighing 30-54 kg would ensure similar exposure across weight bands and 73% of the patients will achieve a target AUC_{0-24} of 363 mg·h/L reportedly associated with successful treatment outcomes. The strategy proposed here reduces the weight bands from four to three: 30–37 kg, 38–70 kg and >70 kg. Monte Carlo simulations using population pharmacokinetic models for co-administered drugs of the FDC suggest that adding a single FDC tablet to the currently recommended dose among patients with a weight between 30 and 54 kg is sufficient to balance the exposure (Court *et al.*, 2018; McIlleron & Roscigno, 2017). Simulations also showed reduced pyrazinamide exposure in MDR-TB patients with lower weight. Exposure to pyrazinamide among MDR-TB patients in different weight bands could be balanced by using a dosing strategy of 1 500 mg for patients in the 30- to -50 kg weight band, and 1 750 mg and 2 000 mg for patients weight between 51–70 kg and >70 kg respectively. Another result of the

study is that clearance of pyrazinamide increased by 14% from the first day of tuberculosis treatment to day 29 which is consistent with other studies (Denti, Jeremiah, *et al.*, 2015; Smythe, 2016). However, this change was considered too small to warrant a dose modification after the start of treatment.

The simulations used demographic data of patients with drug-susceptible tuberculosis from South Africa and West Africa, hence providing a wide distribution of patient characteristics. However, these patients might be different from MDR-TB patients with regards to the influence of disease severity on the pharmacokinetics of antituberculosis drugs. Another limitation was the non-availability of MICs for pyrazinamide to compute MIC adjusted PK-PD indices that may be more reliable than AUC_{0-24} in predicting exposure-response relationships.

8.3 The effect of increased dose of rifampicin and efavirenz-based ART on pharmacokinetics of co-administered drugs

A 50% increased dose of rifampicin did not significantly influence the pharmacokinetics of co-administered drugs, consistent with results from a Tanzanian cohort where AUC_{0-24} and C_{max} were comparable regardless of the dose of up to 20 mg/kg (Aarnoutse *et al.*, 2017). Our increase in the dose of rifampicin was modest hence the effect of rifampicin doses of at least 20 mg/kg on pharmacokinetics of concomitant drugs should be evaluated. Collaborative work done by this author, but not included in this thesis, showed that moxifloxacin clearance was reduced by 29% when administered alone compared to when co-administered with rifampicin (Naidoo *et al.*, 2017). The reduction in exposure to isoniazid, when co-administered with efavirenz-based ART reported in this thesis, has also been reported in a study conducted in Mozambique (Bhatt *et al.*, 2014). In this study, the effect is noticeable in patients who are of fast acetylator status who already achieve lower exposures than slow acetylators.

A limitation of the RAFA study was that the acetylator status for isoniazid elimination had not been determined at the time of this analysis, hence we had to resort to using mixture modelling to separate fast and slow acetylators. Mixture models have been used before for the same purpose, and in our analysis we included the mixture model from the early phases of model development. The proportion of “fast” (which included fast and intermediate) acetylators of aroung 50% based on the mixture model is line with the values reported before in West African countries (Patin *et al.*, 2006; Sabbagh *et al.*, 2008; Smythe, 2016). The precision of the estimates based on the nonparametric bootstrap gives us some level of assurance for stability of models with large covariate effects. There is also need to assess if the site effects reported for pyrazinamide and ethambutol in chapter 6 are not a result of genetic differences between the two sites.

8.4 Drivers of time-to-stable culture conversion and long-term tuberculosis treatment outcomes

To the best of our knowledge, this is the first study applying regression trees and statistical significance testing simultaneously (conditional inference framework) to identify the nonlinear relationship between tuberculosis treatment outcomes, drug exposure and clinical characteristics. Time-to-stable culture conversion was associated with chest X-ray grade, WHO HIV stage prior to tuberculosis diagnosis and early (2 weeks) vs delayed (2 months) initiation of ART. Long-term treatment outcome was correlated with the presence of cavities, patient's level of physical activity and CD4+ cell (<100 vs ≥100 cells/μL). In the parent TB-HAART study, low BMI was significantly associated with poor treatment outcome (Mfinanga *et al.*, 2014), but the association could not be established in our CART analysis of the RAFA study. The main RAFA study reported reduced mortality in patients who received a 50% higher dose of rifampicin and had low CD4+ count (<100 cells/μL) (Merle *et al.*, 2016), but this was not significant in the subset of patients recruited for the pharmacokinetic sub-study. There was no association between drug exposure and tuberculosis treatment outcomes in this study.

In terms of limitation, the dichotomous long-term treatment outcome (death or relapse) recorded does not distinguish between early and late treatment outcome, and the timing of occurrence of the outcome was not available and could not be taken into account. The regression tree method used in this study and other regression tree methods applied to pharmacokinetic data assume no uncertainty in the estimates of drug exposure, which is not true, especially due to between occasion variability. There is need to develop or adapt methods that correct for variability in drug exposure.

8.5 Implications of findings on tuberculosis treatment and research

Rifampicin doses of at least 25 mg/kg have the potential to improve overall tuberculosis treatment outcomes and this would need to be evaluated in larger and longer (~6 months) follow-up studies. The result on the duration of autoinduction suggests that studies assessing rifampicin doses should be stretched at least beyond three weeks, when the steady-state is expected to be achieved. There is need to explore the use of fat-free mass-adjusted dosing, since cumulative evidence shows its superiority over total body weight in driving exposure via allometric scaling for all first-line antituberculosis drugs. On the other hand, an immediate solution would be to add a single tablet of the FDC to patients weighing below 55 kg. Reduced exposure to isoniazid in patients receiving efavirenz-based ART calls for an assessment of this influence on the development of resistance to companion drugs. Strategies need to be put in place for regular monitoring of drug content in tablets distributed within national tuberculosis programmes to reduce the effect of between batch variability, formulation, and storage conditions on drug exposure. The decision trees identified in our analysis could be used towards the implementation of stratified medicine in tuberculosis treatment, since it could reliably identify patients expected to achieve favourable treatment outcomes. This means that more aggressive treatment strategies could be implemented in a subset of patients who are likely to fail treatment, while the chances of toxicity could be reduced by shortening treatment in patients with a better chance of responding.

8.6 Overall summary

This thesis described the pharmacokinetics of first-line antituberculosis drugs in TB/HIV co-infected patients using nonlinear mixed-effects modelling techniques. For rifampicin, the backbone of the treatment regimen, the autoinduction process and saturable pharmacokinetics were characterised and quantified. Furthermore, the thesis shows that not all pathways of rifampicin elimination are saturable, and that desacetyl-rifampicin exhibits saturable pharmacokinetics. The dose-exposure nonlinearity was established as a result of the saturable pharmacokinetics. Higher doses of rifampicin of at least 25 mg/kg are likely to improve overall treatment success. Based on the result presented in this thesis, developing treatment guidelines based on the use of allometric scaling with fat-free mass to account for nonlinear relationships between weight and clearance could guarantee similar exposure to antituberculosis drugs in patients of different body size and composition. The thesis also confirmed the result that exposure to isoniazid is reduced with concomitant intake of efavirenz-based ART, and what is novel is that this effect of efavirenz-based ART is significant in patients of fast NAT2 acetylator status. The baseline characteristics identified using classification and regression trees could be used to profile patients with high or low risk of treatment failure for the implementation of stratified treatment strategies.

References

Aarnoutse RE, Kibiki GS, Reither K, Semvua HH, Haraka F, Mtabho CM, Mpagama SG, van den Boogaard J, *et al.* (2017). Pharmacokinetics, tolerability and bacteriological response of 600, 900 and 1200 mg rifampicin daily in patients with pulmonary TB. *Antimicrobial Agents and Chemotherapy*, *61*(11), e01054-17. https://doi.org/10.1128/AAC.01054-17

Abdool Karim SS, Naidoo K, Grobler A, Padayatchi N, Baxter C, Gray A, Gengiah T, Nair G, *et al.* (2010). Timing of Initiation of Antiretroviral Drugs during Tuberculosis Therapy. *New England Journal of Medicine*, *362*(8), 697–706. https://doi.org/doi:10.1056/NEJMoa0905848

Acocella G. (1978). Clinical pharmacokinetics of rifampicin. *Clinical Pharmacokinetics*, *3*(2), 108–27. https://doi.org/10.2165/00003088-197803020-00002

Acocella G. (1983). Pharmacokinetics and metabolism of rifampin in humans. *Reviews of Infectious Diseases*, *Jul-Aug*, 5 Suppl 3:S428-32. https://doi.org/doi.org/10.1093/clinids/5.Supplement_3.S428

Acocella G, Lamarina A, Nicolis FB, Pagani V, & Segre G. (1972). Kinetic studies on rifampicin. II. Multicompartmental analysis of the serum, urine and bile concentrations in subjects treated for one week. *European Journal of Clinical Pharmacology*, *5*(2), 111–115. https://doi.org/10.1007/BF00561755

Acocella G, Pagani V, Marchetti M, Baroni GC, & Nicolis FB. (1971). Kinetic Studies on Rifampicin. I. Serum Concentration Analysis in Subjects Treated with Different Oral Doses over a Period of Two Weeks. *Chemotherapy*, *16*(6), 356–370. https://doi.org/10.1159/000220750

Adkins JC, & Noble S. (1998). Efavirenz. *Drugs*, *56*(6), 1055–64. https://doi.org/10.2165/00003495-199856060-00014

Alsultan A, & Peloquin C. (2014a). Clinical pharmacology of the anti-tuberculosis drugs. In P. D. O. Davies, G. B. Stephen, & G. Davies (Eds.), *Clinical tuberculosis* (5th ed., pp. 209–228). CRC Press. https://doi.org/10.1201/b16604-19

Alsultan A, & Peloquin CA. (2014b). Therapeutic Drug Monitoring in the Treatment of Tuberculosis: An Update. *Drugs*, *74*(8), 839–854. https://doi.org/10.1007/s40265-014-0222-8

Alsultan A, Savic R, Dooley KE, Weiner M, Whitworth W, Mac Kenzie WR, Peloquin CA, & the Tuberculosis Trials Consortium. (2017). Population Pharmacokinetics of Pyrazinamide in Patients with Tuberculosis. *Antimicrobial Agents and Chemotherapy*, *61*(6), e02625-16. https://doi.org/10.1128/AAC.02625-16

Ameer B, Polk RE, Kline BJ, & Grisafe JP. (1982). Effect of food on ethambutol absorption. *Clinical Pharmacy*, *1*(2), 156–8.

Anderson BJ, & Holford NHG. (2008). Mechanism-Based Concepts of Size and Maturity in Pharmacokinetics. *Annual Review of Pharmacology and Toxicology*, *59*(2), 303–32. https://doi.org/10.1146/annurev.pharmtox.48.113006.094708

Anderson GD. (2008). Gender Differences in Pharmacological Response. *International Review of Neurobiology*, *83*, 1–10. https://doi.org/10.1016/S0074-7742(08)00001-9

Ashokraj Y, Agrawal S, & Panchagnula R. (2008). A decision tree for rapid quality assurance and control of rifampicin-containing oral dosage forms for global distribution for tuberculosis treatment. *Indian Journal of Pharmaceutical Sciences*, *70*(1), 1–4. https://doi.org/10.4103/0250-474X.40323

Azuma J, Ohno M, Kubota R, Yokota S, Nagai T, Tsuyuguchi K, Okuda Y, Takashima T, *et al.* (2013). NAT2 genotype guided regimen reduces isoniazid-induced liver injury and early treatment failure in the 6-month four-drug standard treatment of tuberculosis: A randomized controlled trial for pharmacogenetics-based therapy. *European Journal of Clinical Pharmacology*, *69*(5), 1091–1101. https://doi.org/10.1007/s00228-012-1429-9

Babalik A, Ulus IH, Bakirci N, Kuyucu T, Arpag H, Dagyildizi L, & Capaner E. (2013). Plasma concentrations of isoniazid and rifampin are decreased in adult pulmonary tuberculosis patients with diabetes mellitus. *Antimicrobial Agents and Chemotherapy*, *57*(11), 5740–5742. https://doi.org/10.1128/AAC.01345-13

Banu Rekha V, Balasubramanian R, Swaminathan S, Ramachandran R, Rahman F, Sundaram V, Thyagarajan K, Selvakumar N, *et al.* (2007). Sputum conversion at the end of intensive phase of Category-1 regimen in the treatment of pulmonary tuberculosis patients with diabetes mellitus or HIV infection: An analysis of risk factors. *Indian Journal of Medical Research*, *126*(5), 452–458. Retrieved from http://www.ijmr.org.in/temp/IndianJMedRes1265452-3707356_101753.pdf

Bass JB, Farer LS, Hopewell PC, O'Brien R, Jacobs RF, Ruben F, Snider DE, & Thornton G. (1994). Treatment of tuberculosis and tuberculosis infection in adults and children. American Thoracic Society and The Centers for Disease Control and Prevention. *American Journal of Respiratory and Critical Care Medicine*, *149*(5), 1359–74. https://doi.org/10.1164/ajrccm.149.5.8173779

Batra JK, Venkitasubramanian TA, & Raj HG. (1987). Drug metabolism in experimental tuberculosis: I. Changes in hepatic and pulmonary monooxygenase activities due to infection. *European Journal of Drug Metabolism and Pharmacokinetics*, *12*(2), 109–14. https://doi.org/10.1007/BF03189884

Beal S, Sheiner L, Boeckmann A, & Bauer R. (2013). *NONMEM users' guides (1989–2013)*. Ellicott City, MD, USA: ICON Development Solutions.

Beal SL. (2001). Ways to fit a PK model with some data below the quantification limit. *Journal of Pharmacokinetics and Pharmacodynamics*, *28*(5), 481–504. https://doi.org/10.1023/A:1012299115260

Benator D, Bhattacharya M, Bozeman L, Burman W, Cantazaro A, Chaisson R, Gordin F, Horsburgh CR, *et al.* (2002). Rifapentine and isoniazid once a week versus rifampicin and isoniazid twice a week for treatment of drug-susceptible pulmonary tuberculosis in HIV-negative patients: a randomised clinical trial. *The Lancet*, *360*(9332), 528–34. https://doi.org/10.1016/S0140-6736(02)09742-8

Bergstrand M, Hooker AC, Wallin JE, & Karlsson MO. (2011). Prediction-corrected visual predictive checks for diagnosing nonlinear mixed-effects models. *The AAPS Journal*, *13*(2), 143–51. https://doi.org/10.1208/s12248-011-9255-z

Bhatt NB, Barau C, Amin A, Baudin E, Meggi B, Silva C, Furlan V, Grinsztejn B, *et al.* (2014). Pharmacokinetics of rifampin and isoniazid in tuberculosis-HIV-coinfected patients receiving nevirapine- or efavirenz-based antiretroviral treatment. *Antimicrobial Agents and Chemotherapy*, *58*(6), 3182–90. https://doi.org/10.1128/AAC.02379-13

Bhutani H, Mariappan TT, & Singh S. (2004). The physical and chemical stability of anti-tuberculosis fixed-dose combination products under accelerated climatic conditions. *The International Journal of Tuberculosis and Lung Disease*, *8*(9), 1073–1080. Retrieved from http://www.ingentaconnect.com/content/iuatld/ijtld/2004/00000008/00000009/art00006

Bobrowitz ID, & Robins DE. (1967). Ethambutol-isoniazid versus PAS-isoniazid in original treatment of pulmonary tuberculosis. *The American Review of Respiratory Disease*, *96*(3), 428–38. https://doi.org/10.1164/arrd.1967.96.3.428

Boeree MJ, Diacon AH, Dawson R, Narunsky K, du Bois J, Venter A, Phillips PPJ, Gillespie SH, *et al.* (2015). A dose-ranging trial to optimize the dose of rifampin in the treatment of tuberculosis. *American Journal of Respiratory and Critical Care Medicine*, *191*(9), 1058–1065. https://doi.org/10.1164/rccm.201407-1264OC

Boeree MJ, Heinrich N, Aarnoutse R, Diacon AH, Dawson R, Rehal S, Kibiki GS, Churchyard G, *et al.* (2017). High-dose rifampicin, moxifloxacin, and SQ109 for treating tuberculosis: a multi-arm, multi-stage randomised controlled trial. *The Lancet Infectious Diseases*, *17*(1), 39–49. https://doi.org/10.1016/S1473-3099(16)30274-2

Boman G, & Ringberger VA. (1974). Binding of rifampicin by human plasma proteins. *European Journal of Clinical Pharmacology*, *7*(5), 369–373. https://doi.org/10.1007/BF00558209

Bonate PL. (2011). *Pharmacokinetic-pharmacodynamic modeling and simulation* (2nd ed.). New York: Springer US.

Bose PD, Sarma MP, Medhi S, Das BC, Husain SA, & Kar P. (2011). Role of polymorphic N-acetyl transferase2 and cytochrome P4502E1 gene in antituberculosis treatment-induced hepatitis. *Journal of Gastroenterology and Hepatology*, *26*(2), 312–318. https://doi.org/10.1111/j.1440-1746.2010.06355.x

Bou-Hamad I, Larocque D, & Ben-Ameur H. (2011). A review of survival trees. *Statistics Surveys*, *5*(1), 44–71. https://doi.org/10.1214/09-SS047

Brennan PJ, & Nikaido H. (1995). The envelope of mycobacteria. *Annual Review of Biochemistry*, *64*(1), 29–63. https://doi.org/10.1146/annurev.bi.64.070195.000333

British Medical Research Council. (1981). Controlled trial of four thrice-weekly regimens and a daily regimen all given for 6 months for pulmonary tuberculosis. *The Lancet*, *1*(8213), 171–4. https://doi.org/10.1016/S0140-6736(81)90057-X

British Thoracic Association. (1982). A controlled trial of six months chemotherapy in pulmonary tuberculosis. Second report: results during the 24 months after the end of chemotherapy. British Thoracic Association. *The American Review of Respiratory Disease*, *126*(3), 460–2. https://doi.org/10.1164/arrd.1982.126.3.460

Burman WJ, Gallicano K, & Peloquin C. (2001). A population pharmacokinetic turnover and surge-function model for describing melatonin biological rhythm in healthy male subjects. *Clinical Pharmacokinetics*, *40*(5), 327–41. https://doi.org/10.2165/00003088-200140050-00002

Caetano Mota P, Carvalho A, Valente I, Braga R, & Duarte R. (2012). Predictors of delayed sputum smear and culture conversion among a Portuguese population with pulmonary tuberculosis. *Revista Portuguesa de Pneumologia (English Edition)*, *18*(2), 72–79.

https://doi.org/10.1016/J.RPPNEN.2012.01.004

Capuano SV, Croix DA, Pawar S, Zinovik A, Myers A, Lin PL, Bissel S, Fuhrman C, *et al.* (2003). Experimental Mycobacterium tuberculosis infection of cynomolgus macaques closely resembles the various manifestations of human M. tuberculosis infection. *Infection and Immunity*, *71*(10), 5831–5844. https://doi.org/10.1128/IAI.71.10.5831-5844.2003

Chan J, Fan XD, Hunter SW, Brennan PJ, & Bloom BR. (1991). Lipoarabinomannan, a possible virulence factor involved in persistence of Mycobacterium tuberculosis within macrophages. *Infection and Immunity*, *59*(5), 1755–61. Retrieved from http://iai.asm.org/content/59/5/1755.long

Charles B, Touitou Y, & Selmaoui B. (2009). A population pharmacokinetic turnover and surge-function model for describing melatonin biological rhythm in healthy male subjects. *Journal of Pharmaceutical Sciences*, *98*(2), 782–790. https://doi.org/10.1002/jps.21407

Chen B, Li J-H, Xu Y-M, Wang J, & Cao X-M. (2006). The influence of NAT2 genotypes on the plasma concentration of isoniazid and acetylisoniazid in Chinese pulmonary tuberculosis patients. *Clinica Chimica Acta*, *365*(1), 104–108. https://doi.org/10.1016/j.cca.2005.08.012

Chen J, & Raymond K. (2006). Roles of rifampicin in drug-drug interactions: underlying molecular mechanisms involving the nuclear pregnane X receptor. *Annals of Clinical Microbiology and Antimicrobials*, *5*(3). https://doi.org/10.1186/1476-0711-5-3

Chideya S, Winston CA, Peloquin CA, Bradford WZ, Hopewell PC, Wells CD, Reingold AL, Kenyon TA, *et al.* (2009). Isoniazid, rifampin, ethambutol, and pyrazinamide pharmacokinetics and treatment outcomes among a predominantly hiv-infected cohort of adults with tuberculosis from Botswana. *Clinical Infectious Diseases*, *48*(12), 1685–1694. https://doi.org/10.1086/599040

Chigutsa E, McIlleron H, & Holford NHG. (2010). Parallel first order and mixed order elimination of pyrazinamide in South African patients with tuberculosis. In *Population Approach Group Europe (19)* (p. Abstr 1946). Berlin, Germany. Retrieved from https://www.page-meeting.org/?abstract=1946

Chigutsa E, Pasipanodya JG, Visser ME, Van Helden PD, Smith PJ, Sirgel FA, Gumbo T, & McIlleron H. (2015). Impact of nonlinear interactions of pharmacokinetics and mics on sputum bacillary kill rates as a marker of sterilizing effect in tuberculosis. *Antimicrobial Agents and Chemotherapy*, *59*(1), 38–45. https://doi.org/10.1128/AAC.03931-14

Chigutsa E, Patel K, Denti P, Visser M, Maartens G, Kirkpatrick CMJ, McIlleron H, & Karlsson MO. (2013). A time-to-event pharmacodynamic model describing treatment response in patients with pulmonary tuberculosis using days to positivity in automated liquid mycobacterial culture. *Antimicrobial Agents and Chemotherapy*, *57*(2), 789–795. https://doi.org/10.1128/aac.01876-12

Chigutsa E, Visser ME, Swart EC, Denti P, Pushpakom S, Egan D, Holford NHG, Smith PJ, *et al.* (2011). The SLCO1B1 rs4149032 polymorphism is highly prevalent in South Africans and is associated with reduced rifampin concentrations: dosing implications. *Antimicrobial Agents and Chemotherapy*, *55*(9), 4122–7. https://doi.org/10.1128/AAC.01833-10

Chirehwa MT, Rustomjee R, Mthiyane T, Onyebujoh P, Smith P, McIlleron H, & Denti P. (2016). Model-Based Evaluation of Higher Doses of Rifampin Using a Semimechanistic Model Incorporating Autoinduction and Saturation of Hepatic Extraction. *Antimicrobial Agents and Chemotherapy*, *60*(1), 487–94. https://doi.org/10.1128/AAC.01830-15

Choudhri SH, Hawken M, Gathua S, Minyiri GO, Watkins W, Sahai J, Sitar DS, Aoki FY, *et al.* (1997). Pharmacokinetics of Antimycobacterial Drugs in Patients with Tuberculosis, AIDS, and Diarrhea. *Clinical Infectious Diseases*, *25*(1), 104–111. https://doi.org/10.1086/514513

Ciampi A, Thiffault J, Nakache JP, & Asselain B. (1986). Stratification by stepwise regression, correspondence analysis and recursive partition: a comparison of three methods of analysis for survival data with covariates. *Computational Statistics and Data Analysis*, *4*(3), 185–204. https://doi.org/10.1016/0167-9473(86)90033-2

Clemmesen JO, Tygstrup N, & Ott P. (1998). Hepatic plasma flow estimated according to fick's principle in patients with hepatic encephalopathy: Evaluation of indocyanine green and d-sorbitol as test substances. *Hepatology*, *27*(3), 666–673. https://doi.org/10.1002/hep.510270305

Cockcroft DW, & Gault H. (1976). Prediction of Creatinine Clearance from Serum Creatinine. *Nephron*, *16*(1), 31–41. https://doi.org/10.1159/000180580

Cornish-Bowden A. (2015). One hundred years of Michaelis–Menten kinetics. *Perspectives in Science*, *4*(1), 3–9. https://doi.org/10.1016/J.PISC.2014.12.002

Court R, Chirehwa MT, Wiesner L, Wright B, Smythe WA, Kramer N, Matji R, Roscigno G, *et al.* (2018). Quality assurance of rifampicin-containing fixed drug combinations in South Africa – a pragmatic response. *The International Journal of Tuberculosis and Lung Disease*, Accepted.

Dartois V. (2014). The path of anti-tuberculosis drugs: from blood to lesions to mycobacterial cells. *Nature Reviews. Microbiology*, *12*(3), 159–67. https://doi.org/10.1038/nrmicro3200

Dartois V, & Barry CE. (2010). Clinical Pharmacology and Lesion Penetrating Properties of Second- and Third-Line Antituberculous Agents Used in the Management of Multidrug-Resistant (MDR) and Extensively-Drug Resistant (XDR) Tuberculosis. *Current Clinical Pharmacology*, *5*(2), 96–114. https://doi.org/10.2174/157488410791110797

Davis RB, & Anderson JR. (1989). Exponential survival trees. *Statistics in Medicine*, *8*(8), 947–961. https://doi.org/10.1002/sim.4780080806

de Kock L, Sy SKB, Rosenkranz B, Diacon AH, Prescott K, Hernandez KR, Yu M, Derendorf H, *et al.* (2014). Pharmacokinetics of para-aminosalicylic acid in HIV-uninfected and HIV-coinfected tuberculosis patients receiving antiretroviral therapy, managed for multidrug-resistant and extensively drug-resistant tuberculosis. *Antimicrobial Agents and Chemotherapy*, *58*(10), 6242–50. https://doi.org/10.1128/AAC.03073-14

De Rose A, & Pallara A. (1997). Survival trees: an alternative non-parametric multivariate technique for life history analysis. *European Journal of Population*, *13*(3), 223–241. https://doi.org/10.1023/A:1005844818027

de Steenwinkel JEM, Aarnoutse RE, de Knegt GJ, ten Kate MT, Teulen M, Verbrugh HA, Boeree MJ, van Soolingen D, *et al.* (2013). Optimization of the Rifampin Dosage to

Improve the Therapeutic Efficacy in Tuberculosis Treatment Using a Murine Model. *American Journal of Respiratory and Critical Care Medicine*, *187*(10), 1127–1134. https://doi.org/10.1164/rccm.201207-1210OC

Decroix G, Kreis B, Sors C, Birembaum J, Lirzin M, & Canetti G. (1969). Comparison between regimes of rifampicin-isoniazid administered daily and administered twice a week (initial results of a comparative study conducted in 4 medical services of the Parisian region). *Rev Tuberc Pneumol*, *33*(6), 751–68.

Deguchi T, Mashimo M, & Suzuki T. (1990). Correlation between acetylator phenotypes and genotypes of polymorphic arylamine N-acetyltransferase in human liver. *The Journal of Biological Chemistry*, *265*(22), 12757–60. https://doi.org/10.1128/AAC.39.3.694

Deng L, Mikusova K, Robuck KG, Scherman M, Brennan PJ, & McNeil MR. (1995). Recognition of multiple effects of ethambutol on metabolism of mycobacterial cell envelope. *Antimicrobial Agents and Chemotherapy*, *39*(3), 694–701. https://doi.org/10.1128/AAC.39.3.694

Denti P, Gonzalez-Martinez C, Winckler J, Bekker A, Zar H, Davies G, van Rie A, & McIlleron H. (2017). Pharmacokinetics of rifampicin in African children: Evaluation of the new WHO dosing guidelines. In *10th International workshop on pharmacology of tuberculosis drugs*. Atlanta, USA. Retrieved from http://regist2.virology-education.com/2017/10TBPK/12_Denti.pdf

Denti P, Jeremiah K, Chigutsa E, Faurholt-Jepsen D, PrayGod G, Range N, Castel S, Wiesner L, *et al.* (2015). Pharmacokinetics of isoniazid, pyrazinamide, and ethambutol in newly diagnosed pulmonary TB patients in Tanzania. *PloS One*, *10*(10), e0141002. https://doi.org/10.1371/journal.pone.0141002

Denti P, Martinson N, Cohn S, Mashabela F, Hoffmann J, Msandiwa R, Castel S, Wiesner L, *et al.* (2015). Population pharmacokinetics of rifampin in pregnant women with tuberculosis and HIV coinfection in Soweto, South Africa. *Antimicrobial Agents and Chemotherapy*, *60*(3), 1234–41. https://doi.org/10.1128/AAC.02051-15

Denti P, Smythe W, Simonsson USH, Rustomjee R, Onyebujoh P, Smith P, & McIlleron H. (2010). A population pharmacokinetic model for rifampicin auto-induction. In *The 3rd international workshop on clinical pharmacology of TB drugs*. Boston, USA. Retrieved from http://regist2.virology-education.com/3tb/docs/12_denti.pdf

Devaleenal Daniel B, Ramachandran G, & Swaminathan S. (2017). The challenges of pharmacokinetic variability of first-line anti-TB drugs. *Expert Review of Clinical Pharmacology*, *10*(1), 47–58. https://doi.org/10.1080/17512433.2017.1246179

Diacon AH, Dawson R, von Groote-Bidlingmaier F, Symons G, Venter A, Donald PR, van Niekerk C, Everitt D, *et al.* (2012). 14-day bactericidal activity of PA-824, bedaquiline, pyrazinamide, and moxifloxacin combinations: a randomised trial. *The Lancet*, *380*(9846), 986–993. https://doi.org/10.1016/S0140-6736(12)61080-0

Diacon AH, Patientia RF, Venter A, van Helden PD, Smith PJ, McIlleron H, Maritz JS, & Donald PR. (2007). Early bactericidal activity of high-dose rifampin in patients with pulmonary tuberculosis evidenced by positive sputum smears. *Antimicrob Agents Chemother*, *51*(8), 2994–2996. https://doi.org/10.1128/aac.01474-06

Dickinson JM, & Mitchison DA. (1981). Experimental models to explain the high sterilizing activity of rifampin in the chemotherapy of tuberculosis. *The American Review of*

Respiratory Disease, *123*(4 Pt 1), 367–71. https://doi.org/10.1164/arrd.1981.123.4.367

Domínguez-Castellano A, Muniain MA, Rodriguez-Baño J, Garcia M, Rios MJ, Galvez J, & Perez-Cano R. (2003). Factors associated with time to sputum smear conversion in active pulmonary tuberculosis. *The International Journal of Tuberculosis and Lung Disease : The Official Journal of the International Union against Tuberculosis and Lung Disease*, *7*(5), 432–8. Retrieved from http://www.ncbi.nlm.nih.gov/pubmed/12757043

Donald PR, & McIlleron H. (2009). Antituberculosis drugs. In H. S. Schaaf, A. Zumla, J. M. Grange, M. C. Raviglione, W. W. Yew, J. R. Starke, M. Pai, & P. R. Donald (Eds.), *Tuberculosis: A comprehensive clinical reference* (pp. 608–617). London: Elsevier Inc. https://doi.org/10.1016/B978-1-4160-3988-4.00059-7

Donald PR, Parkin DP, Seifart HI, Schaaf HS, van Helden PD, Werely CJ, Sirgel FA, Venter A, *et al.* (2007). The influence of dose and N-acetyltransferase-2 (NAT2) genotype and phenotype on the pharmacokinetics and pharmacodynamics of isoniazid. *European Journal of Clinical Pharmacology*, *63*(7), 633–9. https://doi.org/10.1007/s00228-007-0305-5

Donald PR, & Schaaf HS. (2011). Isoniazid Pharmacokinetics and Efficacy in Adults. In P. R. Donald & P. D. van Helden (Eds.), *Antituberculosis Chemotherapy* (Vol. 40, pp. 25–31). Basel: Progress in Respiratory Research. https://doi.org/10.1159/000323628

Donald PR, Sirgel FA, Botha FJ, Seifart HI, Parkin DP, Vandenplas ML, Van de Wal BW, Maritz JS, *et al.* (1997). The early bactericidal activity of isoniazid related to its dose size in pulmonary tuberculosis. *American Journal of Respiratory and Critical Care Medicine*, *156*(3 Pt 1), 895–900. https://doi.org/10.1164/ajrccm.156.3.9609132

Donald PR, Sirgel FA, Venter A, Parkin DP, Seifart HI, van de Wal BW, Werely C, van Helden PD, *et al.* (2004). The influence of human N-acetyltransferase genotype on the early bactericidal activity of isoniazid. *Clinical Infectious Diseases : An Official Publication of the Infectious Diseases Society of America*, *39*(10), 1425–30. https://doi.org/10.1086/424999

Dorman SE, Johnson JL, Goldberg S, Muzanye G, Padayatchi N, Bozeman L, Heilig CM, Bernardo J, *et al.* (2009). Substitution of Moxifloxacin for Isoniazid during Intensive Phase Treatment of Pulmonary Tuberculosis. *American Journal of Respiratory and Critical Care Medicine*, *180*(3), 273–280. https://doi.org/10.1164/rccm.200901-0078OC

Dosne A-G, Bergstrand M, & Karlsson MO. (2017). An automated sampling importance resampling procedure for estimating parameter uncertainty. *Journal of Pharmacokinetics and Pharmacodynamics*, *44*(6), 509–520. https://doi.org/10.1007/s10928-017-9542-0

Ellard GA. (1969). Absorption, metabolism and excretion of pyrazinamide in man. *Tubercle*, *50*(2), 144–158. https://doi.org/10.1016/0041-3879(69)90020-8

Ellard GA. (1976). Variations between individuals and populations in the acetylation of isoniazid and its significance for the treatment of pulmonary tuberculosis. *Clinical Pharmacology & Therapeutics*, *19*(5part2), 610–625. https://doi.org/10.1002/cpt1976195part2610

Ellard GA. (1984). The potential clinical significance of the isoniazid acetylator phenotype in the treatment of pulmonary tuberculosis. *Tubercle*, *65*(3), 211–227. https://doi.org/10.1016/0041-3879(84)90079-5

Ellard GA, & Gammon PT. (1976). Pharmacokinetics of isoniazid metabolism in man. *Journal of Pharmacokinetics and Biopharmaceutics*, *4*(2), 83–113. https://doi.org/doi.org/10.1007/BF01086149

Endrenyi L, & Yan W. (1993). Variation of Cmax and Cmax/AUC in investigations of bioequivalence. *International Journal of Clinical Pharmacology, Therapy, and Toxicology*, *31*(4), 184–9. Retrieved from https://www.researchgate.net/publication/14698239

Ette EI, & Williams PJ. (2004). Population Pharmacokinetics II: Estimation Methods. *Annals of Pharmacotherapy*, *38*(11), 1907–1915. https://doi.org/10.1345/aph.1E259

Field SK. (2015). Bedaquiline for the treatment of multidrug-resistant tuberculosis: great promise or disappointment? *Therapeutic Advances in Chronic Disease*, *6*(4), 170–84. https://doi.org/10.1177/2040622315582325

Flynn JL, & Chan J. (2001). Immunology of Tuberculosis. *Annual Review of Immunology*, *19*(1), 93–129. https://doi.org/10.1146/annurev.immunol.19.1.93

Forget EJ, & Menzies D. (2006). Adverse reactions to first-line antituberculosis drugs. *Expert Opinion on Drug Safety*, *5*(2), 231–249. https://doi.org/10.1517/14740338.5.2.231

Fox W. (1981). Whither short-course chemotherapy? *British Journal of Diseases of the Chest*, *75*(4), 331–357. https://doi.org/10.1016/0007-0971(81)90022-X

Frame B. (2007). Mixture Modeling with NONMEM V. In E. I. Ette & Williams Paul J. (Eds.), *Pharmacometrics: The Science of Quantitative Pharmacology* (pp. 723–757). Hoboken, NJ, USA: John Wiley & Sons, Inc. https://doi.org/10.1002/9780470087978.ch28

Fretland AJ, Leff MA, Doll MA, & Hein DW. (2001). Functional characterization of human N-acetyltransferase 2 (NAT2) single nucleotide polymorphisms. *Pharmacogenetics*, *11*(3), 207–215. https://doi.org/10.1097/00008571-200104000-00004

Fu W, & Simonoff JS. (2017). Survival trees for interval-censored survival data. *Statistics in Medicine*, *36*(30), 4831–4842. https://doi.org/10.1002/sim.7450

Gabrielsson J, & Weiner D. (2007). *Pharmacokinetic and pharmacodynamic data analysis : concepts and applications* (5th ed.). Stockholm: Swedish Pharmaceutical Press.

García-García M de L, Ponce-de-León A, García-Sancho MC, Ferreyra-Reyes L, Palacios-Martínez M, Fuentes J, Kato-Maeda M, Bobadilla M, *et al.* (2002). Tuberculosis-related deaths within a well-functioning DOTS control program. *Emerging Infectious Diseases*, *8*(11), 1327–1333. https://doi.org/10.3201/eid0811.020021

Geiseler PJ, Manis RD, & Maddux MS. (1985). Dosage of antituberculous drugs in obese patients. *The American Review of Respiratory Disease*, *131*(6), 944–6. https://doi.org/10.1164/arrd.1985.131.6.944

Gillespie SH, Crook AM, McHugh TD, Mendel CM, Meredith SK, Murray SR, Pappas F, Phillips PPJ, *et al.* (2014). Four-Month Moxifloxacin-Based Regimens for Drug-Sensitive Tuberculosis. *New England Journal of Medicine*, *371*(17), 1577–1587. https://doi.org/10.1056/NEJMoa1407426

Girling DJ. (1977). The hepatic toxicity of antituberculosis regimens containing isoniazid, rifampicin and pyrazinamide. *Tubercle*, *59*(1), 13–32. https://doi.org/10.1016/0041-

3879(77)90022-8

Gordi T, Xie R, Huong NV, Huong DX, Karlsson MO, & Ashton M. (2005). A semiphysiological pharmacokinetic model for artemisinin in healthy subjects incorporating autoinduction of metabolism and saturable first-pass hepatic extraction. *British Journal of Clinical Pharmacology*, *59*(2), 189–98. https://doi.org/10.1111/j.1365-2125.2004.02321.x

Gordon L, & Olshen RA. (1985). Tree-structured survival analysis. *Cancer Treatment Reports*, *69*(10), 1065–9.

Goutelle S, Bourguignon L, Maire PH, Van Guilder M, Conte JE, & Jelliffe RW. (2009). Population modeling and monte carlo simulation study of the pharmacokinetics and antituberculosis pharmacodynamics of rifampin in lungs. *Antimicrobial Agents and Chemotherapy*, *53*(7), 2974–2981. https://doi.org/10.1128/AAC.01520-08

Grange JM. (2009). The genus mycobacterium and the mycobacterium tuberculosis complex. In H. S. Schaaf, A. Zumla, J. M. Grange, M. C. Raviglione, W. W. Yew, J. R. Starke, M. Pai, & P. R. Donald (Eds.), *Tuberculosis: A comprehensive clinical reference* (pp. 44–59). London: Elsevier Inc. https://doi.org/10.1016/B978-1-4160-3988-4.00006-8

Green B, & Duffull SB. (2004). What is the best size descriptor to use for pharmacokinetic studies in the obese? *British Journal of Clinical Pharmacology*, *58*(2), 119–33. https://doi.org/10.1111/j.1365-2125.2004.02157.x

Güler M, Ünsal E, Dursun B, AydIn Ö, & Capan N. (2006). Factors influencing sputum smear and culture conversion time among patients with new case pulmonary tuberculosis. *International Journal of Clinical Practice*, *61*(2), 231–235. https://doi.org/10.1111/j.1742-1241.2006.01131.x

Gumbo T. (2010). Chemotherapy of tuberculosis, mycobacterium avium complex disease, and leprosy. In L. L. Brunton, B. A. Chabner, & B. C. Knollmann (Eds.), *The pharmacological basis of therapeutics* (12th ed., pp. 1549–1570). New York: McGraw Hill Medical.

Gumbo T, Chigutsa E, Pasipanodya J, Visser M, van Helden PD, Sirgel FA, & McIlleron H. (2014). The pyrazinamide susceptibility breakpoint above which combination therapy fails. *The Journal of Antimicrobial Chemotherapy*, *69*(9), 2420–5. https://doi.org/10.1093/jac/dku136

Gumbo T, Dona CS, Meek C, & Leff R. (2009). Pharmacokinetics-pharmacodynamics of pyrazinamide in a novel in vitro model of tuberculosis for sterilizing effect: a paradigm for faster assessment of new antituberculosis drugs. *Antimicrobial Agents and Chemotherapy*, *53*(8), 3197–3204. https://doi.org/10.1128/AAC.01681-08

Gumbo T, Louie A, Deziel MR, Liu W, Parsons LM, Salfinger M, & Drusano GL. (2007). Concentration-dependent mycobacterium tuberculosis killing and prevention of resistance by rifampin. *Antimicrobial Agents and Chemotherapy*, *51*(11), 3781–3788. https://doi.org/10.1128/aac.01533-06

Gumbo T, Louie A, Liu W, Ambrose PG, Bhavnani SM, Brown D, & Drusano GL. (2007). Isoniazid's bactericidal activity ceases because of the emergence of resistance, not depletion of mycobacterium tuberculosis in the log phase of growth tuberculosis in the Log Phase of Growth. *The Journal of Infectious Diseases*, *195*(2), 194–201. https://doi.org/10.1086/510247

Gumbo T, Louie A, Liu W, Brown D, Ambrose PG, Bhavnani SM, & Drusano GL. (2007). Isoniazid bactericidal activity and resistance emergence: integrating pharmacodynamics and pharmacogenomics to predict efficacy in different ethnic populations. *Antimicrobial Agents and Chemotherapy*, *51*(7), 2329–36. https://doi.org/10.1128/AAC.00185-07

Hall RG, Swancutt MA, Meek C, Leff RD, & Gumbo T. (2012). Ethambutol pharmacokinetic variability is linked to body mass in overweight, obese, and extremely obese people. *Antimicrobial Agents and Chemotherapy*, *56*(3), 1502–7. https://doi.org/10.1128/AAC.05623-11

Hanrahan CF, Golub JE, Mohapi L, Tshabangu N, Modisenyane T, Chaisson RE, Gray GE, McIntyre JA, *et al.* (2010). Body mass index and risk of tuberculosis and death. *AIDS*, *24*(10), 1501–8. https://doi.org/10.1097/QAD.0b013e32833a2a4a

Hartkoorn RC, Chandler B, Owen A, Ward SA, Bertel Squire S, Back DJ, & Khoo SH. (2007). Differential drug susceptibility of intracellular and extracellular tuberculosis, and the impact of P-glycoprotein. *Tuberculosis*, *87*(3), 248–255. https://doi.org/10.1016/J.TUBE.2006.12.001

Heifets L, & Lindholm-Levy P. (1992). Pyrazinamide sterilizing activity in vitro against semidormant Mycobacterium tuberculosis bacterial populations. *The American Review of Respiratory Disease*, *145*(5), 1223–5. https://doi.org/10.1164/ajrccm/145.5.1223

Hein DW, Doll MA, Fretland AJ, Leff MA, Webb SJ, Xiao GH, Devanaboyina US, Nangju NA, *et al.* (2000). Molecular genetics and epidemiology of the NAT1 and NAT2 acetylation polymorphisms. *Cancer Epidemiology Biomarkers and Prevention*.

Hesseling AC, Walzl G, Enarson DA, Carroll NM, Duncan K, Lukey PT, Lombard C, Donald PR, *et al.* (2010). Baseline sputum time to detection predicts month two culture conversion and relapse in non-HIV-infected patients. *International Journal of Tuberculosis and Lung Disease*, *14*(5), 560–570. Retrieved from http://www.ingentaconnect.com/content/iuatld/ijtld/2010/00000014/00000005/art00008

Hickman D, & Sim E. (1991). N-acetyltransferase polymorphism: Comparison of phenotype and genotype in humans. *Biochemical Pharmacology*, *42*(5), 1007–1014. https://doi.org/10.1016/0006-2952(91)90282-A

Hirano K, Takahashi M, Kazumi Y, Fukasawa Y, & Abe C. (1997). Mutation in pncA is a major mechanism of pyrazinamide resistance in mycobacterium tuberculosis. *Tubercle and Lung Disease : The Official Journal of the International Union against Tuberculosis and Lung Disease*, *78*(2), 117–22. https://doi.org/10.1016/S0962-8479(98)80004-X

Holford N. (2013). A time to event tutorial for pharmacometricians. *CPT: Pharmacometrics & Systems Pharmacology*, *2*(5), e43. https://doi.org/10.1038/psp.2013.18

Hopewell PC. (2010). Treatment of Tuberculosis. In M. C. Raviglione (Ed.), *Tuberculosis: the essentials* (4th ed., p. 390). New York: Informa Healthcare USA Inc.

Hothorn T, Hornik K, & Zeileis A. (2006). Unbiased recursive partitioning: A conditional inference framework. *Journal of Computational and Graphical Statistics*, *15*(3), 651–674. https://doi.org/10.1198/106186006X133933

Huang Y, Chern H-D, Su W-J, Wu J-C, Chang S-C, Chiang C-H, Chang F-Y, & Lee S-D. (2003). Cytochrome P450 2E1 genotype and the susceptibility to antituberculosis drug-

induced hepatitis. *Hepatology*, *37*(4), 924–930. https://doi.org/10.1053/jhep.2003.50144

Hutchings A, Monie R, Spragg B, & Routledge P. (1983). A method to prevent the loss of isoniazid and acetylisoniazid in human plasma. *British Journal of Clinical Pharmacology*, *15*(2), 263–266. https://doi.org/10.1111/j.1365-2125.1983.tb01496.x

Hutchings A, Monie R, Spragg B, & Routledge P. (1988). Saliva and plasma concentrations of isoniazid and acetylisoniazid in man. *British Journal of Clinical Pharmacology*, *25*(5), 585–589. https://doi.org/10.1111/j.1365-2125.1988.tb03349.x

James G, Witten D, Hastie T, & Tibshirani R. (2013). *An Introduction to Statistical Learning* (Vol. 103). New York: Springer. https://doi.org/10.1007/978-1-4614-7138-7

Janmahasatian S, Duffull SB, Ash S, Ward LC, Byrne NM, & Green B. (2005). Quantification of Lean Bodyweight. *Clinical Pharmacokinetics*, *44*(10), 1051–1065. https://doi.org/10.2165/00003088-200544100-00004

Jayaram R, Gaonkar S, Kaur P, Suresh BL, Mahesh BN, Jayashree R, Nandi V, Bharat S, *et al.* (2003). Pharmacokinetics-pharmacodynamics of rifampin in an aerosol infection model of tuberculosis. *Antimicrobial Agents and Chemotherapy*, *47*(7), 2118–2124. https://doi.org/10.1128/AAC.47.7.2118-2124.2003

Jayaram R, Shandil RK, Gaonkar S, Kaur P, Suresh BL, Mahesh BN, Jayashree R, Nandi V, *et al.* (2004). Isoniazid pharmacokinetics-pharmacodynamics in an aerosol infection model of tuberculosis. *Antimicrobial Agents and Chemotherapy*, *48*(8), 2951–7. https://doi.org/10.1128/AAC.48.8.2951-2957.2004

Jeanes CW, Jessamine AG, & Eidus L. (1972). Treatment of chronic drug-resistant pulmonary tuberculosis with rifampin and ethambutol. *Canadian Medical Association Journal*, *106*(8), 884–8. Retrieved from https://www.ncbi.nlm.nih.gov/pmc/articles/PMC1940582/

Jeremiah K, Denti P, Chigutsa E, Faurholt-Jepsen D, PrayGod G, Range N, Castel S, Wiesner L, *et al.* (2014). Nutritional supplementation increases rifampin exposure among tuberculosis patients coinfected with HIV. *Antimicrobial Agents and Chemotherapy*, *58*(6), 3468–74. https://doi.org/10.1128/AAC.02307-13

Jindani A, Aber VR, Edwards EA, & Mitchison DA. (1980). The early bactericidal activity of drugs in patients with pulmonary tuberculosis. *The American Review of Respiratory Disease*, *121*(6), 939–49. https://doi.org/10.1164/arrd.1980.121.6.939

Jindani A, Doré CJ, & Mitchison DA. (2003). Bactericidal and sterilizing activities of antituberculosis drugs during the first 14 days. *American Journal of Respiratory and Critical Care Medicine*, *167*(10), 1348–54. https://doi.org/10.1164/rccm.200210-1125OC

Jönsson S, Davidse A, Wilkins J, Van der Walt J-S, Simonsson USH, Karlsson MO, Smith P, & McIlleron H. (2011). Population pharmacokinetics of ethambutol in South African tuberculosis patients. *Antimicrobial Agents and Chemotherapy*, *55*(9), 4230–7. https://doi.org/10.1128/AAC.00274-11

Juréen P, Werngren J, Toro JC, & Hoffner S. (2008). Pyrazinamide resistance and pncA gene mutations in mycobacterium tuberculosis. *Antimicrobial Agents and Chemotherapy*, *52*(5), 1852–1854. https://doi.org/10.1128/AAC.00110-08

Karlsson MO, & Sheiner LB. (1993). The importance of modeling interoccasion variability in population pharmacokinetic analyses. *Journal of Pharmacokinetics and Biopharmaceutics*, *21*(6), 735–50. https://doi.org/doi.org/10.1007/BF01113502

Keizer RJ, Jansen RS, Rosing H, Thijssen B, Beijnen JH, Schellens JHM, & Huitema ADR. (2015). Incorporation of concentration data below the limit of quantification in population pharmacokinetic analyses. *Pharmacology Research & Perspectives*, *3*(2), e00131. https://doi.org/10.1002/prp2.131

Keizer RJ, Karlsson MO, & Hooker A. (2013). Modeling and Simulation Workbench for NONMEM: Tutorial on Pirana, PsN, and Xpose. *CPT: Pharmacometrics & Systems Pharmacology*, *2*(6), e50. https://doi.org/10.1038/psp.2013.24

Kergueris MF, Bourin M, & Larousse C. (1986). Pharmacokinetics of isoniazid: Influence of age. *European Journal of Clinical Pharmacology*, *30*(3), 335–340. https://doi.org/10.1007/BF00541539

Kinzig-Schippers M, Tomalik-Scharte D, Jetter A, Scheidel B, Jakob V, Rodamer M, Cascorbi I, Doroshyenko O, *et al.* (2005). Should we use n-acetyltransferase type 2 genotyping to personalize isoniazid doses? *Antimicrobial Agents and Chemotherapy*, *49*(5), 1733–1738. https://doi.org/10.1128/AAC.49.5.1733-1738.2005

Knechel NA. (2009). Tuberculosis: pathophysiology, clinical features, and diagnosis. *Critical Care Nurse*, *29*(2), 34–43. https://doi.org/10.4037/ccn2009968

Konno K, Feldmann FM, & McDermott W. (1967). Pyrazinamide Susceptibility and Amidase Activity of Tubercle Bacilli. *American Review of Respiratory Disease*, *95*(3), 461–469. https://doi.org/10.1164/arrd.1967.95.3.461

Kwara A, Enimil A, Gillani FS, Yang H, Sarfo AM, Dompreh A, Ortsin A, Osei-Tutu L, *et al.* (2016). Pharmacokinetics of first-line antituberculosis drugs using WHO revised dosage in children with tuberculosis with and without HIV coinfection. *Journal of the Pediatric Infectious Diseases Society*, *5*(4), 356–365. https://doi.org/10.1093/jpids/piv035

Lacroix C, Hoang TP, Nouveau J, Guyonnaud C, Laine G, Duwoos H, & Lafont O. (1989). Pharmacokinetics of pyrazinamide and its metabolites in healthy subjects. *European Journal of Clinical Pharmacology*, *36*(4), 395–400. https://doi.org/doi.org/10.1007/BF00558302

Lacroix C, Tranvouez JL, Phan Hoang T, Duwoos H, & Lafont O. (1990). Pharmacokinetics of pyrazinamide and its metabolites in patients with hepatic cirrhotic insufficiency. *Arzneimittelforschung*, *40*(1), 76–79.

Lalloo UG. (2009). Efavirenz and Nevirapine Interactions with Rifampicin: Resolving the Dilemmas? *Clinical Infectious Diseases*, *48*(12), 1760–1762. https://doi.org/10.1086/599115

Laserson KF, Kenyon AS, Kenyon TA, Layloff T, & Binkin NJ. (2001). Substandard tuberculosis drugs on the global market and their simple detection. *International Journal of Tuberculosis and Lung Disease*, *5*(5), 448–454. Retrieved from http://www.ingentaconnect.com/content/iuatld/ijtld/2001/00000005/00000005/art00009

Lavielle M. (2014). *Mixed effects models for the population approach : models, tasks, methods and tools*. London: Chapman and Hall/CRC.

Lee C-N, & Heifets LB. (1987). Determination of minimal inhibitory concentrations of antituberculosis drugs by radiometric and conventional methods. *American Review of Respiratory Disease*, *136*(2), 349–352. https://doi.org/10.1164/ajrccm/136.2.349

Lee CS, Brater DC, Gambertoglio JG, & Benet LZ. (1980). Disposition kinetics of ethambutol in man. *Journal of Pharmacokinetics and Biopharmaceutics*, *8*(4), 335–46. https://doi.org/doi.org/10.1007/BF01059382

Lee CS, Gambertoglio JG, Brater DC, & Benet LZ. (1977). Kinetics of oral ethambutol in the normal subject. *Clinical Pharmacology and Therapeutics*, *22*(5 Pt 1), 615–21. https://doi.org/10.1002/cpt1977225part1615

Lee REB, Li W, Chatterjee D, & Lee RE. (2004). Rapid structural characterization of the arabinogalactan and lipoarabinomannan in live mycobacterial cells using 2D and 3D HR-MAS NMR: structural changes in the arabinan due to ethambutol treatment and gene mutation are observed. *Glycobiology*, *15*(2), 139–151. https://doi.org/10.1093/glycob/cwh150

Leff MA, Fretland AJ, Doll MA, & Hein DW. (1999). Novel human N-acetyltransferase 2 alleles that differ in mechanism for slow acetylator phenotype. *The Journal of Biological Chemistry*, *274*(49), 34519–22. https://doi.org/10.1074/JBC.274.49.34519

Lin H-C, Yu M-C, Liu H-J, & Bai K-J. (2014). Impact of food intake on the pharmacokinetics of first-line antituberculosis drugs in Taiwanese tuberculosis patients. *Journal of the Formosan Medical Association*, *113*(5), 291–7. https://doi.org/10.1016/j.jfma.2014.01.015

Lindbom L, Pihlgren P, & Jonsson EN. (2005). PsN-Toolkit—A collection of computer intensive statistical methods for non-linear mixed effect modeling using NONMEM. *Computer Methods and Programs in Biomedicine*, *79*(3), 241–257. https://doi.org/10.1016/j.cmpb.2005.04.005

Liu J, Rosenberg EY, & Nikaido H. (1995). Fluidity of the lipid domain of cell wall from Mycobacterium chelonae. *Proceedings of the National Academy of Sciences of the United States of America*, *92*(24), 11254–8. Retrieved from https://www.jstor.org/stable/2368784

Liu Y, Pertinez H, Ortega-Muro F, Alameda-Martin L, Harrison T, Davies G, Coates A, & Hu Y. (2017). Optimal doses of rifampicin in the standard drug regimen to shorten tuberculosis treatment duration and reduce relapse by eradicating persistent bacteria. *Journal of Antimicrobial Chemotherapy*. https://doi.org/10.1093/jac/dkx467

Long MW, Snider DE, & Farer LS. (1979). U.S. Public Health Service Cooperative Trial of Three Rifampin-Isoniazid Regimens in Treatment of Pulmonary Tuberculosis. *American Review of Respiratory Disease*, *119*(6), 879–894. https://doi.org/10.1164/arrd.1979.119.6.879

Loos U, Musch E, Jensen JC, Mikus G, Schwabe HK, & Eichelbaum M. (1985). Pharmacokinetics of oral and intravenous rifampicin during chronic administration. *Klinische Wochenschrift*, *63*(23), 1205–1211. https://doi.org/10.1007/BF01733779

Malhotra KK. (2003). Treatment of tuberculosis in chronic renal failure, maintenance dialysis and renal transplant. *Transplantation*, *13*(1), 69–71. Retrieved from http://medind.nic.in/iav/t03/i2/iavt03i2p69.pdf

Mattila MJ, Linnoila M, Seppälä T, & Koskinen R. (1978). Effect of aluminium hydroxide and glycopyrrhonium on the absorption of ethambutol and alcohol in man. *British Journal of Clinical Pharmacology*, *5*(2), 161–6. https://doi.org/10.1111/j.1365-2125.1978.tb01618.x

McIlleron H, Meintjes G, Burman WJ, & Maartens G. (2007). Complications of Antiretroviral Therapy in Patients with Tuberculosis: Drug Interactions, Toxicity, and Immune Reconstitution Inflammatory Syndrome. *The Journal of Infectious Diseases*, *196*(s1), S63–S75. https://doi.org/10.1086/518655

McIlleron H, Norman J, Kanyok TP, Fourie PB, Horton J, & Smith PJ. (2007). Elevated gatifloxacin and reduced rifampicin concentrations in a single-dose interaction study amongst healthy volunteers. *The Journal of Antimicrobial Chemotherapy*, *60*(6), 1398–401. https://doi.org/10.1093/jac/dkm393

McIlleron H, Rustomjee R, Vahedi M, Mthiyane T, Denti P, Connolly C, Rida W, Pym A, *et al.* (2012). Reduced antituberculosis drug concentrations in HIV-infected patients who are men or have low weight: implications for international dosing guidelines. *Antimicrobial Agents and Chemotherapy*, *56*(6), 3232–8. https://doi.org/10.1128/AAC.05526-11

McIlleron H, Wash P, Burger A, Norman J, Folb PI, & Smith P. (2006). Determinants of rifampin, isoniazid, pyrazinamide, and ethambutol pharmacokinetics in a cohort of tuberculosis patients. *Antimicrobial Agents and Chemotherapy*, *50*(4), 1170–1177. https://doi.org/10.1128/aac.50.4.1170-1177.2006

McIlleron HM, & Roscigno G. (2017). *Proposal to DOH for improved dosing of rifampicin in South African TB patients*. Cape Town, South Africa.

Mehta JB, Shantaveerapa H, Byrd RPJ, Morton SE, Fountain F, & Roy TM. (2001). Utility of rifampin blood levels in the treatment and follow-up of active pulmonary tuberculosis in patients who were slow to respond to routine directly observed therapy. *Chest*, *120*(5), 1520–1524. https://doi.org/10.1378/chest.120.5.1520

Melander A, Danielson K, Hanson A, Jansson L, Rerup JC, Scherstén B, Thulin T, & Wåhlin E. (1976). Reduction of isoniazid bioavailability in normal men by concomitant intake of food. *Acta Medica Scandinavica*, *200*(1–6), 93–97. https://doi.org/10.1111/j.0954-6820.1976.tb08202.x

Merle CS, Floyd S, Ndiaye A, Galperine T, Furco A, de Jong BC, Mcilleron HM, Glynn J, *et al.* (2016). High-dose rifampicin tuberculosis treatment regimen to reduce 12-month mortality of TB/HIV co-infected patients: the RAFA trial results. In *21st International AIDS Conference*. Durban, South Africa.

Mesfin YM, Hailemariam D, Biadgilign S, & Kibret KT. (2014). Association between HIV/AIDS and multi-drug resistance tuberculosis: a systematic review and meta-analysis. *PloS One*, *9*(1), e82235. https://doi.org/10.1371/journal.pone.0082235

Mfinanga SG, Kirenga BJ, Chanda DM, Mutayoba B, Mthiyane T, Yimer G, Ezechi O, Connolly C, *et al.* (2014). Early versus delayed initiation of highly active antiretroviral therapy for HIV-positive adults with newly diagnosed pulmonary tuberculosis (TB-HAART): a prospective, international, randomised, placebo-controlled trial. *The Lancet. Infectious Diseases*, *14*(7), 563–71. https://doi.org/10.1016/S1473-3099(14)70733-9

Mitchison D. (1979). Basic mechanisms of chemotherapy. *Chest*, *76*(6 Suppl), 771–81. https://doi.org/10.1378/chest.76.6_Supplement.771

Mitchison DA. (1985). The action of antituberculosis drugs in short-course chemotherapy. *Tubercle*, *66*(3), 219–225. https://doi.org/10.1016/0041-3879(85)90040-6

Mitchison DA. (2000). Role of individual drugs in the chemotherapy of tuberculosis. *The International Journal of Tuberculosis and Lung Disease*, *4*(9), 796–806.

Mitchison DA. (2005). The diagnosis and therapy of tuberculosis during the past 100 years. *American Journal of Respiratory and Critical Care Medicine*, *171*(7), 699–706. https://doi.org/10.1164/rccm.200411-1603OE

Mitchison DA, & Fourie PB. (2010). The near future: improving the activity of rifamycins and pyrazinamide. *Tuberculosis (Edinb)*, *90*(3), 177–181. https://doi.org/10.1016/j.tube.2010.03.005

Monolix version 2016R1. (2016). A software for the analysis of nonlinear mixed effects models. Antony, France: Lixoft SAS. Retrieved from http://lixoft.com/products/monolix/

Mould DR, & Upton RN. (2013). Basic concepts in population modeling, simulation, and model-based drug development-part 2: introduction to pharmacokinetic modeling methods. *CPT: Pharmacometrics & Systems Pharmacology*, *2*(April), e38. https://doi.org/10.1038/psp.2013.14

Mouton JW, Dudley MN, Cars O, Derendorf H, & Drusano GL. (2005). Standardization of pharmacokinetic/pharmacodynamic (PK/PD) terminology for anti-infective drugs: an update. *The Journal of Antimicrobial Chemotherapy*, *55*(5), 601–7. https://doi.org/10.1093/jac/dki079

Mouton RP, Mattie H, Swart K, Kreukniet J, & de Wad J. (1979). Blood levels of rifampicin, desacetylrifampicin and isoniazid during combined therapy. *Journal of Antimicrobial Chemotherapy*, *5*(4), 447–454. https://doi.org/10.1093/jac/5.4.447

Mupere E, Malone L, Zalwango S, Chiunda A, Okwera A, Parraga I, Stein CM, Tisch DJ, *et al.* (2012). Lean tissue mass wasting is associated with increased risk of mortality among women with pulmonary tuberculosis in urban Uganda. *Annals of Epidemiology*, *22*(7), 466–73. https://doi.org/10.1016/j.annepidem.2012.04.007

Naidoo A, Chirehwa M, McIlleron H, Naidoo K, Essack S, Yende-Zuma N, Kimba-Phongi E, Adamson J, *et al.* (2017). Effect of rifampicin and efavirenz on moxifloxacin concentrations when co-administered in patients with drug-susceptible TB. *Journal of Antimicrobial Chemotherapy*, *72*(5), 1441–1449. https://doi.org/10.1093/jac/dkx004

National Institute of Allegy and Infectious Diseases. (2001). *Division of Microbiology and Infectious Diseases Adult Toxicity Table*. Retrieved from https://www.niaid.nih.gov/dmid/clinresearch/dmidadulttoxtable.doc

Neugarten J, Gallo GR, & Baldwin DS. (1983). Rifampin-induced nephrotic syndrome and acute interstitial nephritis. *Am J Nephrol*, *3*(1), 38–42. https://doi.org/10.1159/000166685

Niemi M, Backman JT, Fromm MF, Neuvonen PJ, & Kivisto KT. (2003). Pharmacokinetic interactions with rifampicin. *Clinical Pharmacokinetics*, *42*(9), 819–850. https://doi.org/10.2165/00003088-200342090-00003

Nikaido H. (2001). Preventing drug access to targets: cell surface permeability barriers and active efflux in bacteria. *Seminars in Cell & Developmental Biology*, *12*(3), 215–223.

https://doi.org/10.1006/SCDB.2000.0247

Nuermberger E, & Grosset J. (2004). Pharmacokinetic and pharmacodynamic issues in the treatment of mycobacterial infections. *European Journal of Clinical Microbiology and Infectious Diseases*, *23*(4), 243–255. https://doi.org/10.1007/s10096-004-1109-5

Pargal A, & Rani S. (2001). Non-linear pharmacokinetics of rifampicin in healthy Asian Indian volunteers. *The International Journal of Tuberculosis and Lung Disease*, *5*(1), 70–79. Retrieved from http://www.ingentaconnect.com/content/iuatld/ijtld/2001/00000005/00000001/art00011

Parkin DP, Vandenplas S, Botha FJ, Vandenplas ML, Seifart HI, van Helden PD, van der Walt BJ, Donald PR, *et al.* (1997). Trimodality of isoniazid elimination: phenotype and genotype in patients with tuberculosis. *Am J Respir Crit Care Med*, *155*(5), 1717–1722. https://doi.org/10.1164/ajrccm.155.5.9154882

Pasipanodya JG, McIlleron H, Burger A, Wash PA, Smith P, & Gumbo T. (2013). Serum drug concentrations predictive of pulmonary tuberculosis outcomes. *The Journal of Infectious Diseases*, *208*(9), 1464–73. https://doi.org/10.1093/infdis/jit352

Pasipanodya JG, Srivastava S, & Gumbo T. (2012). Meta-analysis of clinical studies supports the pharmacokinetic variability hypothesis for acquired drug resistance and failure of antituberculosis therapy. *Clinical Infectious Diseases*, *55*(2), 169–77. https://doi.org/10.1093/cid/cis353

Patin E, Harmant C, Kidd KK, Kidd J, Froment A, Mehdi SQ, Sica L, Heyer E, *et al.* (2006). Sub-Saharan African coding sequence variation and haplotype diversity at the *NAT2* gene. *Human Mutation*, *27*(7), 720–720. https://doi.org/10.1002/humu.9438

Peets EA, Sweeney WM, Place VA, & Buyske DA. (1965). The absorption, excretion, and metabolic fate of ethambutol in man. *The American Review of Respiratory Disease*, *91*(1), 51–8. https://doi.org/10.1164/arrd.1965.91.1.51

Peloquin CA. (2002). Therapeutic drug monitoring in the treatment of tuberculosis. *Drugs*, *62*(15), 2169–2183. https://doi.org/10.2165/00003495-200262150-00001

Peloquin CA, Bulpitt AE, Jaresko GS, Jelliffe RW, Childs JM, & Nix DE. (1999). Pharmacokinetics of ethambutol under fasting conditions, with food, and with antacids. *Antimicrobial Agents and Chemotherapy*, *43*(3), 568–72. Retrieved from http://aac.asm.org/content/43/3/568.full

Peloquin CA, Bulpitt AE, Jaresko GS, Jelliffe RW, James GT, & Nix DE. (1998). Pharmacokinetics of pyrazinamide under fasting conditions, with food, and with antacids. *Pharmacotherapy*, *18*(6), 1205–1211. https://doi.org/10.1002/j.1875-9114.1998.tb03138.x

Peloquin CA, Jaresko GS, Yong CL, Keung ACF, Bulpitt AE, & Jelliffe RW. (1997). Population pharmacokinetic modeling of isoniazid, rifampin, and pyrazinamide. *Antimicrobial Agents and Chemotherapy*, *41*(12), 2670–2679. Retrieved from http://aac.asm.org/content/41/12/2670

Peloquin CA, Namdar R, Dodge AA, & Nix DE. (1999). Pharmacokinetics of isoniazid under fasting conditions, with food, and with antacids. *The International Journal of Tuberculosis and Lung Disease*, *3*(8), 703–710. Retrieved from http://www.ingentaconnect.com/content/iuatld/ijtld/1999/00000003/00000008/art00009

Peloquin CA, Namdar R, Singleton MD, & Nix DE. (1999). Pharmacokinetics of Rifampin Under Fasting Conditions, With Food, and With Antacids. *Chest*, *115*(1), 12–18. https://doi.org/10.1378/CHEST.115.1.12

Pepper DJ, Marais S, Wilkinson RJ, Bhaijee F, Maartens G, McIlleron H, De Azevedo V, Cox H, *et al.* (2010). Clinical deterioration during antituberculosis treatment in Africa: Incidence, causes and risk factors. *BMC Infectious Diseases*, *10*(1), 83. https://doi.org/10.1186/1471-2334-10-83

Perlman DC, Segal Y, Rosenkranz S, Rainey PM, Remmel RP, Salomon N, Hafner R, & Peloquin CA. (2005). The clinical pharmacokinetics of rifampin and ethambutol in HIV-infected persons with tuberculosis. *Clinical Infectious Diseases*, *41*(11), 1638–1647. https://doi.org/10.1086/498024

Prakash J, Velpandian T, Pande JN, & Gupta SK. (2003). Serum rifampicin levels in patients with tuberculosis: Effect of P-glycoprotein and CYP3A4 blockers on its absorption. *Clinical Drug Investigation*, *23*(7), 463–472. https://doi.org/10.2165/00044011-200323070-00005

Pulido F, Peña J-M, Rubio R, Moreno S, González J, Guijarro C, Costa J-R, & Vázquez J-J. (1997). Relapse of Tuberculosis After Treatment in Human Immunodeficiency Virus—Infected Patients. *Archives of Internal Medicine*, *157*(2), 227. https://doi.org/10.1001/archinte.1997.00440230105014

R Core Team. (2017). R: A Language and Environment for Statistical Computing. Vienna, Austria. Retrieved from http://www.r-project.org/

Radke BR. (2003). A demonstration of interval-censored survival analysis. *Preventive Veterinary Medicine*, *59*(4), 241–256. https://doi.org/10.1016/S0167-5877(03)00103-X

Ralph AP, Ardian M, Wiguna A, Maguire GP, Becker NG, Drogumuller G, Wilks MJ, Waramori G, *et al.* (2010). A simple, valid, numerical score for grading chest x-ray severity in adult smear-positive pulmonary tuberculosis. *Thorax*, *65*(10), 863–9. https://doi.org/10.1136/thx.2010.136242

Ramakrishnan L. (2012). Revisiting the role of the granuloma in tuberculosis. *Nature Reviews Immunology*, *12*(5), 352. https://doi.org/10.1038/nri3211

Rastogi N, Labrousse V, & Goh KS. (1996). In vitro activities of fourteen antimicrobial agents against drug susceptible and resistant clinical isolates of mycobacterium tuberculosis and comparative intracellular activities against the virulent H37Rv strain in human macrophages. *Current Microbiology*, *33*(3), 167–75. https://doi.org/10.1007/s002849900095

Raynaud C, Laneelle M-A, Senaratne RH, Draper P, Laneelle G, & Daffe M. (1999). Mechanisms of pyrazinamide resistance in mycobacteria: importance of lack of uptake in addition to lack of pyrazinamidase activity. *Microbiology*, *145*(6), 1359–1367. https://doi.org/10.1099/13500872-145-6-1359

Requena-Méndez A, Davies G, Waterhouse D, Ardrey A, Jave O, López-Romero SL, Ward SA, & Moore DAJ. (2014). Effects of dosage, comorbidities, and food on isoniazid pharmacokinetics in Peruvian tuberculosis patients. *Antimicrobial Agents and Chemotherapy*, *58*(12), 7164–70. https://doi.org/10.1128/AAC.03258-14

Rey-Jurado E, Tudó G, Martínez JA, & González-Martín J. (2012). Synergistic effect of two

combinations of antituberculous drugs against Mycobacterium tuberculosis. *Tuberculosis*, *92*(3), 260–3. https://doi.org/10.1016/j.tube.2012.01.005

Rhoades ER, Frank AA, & Orme IM. (1997). Progression of chronic pulmonary tuberculosis in mice aerogenically infected with virulent Mycobacterium tuberculosis. *Tubercle and Lung Disease*, *78*(1), 57–66. https://doi.org/10.1016/S0962-8479(97)90016-2

Rockwood N, Meintjes G, Chirehwa M, Wiesner L, McIlleron H, Wilkinson RJRJ, & Denti P. (2016). HIV-1 coinfection does not reduce exposure to rifampin, isoniazid, and pyrazinamide in South African tuberculosis outpatients. *Antimicrobial Agents and Chemotherapy*, *60*(10), 6050–9. https://doi.org/10.1128/AAC.00480-16

Rockwood N, Pasipanodya JG, Denti P, Sirgel F, Lesosky M, Gumbo T, Meintjes G, McIlleron H, *et al.* (2017). Concentration-Dependent Antagonism and Culture Conversion in Pulmonary Tuberculosis. *Clinical Infectious Diseases*, *64*(10), 1350–1359. https://doi.org/10.1093/cid/cix158

Roy P Das, Majumder M, & Roy B. (2008). Pharmacogenomics of anti-TB drugs-related hepatotoxicity. *Pharmacogenomics*, *9*(3), 311–321. https://doi.org/10.2217/14622416.9.3.311

RStudio. (2014). RStudio: Integrated development environment for R. Boston, MA. Retrieved from http://www.rstudio.org/

Ruslami R, Nijland HMJ, Alisjahbana B, Parwati I, van Crevel R, & Aarnoutse RE. (2007). Pharmacokinetics and Tolerability of a Higher Rifampin Dose versus the Standard Dose in Pulmonary Tuberculosis Patients. *Antimicrobial Agents and Chemotherapy*, *51*(7), 2546–2551. https://doi.org/10.1128/aac.01550-06

Sabbagh A, Langaney A, Darlu P, Gérard N, Krishnamoorthy R, & Poloni ES. (2008). Worldwide distribution of NAT2 diversity: Implications for NAT2 evolutionary history. *BMC Genetics*, *9*(1), 21. https://doi.org/10.1186/1471-2156-9-21

Sahota T, & Della Pasqua O. (2012). Feasibility of a fixed-dose regimen of pyrazinamide and its impact on systemic drug exposure and liver safety in patients with tuberculosis. *Antimicrobial Agents and Chemotherapy*, *56*(11), 5442–5449. https://doi.org/10.1128/AAC.05988-11

Saktiawati AMI, Sturkenboom MGG, Stienstra Y, Subronto YW, Sumardi, Kosterink JGW, van der Werf TS, & Alffenaar J-WC. (2016). Impact of food on the pharmacokinetics of first-line anti-TB drugs in treatment-naive TB patients: a randomized cross-over trial. *Journal of Antimicrobial Chemotherapy*, *71*(3), 703–710. https://doi.org/10.1093/jac/dkv394

Saleri N, Dembele SM, Villani P, Carvalho ACC, Cusato M, Bonkoungou V, Nacanabo R, Kouanda S, *et al.* (2012). Systemic exposure to rifampicin in patients with tuberculosis and advanced HIV disease during highly active antiretroviral therapy in Burkina Faso. *Journal of Antimicrobial Chemotherapy*, *67*(2), 469–472. https://doi.org/10.1093/jac/dkr445

Savic R, Jonker D, Kerbusch T, & Karlsson M. (2007). Implementation of a transit compartment model for describing drug absorption in pharmacokinetic studies. *Journal of Pharmacokinetics and Pharmacodynamics*, *34*(5), 711–726. https://doi.org/10.1007/s10928-007-9066-0

Scales MDG, & Timbrell JA. (1982). Studies on hydrazine hepatotoxicity. 1. Pathological findings. *Journal of Toxicology and Environmental Health*, *10*(6), 941–953. https://doi.org/10.1080/15287398209530308

Schaaf HS, Parkin DP, Seifart HI, Werely CJ, Hesseling PB, van Helden PD, Maritz JS, & Donald PR. (2005). Isoniazid pharmacokinetics in children treated for respiratory tuberculosis. *Archives of Disease in Childhood*, *90*(6), 614–618. https://doi.org/10.1136/adc.2004.052175

Schon T, Jureen P, Giske CG, Chryssanthou E, Sturegard E, Werngren J, Kahlmeter G, Hoffner SE, *et al.* (2009). Evaluation of wild-type MIC distributions as a tool for determination of clinical breakpoints for Mycobacterium tuberculosis. *Journal of Antimicrobial Chemotherapy*, *64*(4), 786–793. https://doi.org/10.1093/jac/dkp262

Schuetz EG, Schinkel AH, Relling M V, & Schuetz JD. (1996). P-glycoprotein: a major determinant of rifampicin-inducible expression of cytochrome P4503A in mice and humans. *Proceedings of the National Academy of Sciences of the United States of America*, *93*(9), 4001–5. https://doi.org/10.1073/pnas.93.9.4001

Segal MR. (1988). Regression Trees for Censored Data. *Biometrics*, *44*(1), 35–47. https://doi.org/10.2307/2531894

Seifart HI, Parkin DP, & Donald PR. (1991). Stability of isoniazid, rifampin and pyrazinamide in suspensions used for the treatment of tuberculosis in children. *The Pediatric Infectious Disease Journal*, *10*(11), 827–31. https://doi.org/10.1097/00006454-199111000-00007

Semvua HH, Kibiki GS, Kisanga ER, Boeree MJ, Burger DM, & Aarnoutse R. (2015). Pharmacological Interactions Between Rifampicin and Antiretroviral Drugs. *Therapeutic Drug Monitoring*, *37*(1), 22–32. https://doi.org/10.1097/FTD.0000000000000108

Seng K-Y, Hee K-H, Soon G-H, Chew N, Khoo SH, & Lee LS-U. (2015a). Population pharmacokinetic analysis of isoniazid, acetylisoniazid, and isonicotinic acid in healthy volunteers. *Antimicrobial Agents and Chemotherapy*, *59*(11), 6791–9. https://doi.org/10.1128/AAC.01244-15

Seng K-Y, Hee K-H, Soon G-H, Chew N, Khoo SH, & Lee LS-U. (2015b). Population pharmacokinetics of rifampicin and 25-deacetyl-rifampicin in healthy Asian adults. *The Journal of Antimicrobial Chemotherapy*, *70*(12), 3298–306. https://doi.org/10.1093/jac/dkv268

Shastri S, Naik B, Shet A, Rewari B, & De Costa A. (2013). TB treatment outcomes among TB-HIV co-infections in Karnataka, India: how do these compare with non-HIV tuberculosis outcomes in the province? *BMC Public Health*, *13*(1), 838. https://doi.org/10.1186/1471-2458-13-838

Shih T-Y, Pai C-Y, Yang P, Chang W-L, Wang N-C, & Hu OY-P. (2013). A novel mechanism underlies the hepatotoxicity of pyrazinamide. *Antimicrobial Agents and Chemotherapy*, *57*(4), 1685–90. https://doi.org/10.1128/AAC.01866-12

Sim E, Abuhammad A, & Ryan A. (2014). Arylamine N-acetyltransferases: from drug metabolism and pharmacogenetics to drug discovery. *British Journal of Pharmacology*, *171*(11), 2705–25. https://doi.org/10.1111/bph.12598

Singh S, & Mohan B. (2003). A pilot stability study on four-drug fixed-dose combination anti-

tuberculosis products. *The International Journal of Tuberculosis and Lung Disease*, *7*(3), 298–303. Retrieved from http://www.ingentaconnect.com/content/iuatld/ijtld/2003/00000007/00000003/art00019

Sirgel FA, Fourie PB, Donald PR, Padayatchi N, Rustomjee R, Levin J, Roscigno G, Norman J, *et al.* (2005). The early bactericidal activities of rifampin and rifapentine in pulmonary tuberculosis. *American Journal of Respiratory and Critical Care Medicine*, *172*(1), 128–135. https://doi.org/10.1164/rccm.200411-1557OC

Sloan DJ, McCallum AD, Schipani A, Egan D, Mwandumba HC, Ward SA, Waterhouse D, Banda G, *et al.* (2017). Genetic determinants of the pharmacokinetic variability of rifampin in Malawian adults with pulmonary tuberculosis. *Antimicrobial Agents and Chemotherapy*, *61*(7), e00210-17. https://doi.org/10.1128/AAC.00210-17

Smythe W, Khandelwal A, Merle C, Rustomjee R, Gninafon M, Bocar Lo M, Sow OB, Olliaro PL, *et al.* (2012). A semimechanistic pharmacokinetic-enzyme turnover model for rifampin autoinduction in adult tuberculosis patients. *Antimicrobial Agents and Chemotherapy*, *56*(4), 2091–8. https://doi.org/10.1128/AAC.05792-11

Smythe WA. (2016). *Characterizing population pharmacokinetic/pharmacodynamic relationships in pulmonary tuberculosis infected adults using nonlinear mixed effects modelling*. (Doctoral thesis, University of Cape Town). Retrieved from https://open.uct.ac.za/bitstream/item/23227/thesis_hsf_2016_smythe_wynand_anton.pdf

Somoskovi A, Parsons LM, & Salfinger M. (2001). The molecular basis of resistance to isoniazid, rifampin, and pyrazinamide in mycobacterium tuberculosis. *Respiratory Research*, *2*(3), 164–8. https://doi.org/10.1186/rr54

Srivastava S, Musuka S, Sherman C, Meek C, Leff R, & Gumbo T. (2010). Efflux-pump-derived multiple drug resistance to ethambutol monotherapy in mycobacterium tuberculosis and the pharmacokinetics and pharmacodynamics of ethambutol. *The Journal of Infectious Diseases*, *201*(8), 1225–31. https://doi.org/10.1086/651377

Steele MA, & Des Prez RM. (1988). The role of pyrazinamide in tuberculosis chemotherapy. *Chest*, *94*(4), 845–850. https://doi.org/10.1378/chest.94.4.845

Steingart KR, Jotblad S, Robsky K, Deck D, Hopewell PC, Huang D, & Nahid P. (2011). Higher-dose rifampin for the treatment of pulmonary tuberculosis: A systematic review. *The International Journal of Tuberculosis and Lung Disease*, *15*(3), 305–316. Retrieved from http://www.ingentaconnect.com/content/iuatld/ijtld/2011/00000015/00000003/art00004

Sturkenboom MGG, van der Lijke H, Jongedijk EM, Kok WT, Greijdanus B, Uges DRA, & Alffenaar J-WC. (2015). Quantification of isoniazid, pyrazinamide and ethambutol in serum using liquid chromatography-tandem mass spectrometry. *Journal of Applied Bioanalysis*, *1*(3), 89–98. https://doi.org/10.17145/jab.15.015

Suo J, Chang C-EE, Lin TP, & Heifets LB. (1988). Minimal inhibitory concentrations of isoniazid, rifampin, ethambutol, and streptomycin against mycobacterium tuberculosis strains isolated before treatment of patients in Taiwan. *The American Review of Respiratory Disease*, *138*(4), 999–1001. https://doi.org/10.1164/ajrccm/138.4.999

Svensson EM, & Karlsson MO. (2017). Modelling of mycobacterial load reveals bedaquiline's exposure–response relationship in patients with drug-resistant TB.

Journal of Antimicrobial Chemotherapy. https://doi.org/10.1093/jac/dkx317

Svensson EM, Svensson RJ, Te Brake L, Boeree MJ, Heinrich N, Churchyard G, Dawson R, Diacon AH, *et al.* (2017). Linking rifampicin exposure to treatment response over six months in patients with pulmonary tuberculosis. In *Population Approach Group Europe (26)* (p. Abstr 7263). Retrieved from www.page-meeting.org/?abstract=7263

Svensson RJ, Aarnoutse RE, Diacon AH, Dawson R, Gillespie SH, Boeree MJ, & Simonsson USH. (2017). A Population Pharmacokinetic Model Incorporating Saturable Pharmacokinetics and Autoinduction for High Rifampicin Doses. *Clinical Pharmacology & Therapeutics*. https://doi.org/10.1002/cpt.778

Swaminathan S, Pasipanodya JG, Ramachandran G, Hemanth Kumar AK, Srivastava S, Deshpande D, Nuermberger E, & Gumbo T. (2016). Drug Concentration Thresholds Predictive of Therapy Failure and Death in Children With Tuberculosis: Bread Crumb Trails in Random Forests. *Clinical Infectious Diseases*, *63*(suppl 3), S63–S74. https://doi.org/10.1093/cid/ciw471

Takayama K, & Kilburn JO. (1989). Inhibition of synthesis of arabinogalactan by ethambutol in Mycobacterium smegmatis. *Antimicrobial Agents and Chemotherapy*, *33*(9), 1493–9. Retrieved from http://aac.asm.org/content/33/9/1493.full.pdf

Tappero JW, Bradford WZ, Agerton TB, Hopewell P, Reingold AL, Lockman S, Oyewo A, Talbot EA, *et al.* (2005). Serum concentrations of antimycobacterial drugs in patients with pulmonary tuberculosis in Botswana. *Clinical Infectious Diseases*, *41*(4), 461–9. https://doi.org/10.1086/431984

Telzak EE, Fazal BA, Pollard CL, Turett GS, Justman JE, & Blum S. (1997). Factors Influencing Time to Sputum Conversion Among Patients with Smear-Positive Pulmonary Tuberculosis. *Clinical Infectious Diseases*, *25*(3), 666–670. https://doi.org/10.1086/513772

Timmins GS, & Deretic V. (2006). Mechanisms of action of isoniazid. *Molecular Microbiology*, *62*(5), 1220–1227. https://doi.org/10.1111/j.1365-2958.2006.05467.x

Upton RN, & Mould DR. (2014). Basic concepts in population modeling, simulation, and model-based drug development: part 3-introduction to pharmacodynamic modeling methods. *CPT: Pharmacometrics & Systems Pharmacology*, *3*(1), e88. https://doi.org/10.1038/psp.2013.71

Urso R, Blardi P, & Giorgi G. (2002). A short introduction to pharmacokinetics. *European Review for Medical and Pharmacological Sciences*, *6*(2), 33–44. https://doi.org/10.1016/B978-0-7020-2793-2.00003-7

US Public Health Service. (1959). Hepatic toxicity of pyrazinamide used with isoniazid in tuberculous patients. *American Review of Respiratory Disease*, *80*(3), 371–387. Retrieved from http://www.atsjournals.org/doi/abs/10.1164/arrd.1959.80.3.371

van Ingen J, Aarnoutse RE, Donald PR, Diacon AH, Dawson R, Plemper van Balen G, Gillespie SH, & Boeree MJ. (2011). Why do we use 600 mg of rifampicin in tuberculosis treatment? *Clinical Infectious Diseases*, *52*(9), e194-9. https://doi.org/10.1093/cid/cir184

Van Lettow M, Kumwenda JJ, Harries AD, Whalen CC, Taha TE, Kumwenda N, Kang'Ombe C, & Semba RD. (2004). Malnutrition and the severity of lung disease in adults with

pulmonary tuberculosis in Malawi. *International Journal of Tuberculosis and Lung Disease*, *8*(2), 211–217. Retrieved from http://www.ingentaconnect.com/contentone/iuatld/ijtld/2004/00000008/00000002/art00008

Vernon AA. (2011). Current Standard Treatment. In P. R. Donald & P. D. van Helden (Eds.), *Antituberculosis Chemotherapy* (Vol. 40, pp. 61–72). Basel: Karger Publishers. https://doi.org/10.1159/000330479

Vinnard C, Ravimohan S, Tamuhla N, Pasipanodya J, Srivastava S, Modongo C, Zetola NM, Weissman D, *et al.* (2017). Pyrazinamide clearance is impaired among HIV/tuberculosis patients with high levels of systemic immune activation. *PLOS ONE*, *12*(11), e0187624. https://doi.org/10.1371/journal.pone.0187624

Visser ME, Stead MC, Walzl G, Warren R, Schomaker M, Grewal HMS, Swart EC, & Maartens G. (2012). Baseline Predictors of Sputum Culture Conversion in Pulmonary Tuberculosis: Importance of Cavities, Smoking, Time to Detection and W-Beijing Genotype. *PLoS ONE*, *7*(1), e29588. https://doi.org/10.1371/journal.pone.0029588

Wallis R, Doherty T, Onyebujoh P, Vahedi M, Laang H, Olesen O, Parida S, & Zumla A. (2009). Biomarkers for tuberculosis disease activity, cure, and relapse. *The Lancet Infectious Diseases*, *9*(3), 162–172. https://doi.org/10.1016/S1473-3099(09)70042-8

Wallis RS, & Johnson JL. (2009). Chapter 70 – Immunotherapy of tuberculosis. In *Tuberculosis* (pp. 718–726). https://doi.org/10.1016/B978-1-4160-3988-4.00070-6

Wang P-Y, Xie S-Y, Hao Q, Zhang C, & Jiang B-F. (2012). NAT2 polymorphisms and susceptibility to anti-tuberculosis drug-induced liver injury: a meta-analysis. *The International Journal of Tuberculosis and Lung Disease*, *16*(5), 589–95. https://doi.org/10.5588/ijtld.11.0377

Wang P, Pradhan K, Zhong X-B, & Ma X. (2016). Isoniazid metabolism and hepatotoxicity. *Acta Pharmaceutica Sinica. B*, *6*(5), 384–392. https://doi.org/10.1016/j.apsb.2016.07.014

Weber WW, & Hein DW. (1979). Clinical pharmacokinetics of isoniazid. *Clinical Pharmacokinetics*, *4*(6), 401–422. https://doi.org/10.2165/00003088-197904060-00001

Weiner IM, & Tinker JP. (1972). Pharmacology of pyrazinamide: metabolic and renal function studies related to the mechanism of drug-induced urate retention. *The Journal of Pharmacology and Experimental Therapeutics*, *180*(2), 411–34. Retrieved from http://jpet.aspetjournals.org/content/180/2/411.long

Wilkins JJ, Langdon G, McIlleron H, Pillai G, Smith PJ, & Simonsson US. (2006). Variability in the population pharmacokinetics of pyrazinamide in South African tuberculosis patients. *European Journal of Clinical Pharmacology*, *62*(9), 727–735. https://doi.org/10.1007/s00228-006-0141-z

Wilkins JJ, Langdon G, McIlleron H, Pillai G, Smith PJ, & Simonsson US. (2011). Variability in the population pharmacokinetics of isoniazid in South African tuberculosis patients. *British Journal of Clinical Pharmacology*, *72*(1), 51–62. https://doi.org/10.1111/j.1365-2125.2011.03940.x

Wilkins JJ, Savic RM, Karlsson MO, Langdon G, McIlleron H, Pillai G, Smith PJ, & Simonsson USH. (2008). Population pharmacokinetics of rifampin in pulmonary

tuberculosis patients, including a semimechanistic model to describe variable absorption. *Antimicrobial Agents and Chemotherapy*, *52*(6), 2138–48. https://doi.org/10.1128/AAC.00461-07

Williams PJ, & Ette EI. (2007). Pharmacometrics: Impacting Drug Development and Pharmacotherapy. In E. I. Ette & P. J. Williams (Eds.), *Pharmacometrics : the science of quantitative pharmacology* (p. 1205). Hoboken, New Jersey: John Wiley & Sons.

Wiltshire CS, Lamorde M, Scherrer A, Musaazi J, Corti N, Allan B, Nakijoba R, Nalwanga D, *et al.* (2014). Low isoniazid and rifampicin concentrations in TB/HIV co-infected patients in Uganda. *Journal of the International AIDS Society*, *17*(4 Suppl 3), 19585. https://doi.org/10.7448/IAS.17.4.19585

World Health Organization. (2003). *Treatment of tuberculosis: Guidelines for national programmes* (3rd ed.). Geneva, Switzerland. https://doi.org/WHO/CDS/TB/2003.313

World Health Organization. (2009). *Management of MDR-TB: A field guide A companion document to Guidelines for the programmatic management of drug-resistant tuberculosis*. Geneva, Switzerland: WHO/HTM/TB/2008.402a. Retrieved from http://apps.who.int/iris/bitstream/10665/44163/1/9789241547765_eng.pdf

World Health Organization. (2010a). *Antiretroviral therapy for HIV infection in adults and adolescents: recommendations for a public health approach. 2010 revision* (WHO/CDS/TB). Geneva, Switzerland.

World Health Organization. (2010b). *Guidelines for treatment of tuberculosis* (4th ed.). Geneva, Switzerland: WHO/HTM/TB/2009.420. World Health Organization.

World Health Organization. (2010c). *Treatment of tuberculosis: guidelines* (No. WHO/HTM/TB/2009.420, 4th ed.). Geneva, Switzerland: World Helath Organization. Retrieved from http://www.who.int/tb/publications/2010/9789241547833/en/

World Health Organization. (2016). *Global Tuberculosis Report 2016*. Geneva, Switzerland: WHO/HTM/TB/2016.13. Retrieved from http://apps.who.int/iris/bitstream/10665/250441/1/9789241565394-eng.pdf

World Health Organization, International Union Against Tuberculosis and Lung Disease, & Royal Netherlands Tuberculosis Association. (2001). Revised international definitions in tuberculosis control. *The International Journal of Tuberculosis and Lung Disease*, *5*(3), 213–5. Retrieved from http://www.ingentaconnect.com/contentone/iuatld/ijtld/2001/00000005/00000003/art00003

Yeager R, Munroe W, & Dessau F. (1952). Pyrazinamide (aldinamide) in the treatment of pulmonary. *American Review of Tuberculosis*, *65*(5), 523.

Yen Y-F, Chuang P-H, Yen M-Y, Lin S-Y, Chuang P, Yuan M-J, Ho B-L, Chou P, *et al.* (2016). Association of Body Mass Index With Tuberculosis Mortality: A Population-Based Follow-Up Study. *Medicine*, *95*(1), e2300. https://doi.org/10.1097/MD.0000000000002300

Zachariah R, Spielmann MP, Harries AD, & Salaniponi FML. (2002). Moderate to severe malnutrition in patients with tuberculosis is a risk factor associated with early death. *Transactions of the Royal Society of Tropical Medicine and Hygiene*, *96*(3), 291–294. https://doi.org/10.1016/S0035-9203(02)90103-3

Zannikos P, & Argenti D. (2004). Analysis of Urine Excretion Data. In P. L. Bonate & D. Howard (Eds.), *Pharmacokinetics in drug development: Clinical Study Design and Analysis (Volume 1)* (pp. 267–289). Arlington,VA: AAPS Press.

Zent C, & Smith P. (1995). Study of the effect of concomitant food on the bioavailability of rifampicin, isoniazid and pyrazinamide. *Tubercle and Lung Disease*, *76*(2), 109–113. https://doi.org/10.1016/0962-8479(95)90551-0

Zhang Y, Heym B, Allen B, Young D, & Cole S. (1992). The catalase-peroxidase gene and isoniazid resistance of Mycobacterium tuberculosis. *Nature*, *358*(6387), 591–593. https://doi.org/10.1038/358591a0

Zhang Y, & Mitchison D. (2003). The curious characteristics of pyrazinamide: a review. *The International Journal of Tuberculosis and Lung Disease*, *7*(1), 6–21. Retrieved from http://www.ingentaconnect.com/content/iuatld/ijtld/2003/00000007/00000001/art00004

Zhang Y, Scorpio A, Nikaido H, Sun Z, Unlike A, & Organi- WH. (1999). Role of Acid pH and De cient Ef ux of Pyrazinoic Acid in Unique Susceptibility of. *Microbiology*, *181*(7), 2044–2049. Retrieved from http://jb.asm.org/content/181/7/2044.full

Zhang Y, Wade MM, Scorpio A, Zhang H, & Sun Z. (2003). Mode of action of pyrazinamide: disruption of Mycobacterium tuberculosis membrane transport and energetics by pyrazinoic acid. *The Journal of Antimicrobial Chemotherapy*, *52*(5), 790–5. https://doi.org/10.1093/jac/dkg446

Zheng X, Zheng R, Hu Y, Werngren J, Forsman LD, Mansjö M, Xu B, & Hoffner S. (2016). Determination of MIC Breakpoints for Second-Line Drugs Associated with Clinical Outcomes in Multidrug-Resistant Tuberculosis Treatment in China. *Antimicrobial Agents and Chemotherapy*, *60*(8), 4786–4792. https://doi.org/10.1128/AAC.03008-15

Zhu M, Burman WJ, Starke JR, Stambaugh JJ, Steiner P, Bulpitt AE, Ashkin D, Auclair B, *et al.* (2004). Pharmacokinetics of ethambutol in children and adults with tuberculosis. *International Journal of Tuberculosis and Lung Diseases*, *8*(11), 1360–7. Retrieved from http://www.ingentaconnect.com/content/iuatld/ijtld/2004/00000008/00000011/art00015

Zhu M, Starke JR, Burman WJ, Steiner P, Stambaugh JJ, Ashkin D, Bulpitt AE, Berning SE, *et al.* (2002). Population pharmacokinetic modeling of pyrazinamide in children and adults with tuberculosis. *Pharmacotherapy*, *22*(6), 686–695. https://doi.org/10.1592/phco.22.9.686.34067

Zimmerman M, Lestner J, Prideaux B, O'Brien P, Dias-Freedman I, Chen C, Dietzold J, Daudelin I, *et al.* (2017). Ethambutol partitioning in tuberculous pulmonary lesions explains its clinical efficacy. *Antimicrobial Agents and Chemotherapy*, *61*(9), e00924-17. https://doi.org/10.1128/AAC.00924-17

Appendix 1: NONMEM scripts

Final NONMEM scripts for results presented in chapter 3

```
$SIZES      LVR=50 MAXFCN=100000000
$PROBLEM    RIF_TB_HAART
$INPUT      ID OCC TIME AMT DV MDV CMT EVID BLQ PRESAMP
            ARM0 DRUG NTAB FORM AGE SEX WEIGHT HEIGHT CD4COUNT ARM
            WGTDOSE TABS_TB TRT_DAYS DOSE_IND TAD1 PROB PROB_DESC=DROP VPCTIME DAY FATFM
            MGKGFFM
$DATA       RIF_DATA_CMT16_02_15.csv IGNORE=#
$SUBROUTINE ADVAN13 TRANS1 TOL=9
$MODEL      NCOMPARTMENTS=4 COMP=(ABS DEFDOSE) COMP=(LIVER)
            COMP=(CENTRAL) COMP=(AUC)
;-------------------------------------------------------------------------;
$PK
MXSTEP=50000
;-------------------------------------------------------------------------;
     OCC1=0
     OCC2=0
     OCC3=0
     OCC4=0
     OCC5=0
     OCC6=0
     OCC7=0

     ; Create indicator variables for occasion
     IF(OCC.EQ.1) OCC1=1
     IF(OCC.EQ.2) OCC2=1
     IF(OCC.EQ.3) OCC3=1
     IF(OCC.EQ.4) OCC4=1
     IF(OCC.EQ.5) OCC5=1
     IF(OCC.EQ.6) OCC6=1
     IF(OCC.EQ.7) OCC7=1

     STRAT=0
     IF (OCC==2.OR.OCC==3) STRAT=1
     IF (OCC==4.OR.OCC==5) STRAT=2
     IF (OCC==6.OR.OCC==7) STRAT=3

     STRAT1=0
     IF (DAY>4.AND.DAY<11) STRAT1=1
     IF (DAY>10.AND.DAY<18) STRAT1=2
     IF (DAY>17.AND.DAY<30) STRAT1=3
;-------------------------------------------------------------------------;
     ;ALLOMETRIC SCALING_FFM & WEIGHT
      ;----Fat Free Mass
      IF (SEX.EQ.1) THEN  ; female
          WHSMAX=37.99
          WHS50=35.98
       ELSE        ;males
          WHSMAX=42.92
          WHS50=30.93
     ENDIF

     HTM2 = HEIGHT**2    ; IMPORTANT: HEIGHT is used in meters!!!
     FFM = (WHSMAX*HTM2*WEIGHT)/(WHS50*HTM2+WEIGHT)

     WTSTD=70  ; STANDARD WEIGHT
     FFMSTD=42 ; STANDARD FFM

     ALLOM_CL=(FFM/FFMSTD)**0.75
     ALLOM_V =(FFM/FFMSTD)
;-------------------------------------------------------------------------;
     VPCTIME1=VPCTIME
     IF(VPCTIME.LT.-5) VPCTIME1=-VPCTIME
;-------------------------------------------------------------------------;
     TVV  =THETA(2)*ALLOM_V ; Pop V
     TVKA =THETA(3)         ; Pop KA
     TVBIO=1                ; Pop F
     TVMTT=THETA(6)         ; Pop MTT
     TVNN=THETA(9)          ; Pop NN
;-------------------------HEPATIC CL--------------------------------------;
     TVVH=THETA(10)*ALLOM_V    ; VOLUME OF LIVER WITH ALLOMETRIC SCALLING
     TVQH=THETA(11)*ALLOM_CL   ; PLASMA FLOW RATE
     TVFU=THETA(12)            ; UNBOUND PLASMA FRACTION OF RIF
;-------------------------------------------------------------------------;
```

```
      AA2=A(2)
      AA3=A(3)

      CONC2=AA2/VH
      CONC3=AA3/V

      ; To calculate TAD
      IF(AMT.GT.0) THEN
          TIMEDOSE = TIME
          AMOUNTDOSE = AMT

      ENDIF

      TAD=TIME-TIMEDOSE
      CLH=QH*FU*CLINT/(QH+FU*CLINT)
      ;BIOTOT=BIO*FH

      ; RETRIEVE AUC IN COMPARTMENT
        AUC_T=A(4)
;-------------------------------------------------------------------------;
$THETA  (0,101.194) ; 1. CLBS [L/h]
$THETA  (0,48.1256,100) ; 2. TVV  [L]
$THETA  (0,1.45517,10) ; 3. TVKA [1/h]
$THETA  (0,0.128134,1) ; 4. SIG_PROP
$THETA  (0.04,0.0694115,10) ; 5. SIG_ADD [mg/L]
$THETA  (0,0.593421,5) ; 6. MTT[h]
$THETA  (0,182.349) ; 7. CLSS[L/h]
$THETA  (0,3.76651,10) ; 8. IND50[L/h]
$THETA  (0,15.3162,50) ; 9. NN
$THETA  1 FIX ; 10. VH
$THETA  50 FIX ; 11. PLASMA FLOW
$THETA  0.2 FIX ; 12. FRACTION_UNBOUND
$THETA  (0,1.14667,3) ; 13. log(KM) [log(mg/L)] - natural log with base e
;-------------------------------------------------------------------------;
$OMEGA  0.0538105  ;  1. BSV_CL
$OMEGA  0.0226764  ;  2. BSV_Vd
$OMEGA  0  FIX  ;  3. BSV_Ka
$OMEGA  0  FIX  ; 4. BSV_BIO
$OMEGA  0  FIX  ; 5. BSV_MTT
$OMEGA  BLOCK(1)  0.550578  ; 6. BOV_MTT
$OMEGA  BLOCK(1) SAME
$OMEGA  BLOCK(1) SAME
$OMEGA  BLOCK(1) SAME
$OMEGA  BLOCK(1) SAME
$OMEGA  BLOCK(1) SAME
$OMEGA  BLOCK(1) SAME
$OMEGA  BLOCK(1)  0.00276887  ; 13. BOVBIO
$OMEGA  BLOCK(1) SAME
$OMEGA  BLOCK(1) SAME
$OMEGA  BLOCK(1) SAME
$OMEGA  BLOCK(1) SAME
$OMEGA  BLOCK(1) SAME
$OMEGA  BLOCK(1) SAME
$OMEGA  BLOCK(1)  0.46748  ; 20. BOV_Ka
$OMEGA  BLOCK(1) SAME
$OMEGA  BLOCK(1) SAME
$OMEGA  BLOCK(1) SAME
$OMEGA  BLOCK(1) SAME
$OMEGA  BLOCK(1) SAME
$OMEGA  BLOCK(1) SAME
$OMEGA  BLOCK(1)  0.0273035  ; 27. BOV_CL
$OMEGA  BLOCK(1) SAME
$OMEGA  BLOCK(1) SAME
$OMEGA  BLOCK(1) SAME
$OMEGA  BLOCK(1) SAME
$OMEGA  BLOCK(1) SAME
$OMEGA  BLOCK(1) SAME
$SIGMA  1  FIX  ;   RESIDUAL
;-------------------------------------------------------------------------;
$ESTIMATION MAXEVAL=0 SIGL=10 ATOL=9 METHOD=1 INTER PRINT=1 NOABORT
            NSIG=3 MCETA=1000 RANMETHOD=4P NONINFETA=1 ETASTYPE=1
$ESTIMATION MAXEVAL=9999 SIGL=15 ATOL=9 METHOD=1 INTER PRINT=1 NOABORT
            NSIG=3 MCETA=10 RANMETHOD=4P NONINFETA=1 ETASTYPE=1
```

```
    ; product of a logarith cannot be negative - this would not work
    ; normal Michalis-Mentel equation gives you a rate =k*A = CL*C
    ; but we want to get CL, so you divide the rate by concentration - and get saturable
    clearance
    ; equation is placed in $DES because saturable clearance changes over time
    SAT_CL=0
    IF (CH>0) SAT_CL=VMAX/(1+EXP(-(LOG(CH)-LOGKM))) / (CH)
    ;transformation based on better Emax model, wider search in log parametrisation

    EH  = (SAT_CL*FU)/((SAT_CL*FU)+QH) ; fraction undergoing first pass extraction
    FH  = 1 - EH ;fraction available after 1st pass to go to systemic circulation
    ;CLH = EH * QH ; hepatic clearance

    K20=(QH*EH/VH)
    K23= (QH*FH/VH)
    K32=(QH/V)

    TEMPO=T-TDOS ; this is time after dose, it should always be >= 0
    KTT=0

    DADT(1)=0

     IF(PD.GT.0.AND.TEMPO.GT.0.AND.TEMPO.LT.12) THEN ; This happens only id PD>0, so only if
     a dose has been detected
         KTT=KTR*(TEMPO)
         DADT(1)=EXP(PIZZA+NN*LOG(KTT)-KTT)-KA*A(1)
         DADT(2)=KA*A(1)-K23*A(2)+K32*A(3)-K20*A(2)
         DADT(3)=K23*A(2)-K32*A(3)
       ELSE
         DADT(1)=0
         DADT(2)=-K23*A(2)+K32*A(3)-K20*A(2)
         DADT(3)=K23*A(2)-K32*A(3)
     ENDIF

     DADT(4)=A(3)/V
;-------------------------------------------------------------------------------------------------
------
$ERROR

     IPRED=A(3)/V

     PROP=IPRED*THETA(4)
     ADD=THETA(5)

     LLOQ=0.08
     IMPUTED_BLQ=LLOQ/2

     ; BLQ==2 are consecutive BLQ samples in a series, which I want to disergard
     IF (ICALL/=4.AND.BLQ==2) THEN
         PROP=0
         ADD=IMPUTED_BLQ*1000000 ; Using this large error has the same effect as ignoring,
         expect the record is still there, so I can use it in VPCs.
     ENDIF

     W = SQRT(ADD**2+PROP**2)


     ; Protective code
     IF (W.LE.0.000001) W=0.000001

     IRES=DV-IPRED
     IWRES=IRES/W

     Y = IPRED + W*ERR(1)

     ; For simulation, like in case of VPC
     IF (ICALL==4.AND.Y<=LLOQ) THEN
        Y=IMPUTED_BLQ ; All BLQ values in simulation get imputed to LLOQ/2. This also
        prevents negative values
     ENDIF

     ; Retrieve amount in compartments
     AA1=A(1)
```

```
      CLBS=THETA(1)           ; CL STRAT1=0
      CLSS=THETA(7)           ; CL STEADY STATE
      IND50=THETA(8)          ; INDUCTION HALF LIFE
      TVCL=(CLBS+(CLSS-CLBS)*(1-EXP(-LOG(2)*DAY/IND50)))*ALLOM_CL
;-------------------------------------------------------------------------;
      BSVCL=ETA(1)
      BSVV=ETA(2)
      BSVKA=ETA(3)
      BSVBIO=ETA(4)
      BSVMTT=ETA(5)
      ;-------------------------------------------------------------------------;

      BOVMTT=OCC1*ETA(6)+OCC2*ETA(7)+OCC3*ETA(8)+OCC4*ETA(9)+OCC5*ETA(10)+OCC6*ETA(11)+OCC7*ETA
      (12)

      BOVBIO=OCC1*ETA(13)+OCC2*ETA(14)+OCC3*ETA(15)+OCC4*ETA(16)+OCC5*ETA(17)+OCC6*ETA(18)+OCC7
      *ETA(19)

      BOVKA=OCC1*ETA(20)+OCC2*ETA(21)+OCC3*ETA(22)+OCC4*ETA(23)+OCC5*ETA(24)+OCC6*ETA(25)+OCC7*
      ETA(26)

      BOVCL=OCC1*ETA(27)+OCC2*ETA(28)+OCC3*ETA(29)+OCC4*ETA(30)+OCC5*ETA(31)+OCC6*ETA(32)+OCC7*
      ETA(33)

;-------------------------------------------------------------------------;
      CL=TVCL*EXP(BSVCL+BOVCL)
      V =TVV*EXP(BSVV)
      KA=TVKA*EXP(BSVKA+BOVKA)
      BIO=TVBIO*EXP(BOVBIO)
      MTT=TVMTT*EXP(BOVMTT)
      NN=TVNN
      VH=TVVH
      QH=TVQH
      FU=TVFU

      CLINT=CL

;------------SATURABLE PHARMACOKINETICS---------------------------------------;
       LOGKM = THETA(13) ; LOG KM - claculated from data set - median of max conc in the liver
       VMAX  = CLINT*EXP(LOGKM) ; max enzimatic rate
       ;from eq. CLint = Vmax/KM

;---------------TRANSIT ABSORPTION-----------------------------------------------;
      F1=0 ; I need to set bioavailability in compartment 1 to 0

      KTR = (NN+1)/MTT

      IF (NEWIND/=2.OR.EVID>=3) THEN ; new individual, or reset event
          ; The values read here will be stored in TDOS and PD in this very PK call.
          TNXD=TIME ; Time of the dose
          PNXD=AMT ; Amount. If it's zero, the DE is deactivated.
      ENDIF

      TDOS=TNXD ; This will either save here the temporary values if it's a new individual...
      PD=PNXD ; ...or the values which were read one record ahead during the execution of the
      previous record.

      IF(AMT.GT.0) THEN ; This reads one record ahead and stores the data to be used when
      running the following record
      ; IF(AMT.GT.0.AND.ALAG1.EQ.0) THEN ; Use this instead if there is ALAG, as it will also
      checks if the ALAG is not 0
          TNXD=TIME
          PNXD=AMT
      ENDIF

      PIZZA=LOG(BIO*PD*KTR+0.00001)-GAMLN(NN+1) ; without +0.00001, it won't work with ETAs
      in bioavailability :NM73 version

      S3=V

$DES
     CH = A(2) / VH ; drug conc in liver
     ; set saturable elimindation to zero for pts with negative concentrations in liver
```

```
$COVARIANCE PRINT=E MATRIX=S ATOL=9
$TABLE      FILE=sdtab16.csv FORMAT=, ID OCC TIME TAD VPCTIME DV EVID
            AMT MDV PRED IPRED IRES W IWRES CWRES OBJI AA1 AA2 NOPRINT
            NOAPPEND ONEHEADER WRESCHOL
$TABLE      FILE=patab16.csv FORMAT=, ID OCC TIME CL V KA BIO MTT NN
            TVCL TVV TVKA TVMTT TVNN BSVCL BSVV BSVKA BSVMTT BOVCL
            BOVKA BOVBIO BOVMTT NOPRINT NOAPPEND ONEHEADER
$TABLE      FILE=cotab16.csv FORMAT=, ID OCC TIME STRAT STRAT1 ARM AGE
            SEX WEIGHT HEIGHT CD4COUNT FORM TABS_TB NTAB DRUG AUC_T
            NOPRINT NOAPPEND ONEHEADER
$TABLE      FILE=mytab16.csv FORMAT=, ID OCC TIME TAD VPCTIME1 STRAT
            STRAT1 DV EVID AMT MDV AA1 AA2 AA3 CONC2 CONC3 SAT_CL
            IPRED PRED IWRES WRES CWRES OBJI NPDE CL V KA BIO MTT NN TVCL
            TVV TVKA TVMTT TVNN BSVCL BSVV BSVKA BSVBIO BSVMTT BOVCL
            BOVKA BOVBIO BOVMTT BLQ PRESAMP ARM0 AGE SEX WEIGHT HEIGHT
            CD4COUNT FORM TABS_TB NTAB DRUG DAY
            VPCTIME1 CLH AUC_T NOPRINT NOAPPEND ONEHEADER
```

```
$SIZES      LVR=60 MAXFCN=100000000
$PROBLEM    PZA_TB-HAART_DATA
$INPUT      ID OCC TIME AMT DV MDV EVID BLQ PROB_NEW PROB_DES=DROP ARM DRUG
            NTAB FORM AGE SEX WEIGHT HEIGHT CD4COUNT WGTDOSE TABS_TB SCHEMOG
            SCVIRLOAD SCALBUMIN D0VIRLOAD TREAT_DAYS TAD1 DAY VPCTIME
$DATA      final_PZA_29-01-15.csv IGNORE=#
$SUBROUTINE ADVAN13 TRANS1 TOL=9
$MODEL      NCOMPARTMENTS=2 COMP=(ABS DEFDOSE)
            COMP=(CENTRAL DEFOBSERVATION)
;-------------------------------------------------------------------------;
$PK
MXSTEP=50000
     OCC1=0
     OCC2=0
     OCC3=0
     OCC4=0
     OCC5=0
     OCC6=0
     OCC7=0

     IF(OCC.EQ.1) OCC1=1      ; Create indicator variable for occasion 1 to 7
     IF(OCC.EQ.2) OCC2=1
     IF(OCC.EQ.3) OCC3=1
     IF(OCC.EQ.4) OCC4=1
     IF(OCC.EQ.5) OCC5=1
     IF(OCC.EQ.6) OCC6=1
     IF(OCC.EQ.7) OCC7=1

     STRAT=0
     IF (OCC==2.OR.OCC==3) STRAT=1
     IF (OCC==4.OR.OCC==5) STRAT=2
     IF (OCC==6.OR.OCC==7) STRAT=3

     STRAT1=0
     IF (DAY>4.AND.DAY<11) STRAT1=1
     IF (DAY>10.AND.DAY<18) STRAT1=2
     IF (DAY>17.AND.DAY<30) STRAT1=3
      ;LGVLOAD=LOG(SCVIRLOAD)
;-------------------------------------------------------------------------;
     ;ALLOMETRIC SCALING_FFM & WEIGHT
      ;----Fat Free Mass
      IF (SEX.EQ.1) THEN  ; female
          WHSMAX=37.99
          WHS50=35.98
       ELSE        ;males
          WHSMAX=42.92
          WHS50=30.93
     ENDIF

     HTM2 = HEIGHT**2    ; IMPORTANT: HEIGHT is used in meters!!!
     FFM = (WHSMAX*HTM2*WEIGHT)/(WHS50*HTM2+WEIGHT)

     WTSTD=55.2  ; STANDARD WEIGHT
     FFMSTD=42.20205 ; STANDARD FFM

     ALLOM_CL=(FFM/FFMSTD)**0.75
     ALLOM_V =(FFM/FFMSTD)

;-------------------------------------------------------------------------;
     TVV  =THETA(2)*ALLOM_V  ; Pop V
     TVKA =THETA(3)  ; Pop KA
     SIG_PROP=THETA(4) ; Sigma_PROP
     SIG_ADD=THETA(5)  ; Sigma_ADD
     TVBIO=1              ; BIO
     TVMTT=THETA(6)   ; MTT
     TVNN=THETA(7)    ;NN
;-------------------------------------------------------------------------;
     CLBS=THETA(1)          ; CL DAY0
     CL28=THETA(8)          ; CL DAY28
     NATVCL=CLBS + (CL28-CLBS)*(DAY/28)
     TVCL=NATVCL*ALLOM_CL
;-------------------------------------------------------------------------;
     ; DEFINE ETAS
```

```
;-------------------------------------------------------------------------;
      BSVCL= ETA(1)       ; BSV_CL
      BSVV = ETA(2)       ; BSV_V
      BSVKA= ETA(3)       ; BSV_KA
      BSVBIO=ETA(4)       ; BSV_BIO
      BSVMTT=ETA(5)       ; BSV_MTT


      BOVCL=OCC1*ETA(6)+OCC2*ETA(7)+OCC3*ETA(8)+OCC4*ETA(9)+OCC5*ETA(10)+OCC6*ETA(11)+OCC7*ETA(
      12)

      BOVKA=OCC1*ETA(13)+OCC2*ETA(14)+OCC3*ETA(15)+OCC4*ETA(16)+OCC5*ETA(17)+OCC6*ETA(18)+OCC7*
      ETA(19)

      BOVBIO=OCC1*ETA(20)+OCC2*ETA(21)+OCC3*ETA(22)+OCC4*ETA(23)+OCC5*ETA(24)+OCC6*ETA(25)+OCC7
      *ETA(26)

      BOVMTT=OCC1*ETA(27)+OCC2*ETA(28)+OCC3*ETA(29)+OCC4*ETA(30)+OCC5*ETA(31)+OCC6*ETA(32)+OCC7
      *ETA(33)
;-------------------------------------------------------------------------;
      VARCL=BSVCL+BOVCL

      CL=TVCL*EXP(VARCL)
      V =TVV*EXP(BSVV)          ; V  in L
      KA=TVKA*EXP(BSVKA+BOVKA)       ; Absorption rate constant
      BIO=TVBIO*EXP(BSVBIO+BOVBIO)     ; Fraction of dose absorbed by first order process
      MTT=TVMTT*EXP(BOVMTT+BSVMTT)                        ;MTT
      NN=TVNN                      ;NN
      K=CL/V

;-----------------TRANSIT
COMPARTMENT-----------------------------------------------------------;
      F1=0 ; I need to set bioavailability in compartment 1 to 0

      KTR = (NN+1)/MTT

      IF (NEWIND/=2.OR.EVID>=3) THEN ; new individual, or reset event
          ; The values read here will be stored in TDOS and PD in this very PK call.
         TNXD=TIME ; Time of the dose
          PNXD=AMT ; Amount. If it's zero, the DE is deactivated.
      ENDIF

      TDOS=TNXD ; This will either save here the temporary values if it's a new individual...
      PD=PNXD ; ...or the values which were read one record ahead during the execution of the
      previous record.

      IF(AMT.GT.0) THEN ; This reads one record ahead and stores the data to be used when
      running the following record
      ; IF(AMT.GT.0.AND.ALAG1.EQ.0) THEN ; Use this instead if there is ALAG, as it will also
      checks if the ALAG is not 0
          TNXD=TIME
          PNXD=AMT
      ENDIF


      PIZZA=LOG(BIO*PD*KTR+0.00001)-GAMLN(NN+1); without +0.00001, it won't work with ETAs in
      bioavailability

      S2=V
;-------------------------------------------------------------------------;
$DES

      TEMPO=T-TDOS ; this is time after dose, it should always be >= 0
      KTT=0

      DADT(1)=0

      IF(PD.GT.0.AND.TEMPO.GT.0) THEN ; This happens only id PD>0, so only if a dose has been
      detected
          KTT=KTR*(TEMPO)
          DADT(1)=EXP(PIZZA+NN*LOG(KTT)-KTT)-KA*A(1)
      ENDIF
```

```
      DADT(2)=KA*A(1)-K*A(2)


;-------------------------------------------------------------------------;
$ERROR
      IPRED  = A(2)/V
      IRES   = DV - IPRED

      W=SQRT((SIG_PROP*IPRED)**2+SIG_ADD**2)      ; Residual SD
      IF(W.LE.0.0001) W=0.0001
      IWRES=IRES/W
      Y=IPRED+W*EPS(1)

      IF(AMT.GT.0) THEN
         TIMEDOSE = TIME
         AMOUNTDOSE = AMT
      ENDIF

      TAD=TIME-TIMEDOSE

      LLOQ=0.2
      IMPUTED_BLQ=LLOQ/2

      ; For simulation, like in case of VPC -LOQ
      IF(ICALL==4.AND.Y<=LLOQ) THEN
         Y=IMPUTED_BLQ ; All BLQ values in simulation get imputed to LLOQ/2. This also
         prevents negative values
      ENDIF


      AA1=A(1)
      AA2=A(2)


;-------------------------------------------------------------------------;
$THETA  (0,3.3242,10) ; 1. CLBS[L/h]
$THETA  (0,42.4347,100) ; 2. TVV [L]
$THETA  (0,3.54661,10) ; 3. TVKA
$THETA  (0,0.0437718,2) ; 4. Sigma_prop
$THETA  (0,1.51731,10) ; 5. Sigma_add [mg/L]
$THETA  (0,0.466387,5) ; 6. TVMTT [h]
$THETA  5 FIX ; 7. NN
$THETA  (0,3.81853,10) ; 8. CL28[L/h]
;-------------------------------------------------------------------------;
$OMEGA  0.0267624  ;  1. BSV_CL
$OMEGA  0  FIX  ;  2. BSV_Vd
$OMEGA  0  FIX  ;  3. BSV_Ka
$OMEGA  0.0111415  ; 4. BSV_BIO
$OMEGA  0  FIX  ; 5. BSV_MTT
$OMEGA  BLOCK(1)  0.0156762  ;  5. BOV_CL
$OMEGA  BLOCK(1) SAME
$OMEGA  BLOCK(1) SAME
$OMEGA  BLOCK(1) SAME
$OMEGA  BLOCK(1) SAME
$OMEGA  BLOCK(1) SAME
$OMEGA  BLOCK(1) SAME
$OMEGA  BLOCK(1)  0.65175  ; 12. BOV_Ka
$OMEGA  BLOCK(1) SAME
$OMEGA  BLOCK(1) SAME
$OMEGA  BLOCK(1) SAME
$OMEGA  BLOCK(1) SAME
$OMEGA  BLOCK(1) SAME
$OMEGA  BLOCK(1) SAME
$OMEGA  BLOCK(1)  0.0138166  ; 19. BOV_BIO
$OMEGA  BLOCK(1) SAME
$OMEGA  BLOCK(1) SAME
$OMEGA  BLOCK(1) SAME
$OMEGA  BLOCK(1) SAME
$OMEGA  BLOCK(1) SAME
$OMEGA  BLOCK(1) SAME
$OMEGA  BLOCK(1)  0.543944  ; 26. BOV_MTT
$OMEGA  BLOCK(1) SAME
$OMEGA  BLOCK(1) SAME
```

```
$OMEGA  BLOCK(1) SAME
$OMEGA  BLOCK(1) SAME
$OMEGA  BLOCK(1) SAME
$OMEGA  BLOCK(1) SAME
$SIGMA  1  FIX  ; 25. RESIDUAL
;------------------------------------------------------------------------;
$ESTIMATION MAXEVAL=0 SIGL=10 ATOL=9 METHOD=1 INTER PRINT=1 NOABORT
            NSIG=3 MCETA=2000 RANMETHOD=4P NONINFETA=1 ETASTYPE=1
$ESTIMATION MAXEVAL=9999 SIGL=10 ATOL=9 METHOD=1 INTER PRINT=1 NOABORT
            NSIG=3 MCETA=50 RANMETHOD=4P NONINFETA=1 ETASTYPE=1
$COVARIANCE PRINT=E MATRIX=S ATOL=9
$TABLE      WRESCHOL FILE=sdtab11.csv FORMAT=, ID OCC TIME VPCTIME TAD
            DV EVID AMT MDV PRED IPRED IRES IWRES CWRES OBJI AA1 AA2
            NOPRINT NOAPPEND ONEHEADER
$TABLE      FILE=patab11.csv FORMAT=, ID OCC TIME TAD CL V KA BIO K
            MTT NN TVV TVBIO TVKA TVMTT TVNN TVCL BSVCL BSVV BOVCL
            BOVKA BOVBIO BOVMTT NOPRINT NOAPPEND ONEHEADER
$TABLE      FILE=cotab11.csv FORMAT=, ID OCC TIME STRAT ARM AGE SEX
            WEIGHT HEIGHT CD4COUNT FORM TABS_TB NTAB DRUG NOPRINT
            NOAPPEND ONEHEADER
$TABLE      FILE=mytab11.csv FORMAT=, ID OCC TIME TAD DV EVID AMT MDV
            AA1 AA2 IPRED PRED IWRES WRES CWRES OBJI CL V KA K BIO MTT
            NN TVV TVBIO TVKA TVMTT TVNN TVCL BSVCL BSVV BSVKA BSVBIO
            BSVMTT BOVCL BOVKA BOVBIO BOVMTT ARM AGE SEX WEIGHT HEIGHT
            CD4COUNT FORM NTAB DRUG STRAT TREAT_DAYS SCVIRLOAD
            SCTOTBIL SCALBUMIN SCHEMOG SCCREAT D0VIRLOAD WGTDOSE
            STRAT1 DAY VPCTIME FFM NOPRINT NOAPPEND ONEHEADER
```

```
$SIZES      MAXFCN=100000000 PD=-1000 LVR=-150 LTH=-200
$PROBLEM    INH-RAFA
$INPUT      ID SAMPLENO OCC TIME AMT MDV EVID DVID DV CMT ADDL II BLQ SITE1BENIN BATCH
DEFROST1YES
            ARM NTAB VOMIT1Y RIFTABS INC_WEIGHT INC_ARM VPCTIME FDCBATCH SDBATCH
            PK04_MISSTBTREAT
            PK04_MISSTBDAYS PK04_WEIGHT PK04_HEMOGLO PK04_WHITECELL PK04_PLAQ PK04_NEUTRO
            PK04_CREAT PK04_ASAT PK04_PHOSPHATE PK04_ALAT PK04_BILIR PK04_GGT SEL_SEX
            SEL_HEIGHT SEL_WEIGHT  SEL_CD4COUNT SEL_VLOAD AGE DVGROUP ACTYLSTATUS
$DATA      INH-PAR_MET02-05-2016ACETYL.csv IGNORE=#

$SUBROUTINE ADVAN13 TRANS1
$MODEL      NCOMPARTMENTS=6 COMP=(ABS DEFDOSE) COMP=(LIVER) COMP=(CENTRAL DEFOBS)
            COMP=(PERI) COMP=(MET) COMP=(AUC)
;------------------------------------------------------------------------------;
$PK

      DVIDACETYL=1
      IF(ACTYLSTATUS==2.AND.DVID==1) DVIDACETYL=2
      IF(ACTYLSTATUS==1.AND.DVID==2) DVIDACETYL=3
      IF(ACTYLSTATUS==2.AND.DVID==2) DVIDACETYL=4
;------------------------------------------------------------------------------;
     OCC1=0
     OCC2=0

     ; Create indicator variables for occasion
     IF(OCC.EQ.1) OCC1=1
     IF(OCC.EQ.2) OCC2=1

     ;ALLOMETRIC SCALING_FFM & WEIGHT
     SEX = SEL_SEX
     HEIGHT = SEL_HEIGHT/100  ; HEIGHT IN METRES

      ;----Fat Free Mass
      IF (SEX.EQ.1) THEN  ; female
          WHSMAX=37.99
          WHS50=35.98
      ELSE        ;males
          WHSMAX=42.92
          WHS50=30.93
     ENDIF

     WEIGHTPK=WEIGHT
     IF (WEIGHT==999) WEIGHTPK=PK04_WEIGHT

     HEIGHT2 = HEIGHT**2    ; IMPORTANT: HEIGHT is used in meters!!!
     FFM = (WHSMAX*HEIGHT2*WEIGHTPK)/(WHS50*HEIGHT2+WEIGHTPK)

     WTSTD=52  ; STANDARD WEIGHT
     FFMSTD=43.34 ; STANDARD FFM

     ALLOM_CL=(FFM/FFMSTD)**0.75
     ALLOM_V =(FFM/FFMSTD)

     ;ALLOM_CL=(WEIGHTPK/WTSTD)**0.75
     ;ALLOM_V =(WEIGHTPK/WTSTD)
;------------------------------------------------------------------------------;
     ;COVARIATES
     COVLOT=0
     IF(FDCBATCH==5) COVLOT=1
     IF(FDCBATCH==6) COVLOT=1
     COVLOT_BIO=1 + THETA(20)*COVLOT

     ;;; CLARM-DEFINITION START
      CLARM = 1  ; Standard treatment + ARM3
     IF(ARM.EQ.1) CLARM = ( 1 + THETA(10))
     ;;; CLARM-DEFINITION END

     COVARM_CL=CLARM
;------------------------------------------------------------------------------;
     ;MIXTURE FOR CLEARANCE
```

```
      ;Sim_start
      IF(MIXNUM.EQ.1) THEN
         TVCL=THETA(1)*ALLOM_CL*COVARM_CL
      ELSE
         TVCL=THETA(8)*ALLOM_CL*COVARM_CL
      ENDIF

      ;IF(ACTYLSTATUS.EQ.1) THEN
      ;   TVCL=THETA(1)*ALLOM_CL*COVARM_CL
      ;ELSE
      ;   TVCL=THETA(8)*ALLOM_CL*COVARM_CL
      ;ENDIF

      ;Sim_end
;-------------------------------------------------------------------------;
      TVVCEN  =THETA(2)*ALLOM_V          ; Pop V
      TVKA =THETA(3)             ; Pop KA
      TVBIO= 1*COVLOT_BIO
      TVQ4=THETA(6)*ALLOM_CL             ; INTERCOMPARTMENTAL CLEARANCE
      TVVPER=THETA(7)*ALLOM_V             ; VOLUME-PERI
      TVCLMET=THETA(11)*ALLOM_CL        ; CLEARANCE METABOLITE
      TVVMET=THETA(12)*ALLOM_V          ; VOLUME METABOLITE
      TVCLCEN=THETA(18)*ALLOM_CL        ; CLEARANCE CENTRAL
      TVCLUNK=THETA(19)*ALLOM_CL
;-------------------------HEPATIC CL--------------------------------------;
      TVVH=THETA(15)*ALLOM_V     ; VOLUME OF LIVER WITH ALLOMETRIC SCALLING
      TVQH=THETA(16)*ALLOM_CL    ; PLASMA FLOW RATE
      TVFU=THETA(17)             ; UNBOUND PLASMA FRACTION OF INH
;-----------------------VARIABILITY ---------------------------------------;
      BSVCL=ETA(1)
      BSVVCEN=ETA(2)
      BSVKA=ETA(3)
      BSVBIO=ETA(4)

      BOVBIO=ETA(5)
      IF(OCC==1) BOVBIO=ETA(6)

      BSVCLMET=ETA(7)
      BSVVMET=ETA(8)
      BSVCLUNK=ETA(9)
;-------------------------------INDIVIDUAL PARAMETERS ---------------------;
      CL=TVCL*EXP(BSVCL)
      CLUNK=TVCLUNK*EXP(BSVCLUNK)
      VCEN =TVVCEN*EXP(BSVVCEN)
      KA=TVKA*EXP(BSVKA)
      BIO=TVBIO*EXP(BSVBIO+BOVBIO)
      Q4   = TVQ4
      VPER = TVVPER
      VH=TVVH
      QH=TVQH
      FU=TVFU
      CLCEN=TVCLCEN
;--------------------INDV PARS INLCUDING MOLECULAR
RATIO-------------------------------------;
      CLMET = TVCLMET*(179.18/137.139)*EXP(BSVCLMET)
      VMET = TVVMET*(179.18/137.139)*EXP(BSVVMET)
;--------------------HEPATIC EXTRACTION-----------------;
      CLINTACETYL=CL
      CLINTUNK=CLUNK

      EHACETYL=(CLINTACETYL*FU)/(((CLINTACETYL+CLINTUNK)*FU)+QH)
      EHUNK=(CLINTUNK*FU)/(((CLINTACETYL+CLINTUNK)*FU)+QH)
      EH=EHACETYL+EHUNK
      FH   = 1 - EH

      F1=BIO
;--------------------RATE CONSTANTS-----------------;
      K20 =  (QH*EHUNK/VH)
      K25 =(QH*EHACETYL/VH)
      K23 =(QH*FH/VH)
      K32 =(QH/VCEN)
      K34 =  Q4/VCEN
      K43 =  Q4/VPER
```

```
      K50=CLMET/VMET
      K12=KA
      K30=CLCEN/VCEN

      ;Sim_start
      EST=MIXEST
      ;EST=ACTYLSTATUS
      ;Sim_end

      ;SCALING TERMS FOR COMPARTMENTS
      S3 = VCEN
      S5 = VMET

 ;-----------------------------------------------------------------------------------------------
 ------------------------------------------------------------------
$DES
  DADT(1) = - K12*A(1)
  DADT(2) = K12*A(1) - K25*A(2) - K23*A(2) + K32*A(3) - K20*A(2)
  DADT(3) = K23*A(2) - K32*A(3) - K34*A(3) + K43*A(4)
  DADT(4) = K34*A(3) - K43*A(4)
  DADT(5) = K25*A(2)
  DADT(6) = A(3)/V2
;-----------------------------------------------------------------------------------------------
------

$ERROR

      IPRED=F

      ; METABOLITE LLOQ
      LLOQ_MET=0.05
      IMPUTED_BLQ_MET=LLOQ_MET/2

      ;OLD LLOQ
      LLOQ_PARENT=0.1
      ;IMPUTED_BLQ=LLOQ/2
      LLQADDERR=LLOQ_PARENT/5

      ; THIS IS DUMMY LLOQ AFTER BLQ VALUES WERE RELEASED
      LLOD=0.02
      IMPUTED_BLQNEW=0.00849694 ; GEOMETRIC MEAN OF VALUES BELOW LLOD MINUS 2 OUTLIERs

      ; ERROR PARENT
      PROP=IPRED*THETA(4)
      ADD=THETA(5) + LLQADDERR

      ;ERROR METABOLITE
      IF (DVID==2) THEN
          PROP = THETA(13)*IPRED
          ADD = THETA(14) + LLOQ_MET/5
      ENDIF

      W = SQRT(ADD**2+PROP**2)

      ; Protective code
      IF (W.LE.0.000001) W=0.000001

      IRES=DV-IPRED
      IWRES=IRES/W

      Y = IPRED + W*ERR(1)

      ; For simulation, like in case of VPC
      IF (DVID==1) THEN
         LLOQ=LLOD
         IMPUTED_BLQ=0.00429
      ELSE
         IMPUTED_BLQ=LLOQ_MET/2
         LLOQ=LLOQ_MET
     ENDIF

      IF (ICALL==4.AND.Y<=LLOQ) THEN
         Y=IMPUTED_BLQ ; All BLQ values in simulation get imputed to LLOQ/2. This also
```

```
      prevents negative values
    ENDIF

    ; Retrieve amount in compartments
    AA1=A(1)
    AA3=A(3)
    AA5=A(5)

    ; To calculate TAD
    IF(AMT.GT.0) THEN
        TIMEDOSE = TIME
        AMOUNTDOSE = AMT

    ENDIF

    TAD = TIME-TIMEDOSE
    VARBIO = BSVBIO+BOVBIO
    VARAUC = VARBIO-BSVCL
    CLH = (QH*FU*(CLINTACETYL+CLINTUNK)/(QH+FU*(CLINTACETYL+CLINTUNK)))
    AUC_T = A(6)
;-------------------------------------------------------------------------;
;Sim_start
$MIX
     NSPOP=2              ; 2 SUB-POPULATIONS (SLOW AND FAST ACETYLATORS)
     P(1)=THETA(9)        ; PROBABILITY OF FAST ACETYLATOR
     P(2)=1-P(1)          ; PROBABILITY OF SLOW  ACETYLATOR

;Sim_end

$THETA  (0,31.626) ; 1. TVCL FAST [L/h]
$THETA  (0,51.5477,500) ; 2. TVV  [L]
$THETA  (0,1.80687,10) ; 3. TVKA [1/h]
$THETA  (0,0.112689,1) ; 4. SIG_PROP
$THETA  0 FIX ; 5. SIG_ADD [mg/L]
$THETA  (0,0.966365,50) ; 6.  Q[L/h]
$THETA  (0,6.44624,100) ; 7. V3 [L]
$THETA  (0,5.32469) ; 8. TVCL SLOW [L/h]
;Sim_start
$THETA  (0,0.499829,1) ; 9. PROPORTION FAST
;$THETA 0 FIX ; 9. PROPORTION FAST
;Sim_end
$THETA  (-1,0.341713,1) ; 10. ARM1_CL
$THETA  (0,6.08572,50) ; 11. CL_MET
$THETA  (0,32.4116,500) ; 12. V_MET
$THETA  (0,0.0654158,1) ; 13. SIG_PROP_MET
$THETA  0 FIX ; 14. SIG_ADD_MET [mg/L]
$THETA  1 FIX ; 15. VH
$THETA  50 FIX ; 16. PLASMA FLOW
$THETA  0.95 FIX ; 17. FRACTION_UNBOUND
$THETA  0 FIX ; 18. TVCLCEN [L/h]
$THETA  (0,11.3797,50) ; 19. TVCLUNK [L/h]
$THETA  (-1,-0.616143,1) ; 20. LOT_BIO
;-------------------------------------------------------------------------;
$OMEGA  0.127335  ; 1. BSV_CLF
$OMEGA  0.019567  ;  2. BSV_Vd
$OMEGA  0.261996  ;  3. BSV_Ka
$OMEGA  0  FIX  ; 4. BSV_BIO
$OMEGA  BLOCK(1)
 0.0345041  ; 5. BOV_BIO
$OMEGA  BLOCK(1) SAME
$OMEGA  0.0322217  ; 7. BSV_CL_MET
$OMEGA  0  FIX  ; 8. BSV_Vd_MET
$OMEGA  0.0800558  ; 9. BSV_CLUNK
$SIGMA  1  FIX  ;   RESIDUAL
;-------------------------------------------------------------------------;
;Sim_start
$ESTIMATION MAXEVAL=9999 SIGL=10 ATOL=9 METHOD=1 INTER PRINT=1 NOABORT
            NSIG=3 NONINFETA=1 ETASTYPE=1
$COVARIANCE PRINT=E MATRIX=S ATOL=9 UNCONDITIONAL
$TABLE      WRESCHOL FILE=sdtab100.csv FORMAT=, ID OCC VPCTIME TIME
            TAD DV EVID AMT MDV IPRED PRED IWRES WRES CWRESI CWRES
            CPREDI CIPREDI OBJI BSVCL BSVKA BSVVCEN BSVBIO BOVBIO
            VARAUC VARBIO BSVCLMET BSVVMET NOPRINT NOAPPEND ONEHEADER
```

```
$TABLE      FILE=patab100.csv FORMAT=, ID CL VCEN VPER Q4 KA BIO ADD
            PROP CLMET VMET VPER CLCEN NOPRINT NOAPPEND ONEHEADER
$TABLE      FILE=cotab100.csv FORMAT=, ID WEIGHTPK HEIGHT FFM
            PK04_HEMOGLO PK04_WHITECELL PK04_PLAQ PK04_NEUTRO
            PK04_CREAT PK04_ASAT PK04_PHOSPHATE PK04_ALAT PK04_BILIR
            PK04_GGT SEL_CD4COUNT SEL_VLOAD AGE NOPRINT NOAPPEND
            ONEHEADER
$TABLE      FILE=catab100.csv FORMAT=, ID SEX ARM FDCBATCH SDBATCH
            SITE1BENIN BLQ BATCH DVGROUP COVLOT ACTYLSTATUS NOPRINT
            NOAPPEND ONEHEADER
$TABLE      FILE=mytab100.csv FORMAT=, ID OCC TIME TAD DV DVID DVGROUP
            EVID AMT MDV AA1 AA3 AA5 IPRED PRED IWRES WRES CPREDI
            CIPREDI CWRES CWRESI CIWRESI OBJI CL VCEN VPER VMET Q4 KA
            BIO VH CLCEN TVCL TVVH TVVCEN TVCLMET TVVMET TVQ4 TVKA
            TVCLCEN BSVCL BSVVCEN BSVKA BSVBIO BOVBIO BSVCLMET BSVVMET
            VARAUC VARBIO BLQ BATCH SITE1BENIN AGE EST ARM NTAB SEX
            HEIGHT WEIGHTPK FFM FDCBATCH SDBATCH PK04_HEMOGLO
            PK04_WHITECELL PK04_PLAQ PK04_NEUTRO PK04_CREAT PK04_ASAT
            PK04_PHOSPHATE PK04_ALAT PK04_BILIR PK04_GGT SEL_CD4COUNT
            SEL_VLOAD COVLOT VPCTIME ACTYLSTATUS CLH EHACETYL EHUNK EH
            NOPRINT NOAPPEND ONEHEADER
;$SIMULATION ONLYSIMULATION (2239177789 NORMAL)

;Sim_end
```

Final NONMEM scripts for results presented in section 6.1.1

```
$SIZES      MAXFCN=100000000 PD=-1000 LVR=-150 LTH=-200
$PROBLEM    RIF-RAFA ;||
$ABBREVIATED COMRES=2
$INPUT      ID SAMPLENO WHAT=DROP OCC TIME AMT MDV EVID DVID L2 CMT1
            DVOLD=DROP DV LNDV DVBLQOLD=DROP ADDL II BLQOLD=DROP BLQ
            SITE1BENIN BATCH DEFROST1YES PAT_INIT=DROP PAT_AGREED=DROP
            ARM NTAB OLDLOT=DROP EXP_DATE=DROP NTAB_RIF
            OLDLOT_RIF=DROP EXP_DATE_RIF=DROP ARV1_NAME=DROP
            ARV1_DOSE=DROP ARV1_MORNING=DROP ARV1_EVENING=DROP
            ARV2_NAME=DROP ARV2_DOSE=DROP ARV2_MORNING=DROP
            ARV2_EVENING=DROP ARV3_NAME=DROP ARV3_DOSE=DROP
            ARV3_MORNING=DROP ARV3_EVENING=DROP TBDOSE_2DAYSDAT=DROP
            TBDOSE_2DAYSTIM=DROP TBDOSE_1DAYSDAT=DROP
            TBDOSE_1DAYSTIM=DROP NRTI_DAT=DROP NRTI_TIM=DROP
            EFV_DAT=DROP EFV_TIM=DROP PK_DATE=DROP WEIGHT T1=DROP
            TDOSE=DROP T_ARV=DROP BREAKFAST=DROP TBREAKFAST=DROP
            T2=DROP T3=DROP T4=DROP T5=DROP VOMIT1Y TVOMIT=DROP
            NOTES=DROP OTHER_TRT=DROP COURSE_PK=DROP NO_SPECIFY=DROP
            PROTOCOL_VIO=DROP YES_SPECIFY=DROP INITIALS=DROP
            DATE_SIGNED=DROP DOSETIME_PRE=DROP TIME_DOSE=DROP RIFTABS
            DAYSTOPK PKDAY DAY VPCTIME INC_WEIGHT INC_ARM LOT=DROP
            LOT_RIF=DROP FDCBATCH SDBATCH PK04_INTDATE=DROP
            PK04_ATTEND=DROP PK04_MISSTBTREAT PK04_MISSTBDAYS
            PK04_MISSARVTREAT=DROP PK04_MISSARVDAYS=DROP
            PK04_MODARVTREAT=DROP PK04_EXTRAMED=DROP PK04_WEIGHT
            PK04_SMEAR1DT=DROP PK04_SMEAR1=DROP PK04_SMEAR2DT=DROP
            PK04_SMEAR2=DROP PK04_SMEAR3DT=DROP PK04_SMEAR3=DROP
            PK04_BIOTESTDATE=DROP PK04_HEMOGLO PK04_WHITECELL
            PK04_PLAQ PK04_NEUTRO PK04_CREAT PK04_ASAT PK04_PHOSPHATE
            PK04_ALAT PK04_BILIR PK04_GGT SEL_INTDATE=DROP
            SEL_DOBDD=DROP SEL_DOBMM=DROP SEL_DOBYY=DROP SEL_SEX
            SEL_HEIGHT SEL_WEIGHT SEL_SMEAR1DT=DROP SEL_SMEAR1=DROP
            SEL_SMEAR2DT=DROP SEL_SMEAR2=DROP SEL_SMEAR3DT=DROP
            SEL_SMEAR3=DROP SEL_FEVER=DROP SEL_NIGHTSW=DROP
            SEL_WEIGHTLOSS=DROP SEL_COUGH=DROP SEL_HAEMOP=DROP
            SEL_CHESTP=DROP SEL_ST1=DROP SEL_ST2=DROP
            SEL_ST2WTLOSS=DROP SEL_ST2SKIN=DROP SEL_ST2ZONE=DROP
            SEL_ST2INFECT=DROP SEL_ST3=DROP SEL_ST3WTLOSS=DROP
            SEL_ST3DIA=DROP SEL_ST3FEVER=DROP SEL_ST3CAND=DROP
            SEL_ST3LEUCO=DROP SEL_ST3TBP=DROP SEL_ST3BAC=DROP
            SEL_ST3VAGINITE=DROP SEL_ST4=DROP SEL_ST4HIV=DROP
            SEL_ST4PNEUM=DROP SEL_ST4TOXO=DROP SEL_ST4CRYPT=DROP
            SEL_ST4ISOS=DROP SEL_ST4CRYPTO=DROP SEL_ST4CMV=DROP
            SEL_ST4HERPES=DROP SEL_ST4LEMP=DROP SEL_ST4MYCOSE=DROP
            SEL_ST4CAND=DROP SEL_ST4MAC=DROP SEL_ST4SALM=DROP
            SEL_ST4TB=DROP SEL_ST4LYMPH=DROP SEL_ST4KAPOSI=DROP
            SEL_ST4ENCEP=DROP SEL_STHIV=DROP SEL_ACTIVE=DROP
            SEL_XRAYDATE=DROP SEL_XCAVER=DROP SEL_XPUL=DROP
            SEL_XGRADE=DROP SEL_XZONE=DROP SEL_BIOTESTDATE=DROP
            SEL_HEMOGLO=DROP SEL_WHITECELL=DROP SEL_PLAQ=DROP
            SEL_NEUTRO=DROP SEL_CREAT=DROP SEL_ASAT=DROP
            SEL_PHOSPHATE=DROP SEL_ALAT=DROP SEL_BILIR=DROP
            SEL_GGT=DROP SEL_TDATE=DROP SEL_CD4COUNT
            SEL_CD4PERCENT=DROP SEL_VLOAD SEL_TBPULYN=DROP
            SEL_TBMENYN=DROP SEL_TBGANGYN=DROP SEL_TBPLEUYN=DROP
            SEL_TBPERITYN=DROP SEL_TBOSSEYN=DROP SEL_TBPERICYN=DROP
            SEL_TBARTYN=DROP SEL_TBOTHERYN=DROP SEL_TBOTHERTXT=DROP
            SEL_TBEPISODE=DROP SEL_TBREGIMENTXT=DROP LAB_ID=DROP AGE
            DVGROUP PROB PROB_DESC=DROP
$DATA      RIF-PAR_MET2017_12-14.csv IGNORE=# IGNORE=(BLQ==9)
            IGNORE=(BLQ==99) IGNORE=(PROB.GE.1)
$SUBROUTINE ADVAN13 TRANS1 TOL=9
$MODEL      NCOMPARTMENTS=5 COMP=(ABS DEFDOSE) COMP=(LIVERP)
            COMP=(CENTRAL) COMP=(LIVERM) COMP=(CENTMET)
;-------------------------------------------------------------------------------;
$PK
```

```
MXSTEP=50000
;-------------------------------------------------------------------------;
; CREATE DVIDSITE
     DVIDSITE=1
     IF(DVID==1.AND.SITE1BENIN==2)  DVIDSITE=2
     IF(DVID==2.AND.SITE1BENIN==1)  DVIDSITE=3
     IF(DVID==2.AND.SITE1BENIN==2)  DVIDSITE=4

;-------------------------------------------------------------------------;
     OCC1=0
     OCC2=0

     ; Create indicator variables for occasion
     IF(OCC.EQ.1) OCC1=1
     IF(OCC.EQ.2) OCC2=1


     ;ALLOMETRIC SCALING_FFM & WEIGHT
     SEX = SEL_SEX
     HEIGHT = SEL_HEIGHT/100  ; HEIGHT IN METRES


      ;----Fat Free Mass
      IF (SEX.EQ.2) THEN  ; female
          WHSMAX=37.99
          WHS50=35.98
      ELSE        ;males
          WHSMAX=42.92
          WHS50=30.93
     ENDIF

     WEIGHTPK=WEIGHT
     IF (WEIGHT==-999) WEIGHTPK=PK04_WEIGHT

     HEIGHT2 = HEIGHT**2    ; IMPORTANT: HEIGHT is used in meters!!!
     FFM = (WHSMAX*HEIGHT2*WEIGHTPK)/(WHS50*HEIGHT2+WEIGHTPK)

     WTSTD=52  ; STANDARD WEIGHT
     FFMSTD=43.34 ; STANDARD FFM

     ALLOM_CL=(FFM/FFMSTD)**0.75
     ALLOM_V =(FFM/FFMSTD)

     ;ALLOM_CL=(WEIGHTPK/WTSTD)**0.75
     ;ALLOM_V =(WEIGHTPK/WTSTD)
;-------------------------------------------------------------------------;
     ;COVARIATES
      FDCTABS=NTAB
      SDTABS=NTAB_RIF

      PERCENTFDC=FDCTABS/(FDCTABS+SDTABS)
      PERCENTSD=1-PERCENTFDC

     ; LOT
     COVLOT=0
     IF(FDCBATCH==5) COVLOT=1
     IF(FDCBATCH==6) COVLOT=1


     ;;; BIOARM-DEFINITION START
     IF(ARM.EQ.1) BIOARM = 1  ; Early ART arm
     IF(ARM.EQ.2) BIOARM = 1 ; Standard arm
     IF(ARM.EQ.3) BIOARM = ( 1 + THETA(13)) ; High dose rif
     ;;; BIOARM-DEFINITION END

     COVARM_BIO=BIOARM
;-------------------------------------------------------------------------;
     TVCL=THETA(18)*ALLOM_CL          ; CL
     TVV  =THETA(2)*ALLOM_V              ; Pop V
```

```
      TVKA =THETA(3)          ; Pop KA
      TVBIO = (PERCENTFDC*(1+THETA(8)*COVLOT) + PERCENTSD*1)*COVARM_BIO     ;BIO
      TVMTT=THETA(6)          ; MTT
      TVNN=THETA(7)           ; NN
      TVCLUNK=THETA(19)*ALLOM_CL
;--------------------------HEPATIC CL-----------------------------------------;
      TVVH=THETA(10)*ALLOM_V     ; VOLUME OF LIVER WITH ALLOMETRIC SCALLING
      TVQH=THETA(11)*ALLOM_CL    ; PLASMA FLOW RATE
      TVFU=THETA(12)             ; UNBOUND PLASMA FRACTION OF RIF

 ;-------------------------------------------------------------------------------;
      TVCLMET=THETA(14)*ALLOM_CL       ; CLEARANCE METABOLITE
    ; TVVMET=THETA(15)*ALLOM_V          ; VOLUME METABOLITE
;-------------------------------------------------------------------------------;
      BSVCL=ETA(9)
      BSVV=ETA(8)
      BSVKA=ETA(3)
      BSVBIO=ETA(5)
      BSVMTT=ETA(4)


      EXTRA_VAR=THETA(9) ; EXTRA VARIABILITY FOR PREDOSE SAMPLES
      BOVBIO=ETA(6)
      IF(OCC==1) BOVBIO=ETA(7)*EXTRA_VAR  ; extra variability

      BSVCLMET=ETA(2)
      SHAREETA=THETA(15)
     BSVCLUNK=ETA(1)
;-------------------------------------------------------------------------------;
      CL=TVCL*EXP(BSVCL)
      V =TVV*EXP(BSVV)
      KA=TVKA*EXP(BSVKA)
      BIO=TVBIO*EXP(BSVBIO+BOVBIO)
      MTT=TVMTT*EXP(BSVMTT)
      NN=EXP(TVNN)
      VH=TVVH
      QH=TVQH
      FU=TVFU
      CLUNK=TVCLUNK*EXP(BSVCLUNK)
;------INDV PARS INLCUDING MOLECULAR RATIO-----------------------------------;
      CLMET = TVCLMET*EXP(BSVCLMET)
      V5    = TVV*EXP(SHAREETA*BSVCLMET)
      VMET  = V5
;--------------------HEPATIC EXTRACTION-----------------;
      CLINTDEACETYL=CL
      CLINTUNK=CLUNK
      CLINTM  = CLMET
 ;-------------------------SATURABLE--------------------------------------;
      ;Parent
      LOGKM = THETA(1) ; LOG KM - claculated from data set - median of max conc in the liver
      VMAX  = CLINTUNK*EXP(LOGKM) ; max enzimatic rate
       ;from eq. CLint = Vmax/KM

      ; Metabolite
      LOGKMM = THETA(20) ; LOG KM - claculated from data set - median of max conc in the liver
      VMAXM  = CLINTM*EXP(LOGKMM) ; max enzimatic rate
;--------------------TRANSIT-----------------;
; Transit
F1=0 ; I need to set bioavailability in compartment 1 to 0

KTR = (NN+1)/MTT


IF (NEWIND/=2.OR.EVID>=3) THEN ; new individual, or reset event
    ; The values read here will be stored in TDOS and PD in this very PK call.
    TNXD=TIME ; Time of the dose
    PNXD=AMT ; Amount. If it's zero, the DE is deactivated.
ENDIF

TDOS=TNXD ; This will either save here the temporary values if it's a new individual...
PD=PNXD ; ...or the values which were read one record ahead during the execution of the
```

```
previous record.

IF(AMT.GT.0) THEN ; This reads one record ahead and stores the data to be used when running
the following record
; IF(AMT.GT.0.AND.ALAG1.EQ.0) THEN ; Use this instead if there is ALAG, as it will also
checks if the ALAG is not 0
    TNXD=TIME
    PNXD=AMT
ENDIF

; Uncomment this if you have ALAG or if you use ADDL
 IF (DOSTIM.GT.0) THEN ; This will account for the ADDL or lagged doses. It will overwrite
 the time, if it a non-event record
    TNXD=DOSTIM
    PNXD=AMT
 ENDIF

;LNGAM = NN*LOG(NN)-NN+LOG(NN*(1+4*NN*(1+2*NN)))/6+0.572364942 ; approximation of log of
gamma(n), 0.572364942 is LOG(PI)/2
; To speed up the computation, I calculate here all the non-time-varying quantities used in
$DES
;PIZZA=LOG(BIO*PD*KTR+0.00001)-LNGAM ; without +0.00001, it won't work with ETAs in
bioavailability
PIZZA=LOG(BIO*PD*KTR+0.00001)-GAMLN(NN+1) ; without +0.00001, it won't work with ETAs in
bioavailability :NM73 version


; RESET code for CMAX
IF (NEWIND.NE.2.OR.EVID.GE.3) THEN ; Each time I have a new subject, or a reset
    COM(1)=0
    COM(2)=0
    TDOS = 0
ENDIF

     S3=V
     S5=V5

     A_0(1)=0.00001
     A_0(2)=0.00001
     A_0(3)=0.00001
     A_0(4)=0.00001
     A_0(5)=0.00001

     ; Define scaling to adjust moles of parent and metabolite (MET/PAR)
     SCALE_MOLES = 780.9/822.94

$DES







     CH = A(2) / VH ; drug conc in liver
     CP = A(3)/V                ; plasma concentration
     CHM = A(4)/VH ; metabolite conc in liver

     IF (CP.GE.COM(1)) THEN
        COM(1) = CP             ; CMAX
        COM(2) = T - TDOS       ; TIME OF CMAX
     ENDIF

;---------------SATURATION-----------------------------;
     ; Parent
     SAT_CL=0
     IF (CH>0) SAT_CL=VMAX/(1+EXP(-(LOG(CH)-LOGKM))) / (CH)
     ;transformation based on better Emax model, wider search in log parametrisation

     EHDEACETYL=(CLINTDEACETYL*FU)/(((CLINTDEACETYL+SAT_CL)*FU)+QH)  ; fraction undergoing
```

```
      first pass extraction to de-acetylrif
      EHUNK=(SAT_CL*FU)/(((SAT_CL+CLINTDEACETYL)*FU)+QH)      ; fraction to other metabolites
      EH=EHDEACETYL+EHUNK                                  ; total fraction metabolised
      FH  = 1 - EH

      ; Metabolite
      SAT_CLM=0
      IF (CHM>0) SAT_CLM=VMAXM/(1+EXP(-(LOG(CHM)-LOGKMM))) / (CHM)

      EHM  = (SAT_CLM*FU)/((SAT_CLM*FU)+QH)
      FHM  = 1 - EHM ;fraction available after 1st pass to go to systemic circulation
      CLHM = EHM * QH ; hepatic clearance

;---------------RATES----------------------------;
    ; Parent
      K20 = (QH*EHUNK/VH)
      K24=(QH*EHDEACETYL/VH)
      K23= (QH*FH/VH)
      K32=(QH/V)

    ; Metabolite
      K40 = (QH*EHM/VH)
      K45 = (QH*FHM/VH)
      K54 = (QH/VMET)

      TEMPO=T-TDOS ; this is time after dose, it should always be >= 0
      KTT=0

      DADT(1)=-KA*A(1)

      IF(PD.GT.0.AND.TEMPO.GT.0) THEN ; This happens only id PD>0, so only if a dose has been
      detected
          KTT=KTR*(TEMPO)
          DADT(1)=EXP(PIZZA+NN*LOG(KTT)-KTT)-KA*A(1)
      ENDIF

      DADT(2) = KA*A(1)-K23*A(2)+K32*A(3)-K24*A(2)-K20*A(2)
      DADT(3) = K23*A(2)-K32*A(3)
      DADT(4) = K24*A(2)*SCALE_MOLES-K40*A(4) - K45*A(4) + K54*A(5)
      DADT(5) = K45*A(4) - K54*A(5)

    ; DADT(6)=A(3)/V
;-------------------------------------------------------------------------------------------------
------

$ERROR




      ; Parent
      IPRED_1 = A(3)/V

      LLOQ_1 = 0.117
      PROP_1 = IPRED_1*THETA(4)
      ADD_1  = THETA(5) + LLOQ_1/5
      LOD_1  = LLOQ_1/10

      ; Metabolite
      IPRED_2 = A(5)/VMET

      LLOQ_2 = 0.0391
      PROP_2 = IPRED_2*THETA(16)
      ADD_2  = THETA(17) + LLOQ_2/5
      LOD_2  = LLOQ_2/10

      ; Weighting
```

```
      W_1 = SQRT((ADD_1)**2 + (PROP_1)**2)    ; Parent
      W_2 = SQRT((ADD_2)**2 + (PROP_2)**2)    ; Metabolite

      ; Correlation
      RHO = THETA(21)


      ; Cholesky decomposition
      ERROR_1 = W_1 * EPS(1)
      ERROR_2 = W_2 * ( RHO*EPS(1) + SQRT(1-RHO**2)*EPS(2) )


      ; Redefine IPRED & weighting
      IPRED = IPRED_1
      W = W_1
      ERROR_TERM = ERROR_1

      IF (DVID==2) THEN
         IPRED = IPRED_2
         W     = W_2
         ERROR_TERM = ERROR_2
      ENDIF

      IF (W.LE.0.000001) W=0.000001

      IRES = DV-IPRED
      IWRES = IRES/W


      Y = IPRED + ERROR_TERM

      ; To prevent simulation (ICALL==4) of negative values. It set a positive lower bound
      for Y, so that VPCs in the log-scale can be plotted
      IF (DVID==1.AND.ICALL==4.AND.Y<=LOD_1) Y=LOD_1/2
      IF (DVID==2.AND.ICALL==4.AND.Y<=LOD_2) Y=LOD_2/2


      ; Retrieve amount in compartments
      AA1=A(1)
      AA2=A(2)
      AA3=A(3)
      AA4=A(4)
      AA5=A(5)

      CONC=AA3/V

      CMAX = COM(1) ; CMAX
      TMAX = COM(2) ; TIME OF CMAX

      ; To calculate TAD
      IF(AMT.GT.0) THEN
         TDOS = TIME
          PD = AMT
          ; Reset CMAX code when a new dose is given (e.g. every day)
          COM(1)=0
          COM(2)=0
      ENDIF


      TAD=TIME-TDOS
      VARBIO=BSVBIO+BOVBIO
      VARAUC=VARBIO-BSVCL-BSVCLUNK
      CLH=QH*FU*(CLINTDEACETYL+CLINTUNK)/(QH+FU*(CLINTDEACETYL+CLINTUNK))
      COVLOTDVID = 10*COVLOT + DVID

     ; RETRIEVE AUC IN COMPARTMENT
      ;AUC0_24=A(5)
;-------------------------------------------------------------------------------;
$THETA  (-1,0.825123,5) ; 1. KM [LOG]
$THETA  (0,52.1068,100) ; 2. TVV  [L]
$THETA  (0,1.26812,10) ; 3. TVKA [1/h]
```

```
$THETA  (0,0.133049,1) ; 4. SIG_PROP
$THETA  0.0234 FIX ; 5. SIG_ADD [mg/L]
$THETA  (0,0.522564,1) ; 6. MTT[h]
$THETA  (-1,1.341,5) ; 7. LOG [NN]
$THETA  (-1,-0.627477,1) ; 8. LOT-BIO
$THETA  (1,1.6381,5) ; 9. OCC1BOV
$THETA  1 FIX ; 10. VH
$THETA  50 FIX ; 11. PLASMA FLOW
$THETA  0.2 FIX ; 12. FRACTION_UNBOUND
$THETA  0 FIX ; 13. ARM3_BIO
$THETA  (0,422.678) ; 14. TVCLMET [L/h]
$THETA  0 FIX ; 15. ETA_ADJUSTVMET
$THETA  (0,0.187074,1) ; 16. SIG_PROP_MET
$THETA  0 FIX ; 17. SIG_ADD_MET [mg/L]
$THETA  (0,36.7237,200) ; 18. TVCL [L/h]
$THETA  (0,149.336,200) ; 19. CLUNK
$THETA  (-1,0.481698,5) ; 20. KMM [LOG]
$THETA  (-1.001,0.783376,1.0001) ; 21. RHO
;-------------------------------------------------------------------------;
$OMEGA  BLOCK(2)
 0.444265  ; 1. BSV_CLUNK
 0.0900071 0.0583506  ; 2. BSV_CLMET
$OMEGA  BLOCK(2)
 0.455427  ;  3. BSV_Ka
 0 0.537783  ; 4. BSV_MTT
$OMEGA  0  FIX  ; 5. BSV_BIO
$OMEGA  BLOCK(1)
 0.0543284  ;  6 BOV_BIO
$OMEGA  BLOCK(1) SAME
$OMEGA  0  FIX  ;  8. BSV_Vd
$OMEGA  0.0439974  ;  9. BSV_CL
$SIGMA  1  FIX  ; RESIDUAL_1
$SIGMA  1  FIX  ; RESIDUAL_2
;-------------------------------------------------------------------------;
$ESTIMATION MAXEVAL=9999 SIGL=10 ATOL=9 METHOD=1 INTER PRINT=1 NOABORT
            NSIG=3 NONINFETA=1 ETASTYPE=1 CTYPE=4 MCETA=20
            RANMETHOD=4P
$COVARIANCE PRINT=E MATRIX=S ATOL=9 UNCONDITIONAL
$TABLE      WRESCHOL FILE=sdtab3007c.csv FORMAT=, ID OCC VPCTIME TIME
            TAD DV EVID AMT MDV IPRED PRED IWRES WRES CWRESI CWRES
            CPREDI CIPREDI OBJI BSVCL BSVKA BSVV BSVBIO BSVMTT BOVBIO
            BSVCLMET BSVCLUNK VARAUC VARBIO NOPRINT NOAPPEND ONEHEADER
$TABLE      FILE=patab3007c.csv FORMAT=, ID CL V KA BIO MTT NN VH QH
            FU KTR ADD_1 ADD_2 PROP_1 PROP_2 CLMET V5 NOPRINT NOAPPEND
            ONEHEADER
$TABLE      FILE=cotab3007c.csv FORMAT=, ID WEIGHTPK HEIGHT FFM
            PK04_HEMOGLO PK04_WHITECELL PK04_PLAQ PK04_NEUTRO
            PK04_CREAT PK04_ASAT PK04_PHOSPHATE PK04_ALAT PK04_BILIR
            PK04_GGT SEL_CD4COUNT SEL_VLOAD AGE CLH NOPRINT NOAPPEND
            ONEHEADER
$TABLE      FILE=catab3007c.csv FORMAT=, ID SEX ARM FDCBATCH SDBATCH
            SITE1BENIN BLQ BATCH DVGROUP NOPRINT NOAPPEND ONEHEADER
$TABLE      FILE=mytab3007c.csv FORMAT=, ID OCC TIME TAD DV EVID DVID
            AMT MDV AA1 AA2 AA3 AA4 CONC IPRED PRED IWRES WRES CPREDI
            CIPREDI CWRES CWRESI CIWRESI OBJI CL V KA BIO MTT NN CLMET
            V5 VH QH FU KTR TVCL TVV TVKA TVMTT TVNN TVCLMET BSVCL
            BSVV BSVBIO BSVMTT BSVKA BOVBIO BSVCLMET BSVCLUNK VARAUC
            VARBIO FFM VPCTIME ARM NTAB NTAB_RIF SEX HEIGHT WEIGHTPK
            AGE FDCBATCH SDBATCH PK04_HEMOGLO PK04_WHITECELL PK04_PLAQ
            PK04_NEUTRO PK04_CREAT PK04_ASAT PK04_PHOSPHATE PK04_ALAT
            PK04_BILIR PK04_GGT SEL_CD4COUNT SEL_VLOAD COVLOT CLH
            BATCH DVGROUP CMAX TMAX SAT_CL VMAX DVIDSITE SHAREETA PROB
            NOPRINT NOAPPEND ONEHEADER
```

Final NONMEM scripts for results presented in section 6.1.2

```
$SIZES      MAXFCN=100000000 PD=-1000 LVR=-150 LTH=-200
$PROBLEM    PZA-RAFA
$ABBREVIATED COMRES=2
$INPUT      ID SAMPLENO OCC TIME AMT MDV EVID DV ADDL II BLQ SITE1BENIN BATCH DEFROST1YES
            ARM NTAB RIFTABS NC_WEIGHT INC_ARM VPCTIME FDCBATCH SDBATCH
            PK04_MISSTBTREAT PK04_MISSTBDAYS PK04_WEIGHT PK04_HEMOGLO PK04_WHITECELL
            PK04_PLAQ PK04_NEUTRO PK04_CREAT PK04_ASAT PK04_PHOSPHATE PK04_ALAT PK04_BILIR
            PK04_GGT SEL_SEX SEL_HEIGHT SEL_WEIGHT SEL_CD4COUNT SEL_VLOAD AGE PROB
            PROB_DESC=DROP
$DATA      PZA-RAFA28-11-2017.csv IGNORE=# IGNORE=(PROB.GT.0)

$SUBROUTINE ADVAN13 TRANS1 TOL=9
$MODEL      NCOMPARTMENTS=3 COMP=(ABS DEFDOSE) COMP=(CENTRAL)
            COMP=(AUC)
;------------------------------------------------------------------------------;
$PK

MXSTEP=50000
;------------------------------------------------------------------------------;
     OCC1=0
     OCC2=0

     ; Create indicator variables for occasion
     IF(OCC.EQ.1) OCC1=1
     IF(OCC.EQ.2) OCC2=1

     ;ALLOMETRIC SCALING FFM & WEIGHT
     SEX = SEL_SEX
     HEIGHT = SEL_HEIGHT/100  ; HEIGHT IN METRES

      ;----Fat Free Mass
      IF (SEX.EQ.2) THEN  ; female
          WHSMAX=37.99
          WHS50=35.98
       ELSE        ;males
          WHSMAX=42.92
          WHS50=30.93
     ENDIF

     WEIGHTPK=WEIGHT
     IF (WEIGHT==-999) WEIGHTPK=PK04_WEIGHT

     HEIGHT2 = HEIGHT**2    ; IMPORTANT: HEIGHT is used in meters!!!
     FFM = (WHSMAX*HEIGHT2*WEIGHTPK)/(WHS50*HEIGHT2+WEIGHTPK)

     WTSTD=52  ; STANDARD WEIGHT
     FFMSTD=43.34 ; STANDARD FFM

     ALLOM_CL=(FFM/FFMSTD)**0.75
     ALLOM_V =(FFM/FFMSTD)

     ;ALLOM_CL=(WEIGHTPK/WTSTD)**0.75
     ;ALLOM_V =(WEIGHTPK/WTSTD)
;------------------------------------------------------------------------------;
     ;COVARIATES
     COVLOT56=0
     IF(FDCBATCH==5) COVLOT56=1  ; ERC6202A
     IF(FDCBATCH==6) COVLOT56=1  ; ERC6203A

     COVLOT56_BIO=1+THETA(8)*COVLOT56

     ;;; CLSITE1BENIN-DEFINITION START
     IF(SITE1BENIN.EQ.1) CLSITE1BENIN = 1  ; Most common
     IF(SITE1BENIN.EQ.2) CLSITE1BENIN = ( 1 + THETA(9))
     ;;; CLSITE1BENIN-DEFINITION END

     COVSITE1BENIN_CL=CLSITE1BENIN

     ;CREATININE CLEARANCE - COCKCROFT AND GAULT

     SCR= PK04_CREAT  ; SERUM CREATININE mm3/L

     CRCL_MLMIN=100  ; CREATININE CLEARANCE [ML/MIN]
```

```
      IF(SEX==1) CRCL_MLMIN=1.23*(140-AGE)*WEIGHTPK/SCR  ; MALES
      IF(SEX==2) CRCL_MLMIN=1.04*(140-AGE)*WEIGHTPK/SCR  ; FEMALES

      CRCL=CRCL_MLMIN*0.06*WTSTD/WEIGHTPK   ;[L/h] - WEIGHT-EFFECT
      CRCL_STD=4.53

;-------------------------------------------------------------------------;
      TVCL=THETA(1)*COVSITE1BENIN_CL*ALLOM_CL        ; TVCL
      TVV =THETA(2)*ALLOM_V          ; TVV
      ;TVKA =THETA(3)          ; TVKA
      TVBIO     = THETA(7)*COVLOT56_BIO       ; TVBIO
      TVMTT=THETA(5)          ; TVMTT
      TVNN=THETA(6)           ; TVNN

      BSVCL=ETA(1)
      BSVV=ETA(3)
      ;BSVKA=ETA(3)
      BSVBIO=ETA(2)
      BSVMTT=ETA(4)

      BOVBIO=ETA(5)
      IF(OCC==2) BOVBIO=ETA(6)
 ;-------------------------------------------------------------------------;

      CL=TVCL*EXP(BSVCL)
      V =TVV*EXP(BSVV)
      BIO = TVBIO*EXP(BSVBIO+BOVBIO)
      MTT=TVMTT*EXP(BSVMTT)

      NN=TVNN
      K=CL/V

;-------------------------TRANSIT-------------------------------------------------;
      F1=0 ; I need to set bioavailability in compartment 1 to 0

      KTR = (NN+1)/MTT

      KA=KTR

      IF (NEWIND/=2.OR.EVID>=3) THEN ; new individual, or reset event
          ; The values read here will be stored in TDOS and PD in this very PK call.
          TNXD=TIME ; Time of the dose
          PNXD=AMT ; Amount. If it's zero, the DE is deactivated.
      ENDIF

      TDOS=TNXD ; This will either save here the temporary values if it's a new individual...
      PD=PNXD ; ...or the values which were read one record ahead during the execution of the
      previous record.

      IF(AMT.GT.0) THEN ; This reads one record ahead and stores the data to be used when
      running the following record
      ; IF(AMT.GT.0.AND.ALAG1.EQ.0) THEN ; Use this instead if there is ALAG, as it will also
      checks if the ALAG is not 0
          TNXD=TIME
          PNXD=AMT
      ENDIF

      ; Uncomment this if you have ALAG or if you use ADDL
      IF (DOSTIM.GT.0) THEN ; This will account for the ADDL or lagged doses. It will
      overwrite the time, if it a non-event record
          TNXD=DOSTIM
          PNXD=AMT
      ENDIF

      PIZZA=LOG(BIO*PD*KTR+0.00001)-GAMLN(NN+1) ; without +0.00001, it won't work with ETAs
      in bioavailability :NM73 version

      ; RESET code for CMAX
      IF (NEWIND.NE.2.OR.EVID.GE.3) THEN ; Each time I have a new subject, or a reset
         COM(1)=0
         COM(2)=0
         TDOS = 0
```

```
      ENDIF

      S2=V

      ; INITIALIZE
      A_0(1)=0.000001
      A_0(2)=0.000001
      A_0(3)=0.000001

$DES

      CP=A(2)/V

       IF (CP.GE.COM(1)) THEN
         COM(1) = CP              ; CMAX
         COM(2) = T - TDOS        ; TIME OF CMAX
      ENDIF

      TEMPO=T-TDOS ; this is time after dose, it should always be >= 0
      KTT=0

      DADT(1)=0

      IF(PD.GT.0.AND.TEMPO.GT.0) THEN ; This happens only id PD>0, so only if a dose has been
      detected
          KTT=KTR*(TEMPO)
          DADT(1)=EXP(PIZZA+NN*LOG(KTT)-KTT)-KA*A(1)
      ENDIF

      DADT(2)=KA*A(1)-K*A(2)
      DADT(3)= CP
;-------------------------------------------------------------------------------------------------
------

$ERROR
      IPRED=A(2)/V

      LLOQ=0.02
      IMPUTED_BLQ=LLOQ/2
      ADD_LLOQ=LLOQ/5

      PROP=IPRED*THETA(3)
      ADD=THETA(4)

      W = SQRT(ADD**2+PROP**2)

      ; Protective code
      IF (W.LE.0.000001) W=0.000001

      IRES=DV-IPRED
      IWRES=IRES/W

      Y = IPRED + W*ERR(1)

      ; For simulation, like in case of VPC
      IF (ICALL==4.AND.Y<=LLOQ) THEN
         Y=IMPUTED_BLQ ; All BLQ values in simulation get imputed to LLOQ/2. This also
         prevents negative values
      ENDIF

      ; Retrieve amount in compartments
      AA1=A(1)
      AA2=A(2)
      AUC=A(3)

      CMAX = COM(1) ; CMAX
      TMAX = COM(2) ; TIME OF CMAX

      ; To calculate TAD
      IF(AMT.GT.0) THEN
         TDOS = TIME
          PD = AMT
          ; Reset CMAX code when a new dose is given (e.g. every day)
```

```
      COM(1)=0
      COM(2)=0
   ENDIF


   TAD=TIME-TDOS
   VARBIO=BSVBIO+BOVBIO
   VARAUC=VARBIO-BSVCL
;------------------------------------------------------------------------;
$THETA  (0,3.6509,10) ; 1. TVCL [L/h]
$THETA  (0,35.0166,100) ; 2. TVV  [L]
$THETA  (0,0.108421,1) ; 3. SIG_PROP
$THETA  (0,0.959654,10) ; 4. SIG_ADD [mg/L]
$THETA  (0,0.357306,1) ; 5. MTT[h]
$THETA  1 FIX ; 6. NN
$THETA  1 FIX ; 7. TVBIO
$THETA  (-1,-0.199157,1) ; 8. LOT_BIO
$THETA  (-1,-0.144346,1) ; 9. CLSITE1BENIN1
;------------------------------------------------------------------------;
$OMEGA  0.0711183  ;  1. BSV_CL
$OMEGA  0.0130751  ; 2. BSV_BIO
$OMEGA  0  FIX  ;  3. BSV_Vd
$OMEGA  0.366585  ; 4. BSV_MTT
$OMEGA  BLOCK(1)  0.0126757  ;  5. BOVBIO
$OMEGA  BLOCK(1) SAME
$SIGMA  1  FIX  ;   RESIDUAL
;------------------------------------------------------------------------;
$ESTIMATION MAXEVAL=9999 MSFO=run102.msf SIGL=10 ATOL=9 METHOD=1 INTER
            PRINT=1 NOABORT NSIG=3 NONINFETA=1 ETASTYPE=1 MCETA=50
            RANMETHOD=4P
$COVARIANCE PRINT=E MATRIX=S ATOL=6
$TABLE      FILE=mytab102.csv FORMAT=, ID OCC TIME TAD DV EVID AMT MDV
            AA1 AA2 IPRED PRED IWRES WRES CWRESI CWRES CPREDI CIPREDI
            OBJI CL V KA BIO MTT NN TVCL TVV TVMTT TVNN TVBIO BSVCL
            BSVV BSVBIO BSVMTT BOVBIO VARAUC SEX WEIGHTPK HEIGHT FFM
            VPCTIME ARM FDCBATCH SDBATCH PK04_HEMOGLO PK04_WHITECELL
            PK04_PLAQ PK04_NEUTRO PK04_CREAT PK04_ASAT PK04_PHOSPHATE
            PK04_ALAT PK04_BILIR PK04_GGT SEL_CD4COUNT SEL_VLOAD
            COVLOT56 AGE CRCL CMAX TMAX AUC NOPRINT NOAPPEND ONEHEADER
```

Final NONMEM scripts for results presented in section 6.1.3

```
$SIZES      MAXFCN=100000000 PD=-1000 LVR=-150 LTH=-200
$PROBLEM    EMB-RAFA
$ABBREVIATED COMRES=2
$INPUT      ID SAMPLENO OCC TIME AMT MDV EVID DV ADDL II BLQ SITE1BENIN BATCH DEFROST1YES
ARM NTAB
            WEIGHT VOMIT1Y RIFTABS INC_WEIGHT INC_ARM VPCTIME FDCBATCH SDBATCH
            PK04_MISSTBTREAT
            PK04_MISSTBDAYS PK04_WEIGHT PK04_HEMOGLO PK04_WHITECELL PK04_PLAQ PK04_NEUTRO
            PK04_CREAT
            PK04_ASAT PK04_PHOSPHATE PK04_ALAT PK04_BILIR PK04_GGT SEL_SEX SEL_HEIGHT
            SEL_WEIGHT
            SEL_CD4COUNT SEL_VLOAD AGE PROB
$DATA      EMB-RAFA02-05-2016.csv IGNORE=#
$SUBROUTINE ADVAN13 TRANS1 TOL=9
$MODEL      NCOMPARTMENTS=3 COMP=(ABS DEFDOSE) COMP=(CENTRAL)
            COMP=(PERI) ;COMP=(AUC)
;------------------------------------------------------------------------------;
$PK
MXSTEP=50000
;------------------------------------------------------------------------------;
     OCC1=0
     OCC2=0

     ; Create indicator variables for occasion
     IF(OCC.EQ.1) OCC1=1
     IF(OCC.EQ.2) OCC2=1

     ;ALLOMETRIC SCALING_FFM & WEIGHT
     SEX = SEL_SEX
     HEIGHT = SEL_HEIGHT/100  ; HEIGHT IN METRES

      ;----Fat Free Mass
      IF (SEX.EQ.2) THEN  ; female
          WHSMAX=37.99
          WHS50=35.98
          LBW1=1.07    ; CONSTANT TO MULTIPLY WITH WEIGHT
          LBW2=148     ; CONSTANT TO MULTIPLY WITH WEIGHT*WEIGHT
      ELSE        ;males
          WHSMAX=42.92
          WHS50=30.93
          LBW1=1.10    ; CONSTANT TO MULTIPLY WITH WEIGHT
          LBW2=128     ; CONSTANT TO MULTIPLY WITH WEIGHT*WEIGHT
     ENDIF

     WEIGHTPK=WEIGHT
     IF (WEIGHT==-999) WEIGHTPK=PK04_WEIGHT

     HEIGHT2 = HEIGHT**2    ; IMPORTANT: HEIGHT is used in meters!!!
     FFM = (WHSMAX*HEIGHT2*WEIGHTPK)/(WHS50*HEIGHT2+WEIGHTPK)
     LBW =  LBW1*WEIGHTPK - LBW2*WEIGHTPK*WEIGHTPK/((100*HEIGHT)**2)

     WTSTD=52  ; STANDARD WEIGHT
     FFMSTD=43.34 ; STANDARD FFM
     LBWSTD=43.99  ; STANDARD LBW

     ;ALLOMF_CL=(FFM/FFMSTD)**0.75
     ;ALLOMF_V =(FFM/FFMSTD)

     ALLOM_CL=(WEIGHTPK/WTSTD)**0.75
     ALLOM_V =(WEIGHTPK/WTSTD)
;------------------------------------------------------------------------------;
     ;COVARIATES
     COVLOT=0
     IF(FDCBATCH==5) COVLOT=1
     IF(FDCBATCH==6) COVLOT=1

     COVLOT_BIO=1+THETA(11)*COVLOT

     ;CREATININE CLEARANCE - COCKCROFT AND GAULT

     SCR= PK04_CREAT  ; SERUM CREATININE mm3/L

     ;CRCL_MLMIN=100  ; CREATININE CLEARANCE [ML/MIN]
```

```
      IF(SEX==1) CRCLN=1.23*(140-AGE)*WEIGHTPK/SCR  ; MALES
      IF(SEX==2) CRCLN=1.04*(140-AGE)*WEIGHTPK/SCR  ; FEMALES

      ;CRCL=CRCL_MLMIN*0.06*WTSTD/WEIGHTPK   ;[L/h] - WEIGHT-EFFECT
      CRCLN_STD=75.55  ; ML/MIN

      ; CREATININE CLEARANCE BASED ON LEAN BODY WEIGHT- JAMES
      CRCLJ= ((140-AGE)*LBW)/SCR

      ;COVCRCL_CL=1+THETA(13)*(CRCLN-CRCL_STD)

      ; ARM_BIO
      ARM2_BIO=0
      ARM3_BIO=0

      IF(ARM==2) ARM2_BIO=1
      IF(ARM==3) ARM3_BIO=1

      COVARM3_BIO=1+THETA(12)*ARM3_BIO

      ;;; CLSITE1BENIN-DEFINITION START
      IF(SITE1BENIN.EQ.1) CLSITE1BENIN = 1  ; Most common
      IF(SITE1BENIN.EQ.2) CLSITE1BENIN = ( 1 + THETA(14))
      ;;; CLSITE1BENIN-DEFINITION END

      COVSITE1BENIN_CL=CLSITE1BENIN

      ;;; MTTSITE1BENIN-DEFINITION START
       IF(SITE1BENIN.EQ.1) MTTSITE1BENIN = 1  ; Most common
       IF(SITE1BENIN.EQ.2) MTTSITE1BENIN = ( 1 + THETA(15))
      ;;; MTTSITE1BENIN-DEFINITION END

      ;;; MTT-RELATION START
      COVSITE1BENIN_MTT=MTTSITE1BENIN
      ;;; MTT-RELATION END
;-------------------------------------------------------------------------;
      TVCLNR=THETA(1)*COVSITE1BENIN_CL*ALLOM_CL         ; NON-GFR CLEARANCE
      TVCLR=THETA(13)*COVSITE1BENIN_CL*(CRCLN/CRCLN_STD); GFR CLEARANCE USING WEIGHT IN C-G
      FORMULA
      TVCL= TVCLNR + TVCLR
      TVV2  =THETA(2)*ALLOM_V          ; VOLUME-CENT
      TVKA =THETA(3)/COVSITE1BENIN_MTT         ; Pop KA
      TVBIO=THETA(10)*COVLOT_BIO*COVARM3_BIO              ; BIO
      TVMTT=THETA(6)*COVSITE1BENIN_MTT         ; MTT
      TVNN=THETA(7)          ; NN
      TVQ=THETA(8)*ALLOM_CL           ; INTERCOMPARTMENTAL CLEARANCE
      TVV3=THETA(9)*ALLOM_V           ; VOLUME-PERI

      BSVCL=ETA(1)
      BSVV=ETA(2)
      BSVKA=ETA(3)
      BSVBIO=ETA(4)
      BSVMTT=ETA(5)


      BOVBIO=ETA(6)
      IF(OCC==1) BOVBIO=ETA(7)

;-------------------------------------------------------------------------;
      CL=TVCL*EXP(BSVCL)
      V2 =TVV2*EXP(BSVV)
      KA=TVKA*EXP(BSVKA)
      BIO=TVBIO*EXP(BSVBIO+BOVBIO)
      MTT=TVMTT*EXP(BSVMTT)
      NN=TVNN
      Q     = TVQ
      V3    = TVV3
      K     = CL/V2
      K23   = Q/V2
      K32   = Q/V3
      SC    = V2
```

```
;--------------TRANSIT----------------------------------------------------;
      ; Transit
      F1=0 ; I need to set bioavailability in compartment 1 to 0

      KTR = (NN+1)/MTT

      IF (NEWIND/=2.OR.EVID>=3) THEN ; new individual, or reset event
          ; The values read here will be stored in TDOS and PD in this very PK call.
          TNXD=TIME ; Time of the dose
          PNXD=AMT ; Amount. If it's zero, the DE is deactivated.
      ENDIF

      TDOS=TNXD ; This will either save here the temporary values if it's a new individual...
      PD=PNXD ; ...or the values which were read one record ahead during the execution of the
      previous record.

      IF(AMT.GT.0) THEN ; This reads one record ahead and stores the data to be used when
      running the following record
      ; IF(AMT.GT.0.AND.ALAG1.EQ.0) THEN ; Use this instead if there is ALAG, as it will also
      checks if the ALAG is not 0
          TNXD=TIME
          PNXD=AMT
      ENDIF

      ; Uncomment this if you have ALAG or if you use ADDL
      IF (DOSTIM.GT.0) THEN ; This will account for the ADDL or lagged doses. It will
      overwrite the time, if it a non-event record
          TNXD=DOSTIM
          PNXD=AMT
      ENDIF

      PIZZA=LOG(BIO*PD*KTR+0.00001)-GAMLN(NN+1) ; without +0.00001, it won't work with ETAs
      in bioavailability :NM73 version

      ; RESET code for CMAX
      IF (NEWIND.NE.2.OR.EVID.GE.3) THEN ; Each time I have a new subject, or a reset
          COM(1)=0
          COM(2)=0
          TDOS = 0
      ENDIF

      A_0(1)=0.00001
      A_0(2)=0.00001
      A_0(3)=0.00001
      ;A_0(4)=0.00001

$DES
      CP = A(2)/V2    ; plasma concentration

      IF (CP.GE.COM(1)) THEN
         COM(1) = CP              ; CMAX
         COM(2) = T - TDOS        ; TIME OF CMAX
      ENDIF

      TEMPO=T-TDOS ; this is time after dose, it should always be >= 0
      KTT=0

      DADT(1)=0

      IF(PD.GT.0.AND.TEMPO.GT.0) THEN ; This happens only id PD>0, so only if a dose has been
      detected
          KTT=KTR*(TEMPO)
          DADT(1)=EXP(PIZZA+NN*LOG(KTT)-KTT)-KA*A(1)
      ENDIF

      DADT(2) = KA*A(1) - K*A(2) - K23*A(2) + K32*A(3)
      DADT(3) = K23*A(2) - K32*A(3)
      ;DADT(4)=CP

;-------------------------------------------------------------------------------------------------
------
$ERROR
```

```
      IPRED=A(2)/V2

      LLOQ=0.0844
      IMPUTED_BLQ=LLOQ/2

      LLOQNEW=0.00717 ; LOWEST CONC FROM RELEASED BLQ DATA

      PROP=IPRED*THETA(4)
      ADD=THETA(5) + LLOQ/5

      W = SQRT(ADD**2+PROP**2)

      ; Protective code
      IF (W.LE.0.000001) W=0.000001

      IRES=DV-IPRED
      IWRES=IRES/W

      Y = IPRED + W*ERR(1)

      ; For simulation, like in case of VPC
      IF (ICALL==4.AND.Y<=LLOQNEW) THEN
         Y=LLOQNEW/2 ; All BLQ values in simulation get imputed to LLOQ/2. This also prevents
         negative values
      ENDIF

      ; Retrieve amount in compartments
      AA1=A(1)
      AA2=A(2)
      AA3=A(3)

      CMAX = COM(1) ; CMAX
      TMAX = COM(2) ; TIME OF CMAX

      ; To calculate TAD
      IF(AMT.GT.0) THEN
         TDOS = TIME
          PD = AMT
          ; Reset CMAX code when a new dose is given (e.g. every day)
          COM(1)=0
          COM(2)=0
      ENDIF

      TAD=TIME-TDOS
      BSVVARBIO=BSVBIO+BOVBIO
      BSVVARAUC=BSVVARBIO-BSVCL
      ;AUC=A(4)
;-------------------------------------------------------------------------------;
$THETA  (0,43.1567,100) ; 1. TVCLNR [L/h]
$THETA  (0,226.171,500) ; 2. TVV2  [L]
$THETA  (0,1.5367,10) ; 3. TVKA [1/h]
$THETA  (0,0.13621,1) ; 4. SIG_PROP
$THETA  (0,0.021491,10) ; 5. SIG_ADD [mg/L]
$THETA  (0,1.25061) ; 6. MTT[h]
$THETA  (0,17.0827,50) ; 7. NN
$THETA  (0,47.4921) ; 8.  Q[L/h]
$THETA  (0,412.726) ; 9. V3 [L]
$THETA  1 FIX ; 10. TVBIO
$THETA  (-1,-0.1732,1) ; 11. LOT_ERC6202A-BIO
$THETA  0 FIX ; 12. ARM3-BIO
$THETA  (0,10.6734,100) ; 13. TVCLR
$THETA  (-1,-0.130085,5) ; 14. CLSITE1BENIN1
$THETA  0 FIX ; 15. MTTSITE1BENIN1
;-------------------------------------------------------------------------------;
$OMEGA  0.0176991  ;  1. BSV_CL
$OMEGA  0  FIX  ;  2. BSV_Vd
$OMEGA  0.711355  ;  3. BSV_Ka
$OMEGA  0.057299  ; 4. BSV_BIO
$OMEGA  0.05799  ; 5. BSV_MTT
$OMEGA  BLOCK(1)  0.0217234  ; 6. BOV_BIO
$OMEGA  BLOCK(1) SAME
$SIGMA  1  FIX  ;   RESIDUAL
;-------------------------------------------------------------------------------;
```

```
$ESTIMATION MAXEVAL=9999 MSFO=run1000.msf SIGL=10 ATOL=9 METHOD=1
            INTER PRINT=1 NOABORT NSIG=3 NONINFETA=1 ETASTYPE=1
$COVARIANCE PRINT=E MATRIX=S UNCONDITIONAL ATOL=6
$TABLE      WRESCHOL FILE=sdtab1000.csv FORMAT=, ID OCC VPCTIME TIME
            TAD DV EVID AMT MDV IPRED PRED IWRES WRES CWRESI CWRES
            CPREDI CIPREDI OBJI BSVCL BSVV BSVKA BSVBIO BSVMTT BOVBIO
            BSVVARBIO BSVVARAUC NOPRINT NOAPPEND ONEHEADER
$TABLE      FILE=patab1000.csv FORMAT=, ID CL V2 V3 Q KA BIO MTT NN
            ADD PROP NOPRINT NOAPPEND ONEHEADER
$TABLE      FILE=cotab1000.csv FORMAT=, ID WEIGHTPK HEIGHT FFM
            PK04_HEMOGLO PK04_WHITECELL PK04_PLAQ PK04_NEUTRO
            PK04_CREAT PK04_ASAT AGE CRCLN PK04_PHOSPHATE PK04_ALAT
            PK04_BILIR PK04_GGT SEL_CD4COUNT SEL_VLOAD CRCLJ LBW
            NOPRINT NOAPPEND ONEHEADER
$TABLE      FILE=catab1000.csv FORMAT=, ID ARM SEX COVLOT SITE1BENIN
            BLQ NTAB FDCBATCH NOPRINT NOAPPEND ONEHEADER
$TABLE      FILE=mytab1000.csv FORMAT=, ID OCC TIME TAD DV EVID AMT
            MDV AA1 AA2 IPRED PRED IWRES WRES CWRESI CWRES CPREDI
            CIPREDI OBJI CL V2 V3 Q KA BIO MTT NN TVCL TVV2 TVKA TVMTT
            TVNN TVQ TVV3 BSVCL BSVV BSVKA BSVBIO BSVMTT BOVBIO
            BSVVARBIO BSVVARAUC ARM SEX WEIGHTPK HEIGHT FFM AGE
            VPCTIME FDCBATCH SDBATCH PK04_HEMOGLO PK04_WHITECELL
            PK04_PLAQ PK04_NEUTRO PK04_CREAT PK04_ASAT PK04_PHOSPHATE
            PK04_ALAT PK04_BILIR PK04_GGT SEL_CD4COUNT SEL_VLOAD
            COVLOT CRCLN BLQ CRCLJ LBW CMAX TMAX NOPRINT NOAPPEND
            ONEHEADER
```

Appendix 2: Approval to include publications in the thesis

Subject: Permission to include papers in her PhD Thesis: Mr MT Chirehwa CHRMAX003
From: DOCTORAL DEGREES BOARD <ddb@uct.ac.za>
Date: 2017/11/07 10:15 AM
To: Maxwell Chirehwa <CHRMAX003@myuct.ac.za>, "mtchirehwa@gmail.com" <mtchirehwa@gmail.com>
CC: Adri Winckler <adri.winckler@uct.ac.za>, Mike Lambert <mike.lambert@uct.ac.za>, Paolo Denti <paolo.denti@uct.ac.za>

Dear Mr Chirehwa

I hereby confirm that the Chair of the Doctoral Degrees Board, Professor Phakeng, has **approved** your request to include the two specified publications in your PhD thesis.

In your thesis (after your declaration that it is your own work) please include the following separate signed statement listing the publications that you were given permission to include:
"I confirm that I have been granted permission by the University of Cape Town's Doctoral Degrees Board to include the following publication(s) in my PhD thesis, and where co-authorships are involved, my co-authors have agreed that I may include the publication(s): "

This statement notifies examiners of the publications that you have been granted permission to include.

Kind regards

JANINE ISAACS
DOCTORAL DEGREES BOARD OFFICE
Doctoral Degrees Board Officer
Room 3.04, Masingene Building, Cross Campus Road, Middle Campus
Rondebosch, Cape Town, SOUTH AFRICA , 7700
Email: janine.isaacs@uct.ac.za
Telephone: +27 (0)21 650 2202

Attachments:

Declaration - Inclusion of publications.docx 21.7 KB

Appendix 3: Approval for reprint

Subject: ID: 246169 Permission authorization for WHO copyrighted material
From: <permissions@who.int>
Date: 2017/12/28 1:02 PM
To: <chrmax003@myuct.ac.za>
CC: <permissions@who.int>

Dear Mr Chirehwa

Thank you for your request for permission to reproduce, reprint or translate certain WHO copyrighted material.

On behalf of the World Health Organization, we are pleased to authorize your request to reproduce the WHO materials as detailed in the form below, subject to the terms and conditions of the non-exclusive licence below.

If you have questions regarding this authorization, please contact permissions@who.int.

We thank you for your interest in WHO published materials.

Kind regards,
WHO Permissions team

WORLD HEALTH ORGANIZATION (WHO)

Non-exclusive licence to use selected WHO published materials

You submitted a request, through WHO's online platform, for permission to reprint and reproduce certain WHO copyrighted material (the "Licensed Materials"). This is a legal agreement (the "Agreement") between you and WHO, granting you a licence to use the Licensed Materials subject to the terms and conditions herein.

Read this Agreement in its entirety before using the Licensed Materials.

By using the Licensed Materials, you enter into, and agree to be bound by, this Agreement.

This licence is granted only for original materials belonging to WHO. If any part of the WHO published materials you wish to reproduce are credited by WHO to a source other than WHO, those materials are not covered by this Agreement and are not part of the Licensed Materials. You are responsible for determining if this is the case, and if so, you are responsible for obtaining

any necessary permission from the source of those third-party materials prior to their use.

If you enter into this Agreement on behalf of an organization, by using the Licensed Materials you confirm (represent and warrant) that you are authorized by your organization to enter into this Agreement on the organization's behalf. In such a case, the terms "you" and "your" in this Agreement refer to, and this Agreement applies to, the organization.

WHO grants this licence to you based on the representations and warranties you made in the licence request you submitted through WHO's online platform. If any of those representations and/or warranties are or become false or inaccurate, this licence agreement shall automatically terminate with immediate effect, without prejudice to any other remedies which WHO may have.

If you have questions regarding this Agreement, please contact permissions@who.int.

1. Licence. Subject to the terms and Conditions of this Agreement, WHO grants to you a worldwide, royalty free, non-transferable, non-sublicensable, non-exclusive licence to use, reproduce, publish, and display the Licensed Materials in the manner and using the media indicated in the Permissions Request Form you submitted to WHO (the "Licensed Use"). This licence is limited to the current edition of your publication. Future editions or a different use of the Licensed Materials will require additional permission from WHO. If your request includes translation into different languages, then non-exclusive permission is hereby granted to translate the Licensed Materials into the languages indicated.

2. Retained Rights. Copyright in the Licensed Materials remains vested in WHO, and WHO retains all rights not specifically granted under this Agreement.

3. Mandatory Acknowledgement. In every instance of the Licensed Use, you must make suitable acknowledgement of WHO, either as a footnote or in a reference list at the end of your publication, as follows:

> "Reprinted from Publication title, Vol /edition number, Author(s), Title of article / title of chapter, Pages No., Copyright (Year)."

In addition, If the Licensed Materials originate from the WHO web site, you must also include the URL reference and the date accessed.

Translations of the Licensed Materials should be attributed as follows:

> "Translated with permission of the publisher from Publication title, Vol /edition number, Author(s), Title of article / title of chapter, Pages No., Year."

4. Altering or Modifying the Licensed Materials. As part of the Licensed Use, you may minimally alter or adapt figures and tables in the Licensed Materials to match the style of your publication. Any other alteration or modification of the Licensed Materials (including abbreviations, additions, or deletions) may be made only with the prior written authorization of WHO.

5. Appropriate and Prohibited Uses. You must use the Licensed Materials in a factual and appropriate context. You may not use the Licensed Materials in association with any product marketing, promotional, or commercial activities, including, without limitation, in advertisements, product brochures, company-sponsored web sites, annual reports, or other non-educational publications or distributions.

6. No WHO endorsement. You shall not state or imply that WHO endorses or is affiliated with your publication or the Licensed Use, or that WHO endorses any entity, organization, company, or product.

7. No use of the WHO logo. In no case shall you use the WHO name or emblem, or any abbreviation thereof. Notwithstanding the foregoing, if the WHO name and/or emblem appear as an integral part of the Licensed Materials (e.g. on a map) you may use the name and/or emblem in your use of the License Materials, provided the name and/or logo is not used separately from the Licensed Materials.

8. No Warranties by WHO. All reasonable precautions have been taken by WHO to verify the information contained in the Licensed Materials. However, WHO provides the Licensed Materials to you without warranty of any kind, either expressed or implied, and you are entirely responsible for your use of the Licensed Materials. In no event shall WHO be liable for damages arising from your use of the Licensed Materials.

9. Your Indemnification of WHO. You agree to indemnify WHO for, and hold WHO harmless against, any claim for damages, losses, and/or any costs, including attorneys' fees, arising in any manner whatsoever from your use of the Licensed Materials or for your breach of any of the terms of this Agreement.

10. Termination. The licence and the rights granted under this Agreement shall terminate automatically upon any breach by you of the terms of this Agreement. Further, WHO may terminate this licence at any time with immediate effect for any reason by written notice to you.

11. Entire Agreement, Amendment. This Agreement is the entire agreement between you and WHO with respect to its subject matter. WHO is not bound by any additional terms that may appear in any communication from you. This Agreement may only be amended by mutual written agreement of you and WHO.

12. Headings. Paragraph headings in this Agreement are for reference only.

13. Dispute resolution. Any dispute relating to the interpretation or application of this Agreement shall, unless amicably settled, be subject to conciliation. In the event of failure of the latter, the dispute shall be settled by arbitration. The arbitration shall be conducted in accordance with the modalities to be agreed upon by the parties or, in the absence of agreement, with the rules of arbitration of the International Chamber of Commerce. The parties shall accept the arbitral award

as final.

14. Privileges and immunities. Nothing in or relating to this Agreement shall be deemed a waiver of any of the privileges and immunities enjoyed by WHO under national or international law and/or as submitting WHO to any national court jurisdiction.

***

DataCol Web: Form for requesting permission to reproduce, reprint or translate WHO copyrighted material
==========
ID: 246169

Section: Contact details
---
* Title
* Mr
---
* First name
* Maxwell
---
* Family name
* Chirehwa
---
* Organization/affiliation
* University of Cape Town
---
* Web site address
* www.medicine.uct.ac.za/med/divisions/pharmacology
---
* Type of organization
* University/Academic
---
* If other, please specify
*
---
* If STM signatory, please select
---
* Position
* PhD Student
---
* Telephone
* +27216504861
---
* Address

* K45-21 OLD MAIN BUILDING, GROOTE SCHUUR HOSPITAL, OBSERVATORY, CAPE TOWN, 7925
---
* Country
* South Africa
---
* Email
* chrmax003@myuct.ac.za

Section: Information about WHO material to be reproduced
---
* Full title of WHO material from which the reproduction is to be made
* Global Tuberculosis Report 2017
---
* Website URL where WHO material is published
* http://www.who.int/tb/publications/global_report/en/
---
* ISBN / WHO Reference Number
* 978-92-4-156551-6
---
* Please select the item(s) to be reproduced
* Figure/table
---
* Type of reuse
* Dissertation or thesis
---
* No of item(s) to be reproduced
* 5 items or less
---
* For each item, please provide a reference and page number. If entire document, please state "Entire document".
* FIG. 3.4 Estimated TB incidence rates, 2016
Page 31

Section: Information about your publication
---
* Please provide the title of your publication that the above materials are to be published in
* Population nonlinear mixed-effects modelling of pharmacokinetics and pharmacodynamics of tuberculosis treatment
---
* Publishing format
* PDF
---
* Will you be translating?
* No
---
* If yes, please indicate languages
*
---

* If web please provide URL / If other, please specify
*
---
* Number of copies (if applicable)
*
---
* Target audience and planned distribution
* 3 thesis examiners and thesis will be uploaded on University website
---
* Planned publication/distribution date
* 15 January 2018
---
* If your publication or the material is to be sold, indicate the planned selling price or subscription fee
* NOT SOLD
---
* Is your publication sponsored or funded by an organisation other than your own?
* No
---
* If yes, please provide additional information
*
---
* Will there be any advertising associated with your publication?
* No
---
* If yes, please provide additional information
*
---
* Subject(s) of interest that most correspond to your request
* Tuberculosis
---
* Additional information about your request
*
---
* Approval
* Auto permission
---
* Latest approval modification
---
* WHO Department
* ACP, ACT
---
* Correct WHO URL
* http://www.who.int/tb/publications/global_report/en/

Section: Terms and conditions
---
* By submitting this request you confirm that you will abide by the terms and conditions if WHO

grants you permission.
* I have read and agree with the terms and conditions

Click the following link to access a format view of this record:
http://apps.who.int/datacol/survey.asp?survey_id=258&respondent_id=246169

This email was automatically sent to you by the WHO Intranet Data Collector.
The DataCol can send emails to accounts specified by the Form focalpoint.
